SANDIA REPORT

SAND97-1251 • UC-2010
Unlimited Release
Printed August 1997

Design, Demonstration and Evaluation of a Thermal Enhanced Vapor Extraction System

James Phelan, Bruce Reavis, James Swanson, Wu-Ching Cheng, Harsh Dev, Joseph Enk

Prepared by
Sandia National Laboratories
Albuquerque, New Mexico 87185 and Livermore, California 94550

Sandia is a multiprogram laboratory operated by Sandia Corporation, a Lockheed Martin Company, for the United States Department of Energy under Contract DE-AC04-94AL85000.

Sandia National Laboratories

Issued by Sandia National Laboratories, operated for the United States Department of Energy by Sandia Corporation.

Available to DOE and DOE contractors from
Office of Scientific and Technical Information
P.O. Box 62
Oak Ridge, TN 37831

Prices available from (615) 576-8401, FTS 626-8401

Available to the public from
National Technical Information Service
U.S. Department of Commerce
5285 Port Royal Rd
Springfield, VA 22161

NTIS price codes
Printed copy: A09
Microfiche copy: A01

SAND97–1251
Unlimited Release
Printed August 1997

Distribution
Category UC-2010

Design, Demonstration and Evaluation of a Thermal Enhanced Vapor Extraction System

James Phelan, Bruce Reavis, and James Swanson
Environmental Restoration Technologies Department

Wu-Ching Cheng
Environmental Risk Assessment & Regulatory Analysis

Sandia National Laboratories
P.O. Box 5800
Albuquerque, NM 87185-0719

Harsh Dev and Joseph Enk
Illinois Institute of Technology, Research Institute
10 West 35th St.
Chicago, IL 60616-3799

ABSTRACT

The Thermal Enhanced Vapor Extraction System (TEVES), which combines powerline frequency heating (PLF) and radio frequency (RF) heating with vacuum soil vapor extraction, was used to effectively remove volatile organic compounds (VOCs) and semi-volatile organic compounds (SVOCs) from a pit in the chemical waste landfill (CWL) at Sandia National Laboratories (SNL) within a two month heating period. Volume average temperatures of 83°C and 112°C were reached for the PLF and RF heating periods, respectively, within the 15 ft × 45 ft × 18.5 ft deep treated volume. This resulted in the removal of 243 lb of measured toxic organic compounds (VOCs and SVOCs), 55 gallons of oil, and 11,000 gallons of water from the site. Reductions of up to 99% in total chromatographable organics (TCO) was achieved in the heated zone.

Energy balance calculations for the PLF heating period showed that 36.4% of the heat added went to heating the soil, 38.5% went to evaporating water and organics, 4.2% went to sensible heat in the water, 7.1% went to heating the extracted air, and 6.6% was lost. For the RF heating

period, 54.9% went to heating the soil, 23.5% went to evaporating water and organics, 2.4% went to sensible heat in the water, 7.5% went to heating extracted air, and 9.7% went to losses. Energy balance closure was 92.8% for the PLF heating and 98% for the RF heating. The energy input requirement per unit soil volume heated per unit temperature increase was 1.63 kWH/yd^3 – °C for PLF heating and 0.73 kWH/yd^3 –°C for RF heating.

In the case of VOC removal, the baseline technology is soil vapor extraction (SVE). In the case of SVOC removal or VOC removal from low-permeability soils, the baseline technology is excavation and either on-site or off-site treatment with thermal desorption or incineration. The cost for SVE, excavation and treatment, and TEVES are about $25 to .

$75/$yd^3$, $450 to $600/$yd^3$, and $130 to $170/$yd^3$, respectively. While TEVES cannot compete with SVE for VOC removal in high permeability soils, TEVES is highly competitive with excavation/treatment for removal of SVOCs and VOCs in low permeability soils.

Contents

Figures

Tables

ACRONYMS

A	amp
AC	alternating current
ANSI	American National Standards Institute
ASTM	American Society of Testing and Materials
atm	atmosphere
BGL	below ground level
Btu	British thermal unit
C	Celsius
CERCLA	Comprehensive Environmental Response, Compensation, and Liability Act
CFM	cubic feet per minute
CFR	Code of Federal Regulations
CW	continuous wave
CWL	Chemical Waste Landfill
DCB	dichlozobenzene
DoD	Department of Defense
DOE	Department of Energy
DOE/AL	DOE-Albuquerque Operations Office
DOE/OTD	DOE-Office of Technology Development
DOT	Department of Transportation
EBZ	ethylbenzene
EIS	Environmental Impact Statement
EPA	Environmental Protection Agency
ETCAP	Environmental Technology Cost-Savings Analysis Project
F	Fahrenheit
FCC	Federal Communications Commission
FRE	Freon-113
ft	feet
GAC	Granular Activated Carbon
gal	gallon
GC	gas chromatograph
gpm	gallons per minute
GPR	Ground Penetrating Radar
HDPE	high-density polyethylene
Hp	horsepower
hr	hour
Hz	hertz
IEEE	Institute of Electrical and Electronic Engineers
IITRI	Illinois Institute of Technology Research Institute
IL	Illinois
ISCST	Industrial Source Control Short Term
in	inch
ISM	industrial, scientific, and medical frequency band
KAFB	Kirtland Air Force Base

kg	kilogram
kVA	kilo Volt Amps
kW	kilowatt
kWH	kilowatt hours
lb	pound
LLNL	Lawrence Livermore National Laboratory
LPT	low power test
m	meter
MAG	magnetometer
mbar	millibar
MHz	megahertz
ml	milliliter
NAPL	non aqueous phase liquids
NEPA	National Environmental Policy Act
NM	New Mexico
NMED	New Mexico Environmental Division
OTD	Office of Technology Development
PCBs	polychlorinated biphenyls
PCE	tetrachloroethylene
PEN	pentane
PLC	programmable logic controller
PLF	powerline frequency
ppb	parts per billion
ppm	parts per million
psi	pounds per square inch
PVC	polyvinyl chloride
RCRA	Resource Conservation and Recovery Act
RD&D	Research Development and Demonstration
RF	radio frequency
RFI	radio frequency interference
RFI/CMS	RCRA Facility Investigation/Corrective Measures Study
RI/FS	Remedial Investigation/Feasibility Study
scfm	standard cubic feet per minute
SEAMIST™	Science and Engineering Associates Membrane Instrumentation and Sampling Technique
SERP	Steam Enhanced Recovery Process
SITE	Superfund Innovative Technologies Evaluation
SNL	Sandia National Laboratories
SNL-ER	Sandia National Laboratories - Environmental Restoration
SP	step potential
SVE	soil vapor extraction
SVOC	semi-volatile organic compound
SVVS	Subsurface Volatilization and Ventilation System
TA-III	Technical Area III
TAL	Target Analyte List

TCA	trichloroethane
TCE	trichloroethylene
TCO	total chromatographable organics
TEVES	Thermal Enhanced Vapor Extraction System
TPH	total petroleum hydrocarbons
TV	touch voltage
UEL	Upper explosive limit
V	volt
VOC	volatile organic compound
vol	volume
wt	weight
X-O	o-xylene
XMP	m/p-xylene

This page intentionally left blank.

1.0. INTRODUCTION

1.1 Description of Project

The Thermal Enhanced Vapor Extraction System (TEVES) demonstration project was conceived in the Fall of 1991 as part of a U.S. Department of Energy, Office of Technology Development (DOE/OTD) effort to demonstrate, test, and evaluate enhanced mass removal technologies for volatile organic contamination in soils. The DOE/OTD enhanced mass removal technology effort included other thermal methods such as Dynamic Steam Stripping (which includes Three-Phase alternating current heating [DOE 1995a], Six-Phase alternating current [AC] Heating [DOE 1995b], and Radiofrequency [RF] Dipole Antennae Heating [Jarosch 1994]). The reasons for investment in the enhanced mass removal efforts by DOE/OTD included the recognition that certain contaminant profiles and soil conditions were a challenge to conventional vacuum vapor extraction technology. These conditions included situations where the contaminants were held in low permeability soils, limiting the advective removal of volatile contaminants and the low mass removal rates characteristic of low vapor pressure compounds at ambient temperature.

A hazardous waste disposal site at Sandia National Laboratories (SNL), known as the Chemical Waste Landfill (CWL), was used for the disposal of a wide variety of containerized and free liquids in small unlined disposal cells. Wastes were grouped into categories for co-disposal to limit incompatibility problems with chemical waste groups. As such, all organic chemical wastes were co-disposed with the majority being solvents and waste oils. Since this combination of chemical wastes would significantly lower the vapor pressure of the target solvents, traditional vacuum vapor extraction was expected to have limited success.

The CWL was thought to have three disposal cells that were used for the disposal of organic chemical wastes. These shallow cells were of rectangular dimension and matched the geometry of a soil heating technology developed by the Illinois Institute of Technology Research Institute (IITRI) of Chicago, IL. A partnership was established between the technology development staff of SNL and IITRI to complete the TEVES demonstration at one of the disposal cells of the CWL and is the subject of this report.

Figure 1-1 shows an illustration of the TEVES system indicating the subsurface waste and contaminated soil zones, the RF excitor and reflector (or guard) electrodes, the vapor extraction wells and the vapor recovery and treatment system.

Both powerline frequency (PLF) and radio frequency (RF) heating were tested in the TEVES demonstration, because the two different modes of heating have complementary advantages. The PLF heating is simpler to operate and is less expensive per kWH of energy delivered to the soil. However, PLF will deliver energy only where the electrical conductivity is sufficiently high. Predominantly, this means where the soil moisture is high, so where the soil is heterogeneous, PLF will not heat the soil uniformly. RF heating is able to reach higher temperatures since it does not rely solely on conduction; however, RF requires more complicated equipment and thus is higher in cost per

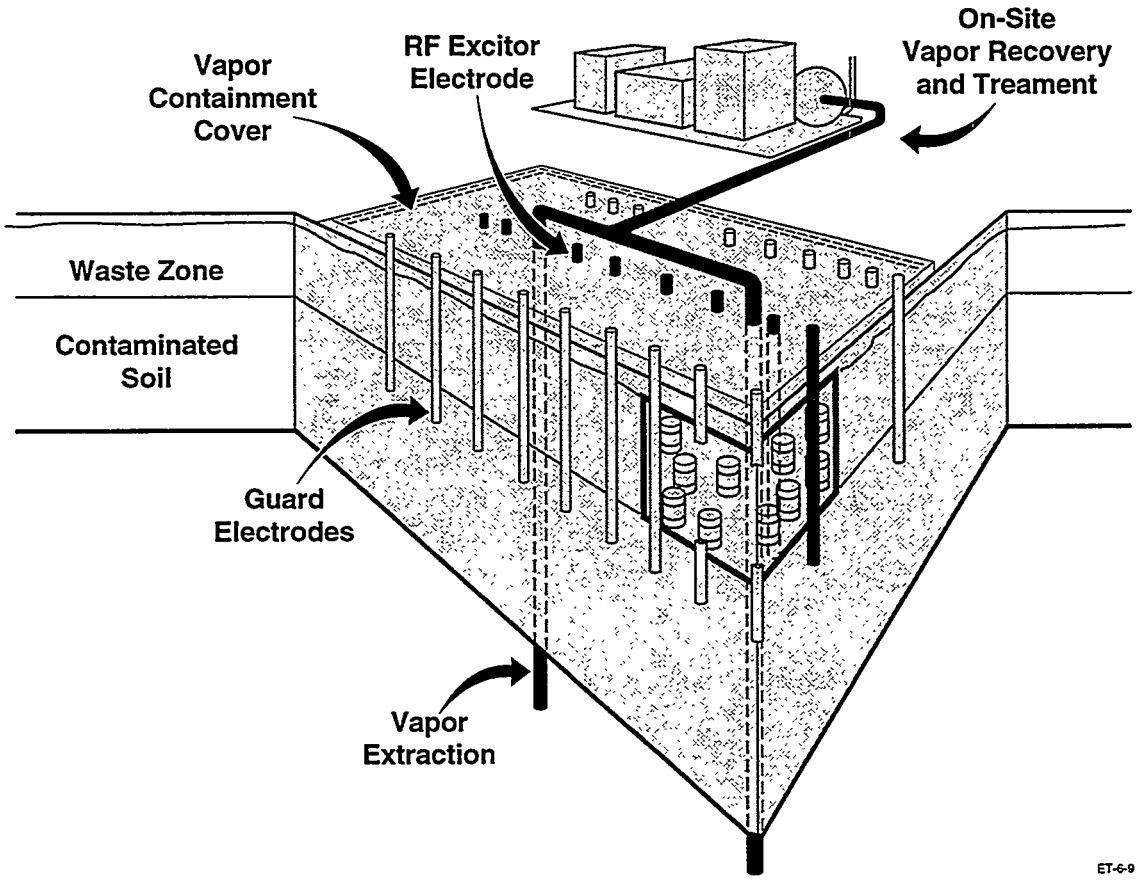

Figure 1-1. Conceptual design of the below ground portion of the heating system.

kWH of energy delivered to the soil. Thus, the design of the demonstration called for a first phase of heating with PLF and a second phase of heating with RF.

1.2 Project Chronology

The TEVES demonstration was conducted in stages over a four year period. The following timetable shows the major stages:

Project Initiation	January 1992
Site and Waste Characterization	April – August 1992
Lab Treatability Studies	August 1992 – July 1993
Permit Application	July – October 1992
Engineering Design	October 1992 – December 1993
Permit Approval	May 1994
Demonstration Period	October 1994 – June 1995
Closure	June 1995 – December 1995
Permit Termination	September 24, 1996

1.3. Demonstration Objectives

The objectives of the project were to demonstrate the technical utility and economic competitiveness of a near full-scale application of soil heating technology in conjunction with soil vapor extraction. The objectives also included determining the following:

- The heating efficiency for PLF and RF heating compared to pre-test estimates.
- The temperatures needed to effectively remove contaminants of varying thermal properties.
- The capability of a traditional thermal catalytic off-gas treatment unit to accept wastes generated by thermal enhancement methods.
- The important operating parameters needed for commercial operations.
- The key cost elements for the process.
- The baseline remediation technologies for volatile organic compounds (VOC) and semi-volatile organic compounds (SVOC) contamination and the niches for which soil heating enhanced vapor extraction is a competitive technology.

This page intentionally left blank.

2.0 SITE AND WASTE DESCRIPTION

SNL is southeast of Albuquerque, NM, in Bernalillo County located within the boundaries of Kirtland Air Force Base (KAFB). Within SNL are five designated technical areas. The area that contains the CWL is Technical Area III (TA–III) (Figure 2–1). The CWL is four miles south of the nearest drinking water supply well and three miles from any natural groundwater discharge point. The water table is approximately 148 m (485 ft) below ground level (BGL), at the CWL.

2.1 Landfill History

The landfill was created in 1962 to accept waste chemicals generated by SNL facilities. To minimize any adverse chemical reactions, individual disposal pits were excavated from the soil for each chemical group. The groups included oxidizers, reducers, acids, metal, and organics. The typical size of these pits is about 15 ft wide by 45 ft long by 15 ft deep. The organic waste disposal cells were given a pit designator of #3, and it is thought that three organic waste disposal cells were used over the lifetime of the CWL. The cell used for TEVES was given the designation, Pit 3–1, indicated in Figure 2–2. The total disposal volume for all organic waste pits was about 100,000 liters of hazardous waste and oils. It is not known how much of this volume went into each of the three organic waste disposal pits. A magnometer and ground penetrating radar survey was conducted to locate buried objects over the entire landfill as part of the baseline environmental restoration effort. This data was used to estimate the number of buried metal objects located in the treatment zone.

The profile of the wastes and an estimate of the quantities placed into all organic waste disposal pits is shown in Table 2–1. These are consistent with the past SNL programs of developing a wide variety of new technologies, with no involvement as a primary industrial manufacturing facility. This is indicated by the wide variety of chemical wastes, many of small quantities, and a limited number of larger quantity organic solvents. Of note is the large proportion of oils (e.g., motor, hydraulic, transformer oils, and heat transfer fluids) that were placed into the organic waste disposal pits. Polychlorinated biphenyls (PCBs) were not found in this waste mixture.

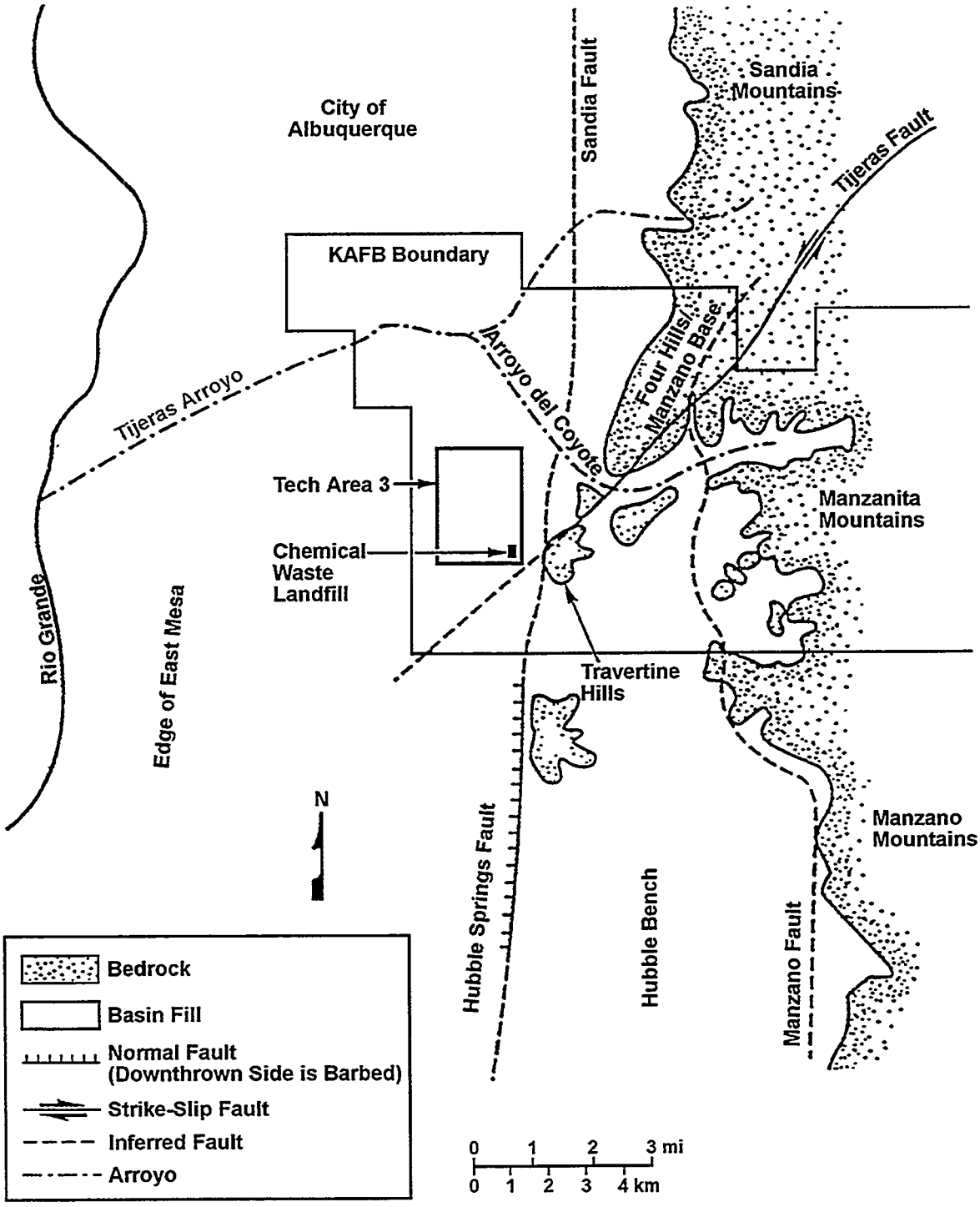

Figure 2-1. Location of Chemical Waste Landfill.

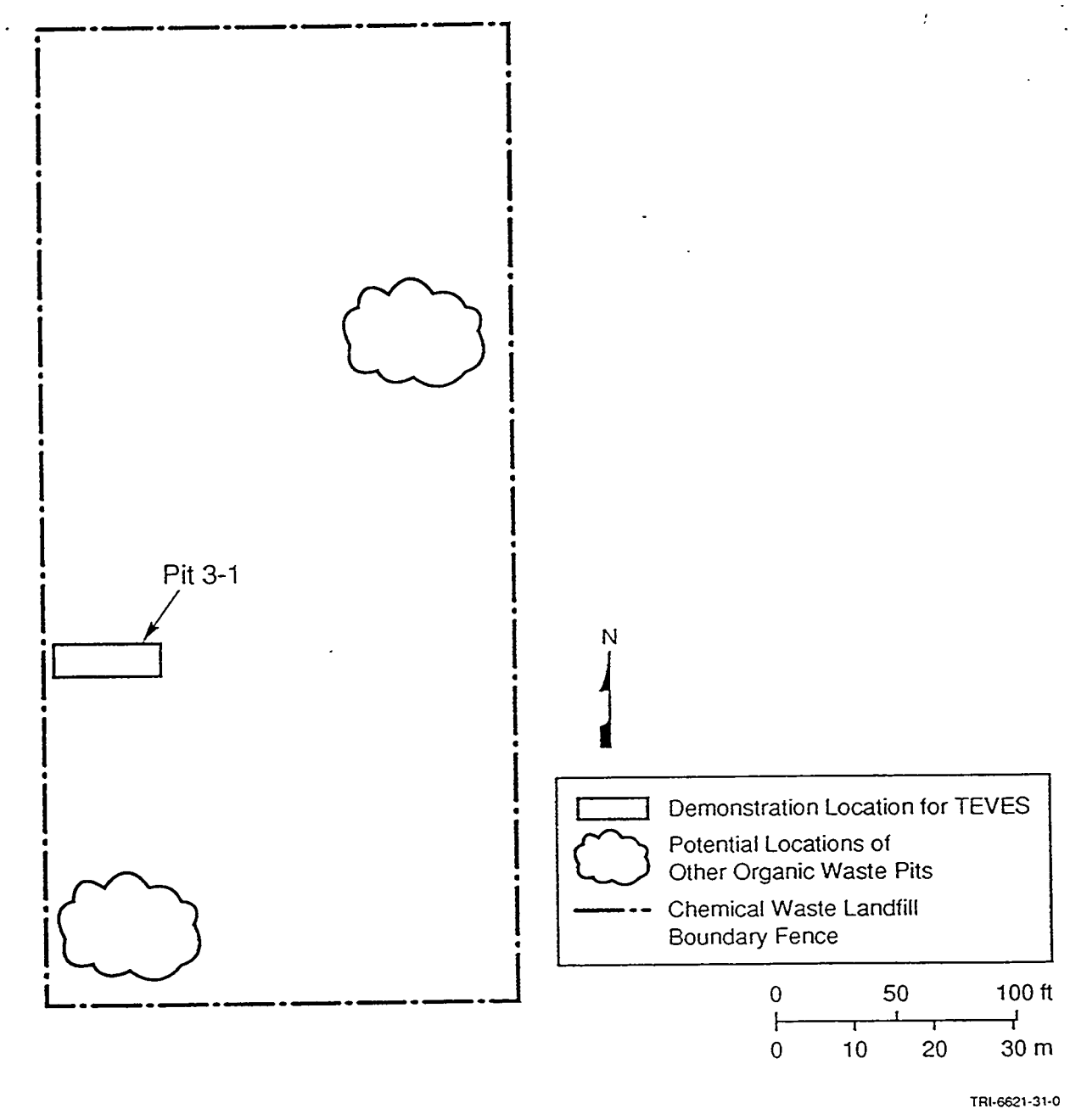

Figure 2-2. Location of TEVES, Pit 3-1.

Table 2–1. Chemical Waste Landfill Disposal Pit Contents — Pit 3
(Recorded Disposals from 1975 to 1982)

Chemical	Volume (liters)
Oil (unidentified)	27,851
Solvents (unidentified)	24,586
Acetone	9,626
Paint and Thinners	4,179
Trichloroethylene	3,669
Organics	2,467
Therminol	2,082
Ethylene Glycol	1,630
Freon	1,543
Alcohol	1,382
Epoxy	1,109
Chloroethane	1,059
Photoresist	1,046
Toluene	914
Dye, Laser Dye Mixes	692
LIX Solvent	513
Tetrahydrofuran	394
Xylene	340
Methyl Ethyl Ketone	313
Chemicals (unidentified)	256
Resins (unidentified)	204
Plasticizer (unidentified)	147
Cleaning Agents/Solvents	100
Polymers (unidentified)	100
Airplane Fuel	76
Glycerin	40
Benzene	30
Nitromethane	18
DOW Sealants/Adhesives	15
Carbon Tetrachloride	13
Methylene Chloride	13
Miscellaneous	7,865
Total	**94,272**

3.0 DEMONSTRATION DESIGN

There were six phases and two stages in the TEVES demonstration design. The first was a project planning stage followed by six phases of the actual demonstration and completed with the technology transfer stage. These included the following:

1. Regulatory Permits
    - National Environmental Policy Act (NEPA)
    - Resource Conservation and Recovery Act, Research Development and Demonstration Permit (RCRA RD&D)
    - Albuquerque/Bernalillo County Air Quality Control Requirements
2. Phase I: Site Investigation
    - Soil sampling and analysis
    - Air-phase permeability measurements
    - Vent well construction
    - Buried metal object evaluation
3. Phase II: Off-Gas System Design
    - Estimate mass-load rate and volume flux
    - Integrated vapor and condensate treatment
4. Phase III: Venting/Heating Design
    - Bench-scale treatability tests
    - PLF heating system design
    - RF heating system design
    - Process monitoring system
    - Electrical safety systems
    - Vacuum extraction system design
    - Electrical service
    - Pre-test modeling
5. Phase IV: Vacuum Venting
    - Ambient temperature venting for three days
    - Establish baseline contaminant load and constituent profile
6. Phase V: Powerline Frequency (PLF) Heating/Venting
    - 60-Hz AC, 100 kW ohmic heating of top 25 ft to 90°C
    - Heat/vent for 30–45 days
    - Establish contaminant load and constituent profile
7. Phase VI: Radio Frequency Heating/Venting
    - 3–6.78 MHz, 100 kW dielectric heating of top 20 ft to 200°C immediately following PLF heating periods
    - Heat/vent for 30–45 days
    - Establish contaminant load and constituent profile
8. Technology Transfer
    - Post demonstration cost analysis
    - Application analysis

3.1 Regulatory Permits

In order to comply with the National Environmental Policy Act (NEPA), an environmental checklist and action description memorandum were submitted to DOE/AL on February 3, 1992. Under the DOE proposed final rule of November 20, 1990, the TEVES proposed action could be considered a temporary pilot-scale waste collection and treatment facility that supports a Comprehensive Environmental Response, Compensation, and Liability Act Remedial Investigation/Feasibility Study (CERCLA RI/FS) or RCRA Facility Investigation/Corrective Measure Study (RFI/CMS) and be considered for a categorical exclusion. On April 10, 1992, the proposed action to perform the TEVES demonstration was categorically excluded from the requirement to prepare NEPA documentation in the form of either an Environmental Assessment or an Environmental Impact Statement (EIS).

The CWL demonstration location was permitted through RCRA as an interim status land disposal facility from 1982 until 1985. Therefore, all hazardous waste treatments performed at the site would require application of RCRA requirements. Options included a full RCRA Part B Permit, a RD&D Permit, or an exclusion under the treatability exemption allowances. The estimated mass of hazardous waste that would be treated by the TEVES would exceed the maximum threshold for the treatability exemption indicating that this option was unavailable. Since the TEVES was considered a demonstration of an innovative technology system, the RCRA RD&D Permit provisions were selected as the appropriate regulatory basis. A RCRA RD&D Permit Application was submitted to the New Mexico Environment Department on October 7, 1992, and after an administrative review, technical review, and public participation in the review process, the permit application was approved on May 24, 1994.

The Albuquerque/Bernalillo County Air Quality Control Board promulgated regulations requiring an Authority to Construct Permit for emissions of hazardous air pollutants in significant amounts. A *significant amount* was defined as any detectable amount. An Authority to Construct Permit Application for TEVES was submitted to the City of Albuquerque on July 29, 1994, and after an administrative review, technical review, and public participation in the review process, the permit was approved on October 11, 1994.

3.2 Phase I Site Investigation

3.2.1 Soil Sampling and Analysis

The soil sampling and analysis effort was performed in April 1992. It included drilling two boreholes to obtain soil samples for hazardous constituents, performing air permeability tests, collecting soil gas samples, and constructing two vapor extraction/soil heating wells. Soil samples were obtained at 5 ft (1.5 m) intervals from the surface to a depth of 50 ft (15 m) and then every 10 ft (3 m) to the bottom of the well using hollow stem auger drilling technology and a combination of continuous core barrel or split spoon soil sampling methods. This was the first

contaminant characterization effort at Pit 3–1 and therefore, a full suite of analytical parameters was specified. The parameters are shown in Table 3–1 (IT 1992a).

Table 3-1. Phase I Analytical Methods

Analyte Group	Method Number
Volatile Organic Compounds (VOCs)	SW846, Method 8240
Semi-volatile Organic Compounds (SVOCs)	SW846, Method 8270
Target Analyte List (TAL) Metals	SW846, Method 3050
Total Chromatographable Organics (TCOs)	ASTM Method D–2887; IERL-RTP Procedures Manual
Polychlorinated Biphenyls (PCBs)	SW846, Method 8080
VOCs in Air	Compendium Method TO–14

Complete results of the Phase I Site Investigation are found in the report, *Results of the TEVES Phase I Site Investigation* (IT 1992b). A summary of the types of VOCs found in the soil and soilgas and their maximum concentrations is shown in Table 3–2. The depth profile showed significant concentrations in the disposal pit (estimated depth 15 ft and down to about 25 ft). There were few contaminants found in soil samples below 30 ft; however, soilgas concentrations were prevalent throughout the bottom of the borehole at around 100 ft. Since the soil heating technologies are effective for residual liquid phase soil contaminants, this effort indicated design depth of 25–30 ft deep.

3.2.2 Air Permeability Tests

A soil gas collection and air permeability test device (SEAMIST™) was used during the field drilling effort. This device uses a fabric membrane inverted into an open borehole that contains tubing attached to pre-determined depth locations (Lowry and Narbutovskih 1991). A small rotary vane vacuum pump is used to extract soil vapors and establish a vacuum on the test zone. Flow and pressure measurements are made and used in an analytical equation to estimate air permeability of the test region (Narbutouskih 1991). After completion of the air permeability tests, summa canisters are attached to the flow tube to collect depth discrete soil vapor samples. The drill crew is maintained on standby for 2–4 hours during this process and can complete well construction activities once the membrane is removed. The results of the air permeability tests are shown in Table 3–3.

Table 3-2. Phase I Maximum Concentration of Soil Contaminants

Detected Analytes	Soil Conc. (ppm)	Soil Gas Conc. (ppm)
Acetone	270	Not Analyzed
Methylene Chloride	0.082	21
Ethylbenzene	230	4
Tetrachloroethene	1,700	150
Toluene	1,300	25
1,1,1-Trichloroethane	250	210
Trichloroethene	540	290
Xylenes (total)	1,100	3
Dichlorodifluoromethane	Not Analyzed	5
Chlorodifluoromethane	Not Analyzed	0.5
n-Pentane	Not Analyzed	56
1,1-Dichloroethene	Not Detected	25
Freon-113	Not Analyzed	86
Carbon Disulfide	Not Detected	Not Detected
Hexane	Not Analyzed	1
1,1-Dichloroethane	Not Detected	5
Chloroform	Not Detected	3
Carbon Tetrachloride	Not Detected	0.5
Benzene	Not Detected	5
1,2-Dichloroethane	Not Detected	1
1,2-Dichloropropane	Not Detected	2
n-Octane	Not Analyzed	8
n-Nonane	Not Analyzed	1
Decane	Not Analyzed	0.2
Trichlorofluoromethane	Not Analyzed	10
n-Heptane	Not Analyzed	1
Cyclohexane	Not Analyzed	1.5
Vinyl Chloride	Not Detected	6
Phenol	6	Not Analyzed
1,4-Dichlorobenzene	4	Not Analyzed
1,2-Dichlorobenzene	2,600	Not Analyzed
2-methylnaphthalene	5	Not Analyzed
Diethylphthalate	3	Not Analyzed
Fluorene	4	Not Analyzed
Phenanthrene	10	Not Analyzed
bis(-Ethylhexylphthalate)	7	Not Analyzed
Crysene	17	Not Analyzed
Di-n-butyl phthalate	65	Not Analyzed
Arochlor 1242	0.1	Not Analyzed
Arochlor 1260	0.1	Not Analyzed
Total Chromatographable Organics	76,000	Not Analyzed

Table 3-3. Air Permeability Test Results (Darcy)

Depth	TEVES1	TEVES2
20 ft	5	63
30 ft	11	6
40 ft	11	5
50 ft	17	7
60 ft	16	47
75 ft	7	17

3.2.3 Vapor Extraction Well Design and Construction

Past field experience by IITRI and the planned area of the heated zone allowed a pre-engineering estimate of the depth for the center excitor row electrodes. Prior to mobilizing the drilling/soil sampling effort, materials for construction of the two vapor extraction wells were acquired. Four-inch diameter type K copper pipe was selected for the electrode conductor for a total length of 18.5 ft. below grade and 1.5 ft. above grade for attachment to the vapor extraction system. The copper pipe was cut at a machine shop with a design to have an equivalent open slot area equal to traditional polyvinyl chloride (PVC) well screen using 0.020 in. slots. Attached to the copper pipe was a 10 ft. section of 4 in. diameter teflon well screen (0.020 in. slot) to allow vapor extraction below the length of the excitor row electrodes. Attached to the teflon pipe was traditional 4 in. PVC well screen (0.020 in. slot) to the bottom of the borehole. The teflon section was used as a thermal break between the copper electrode and PVC extraction well because of the concern about the PVC materials melting or carbonizing if they were attached to the copper. Construction diagrams for these wells (TEVES1 and TEVES2) are found in Appendix F. The extra length of the two vapor extraction wells was for air permeability tests unrelated to the TEVES demonstration (Phelan 1993). The TEVES1 and TEVES2 vapor extraction wells were backfilled with local soil to 30 ft. below grade prior to assembly of the vapor extraction manifold.

3.2.4 Buried Metal Object Evaluation

A commercial ground penetrating radar (GPR) and magnetometer (MAG) survey was performed at the CWL. To improve the reliability of GPR and MAG data interpretation, a new method that combines the data was utilized (McCorkle 1993, Hansel 1992, Hansel and Dalton 1993, Dalton 1992). This effort indicated discrete metal objects located in the demonstration site with a higher density in the southeast quadrant (Figure 3–1). The crosses represent electrode locations. The information provided by this survey was unable to resolve the size or number of buried objects. It is unlikely, however, that waste in containers larger than 55 gallon steel drums was placed into the disposal pit.

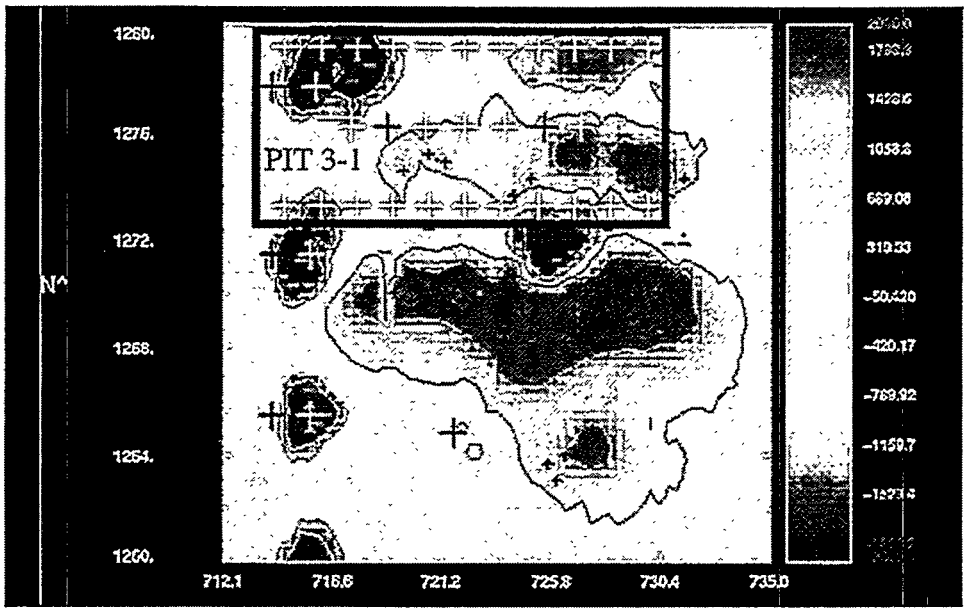

Figure 3-1. Magnetometer survey for buried objects at CWL.

The integrity of the metal containers buried in the ground for 10 to 15 years was unknown. It was possible for a drum to be in relatively good condition or to have been highly corroded from the alkaline soils. Volatile hazardous waste in containers will generate internal container pressure that is a function of the temperature and vapor pressure of the material. With the soil temperatures ranging from 150°C to 200°C planned for the demonstration, it was expected that much of the containerized liquid wastes would be vented and captured by the vacuum extraction system. Table 3–4 shows the vapor pressure of several wastes known to exist in Pit 3–1. The Department of Transportation requirements for pressure integrity of a 55 gallon drum (DOT 17H or 17E) is 36 psi (3 atm) (49 Code of Federal Regulation [CFR] 178.605[d][3]). For most VOCs known to exist in Pit 3–1, the vapor pressure at elevated temperatures will exceed the pressure integrity specification for a 55 gallon drum. This means that hazardous wastes would most likely be vented from drums. The pressure at which venting will occur will be a function of the integrity of the drum. Venting most likely takes place at a localized weakness in the drum such as a localized corrosion, bung opening, ring closure, or a dent/crease.

3.3 Off-Gas Treatment System

3.3.1 Estimated Mass-Load Rate and Volume Flux

Design of the off-gas treatment system required an estimate of the desired volume flow rate of extracted air and mass rate of contaminants expected during soil heating. Using the Phase I soil and soil gas sampling data, estimates of the increased vapor concentrations of the largest contamination contributors were made using the ideal gas law. Table 3–5 shows the estimated

Table 3-4. Vapor Pressures of VOCs as Function of Temperature

Temp (C)	Vapor Pressures (atm)			
	TCE	toluene	xylene	1,2 DCB
20	0.07	0.02	0.00	0.00
30	0.11	0.04	0.01	0.00
40	0.18	0.07	0.02	0.00
50	0.27	0.12	0.03	0.00
60	0.40	0.18	0.05	0.01
70	0.57	0.26	0.08	0.02
80	0.79	0.38	0.13	0.03
90	1.08	0.54	0.19	0.05
100	1.43	0.74	0.28	0.08
110	1.86	1.00	0.40	0.12
120	2.38	1.32	0.56	0.17
130	2.99	1.72	0.77	0.24
140	3.72	2.21	1.04	0.33
150	4.55	2.81	1.38	0.44
200	10.75	7.79	4.75	1.58

(Ref., Boublik et al., 1984)
TCE: Trichloroethylene
DCB: Dichlorobenzene

Table 3-5. Estimated Containment Mass Removal Rates

	mass removal rate (lbs/hr)				
	PCE	TCE	TCA	FRE	Total
ambient temperature	0.1	0.3	0.1	0.1	0.6
powerline frequency heating	1.8	1.0	0.3	0.1	3.2
radiofrequency heating	3.8	1.0	0.3	0.1	5.2

FRE: Freon-113
PCE: tetrachloroethylene
TCA: trichloroethane
TCE: trichloroethylene

contaminant removal rates at the design end-point temperatures of the PLF and RF heating. A volume flux of 200 scfm at 70 in. water vacuum was estimated using the desired subsurface flow radius of influence and the measured air permeabilities.

3.3.2 Integrated Vapor and Condensate Management

The contaminant vapors extracted from the treatment zone were expected to be extracted with water vapor from low to saturated levels. A system was desired that would destroy the organic vapors and minimize the amount of condensate generated.

The off-gas treatment system consisted of an air-to-air condenser to remove excess water vapor from the air stream, an air stripper to remove volatiles from the condensate, a carbon adsorption unit to remove residual organics from the stripped condensate, and a catalytic oxidation unit to destroy organics in the vapor discharge from the condenser and air stripper. Figure 3–2 illustrates the flow.

3.3.2.1 CONDENSER

An air-to-air heat exchanger was designed to remove the water vapor from the soil vapor stream at peak water vapor load rates. It was necessary to use the air-to-air heat exchanger because the catalyst in the thermal catalytic destructor would experience hydrothermal aging and could only be warranted for air streams up to 10% water by volume. A humidity/temperature probe was used to measure the water saturation and temperature at the exit of the condenser. The fan of the heat exchanger was turned on to improve the water vapor removal. The condensate from the condenser accumulates in a day tank until a high level switch is tripped, causing the day tank pump to transport the condensate to the air stripper.

3.3.2.2 AIR STRIPPER

When the high level condensate switch of the day tank closes, the programmable logic controller (PLC) closes the manifold extraction valve 90% (allowing a small extraction to continue on the treatment zone), opens the air stripper valve, and begins pumping condensate at about 1–3 gpm to the top of the flat plate air stripper. Air flow through the stripper is induced by the main vacuum extraction system blower. The stripped VOCs are then carried through the blower and into the Catox unit to be destroyed by catalytic oxidation. A low-level day tank switch would then close and the PLC stops the day tank pump and starts a five-minute timer to allow all liquid in the air stripper to be treated.

3.3.2.3 THERMAL CATALYTIC SYSTEM

The thermal catalytic system was used to treat the uncondensed vapors discharged from the air-to-air heat exchanger and the vapor discharged from the air stripper. The catalytic oxidizer operated at an optimum temperature of about 800°F.

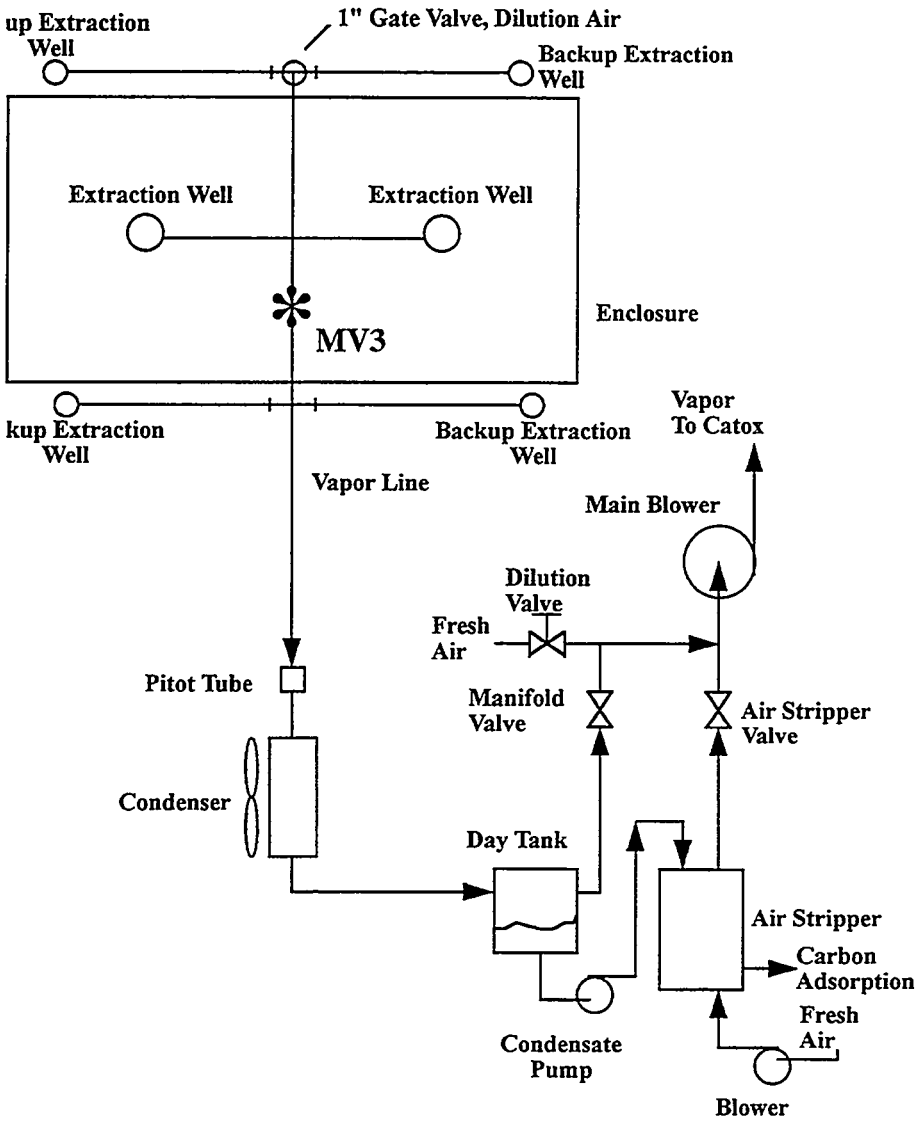

Figure 3-2. Integrated Off-Gas treatment system.

3.3.2.4 CARBON ADSORPTION

A mercury float switch in the bottom compartment of the air stripper is used to activate a pump that moves the treated water through an activated carbon drum for final polishing. The effluent from the activated carbon treatment is discharged into a large tank for storage. Analysis of the liquid is necessary to determine if it would meet discharge requirements for sanitary sewer disposal. These requirements specified no more than 5 ppm Total Toxic Organics (as listed by the City of Albuquerque Wastewater Regulations).

3.4 *In Situ* Heating Design

3.4.1 Bench-Scale Treatability Tests

A treatability study was performed to determine the time/temperature conditions necessary for removal of the soil contaminants found at the CWL Pit 3–1 (Jones et al., 1993). Soil samples collected during the Phase I Site Investigation were subjected to eleven bench-scale tests to determine the expected removal during ambient temperature vacuum extraction, powerline frequency heating, and radiofrequency heating. The experimental setup is shown in Figure 3–3. This figure shows a 1.5-inch diameter stainless steel pipe used as the treatability reactor, heaters used to heat the soil and preheat air or steam being passed through the soil, an air/steam supply line, a condenser used to collect the contaminants from the soil, and a mass flow meter/flow totalizer used to measure the total and instantaneous air flow through the soil. Pre- and post-test analyses for total petroleum hydrocarbons (TPHs) were calibrated against several petroleum standards. Experiment 1 was performed to simulate ambient temperature vacuum extraction. Experiments 2, 3, and 11 simulated the expected end temperature of the powerline frequency heating (80°–85°C). Experiments 4–10 were performed to simulate the effect of various high temperature-time combinations. Experiment 9 failed, due to a high temperature excursion from a failed controller. Experiments 5 and 10 used superheated steam after the native moisture had boiled out of the soil to evaluate the effect of steam sweep on petroleum hydrocarbon removal.

The results of the treatability study are summarized in Table 3–6. Data are presented for the removal of petroleum hydrocarbons in three different boiling ranges, (the gasoline, diesel, and the C_{16} to C_{44} fraction). The data are also grouped according to the treatment temperature ranges. Experiments were performed in three different temperature ranges, one each to represent the three processes: *in situ* venting (20°C); *in situ* heating with PLF process (80°–85°C); and *in situ* heating with the RF process (>100°C).

The results show that *in situ* venting of soil for the diesel fraction, even for as long as 30 days, helps to reduce the concentration of the diesel range organics by only 27%. The removal of diesel may be substantially slower under field conditions that do not provide idealized air sweep of the soil which is the case in the laboratory. Heating the soil to a temperature range of 150°–254°C helped to remove approximately 90%–99% of the diesel fraction. The time needed for this is approximately 160–360 hours (6.7–15 days) depending upon the treatment temperature.

In two experiments, 5 and 10, steam was injected into the soil after the native moisture was boiled out. Comparing Experiment 5 data on diesel to that of Experiment 4, it appears that the addition of steam did not have any beneficial effect compared to air alone. A similar conclusion can be made for Experiment 10. This result shows that the contaminants in this soil did not require added steam for removal.

The removal of gasoline fraction in all temperature ranges was satisfactory. The results show that when the soil is heated to a range of 80°–85°C, the residual concentration of gasoline can be reduced to less than 16 ppm after 6.7 days. Higher temperatures may be used for gasoline

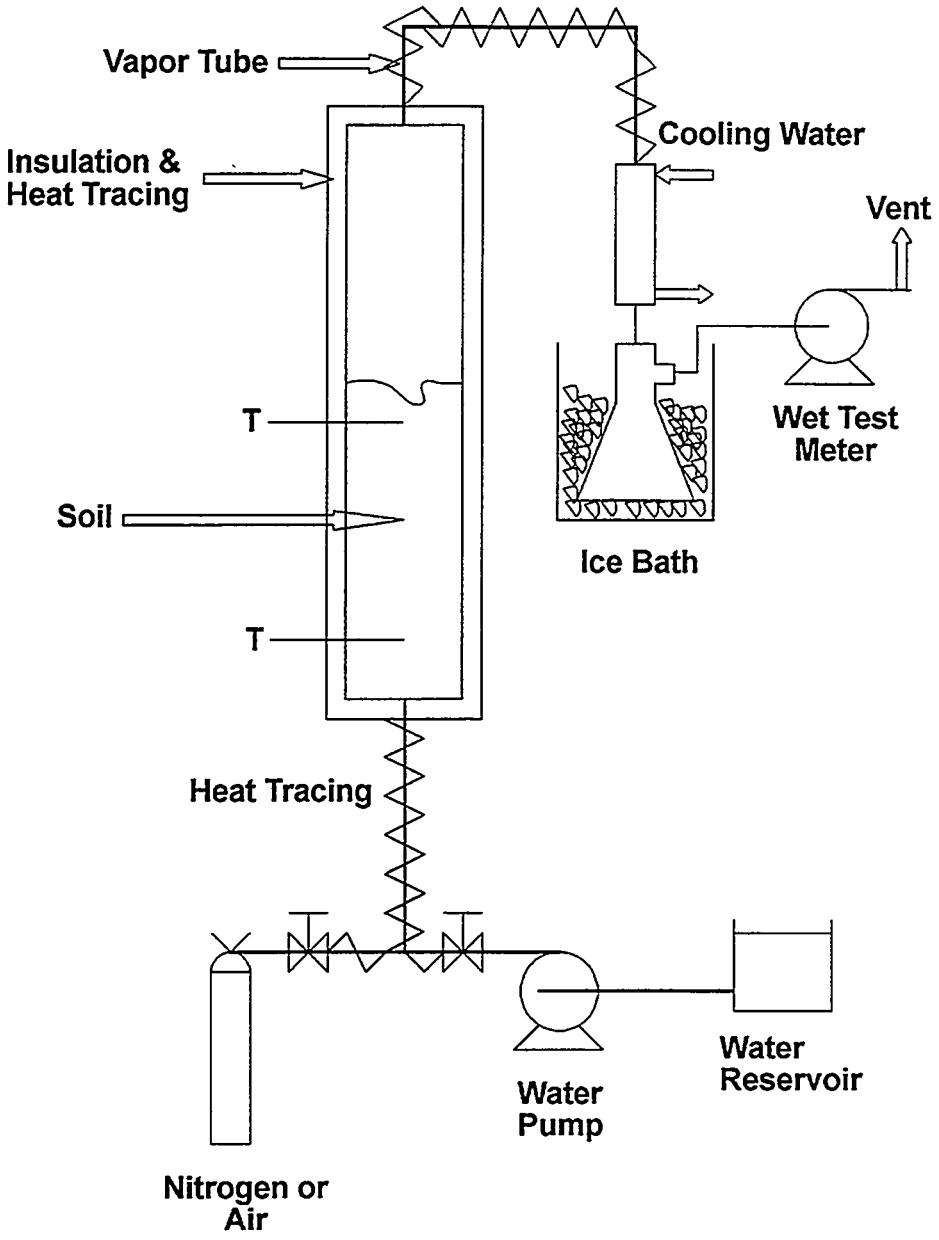

Figure 3-3. Bench-scale treatability test setup.

removal but they are not necessary. At room temperature, the gasoline concentration was reduced to less than 16 ppm after 30 days.

In Experiments 4 and 5, the residual gasoline concentration was higher than that observed in all other experiments, including the 20°C experiment. The reason for the high residual is not clear. It may be related to the much shorter treatment time used in these experiments. In Experiment 5, the high residual concentration may be related to a cold spot (116°C) observed in the bottom half of the soil column.

Table 3-6. Summary of Soil Treatability Experiment Results

			Gasoline Fraction			Diesel Fraction			>C16 Fraction		
Expt. No.	Treatment Temperature (C)	Time at Temperature (hours)	Initial ug/gm	Final ug/gm	Removal %[1]	Initial ug/gm	Final ug/gm	Removal %[1]	Initial ug/gm	Final ug/gm	Removal %[1]
1	20	711	42	<16	> 64	266	205	26	233	233	4
2	82	159	48	11	61	316	161	51	342	161	55
3	83	313	54	11	80	314	154	53	325	154	54
4	121	83	789	43	95	4451	3040	37	3780	3160	22
5	125	77	948	109	89	5236	3486	38	5240	4813	15
6	199	160	614	22	96	2834	24	99	1840	19	99
7	254	159	730	9	>99	3626	10	99	1690	34	98
8	150	166	1050	<16	>98	2310	35	98	1000	380	64
10	175	357	250	<16	>94	1790	11	99	975	210	79
11	84	167	175	<16	>91	2910	1850	38	405	424	0

[1]Percent removal is computed on a dry soil basis.

High removal of hydrocarbons containing 16-44 carbon atoms per molecule was obtained only under high temperature treatment conditions. Thus in Experiments 6 and 7; where the temperature was in the range of 199°C-250°C, 98%-99% removal of the high boiling fraction was obtained in a period of 6–7 days. The residual concentration was 19–34 ppm. At room temperature, there was no removal of this fraction even after 30 days of venting.

These treatability tests indicate that a temperature of about 200°C could be needed for removal of nearly all of the petroleum hydrocarbons; however, lower temperatures may be adequate and were the subject of this field effort.

3.4.2 Design Heat Balance

The heating time is related to the power requirement by an energy balance. This is given in Table 3–7.

The heated volume is,

45 ft long x 16 ft wide x 23 ft deep = 16,560 ft^3.

The density of nearly-dry sand is about 100 lb/ft^3. The total mass of soil to be heated is,

16,560 ft^3 x 100 lb/ft^3 = 1,656,000 lb = 828 tons.

The initial moisture in the top 20 ft was 5 vol % or 3.1 wt %, based on a number of measurements by SNL. This gives a total of,

0.031 x 1,656,000 lb = 51,000 lb water in the heated volume.

Table 3-7. Energy Balance Calculations

Array Dimensions (ft)	45	16	23		
Volume, ft^3,	16,560				
Density, lb/ft^3	100				
Mass, lb	1,656,000				
Moisture, %	3.1				
Moisture, lb	51,336				
Target Temp °C	200				
Initial Temp	15				
PLF HEATING:			**RF HEATING:**		
Final Moisture, %	2		Final Moisture, %	0	
Final Temperature	90		Average Temp, °C	200	
HEAT LOSS:			**HEAT LOSS:**		
Width, Heated ft	3.0		Width, Heated ft	1.5	
Perimeter, ft^2	3582		Perimeter, ft^2	3526	
Mass, lb	1,057,800		Mass, lb	528,900	
HT Capacity	0.22		HT Capacity	0.22	
SENS Heat Btu	35,843,000		SENS Heat Btu	23,038,000	
EVAP HT Btu	0		EVAP HT Btu	16,396,000	
kWH	10,511		kWH	11,564	
PLF HEAT WITHOUT LOSS:			**RF HEAT WITHOUT LOSS:**		
SENS HEAT Btu	58,274,000		SENS HFAT Btu	72,135,000	
EVAP HT Btu	34,216,000		EVAP HT Btu	33,120,000	
kWH	27,123		kWH	30,867	
TOTAL PLF kWH	**37,634**		**TOTAL RF kWH**	**42,431**	
DAYS @ 100kW	**16**		**DAYS @ 100 kW**	**18**	
DAYS @ 75 kW	**21**		**DAYS @ 75 kW**	**24**	
DAYS @ 40 kW	**39**		**DAYS @ 40 kW**	**44**	

The heating will be done in two phases: a PLF phase and an RF phase. Each phase is designated by the two columns in Table 3-7. The PLF phase heated to an average temperature of 90°C and a final moisture of 2%. The RF phase heated to an average temperature of 200°C with no moisture left.

During each phase of heating there will be heat loss to the surrounding soil. This is estimated in Table 3-7. Based on previous experience in field experiments using PLF heating, there was a temperature gradient in the soil surrounding the perimeter of the heated volume with a width of about 6 ft. If the 6-ft-width is heated on the average to half the soil temperature within

the array, it is equivalent to a width of 3 ft heated to 90°C. The perimeter for heat loss is the cross-sectional area of the four outside edges of the array plus the bottom is,

(45 ft x 23 ft x 2) + (16 ft x 23 ft x 2) + (45 x 16) = 3526 ft^2

3526 ft^2 x 3 ft x 100 lb/ft^3 = 1,057,000 lb, the mass of soil outside the target volume whose heating represents heat loss.

With a typical heat capacity of 0.22 Btu/lb–°F, and a heat capacity of 1.0 Btu/lb–°F for the contained moisture, the sensible heat lost to this outside volume is,

1,057,000 lbs x (90 – 15°C) x (9/5)°F x (0.22 + 1.0 x 0.031) = 35,843,000 Btu heat loss,

34,843,000 Btu / 3410 Btu/kWH = 10,511 kWH heat loss.

No account was taken for evaporation of any water in this outside zone since the heat for evaporation would still have to flow through the soil by conduction. This would only amount to a moderate correction.

The target soil volume within the array is heated and dried to 2% moisture by the PLF heating. This is given at the bottom of the first column in Table 3-7. The sensible heat load is,

(1,656,000 lb soil x (0.22 + 1.0 x 0.031) Btu/lb + 2000 gal x 8 lb/gal x 1 Btu/lb) x (90 – 15°C) x (9/5)°F = 58,270,000 Btu.

The energy to evaporate the water from 3.1% to 2% moisture is,

(1,656,000 lb x (0.031 – 0.02) + 2000 gal x 8 lb/gal) x 1000 Btu/lb = 34,216,000 Btu.

The sum of these is the energy required for the target volume,

(58,270,000 + 34,216,000)/3410 = 27,122 kWH.

The total energy is the sum of the required energy plus the loss,

10,511 + 27,122 = 37,634 kWH.

This estimates a value of 0.68 kWH/yd^3 –°C as a figure of merit for PLF heating the target zone to 90°C.

At 100 kW heating rate, the time required is,

34,972 kWH / (100 kW x 24 hr/day) = 16 days.

At a heating rate of 75 kW, it will take 21 days.

The RF heating energy balance is given in the right column of Table 3-7. Again, based on previous experience, the heat loss is assumed to be equivalent to heating a 1.5-ft wide layer of

soil around the perimeter and bottom of the target volume. This is equivalent to a 3-ft layer with a temperature gradient.

The RF heat loss layer is thinner than the PLF heating step because the PLF heating already established most of the heat loss gradient and the gradient increased more slowly with longer time. The mass of this layer is,

$3526\ ft^2 \times 1.5\ ft \times 100\ lb/ft^3 = 528{,}900\ lb.$

The sensible heat to increase the temperature of this mass from 90 to 200°C is,

528,900 lb x (200 – 90°C) x (9/5) °F x 0.22 Btu/lb = 23,038,000 Btu.

The heat loss to evaporate the water in this layer from 3.1 to 0% is,

528,000 lb x (0.031) x 1000 Btu/lb = 16,395,000 Btu.

The sum of the two heat losses is equivalent to,

(23,038,000 + 16,395,000) / 3410 Btu/kWH = 11,564 kWH.

The energy for heating of the target volume is,

1,656,000 lb soil x (200 – 90°C) x (9/5)°F x 0.22 = 72,135,000 Btu sensible heat plus

1,656,000 x (0.02) x 1000 Btu/lb = 33,120,000 Btu evaporative heat.

The sum of these converted to kWH is,

(72,135,000 + 33,120,000) / 3410 Btu/kWH = 30,867 kWH.

The total energy required is the sum,

11,564 + 30,867 = 42,431 kWH.

This estimates a value of 0.63 kWH/yd^3 –°C as a figure of merit for RF heating the target zone from 90 to 200°C.

The time required for heating at 100 kW is,

42,431 kWH / (100 kW x 24 hr/day) = 18 days.

At 75 kW, the time will be longer. That is shown at the bottom of Table 3-7.

The actual heating time required is longer since there will be some downtime to maintain components of the electrical equipment and the vapor treatment system. It is not possible to maintain this rate of energy input at all times. Since this demonstration was experimental, an average power of 75 kWH for both the PLF and RF heating phases was assumed. With this

change from 100 kw to 75 kw, the actual heating times became 21 and 24 days, respectively, for the two phases.

3.4.3 Site Layout

The TEVES system was implemented in Pit 3-1 of the CWL located in the south east corner of TA-III. The location of the CWL was shown on Figure 2-1. Figure 3-4 illustrates the demonstration site layout indicating the relative position of all the major equipment items. The dimensions of the heated pit were 15 ft wide by 45 ft long by 15 ft deep. The actual area within the bounds of the electrodes was 50 ft long by 20 ft wide.

In the TEVES demonstration, soil heating was planned to include the sequential application of PLF and RF heating. The energy was applied to an array of electrodes placed in drilled boreholes arranged around and in the pit. Figure 3-4 shows the location of the trailer-mounted, 200 kW RF power source designated as FRT-86. The trailer marked IITRI 2 contained a 200 kVA multi-tap isolation transformer, which supplied power to the array during 60 Hz heating. The trailer marked IITRI 1 served as an equipment storage area and a control room for the data acquisition system. Vaporized contaminants and water vapor were conveyed to an on-site catalytic oxidation system indicated as CATOX on Figure 3-4. An on-site mobile laboratory is indicated by ML in Figure 3-4.

3.4.4 Heating System Design

3.4.4.1 ELECTRODE ARRAY AND RF SHIELD

Figure 3-5 illustrates the design of the heating system. It consists of three rows of electrodes placed in drilled boreholes. The two outer rows were located approximately 2.5 ft outside the two long sides of the pit. The center row was located in the middle of the pit. Figure 3-6 is a plan view of the electrode array which also shows the scheme for vapor collection. The primary vapor collection points were in the center row of electrodes where the hottest temperatures were anticipated. There were two back-up vapor collection points in each of the two outer rows of electrodes. These were provided in case the primary vapor collection wells or the piping leading up to them failed to perform during the heating cycle. A silicon rubber impregnated glass cloth was used as a vapor barrier. This material was placed on top of the heated zone and it extended approximately 10 ft outside the dimensions of the heated area. Figure 3-7 is a plan view of the electrode borehole locations indicating the electrode numbering system, dimensions, and the length of the electrodes. The electrodes in the two outer rows were made from 3-in schedule 40 aluminum pipe which was capped at both ends. The electrodes in the center row were made from 4-in and 5-in Type K copper tubing.

Figure 3-8 illustrates a vertical longitudinal cross-section drawn through the central row of electrodes. It shows that the central electrodes were placed to a depth of 18.5 ft while the

outer electrodes were placed to a depth of 24 ft. At the bottom of the central electrodes, a brass hemispherical ball was attached. The purpose of this was to enlarge the surface area at the end of the electrodes in order to ameliorate the high current density which accumulates at the tips of the electrodes as a result of an end effect during the application of RF energy.

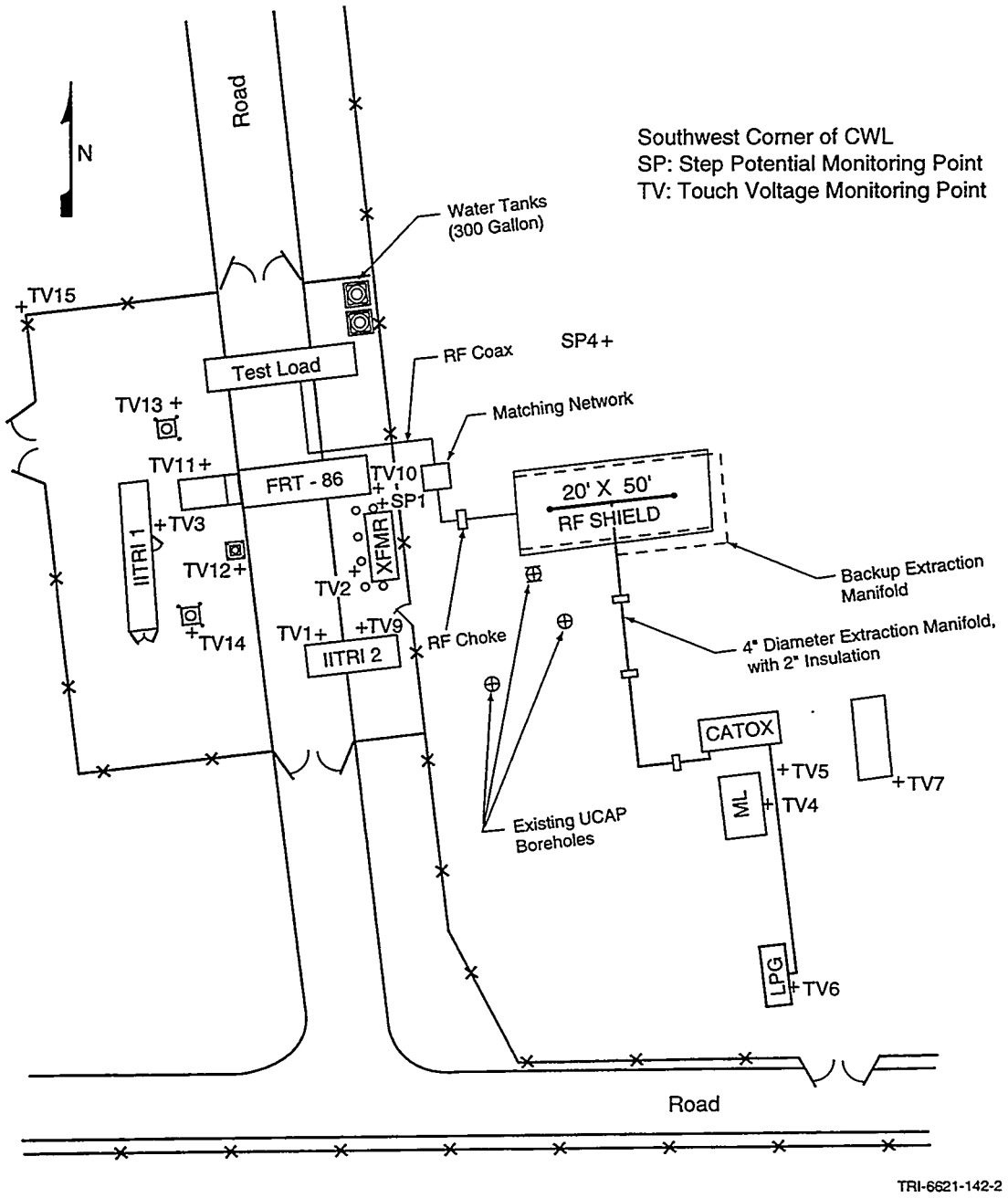

Figure 3-4. TEVES equipment layout.

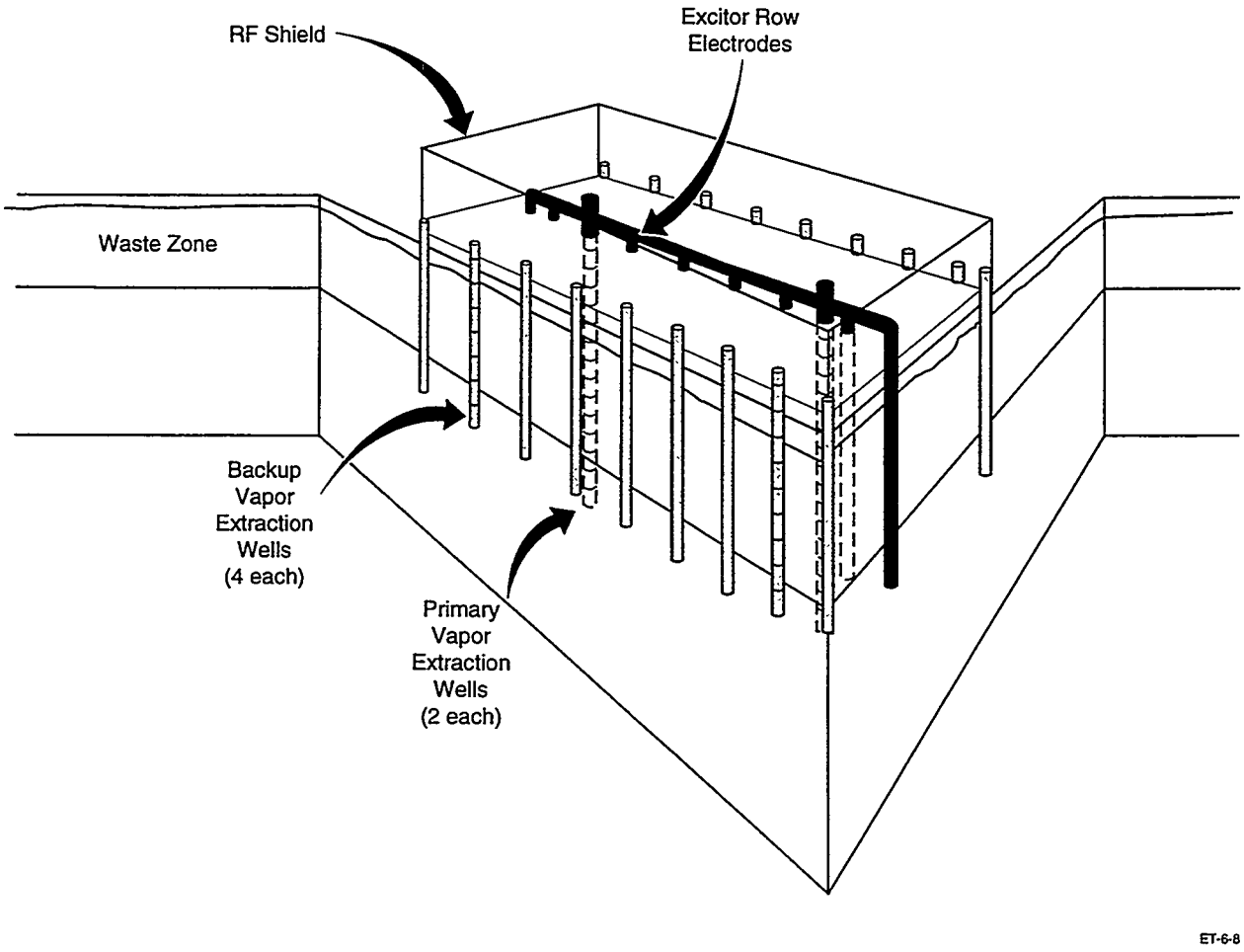

Figure 3-5. Design of heating system.

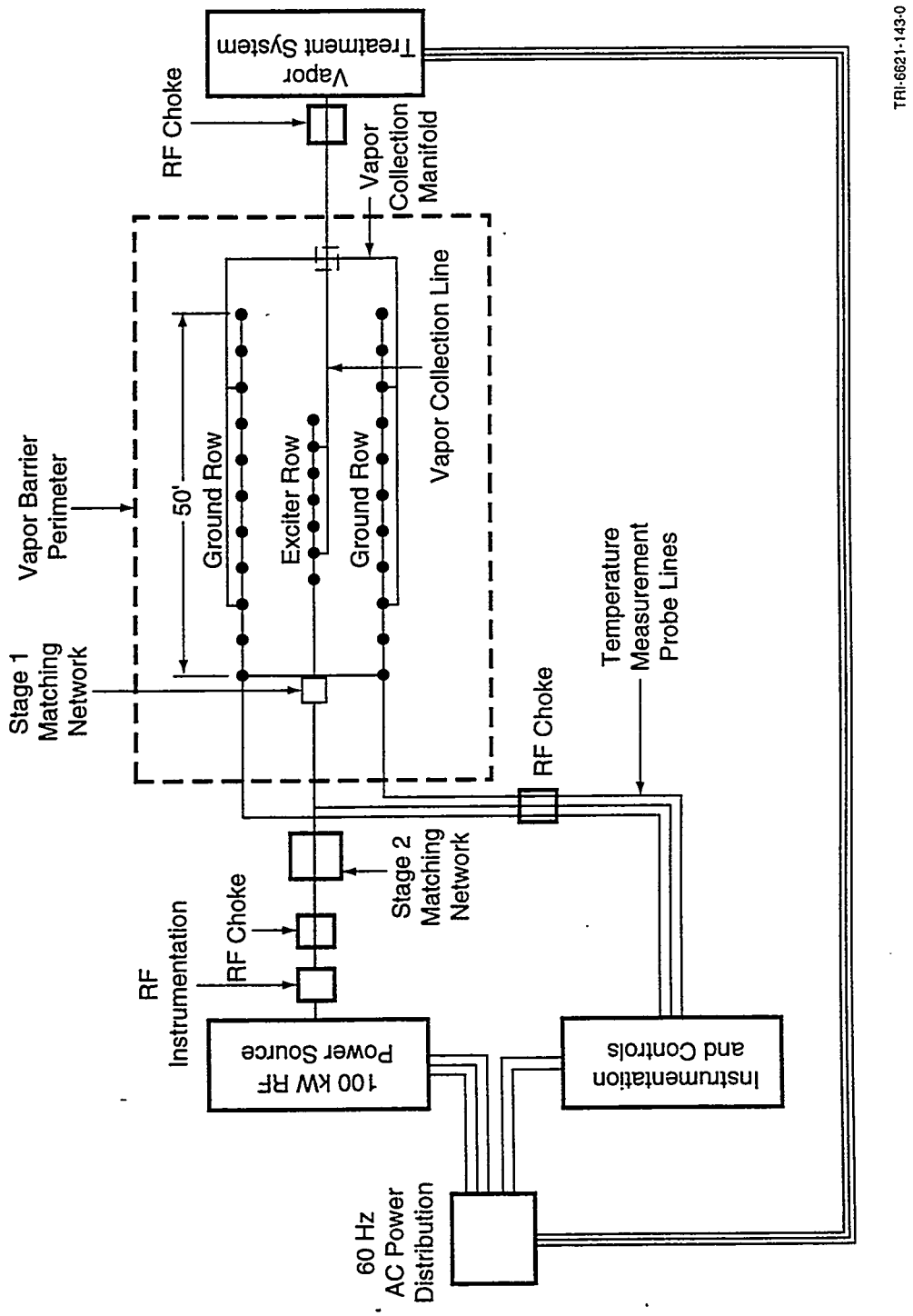

Figure 3-6. Heating system layout.

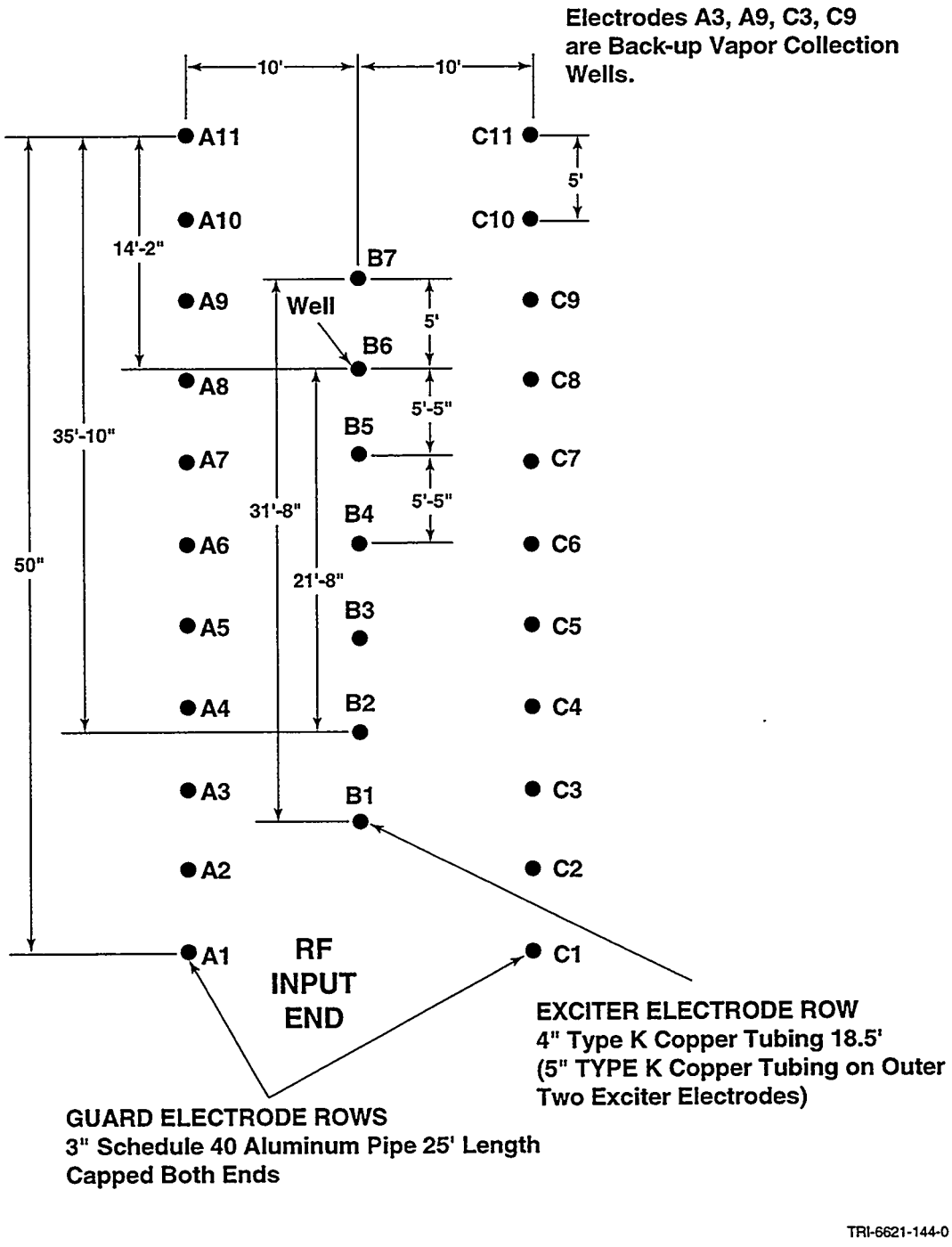

Figure 3-7. Electrode borehole layout.

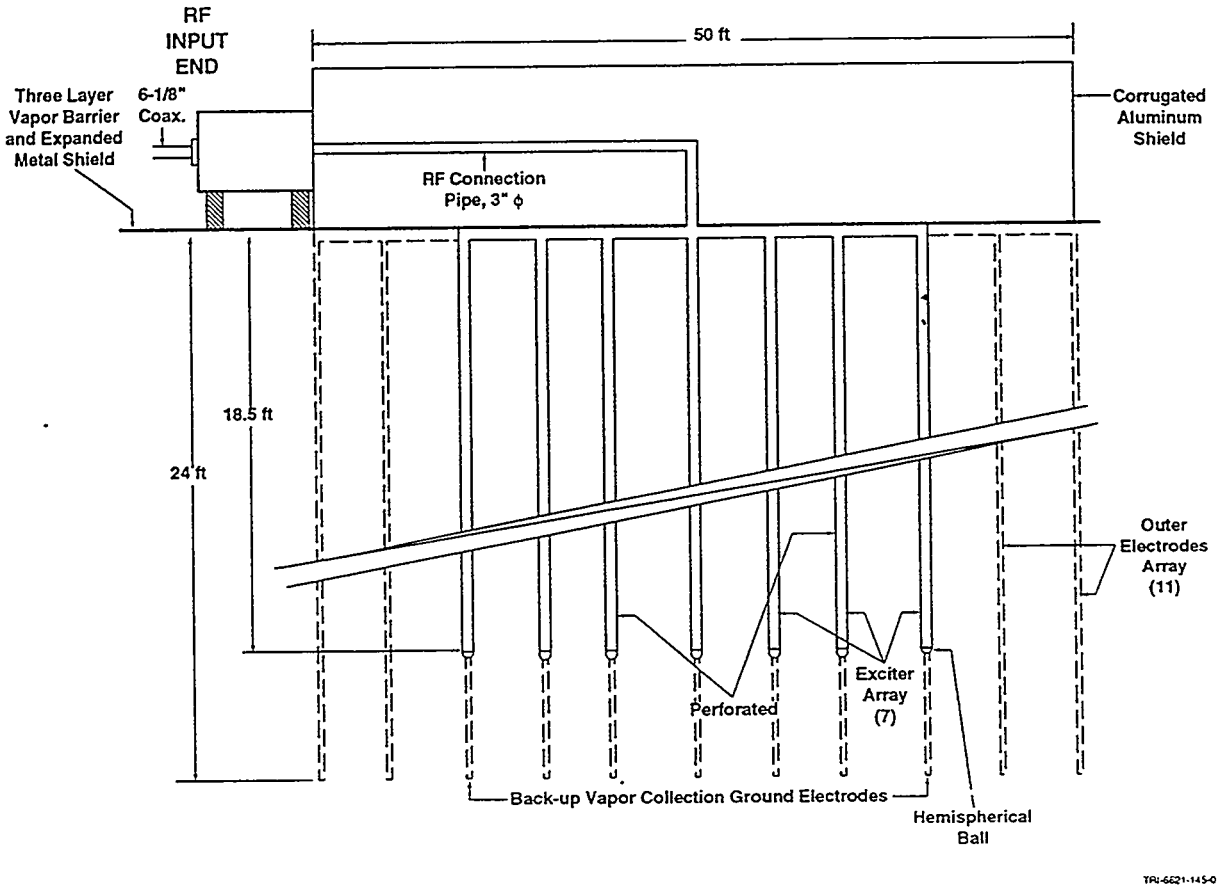

Figure 3-8. Vertical longitudinal cross-section of the electrode array.

An RF shield was placed on top of the electrode array to mitigate any stray emissions during RF heating. The shield was a building-like structure made from corrugated aluminum. The building was designed to span the width and length of the electrode array. Its height was approximately 6 ft. It was set on special footings mounted on the electrodes of the two outer rows. Figure 3-9 is a photograph of the electrode array showing the RF shield and other equipment at the site.

Figure 3-8 illustrates a coaxial RF feed to a matching network housing located at one end of the RF shield. During the RF heating portion of the demonstration, the RF power source was connected to the electrode array by means of a copper coaxial cable connecting to the Stage 1 matching network housing. During PLF heating portion of the demonstration, the coax from the RF power source was disconnected from RF shield at the matching network, and a copper cable was used to supply 60 Hz power from the 200 kW power transformer to the main center row electrode feed.

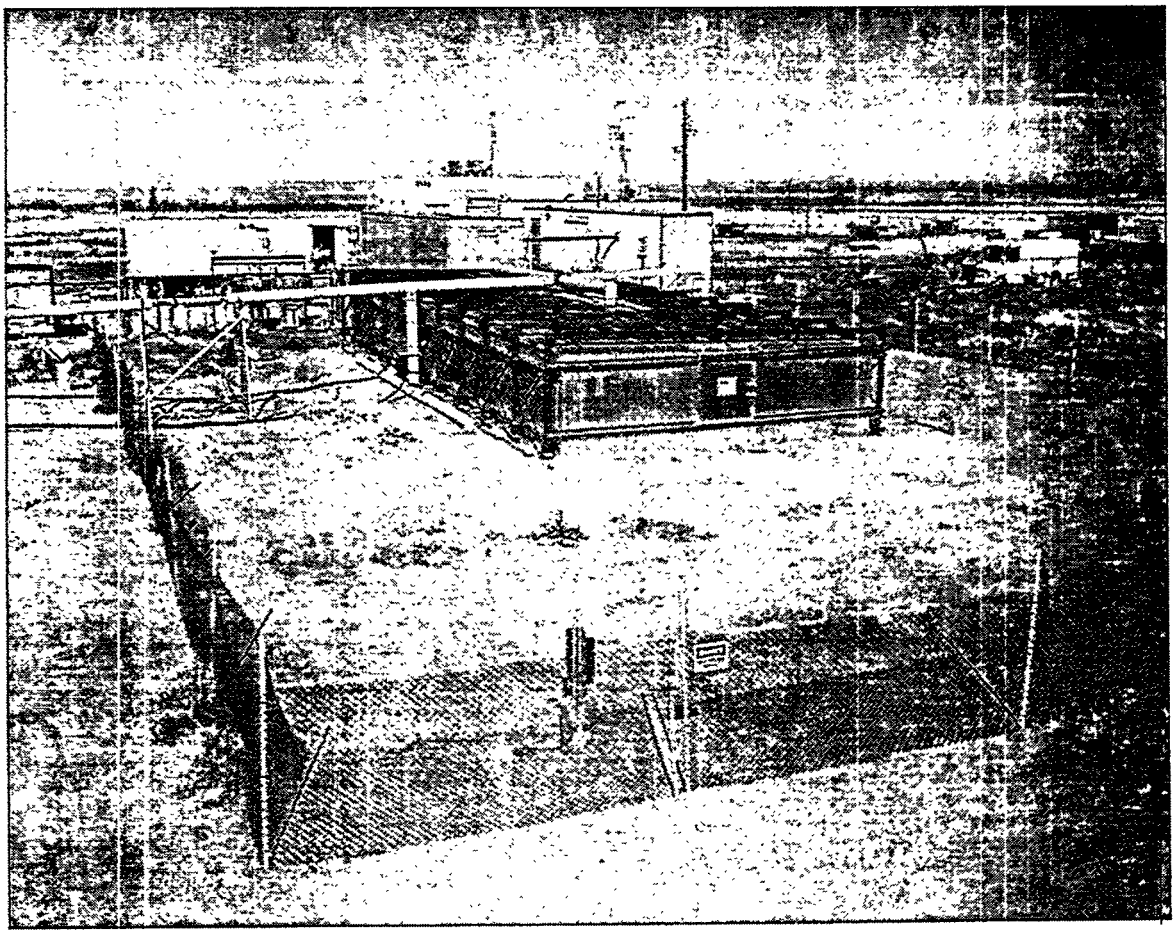

ET-714-0

Figure 3-9. Site photograph, looking westward.

3.4.4.2 VAPOR BARRIER AND THERMAL INSULATION

A vapor barrier was used to cover the heated zone. It extended approximately 10 ft outside the dimensions of the heated area. The vapor barrier was made from a silicone rubber impregnated glass fiber cloth approximately 0.010-in thick. The barrier is suitable for service up to 200°C.

A 2-in thick thermal insulation blanket was placed on top of the vapor barrier. The thermal insulation was covered with a single sheet of high-density polyethylene (HDPE).

3.4.4.3 PLF POWER SOURCE

Figure 3-10 is a block diagram of the power supply to the electrode array. AC power from the 480 V supply was provided to ITRI's multi-tap isolation transformer which in turn supplied power to the electrode array.

Table 3-8 summarizes the various tap settings, voltages, current, and the load impedance necessary to deliver the maximum 200 KVA power into the load. At a given voltage tap setting, the resistance of the load should be equal to or greater than the values listed in the last column in order to stay within the current capacity of the transformer.

The multi-tap transformer and all the associated controls were installed in a 20-ft long trailer. This trailer was parked outside the safety exclusion zone, and PLF power lines were run in PVC conduits through the safety fence into the array.

Table 3-8. Voltage Taps on the PLF Power Transformer

Tap No.	Voltage (V)	Current (A)	Load Resistance for Full 200 KVA power (Ohm)
10	200	1000	0.2
9	400	500	0.8
8	600	333	1.8
7	800	250	3.2
6	1000	200	5
5	1500	133	11.3
4	2000	100	20
3	2500	80	31.3
2	3000	67	44.6
1	4000	50	80

3.4.4.4 WATER INJECTION SYSTEM

In situ PLF heating relies on the electrical conductivity of soil to pass a current through the treatment zone. The presence of soil moisture is essential to keep the soil conductivity high enough to pass the current. As the soil first warms up near the electrodes, loss of moisture leads to the development of a zone of high resistance around the electrodes. In order to ameliorate this effect, water was added to the soil surface around each electrode. Figure 3-11 is a flow diagram of the water injection system as it was initially assembled. During the course of 60 Hz heating, it was observed that the demand for water was higher than anticipated in the center row of electrodes and there was virtually no demand at the outer rows. The system was modified to allow for increased delivery of water at the center electrodes.

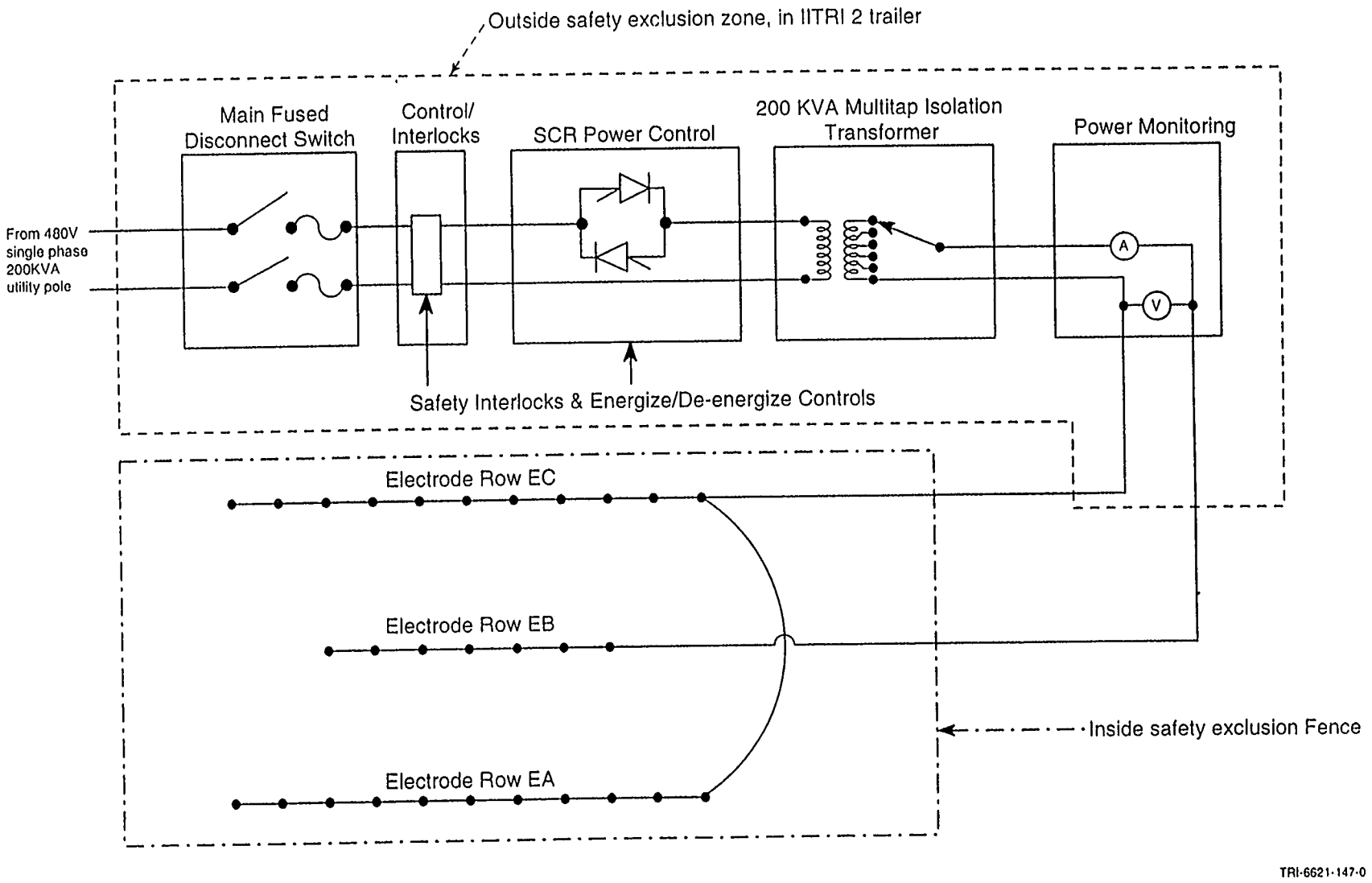

Figure 3-10. Block diagram of the AC power supply to the electrode array.

3.4.4.5 RF POWER SOURCE

The RF transmitters used for the TEVES project had been previously used on a variety of DOE and the Department of Defense (DoD) missions. The AN/FRT-86 transmitter was originally designed and operated as a 200 kW peak power, frequency synthesized, independent sideband, high frequency transmitter for fixed station communication use (NAVSHIPS 1970). Several units were subsequently modified for operation at 200 kW for a DoD project (Arecibo). IITRI obtained one unit (S/N A4) and further modified it for operation at 200 kW continuous wave (CW) at a single frequency for demonstration of the recovery of energy reserves from oil shale and tar sands. Subsequently, Lawrence Livermore National Laboratory (LLNL) acquired these units and used them in ion cyclotron resonant heating experiments. The units were modified to manual tune only and configured as a wide-band power amplifier capable of 200 kW CW or 500 kW short-cycle pulse operation. This use ceased in 1987. This project obtained two transmitters (S/N A4 and A1) and the 225 kW dummy load in 1994. The S/N A4 unit was cleaned, modified, refurbished and tested using the high-power dummy load (using S/N A1 for parts as necessary). The AN/FRT-86 S/N A4 transmitter was successfully refurbished and was capable of 150 kW continuous operation at 6.78 MHz for several hours before being put to use on the TEVES project.

3.4.5 Process Monitoring System

Automated process monitoring included data collected on vapor composition at three locations, sub-surface pressures collected at three depths of four different locations, vapor flow at the vapor manifold, and soil temperatures at the electrodes. Thermal well temperatures were manually monitored during scheduled power shutdowns (two to four times per day).

3.4.5.1 VAPOR COMPOSITION ANALYSIS

The vapor composition was measured at three locations. They were positioned at the vapor manifold upstream of the off-gas treatment system, a location after the condenser, and a location at the stack of the thermal catalytic unit. Heated vapor sampling lines were run from these locations to an on-site lab where a gas chromatograph (GC) with automated valving and method sequence was used to analyze the samples. The GC was a Varian 3400 used with the Star Workstation software. Labview software was used to control the operational sequences. Both the hardware and software are described in detail by Peter and Laguna, 1996.

The automated vapor sampling apparatus consisted of an individual diaphram vacuum pump for each sampling port pulling continuously about 1 CFM through heated, insulated teflon tubes. Vapors were passed through a carbon canister prior to atmospheric discharge. The software initiated a sample analysis based on a predetermined schedule shown in Table 3-9.

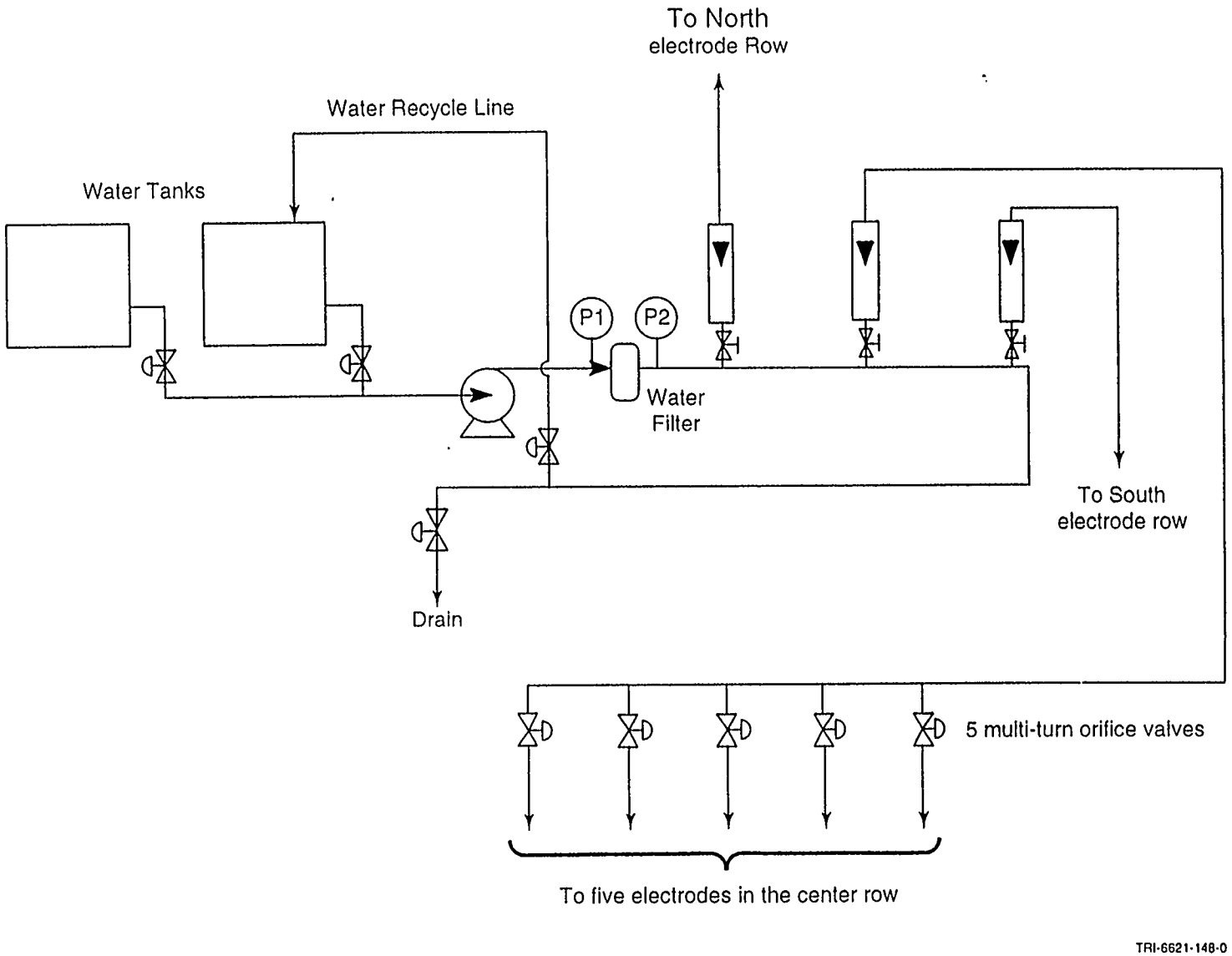

Figure 3-11. Water injection system flow diagram.

Table 3-9. Vapor Sampling Schedule

Time	Run Type
0000	Calibration
0200	Zero Air
0400	Manifold
0600	Post Condenser
0800	Zero Air
1000	Exhaust Stack
1200	Calibration
1400	Zero Air
1600	Manifold
1800	Post Condenser
2000	Zero Air
2200	Exhaust Stack

Table 3-10. Target Compounds Analyzed

pentane	PEN
freon 113	FRE
1,1,1-trichloroethane	TCA
trichloroethylene	TCE
ethyl benzene	EBZ
tetrachloroethylene	PCE
o-xylene	X-O
m/p-xylene	XMP
dichlorobenzene	DCB

A small rotary vane vacuum pump attached to a multi-port valve obtained a side stream sample from one of the three main sample collection lines, a bottle of calibration gas or an ultra-high purity zero air nitrogen gas bottle. The vapor sample was purged through a 1-mL loop in the gas chromatograph oven for three minutes at 100 mL/min, then injected into the column. The gas chromatograph was programmed for a non-isothermal temperature program lasting 90 minutes. The chosen column and temperature program were optimized to separate nine target compounds selected to represent a range of low to high boiling temperature materials identified in the site characterization studies. A flame ionization detector was used to quantify the contaminants of interest. These nine compounds are shown in Table 3–10 with the abbreviations used in the figures showing the analytical results (Section 7.0).

In addition to the nine calibrated analytes, the integrated sum of all peaks detected in ten-minute retention time windows was collected for each chromatographic run. This allowed an evaluation of all material extracted from the treatment zone even if the specific compounds had not been identified and calibrated. However, these results can only be presented in relative form as the units are in peak area sum.

3.4.5.2 SUB-SURFACE PRESSURE

Sub-surface pressures were monitored at four locations to assess the vapor capture in the treatment zone. Figure 3-12 shows the pressure monitoring locations. At each location, a bundle of teflon tubes was placed at depths of 8, 15, and 20 feet. At the bottom end of each tube was a steel screened port. The tubes came out under the vapor blanket to a pressure scanning system. The pressure scanning system consisted of individual solenoid valves connected to each line and to a common manifold. The manifold was connected to a single high-accuracy absolute pressure transducer. A Campbell Scientific 21X data logger was used to activate the solenoid valves and collect the pressure transducer voltage every two hours.

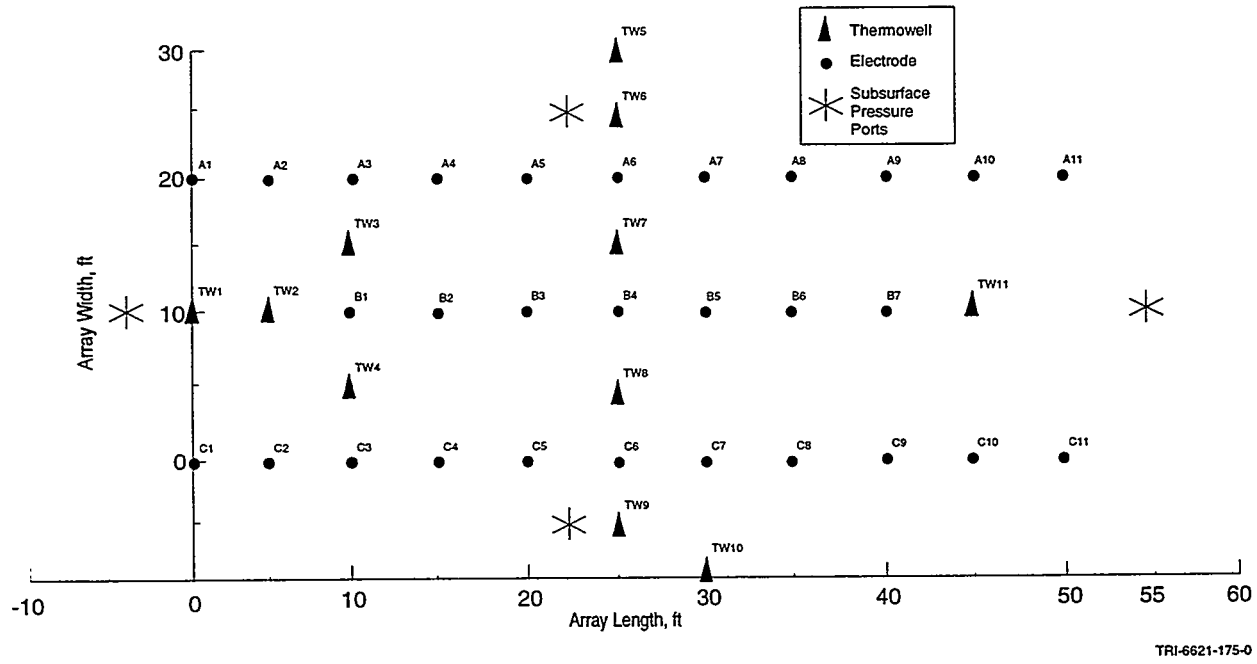

Figure 3-12. Location of thermowells and subsurface pressure ports.

3.4.5.3 VAPOR FLOW

Vapor flows were measured at two locations. One location was at the vapor manifold upstream of the off-gas treatment unit. The flow meter used at the vapor manifold was a Pitot tube. The differential pressure was recorded automatically by the computer used for the subsurface pressure data acquisition. The other site was the pre-Catox location between the blower and oxidizer unit. At the vapor manifold, the flow measured was the soil gas plus dilution air entering from the 1-in dilution valve at the end of the extraction manifold. At the pre-Catox location, the flow measured was the vapor flow at the manifold plus additional dilution air entering from the 3-in hand valve controlled manually by the operator. The flow at the pre-Catox location was an orifice plate with a differential pressure measurement. The operator recorded the flow, once or twice a day, into a log book.

3.4.5.4 SOIL TEMPERATURE

The soil temperature was measured as a function of time and location during the course of the heating cycle. Thermocouples were attached to the inner walls of selected electrodes. The temperature from the two outer rows was measured and monitored at two minute intervals. Figure 3-13 illustrates the location and distribution of the electrode thermocouples.

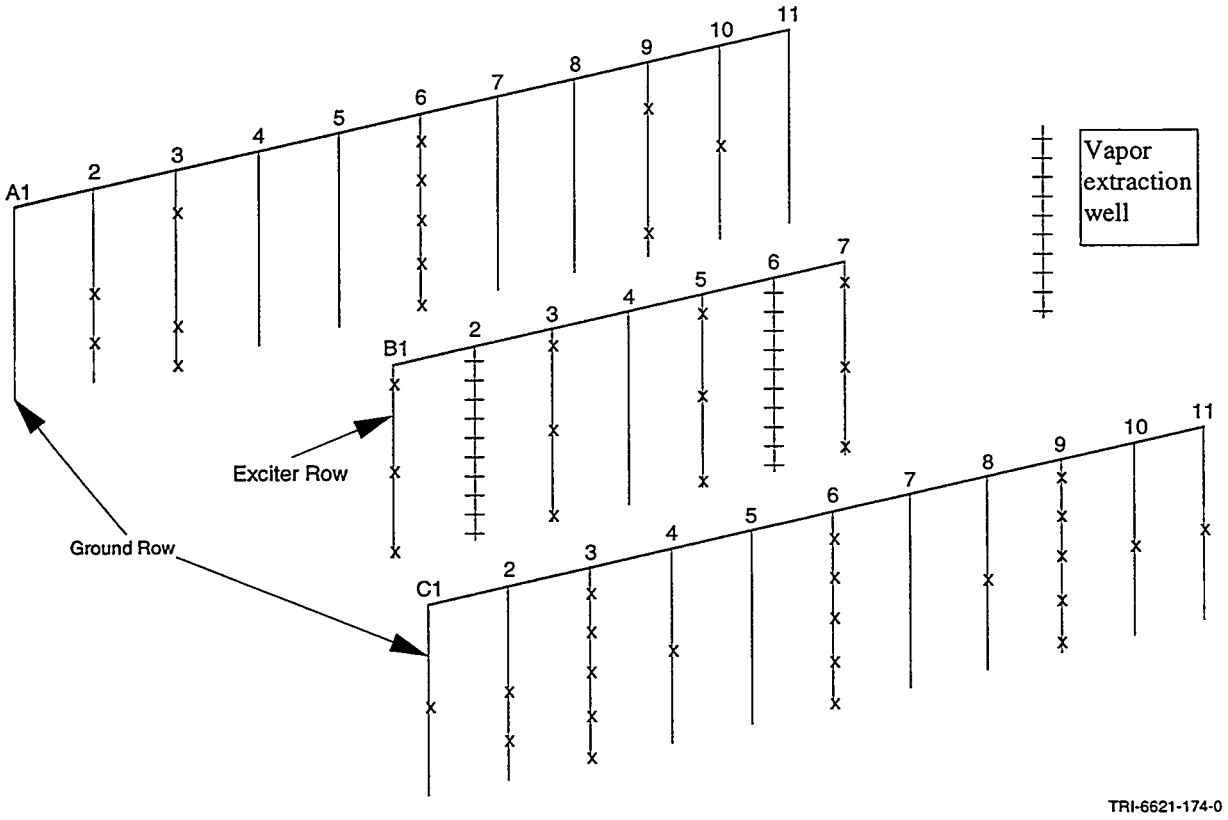

Figure 3-13. Location and distribution of the electrode thermocouples in three dimensions.

A total of 32 thermocouples were attached to the inner walls of the electrodes. A semi-automatic data acquisition system was used to acquire and store the thermocouple data from the electrodes. Figure 3-14 is a schematic flow diagram of the data acquisition system. It consists of a 32 channel multiplexer to which individual thermocouple cables were wired. The multiplexer was connected to a Campbell Scientific CR10 data logger. The data logger displayed the outer row temperatures on a personal computer every two minutes. Every four hours the data logger saved a complete set of temperature readings to its memory. Thus, during a 24 hour period, 6 measurement sets were saved to memory. The center row temperatures were measured manually by switching off the applied power and hooking up a special patch cord to a connector mounted inside the coax located in the Stage 1 matching network housing. Whenever the patch cord was connected, a sensing circuit was completed which activated the data logger for the acquisition of the center row temperature data.

In addition to the electrode thermocouples, eleven thermowells were used to measure the temperature at locations other than the electrode rows. The thermowells were made from Teflon tubes sealed at the bottom end. These tubes were inserted in boreholes drilled through the soil. After insertion, the boreholes were back-filled with soil. Temperature at five different points inside each thermowell was measured by inserting a long-sheathed thermocouple. Figure 3-12 is a plan view of the electrode array on which the location of the thermowell boreholes is indicated.

3.4.6 Electrical Safety Systems

Due to the nature of the vertically emplaced electrode array used for this demonstration and its extension through the soil surface, soil surface voltage gradients occur when the array is electrically energized. In order to restrict access to the area immediately over the subsurface electrode array and the nearby surrounding area, an electrical exclusion zone was established. This exclusion zone was designed to prohibit access to the area where the soil surface voltage gradients were predicted to be above the safe limit of 2 volts per meter. This safe limit was selected based upon American National Standards Institute/Institute of Electrical and Electronic Engineers (ANSI/IEEE) Standard 80 (ANSI/IEEE 1986). It was selected to provide a high level of confidence that no electrical current would be perceived at voltage gradients at or below this limit value.

The placement of the exclusion zone was based on a series of analytical predictions of the soil surface voltage gradients or step potential (SP) contours. Figure 3-15 illustrates the SP contours around the electrode array for an applied energy level of 200 kVA, the maximum output of the PLF power supply. Also shown on this figure is the placement of the exclusion zone boundary. This placement was selected so as to completely contain the area where the soil surface voltage gradient or step potential was above the safe limit. This boundary was established by erecting a 4-foot high bright orange plastic construction fence.

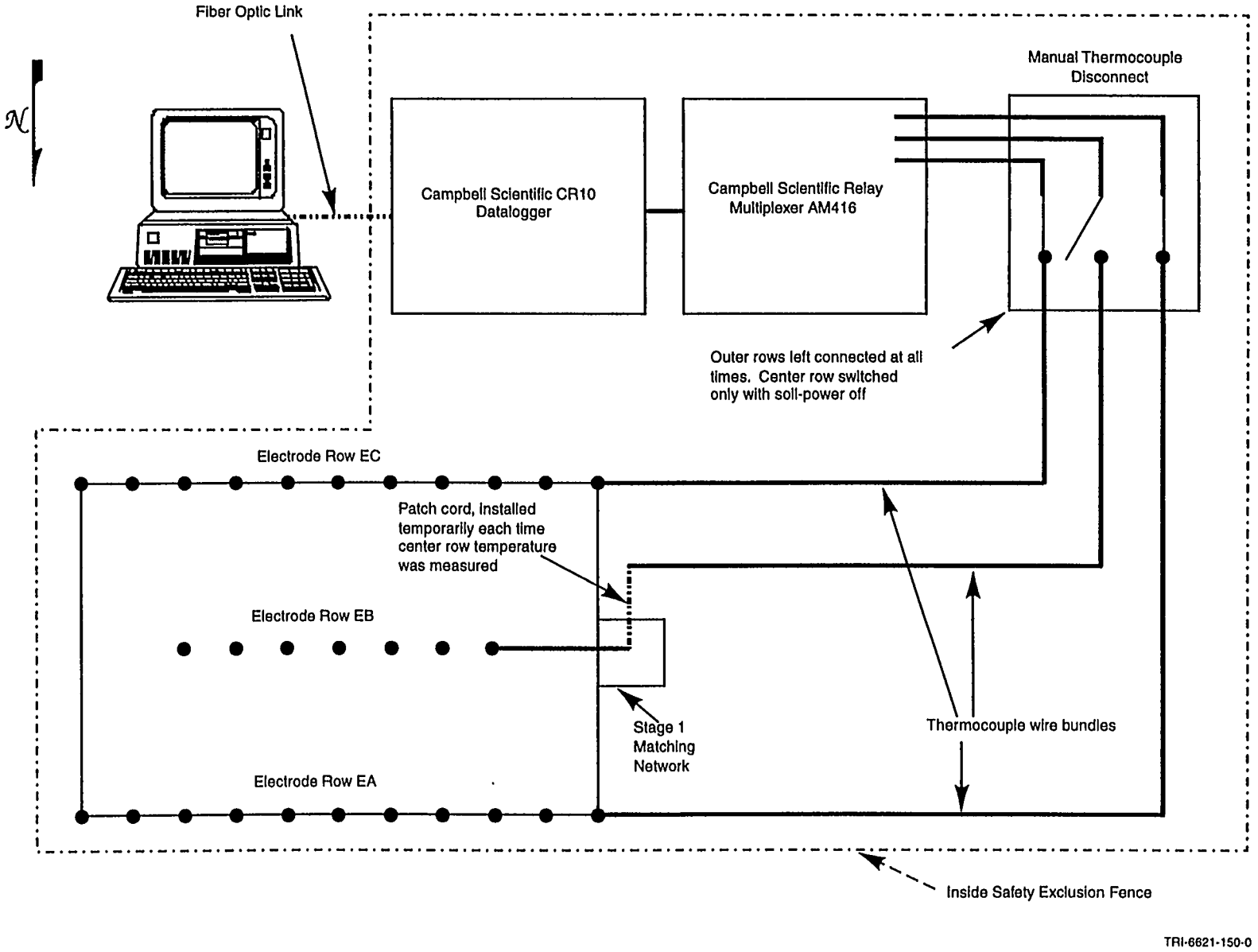

Figure 3-14. Schematic flow diagram of the data acquisition system.

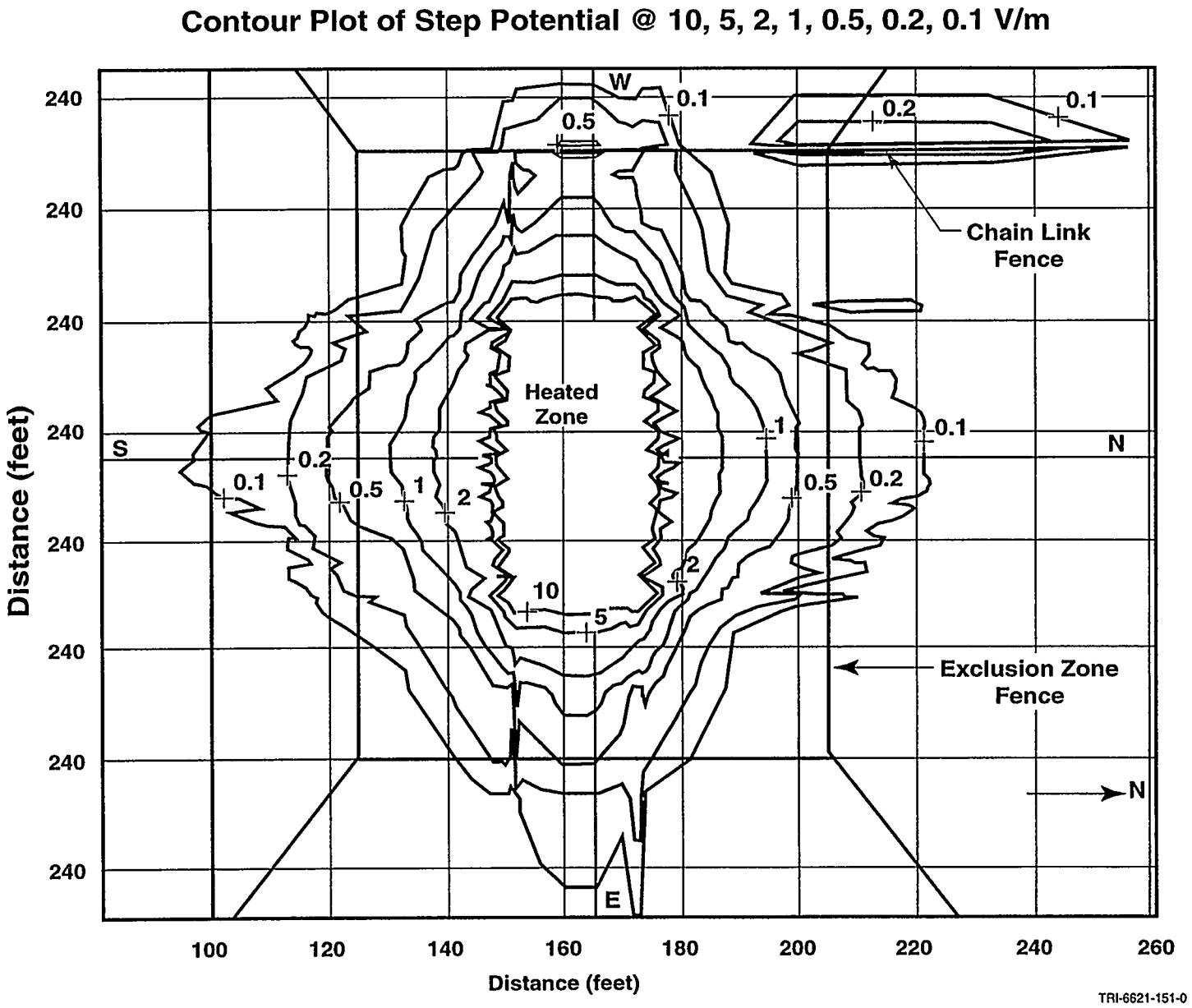

Figure 3-15. Surface step potential contours at soil surface (analytical calculation).

In addition to the site administrative controls, such as the Lockout/Tagout procedure for the PLF power supply used to assure electrical safety, an external interlock string was established to de-energize the PLF power supply's output and remove PLF energy from the subsurface electrode array should any portion of the interlock string be opened. Figure 3-16 illustrates a schematic representation of the external interlock string. The external interlock string consisted of the following:

- A dual beam infrared photo-electric fence located just within the perimeter of the exclusion zone fence.

- Three manually interruptable emergency stop buttons. The first was located in the office trailer, the second was located outside of the exclusion zone fence personnel gate, and the third was located on the vapor collection system's blower platform.

- Contact closures, required in order to energize the electrode array, were located within the thermocouple disconnect box and at the exclusion zone fence personnel gate.

A slightly modified interlock string was used during RF operations. Two outdoor warning strobe lights were mounted atop the PLF power supply. An amber light indicated that the power supply was energized. A red light indicated that PLF power was being applied to the electrode array.

During the course of the demonstration, touch voltage (TV) and step potentials (SPs) were measured regularly at the same designated locations around the demonstration site. Figure 3-17 is a site map giving the locations of the SP and the TV measurement points. The 15 TV points are described in Table 3-11.

SP was measured to estimate the potential difference between the feet of an adult with a average step of one meter. SP was measured by driving two copper clad steel stakes into the ground and measuring the potential difference between them when the electrode array is energized. The separation between the two stakes, mounted on a rigid fiber glass frame, was one meter. At each measurement point, the stakes were driven in two vertical orthogonal planes. The step potential at the point is calculated by the paired measurements.

Touch voltage was measured by noting the potential difference between a metallic object and the ground near it. This was done by connecting one lead of a voltmeter to the metal object and the other lead to an insulated metal stake which was driven into the ground in the vicinity of the object. This method measures the worse case (i.e., highest) potential difference that a person may be subject to when physical contact is made between the body and the metal object while the feet are touching the ground. The safe limit for touch voltage is 6 volts to ground within 6 ft of the metal object.

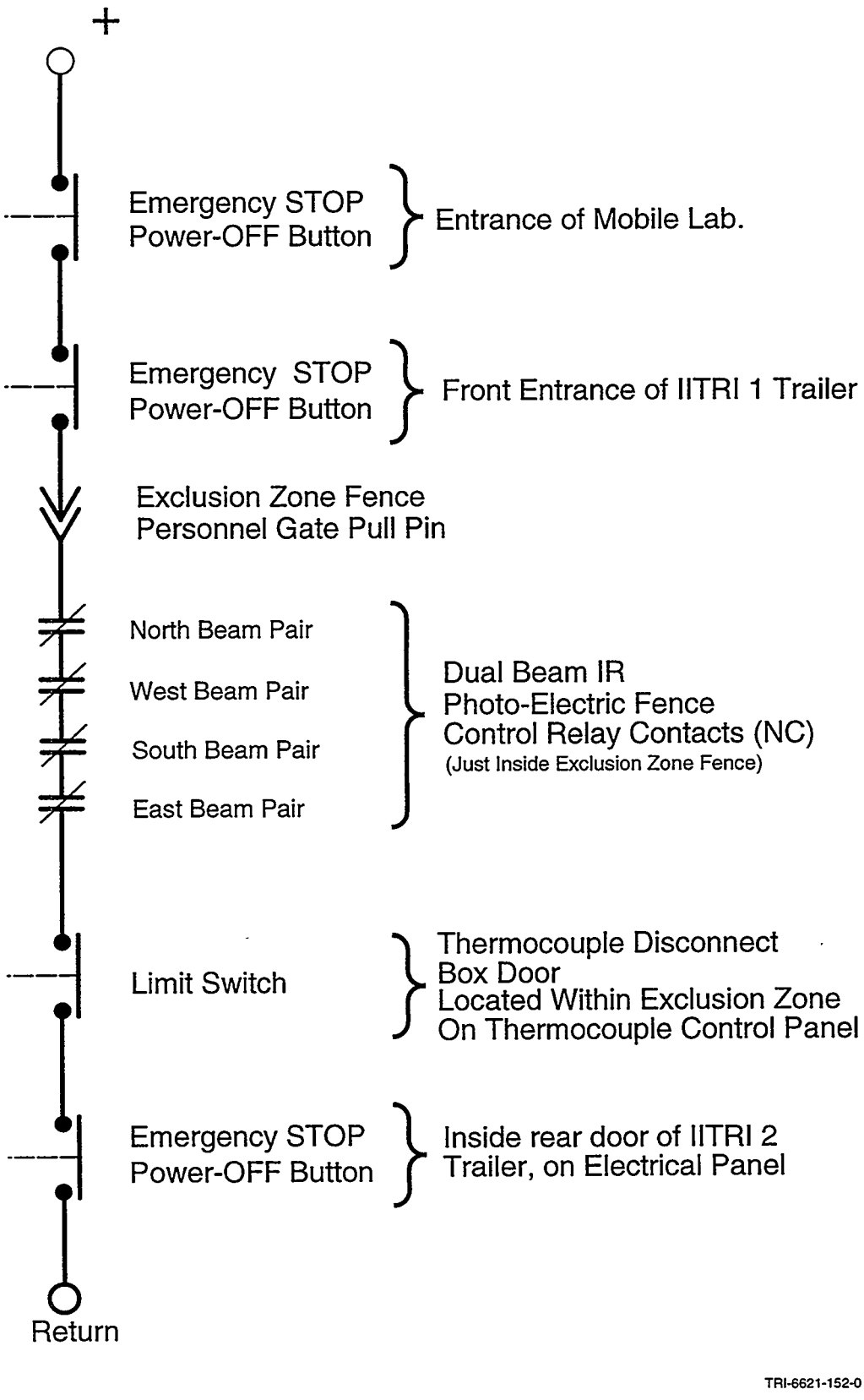

Figure 3-16. PLF power supply external interlock string.

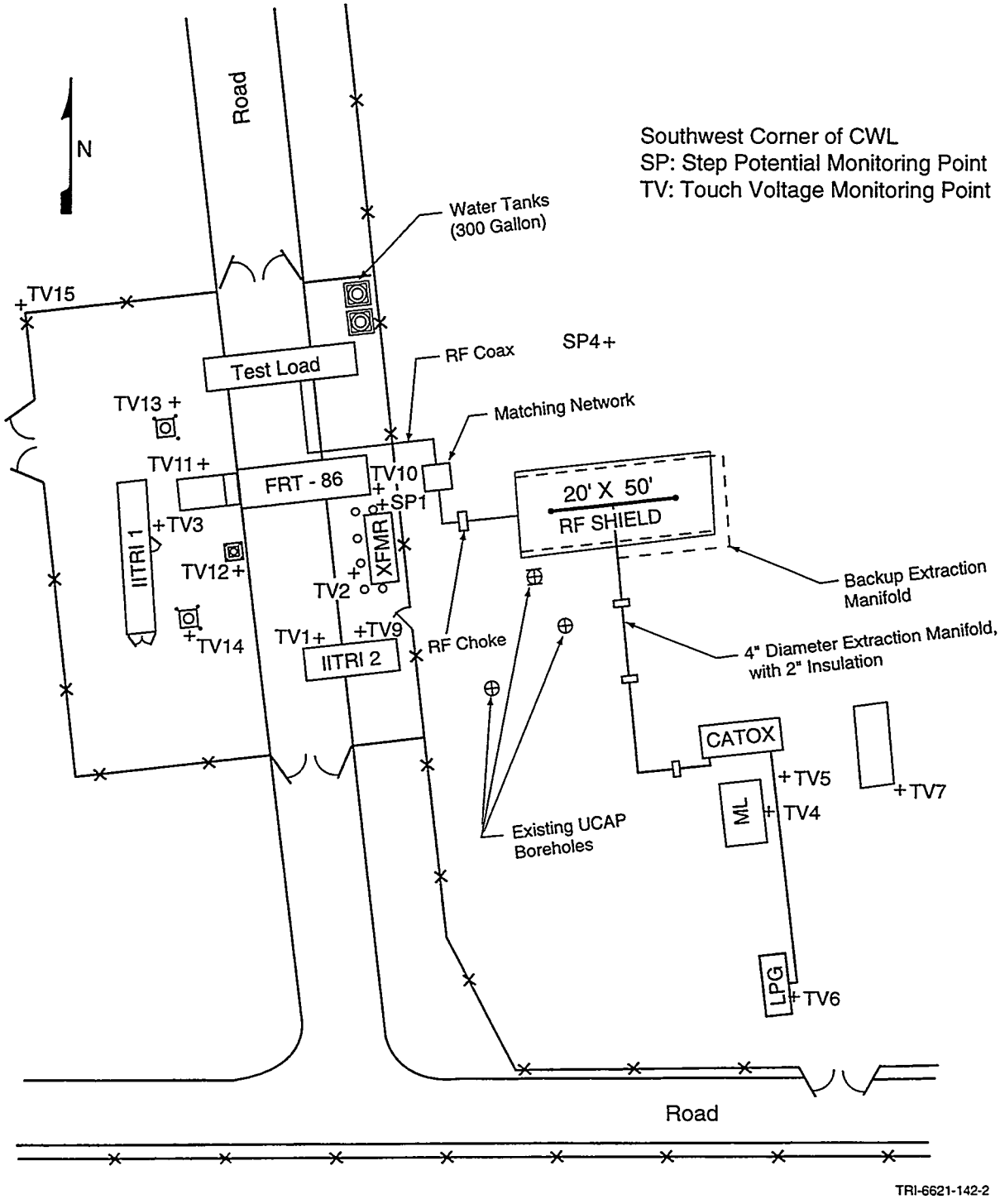

Figure 3-17. Location of step potential and touch voltage measurement points.

Table 3-11. List of Touch Voltage Measurement Points

TV Location No.	Description
1	IITRI 2 trailer door frame
2	Conduit clamp
3	IITRI 1 trailer staircase
4	Door frame of mobile laboratory
5	Corner of CATOX platform
6	Top of propane tank
7	Front of water tanker trailer
8	Test load trailer staircase
9	Fence clamp
10	FRT-86 rear staircase
11	FRT-86 front staircase
12	Frame of high-volume air sampling station
13	Well casing of monitoring well MW3
14	Bolt on casing of monitoring well MW3A
15	Ground cable on pole

Results of these measurements are presented in Section 4.5

3.4.7 Vacuum Extraction System

The vacuum extraction system consisted of a positive displacement blower capable of 200 scfm at 70 inches water vacuum. The extraction manifold was 3-in steel pipe with one watt/ft heat tracing and fiberglass insulation. Two electrodes in the excitor row also acted as vapor extraction wells (B2 and B6) (see Figure 3-6). Four ground row electrodes were also constructed as backup vapor extraction wells (A3, A9, C3 and C9) (see Figure 3-6), but were blocked with blind flanges until a need became apparent.

3.4.8 Electrical Service

Figure 3-18 shows the TEVES power distribution consisting of a pad mounted 750 kVA three-phase transformer, a pad mounted 37.5 kVA single-phase transformer and several fused safety disconnects. Power consumption was monitored by a digital meter which tapped into the secondary side of the 750 kVA transformer via current transformers.

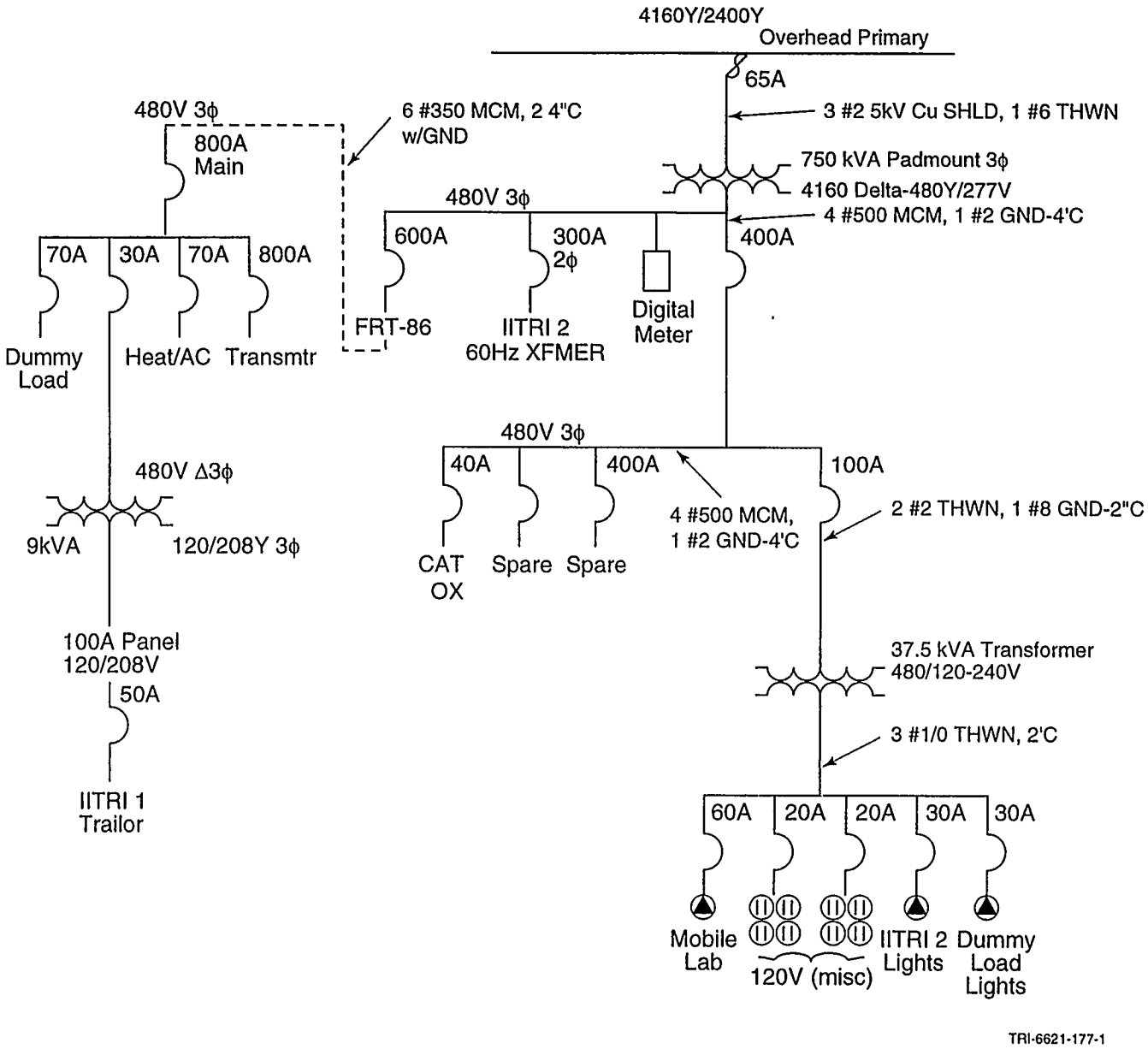

Figure 3-18. TEVES power distribution.

Power for the RF transmitter was supplied through a 600 A, 480 V, three-phase disconnect. Power for the 60 Hz heating transformer was supplied through a 600 A, 480 V, 2 phase disconnect. Only one of these disconnects was operated at any given time.

Power for the catalytic oxidizer unit was supplied by a 40 A, 480 V, three-phase disconnect fed from the 750 KVA secondary via a 400 A disconnect.

A 37.5 KVA, 480V/120-240 V transformer was fed from the 750 KVA secondary by the 400A disconnect in line with a 100 A disconnect. This transformer supplied single phase 120 - 240 V power to a bank of smaller disconnects which in turn supplied power for the onsite mobile laboratory, test trailer lighting and miscellaneous 120 V power requirements.

Power for the "dummy load" trailer and the IITRI 1 trailer was supplied from the distribution panel internal to the FRT-86 transmitter trailer.

The external transformers and disconnects were located on a cement pad directly west of the TEVES test bed, just outside of the landfill fence.

3.4.9 Alternative Heating Schedule

Due to an unexpected malfunction of the vapor treatment unit, PLF heating was stopped after 33 days. The vapor treatment unit was not capable of handling the higher concentrations of VOCs due to the higher temperatures. There was then a 87-day cooldown period while repairs and adjustments were made on the vapor treatment system before RF heating was implemented for 29 days. Thus the original demonstration design detailed on page 3-1, was significantly modified. The most significant change was that the RF heating did not immediately follow the PLF heating; during the 87-day cooldown period, the soil cooled to almost the initial temperature. Thus, the 29 days of RF heating were not sufficient to attain the original demonstration temperature of 200°C.

3.5 Modeling

Modeling of the TEVES test was conducted by Webb (1996) using the TOUGH2 code. The modeling evaluated the fluid flow and heat transfer behavior of the system including the effects on air, water, and a single component non-aqueous phase liquid (NAPL). An initial ortho-xylene inventory of 5%, as the NAPL, was assumed in the heated zone for illustrative purposes. Variations in borehole vacuum, borehole location, and soil permeability were investigated. Simulations indicate that the temperatures in the soil are relatively insensitive to the magnitude of the borehole vacuum or the borehole locations. In contrast, however, the NAPL and liquid water saturation distributions are sensitive to these borehole parameters. As the borehole vacuum and air flow rate through the soil decrease, the possibility of contaminant (NAPL) migration from the heated zone into the surrounding unheated soil increases. For example, for 60 days of heating at 100 kW, a borehole vacuum of 2.5 kPa (10 in. of water), using

extraction wells inside the heated zone, does not result in NAPL migration into the unheated zone; whereas for a borehole vacuum of 0.5 kPa (2 in. of water), there is migration of NAPL into the unheated zone. For extraction using boreholes at the perimeter of the heated zone the likelihood of contaminant movement into the unheated soil is greater than for extraction using boreholes that are in the middle of the heated zone.

This page intentionally left blank.

4.0 POWERLINE FREQUENCY HEATING RESULTS

4.1 Applied Energy

Figure 4-1 shows the applied power during the 33-day powerline frequency (PLF) heating period indicating a maximum power of about 100 kW and average applied power of about 60 kW. Figure 4-2 shows the applied voltage ranged from 400 to 1000 volts and the current from 100 to 250 amps. Integration of the applied PLF power curve, Figure 4-3, gives a cumulative energy use of 45,000 kW-hr/or 1.54×10^8 Btu.

Coincidental to the last day PLF heating, a large pulse of vapors was released from the treatment zone which caused the off-gas treatment system to overheat and automatically shut down. To evaluate the center row electrode temperatures, the manual center-row thermocouple monitor patch cable port was opened and an unexpected release of vapors and steam occurred. The reaction by local non-TEVES project personnel to odors released by this event caused an 87 day delay in the start of the RF heating phase.

4.2 Water Addition

Water was injected into the heated zone in order to improve the electrical conductance of the soil. Table 4-1 gives a summary of the schedule of water addition. The data is superimposed on the applied PLF power data to show that greater water addition rates were required to achieve higher applied PLF power (Figure 4-1). The cumulative amount of water injected into the soil is also important in the heat balance because the added mass of water also needs to be heated. The amount of energy needed to heat up and evaporate the additional water added to the treatment zone totals 21,500 kW-hr. This is about one-half the total energy input by the PLF heating system. The energy required to heat each unit gallon per hour of added water from 15°C to 90°C is about 0.33 kW.

4.3 Temperatures

Figure 4-4 shows the average thermowell temperatures in the soil during the PLF heating period. The temperatures at each depth are averaged for all measurements throughout the array. Thermowell temperatures peaked at about 85°C for the 3-ft and 9-ft depths and were about 40°C for the lower depths. The relatively low temperatures at the 18, 21 and 24 ft depths as compared with at the 3 and 9 ft. depths are probably due to the use of water injection close to the surface. The injected water may not have reached the greater depths and thus the electrical conductivity was less at the greater depths. Therefore, even though the central electrodes were placed to a depth of 18.5 ft and the outer electrodes were placed to a depth of 24 ft., the amount of heating at

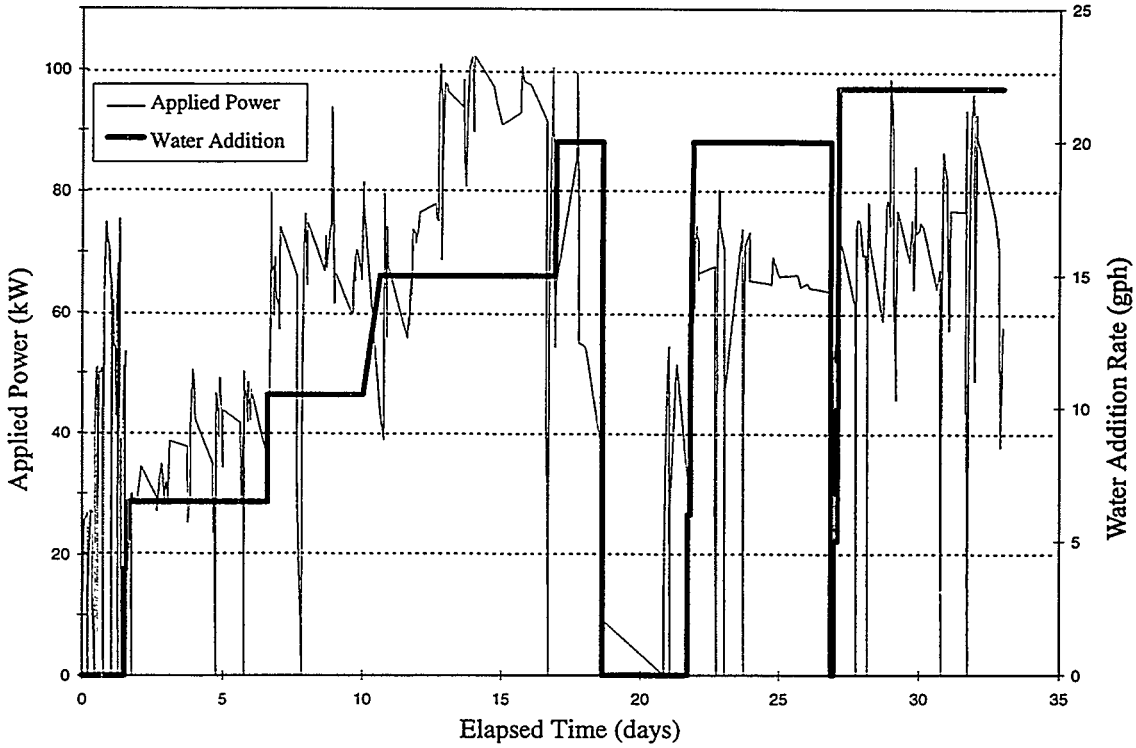

Figure 4-1. PLF heating, applied power.

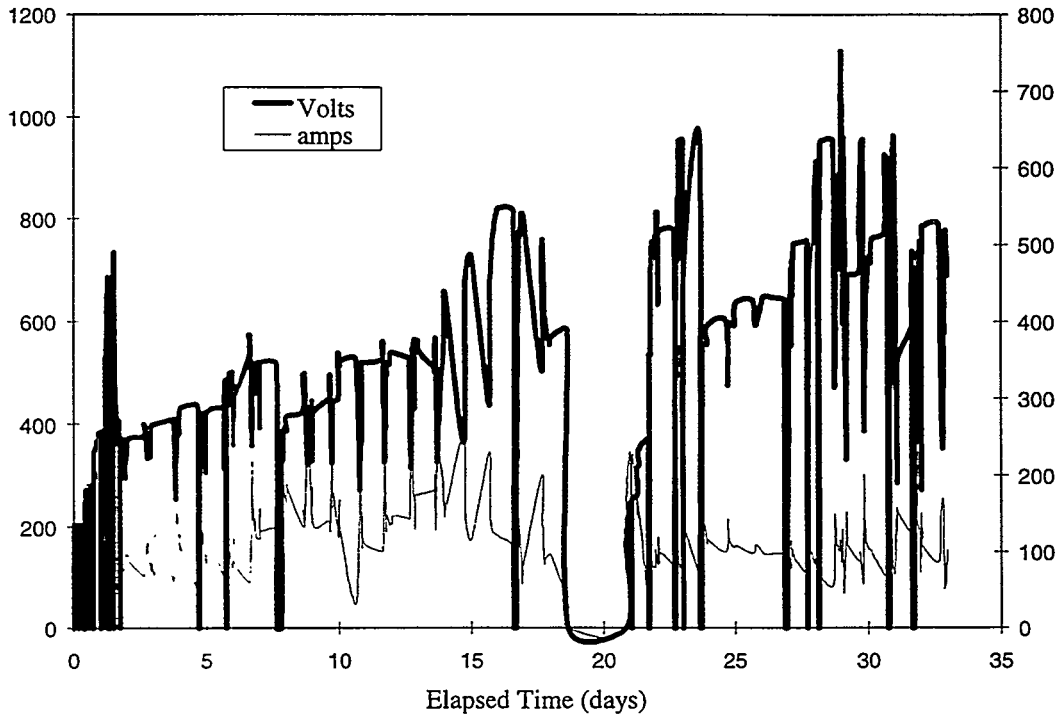

Figure 4-2. PLF heating, applied voltage and current.

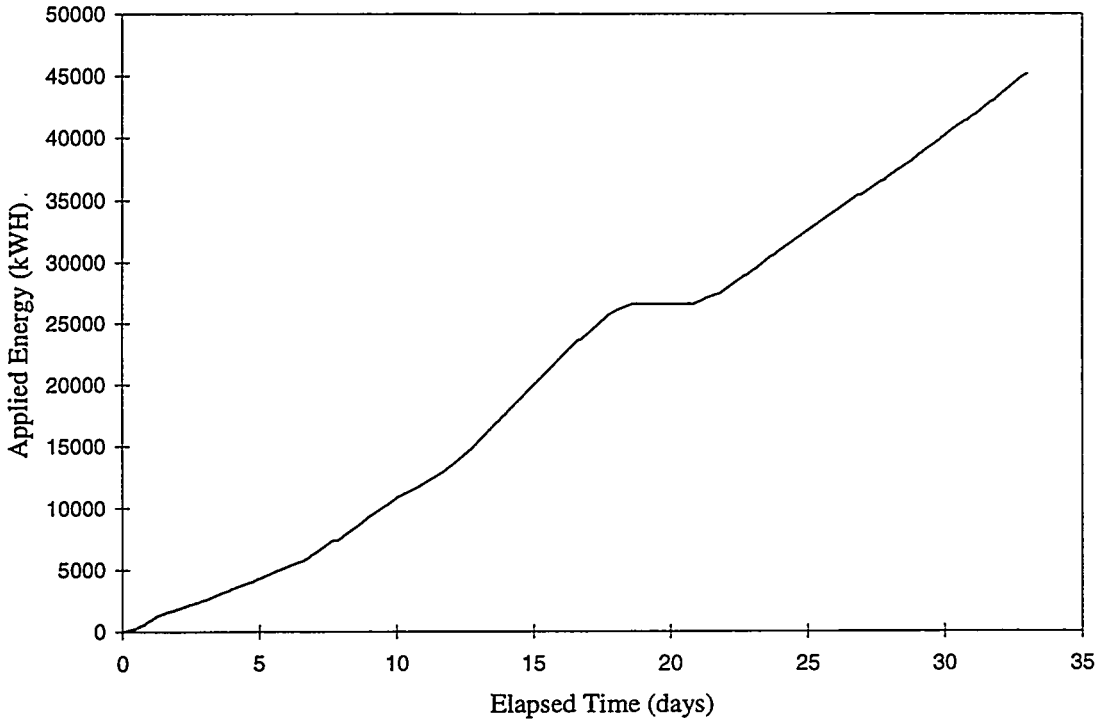

Figure 4-3. PLF heating, cumulative applied power.

Table 4-1. Water Injection During PLF Heating

Elapsed Time (days)	Water Flow (gph)	Incremental Addition (gal)	Cummulative Water (gal)
0	0	0.0	0
1.5	4	0.0	0
1.6	6.5	12.0	12
6.6	10.5	777	789
8.7	0	527	1316
8.8	10.5	0	1316
10.6	15	444	1760
17	20	2298	4058
18.7	0	810	4868
20.9	0	0	4868
21.7	6	0	4868
21.8	12	10	4878
21.8	17	12	4890
21.9	20	26	4915
26.9	0	2400	7315
27	5	0	7315
27.1	10	4	7319
27.1	22	7	7326
32.9	0	3062	10388

the greater depths were significantly less than at the shallow regions. Figures 4-5 through 4-7 show the thermowell temperature profiles at each depth interval of 3 ft, 9 ft, and 18 ft respectively. Figure 4-8 shows the center row electrode temperatures which ranged from 80°C to 140°C. These temperatures are much higher because of the ohmic heating occurring in the body of the electrode when current is being passed through. Figure 4-9 shows the combined outer row temperatures at each depth interval with peak temperatures of about 60°C for the 3-ft and 9-ft depths, and near background of 20°C to 25°C for the lower depth intervals. The prominent drop in temperatures from day 18 to day 21 were due to a failure of the water addition system during a hard freeze causing a significant drop in applied power. Figures 4-10 through 4-12 show the temperature contours from all data sources on day 33 showing the plan view, long-side view and short-side view, respectively. Using a kriging routine with all data, the average temperature for the target treatment volume of 15 ft wide by 45 ft long by 18.5 ft deep was estimated to be 83°C. Using the total applied energy of 45,000 kWH, a volumetric energy requirement for the PLF heating test amounted to 1.63 kWH/yd^3–°C.

4.4 Heat Balance

The PLF energy input was consumed by,

(1) line losses,
(2) heating the soil,
(3) vaporizing water and VOC extracted from the soil,
(4) heating soil moisture
(5) heating the ambient and soil air drawn in by vapor extraction wells,
(6) dissipation of heat from the warmed soil, and
(7) conduction losses through the vapor barrier.

The calculations for these components are shown in Appendix B. The results are summarized in Table 4-2. Several assumptions were made in order to arrive at these results and are described in Appendix B. Other contributions to the heat balance that are not accounted for are heat loss due to condensation of water vapor on the inside of the vapor barrier and radiation heat losses. It was assumed that the initial soil water saturation was 20%.

4.5 Step/Touch Potentials

A low power test (LPT) was conducted on November 8, 1994 by applying approximately 10 kW to the subsurface electrode array. The performance of the PLF power source and its associated metering was verified. Initial measurements of the soil surface step potential were made. The purpose of these measurements was to ensure safe operating conditions for all site personnel, equipment, and facilities at full power (up to 200 kW applied). All measurement data collected during the LPT was extrapolated to full power operating conditions and examined for

any problem areas external to the electrical exclusion zone fence. No problems were identified at these extrapolated values of step potential and touch voltage. Plots of measured versus predicted step potential were made for eight radial directions centered about the electrode array. Figure 4-13 illustrates the data for the measurements made along the East Radial line. The location of the exclusion fence was 55 ft from the center of the array. As the plot indicates, the step potential at the location of the fence was about 1 volt/meter. The other plots are located in Appendix D.

Surface step potential measurements were made on a regular basis during the course of the PLF heating demonstration. The step potential at monitoring point SP2 reached a value of 2 V/meter on November 18, 1994. At this time the southern segment of the exclusion fence was moved further out by 2 meters. It is postulated that the step potentials were greater on the southern side because the neutral power cable was attached on the southern frame of the RF shield.

Initial touch voltage measurements were made on November 9, 1994 at an input power level of 25 kW. All 15 monitoring points were well below the limit of 6 volts even when extrapolated to operation at 200 kW.

Touch voltage measurements were regularly made during the course of the PLF heating demonstration. All readings were below the established limit of 6 volts.

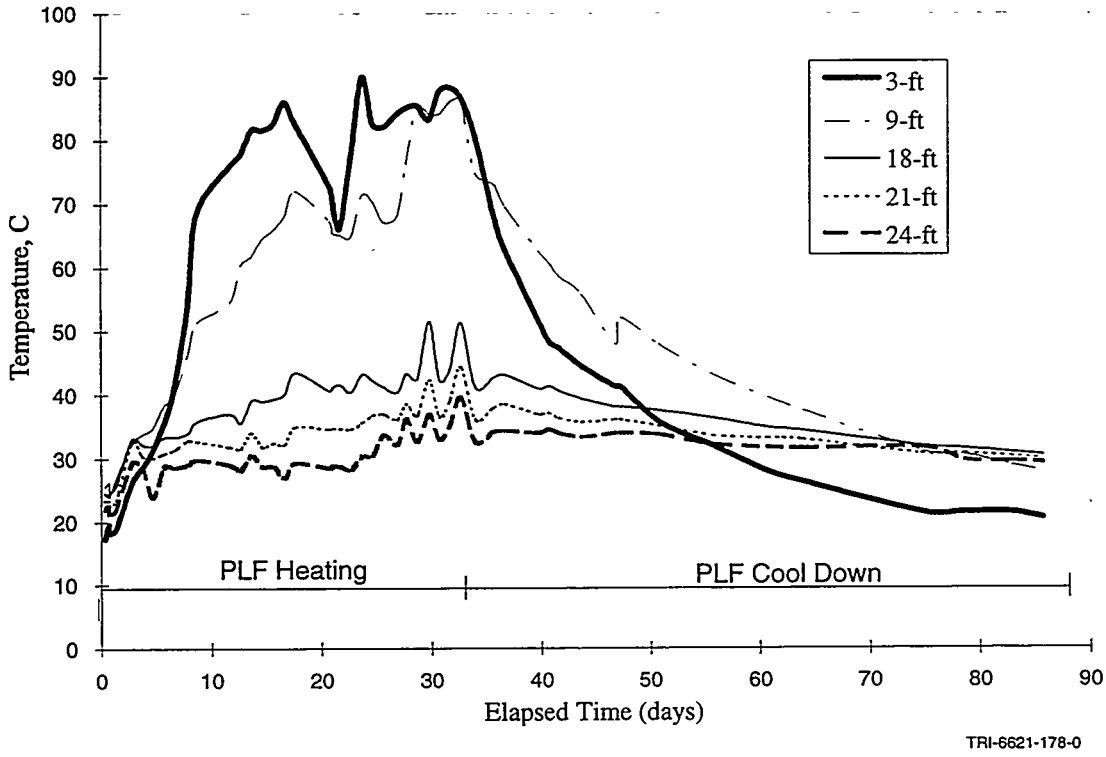

Figure 4-4. PLF heating, thermowell temperatures.

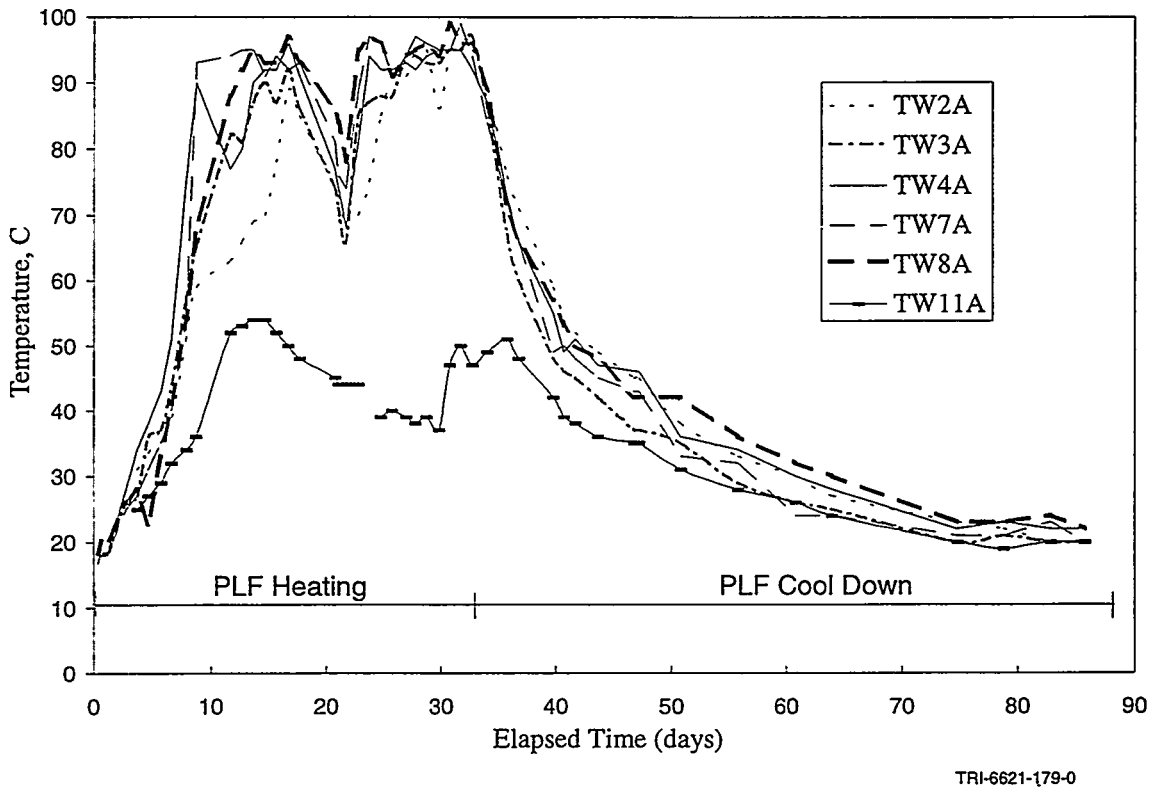

Figure 4-5. Thermowell temperatures at 3-ft depth during PLF heating.

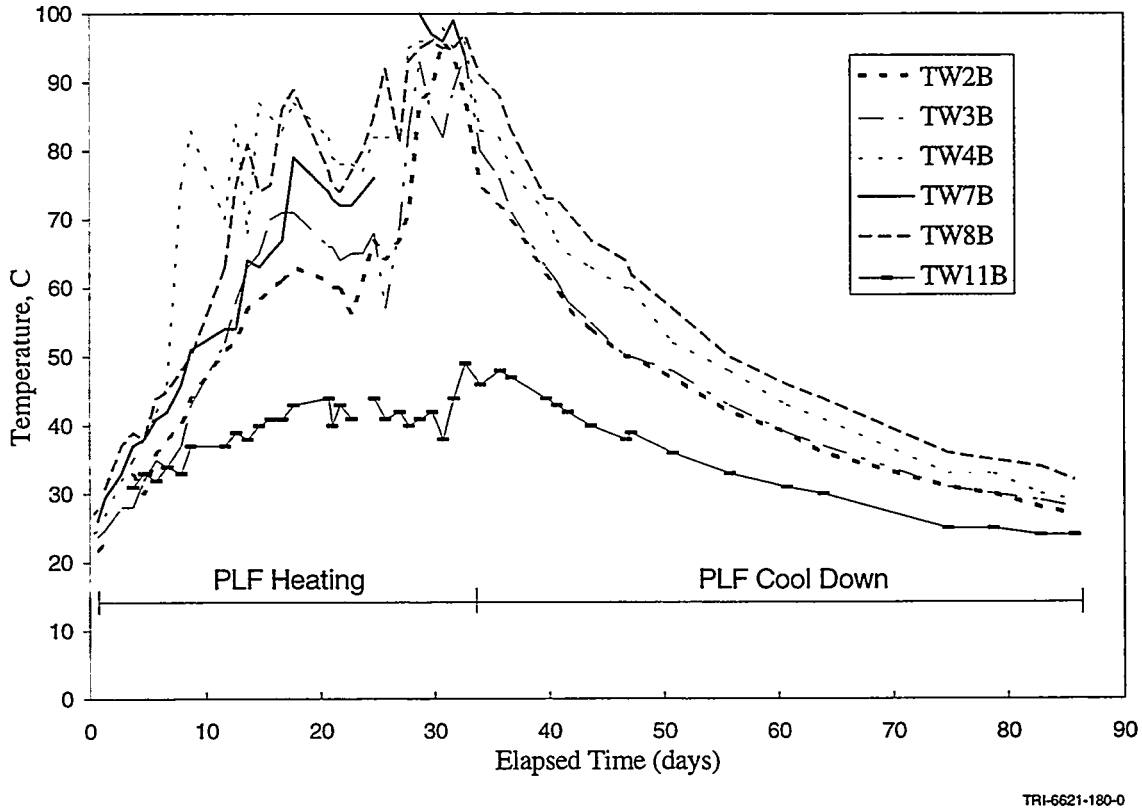

Figure 4-6. Thermowell temperatures at 9-ft depth during PLF heating.

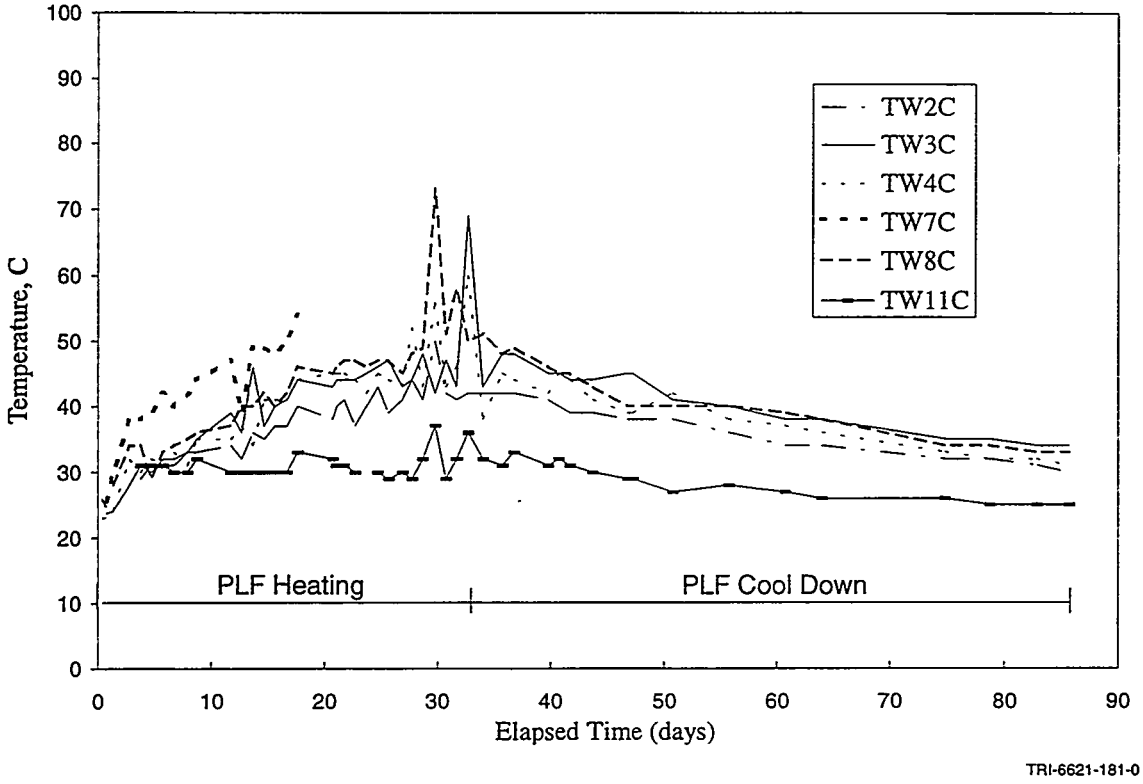

Figure 4-7. Thermowell temperatures at 18-ft depth during PLF heating.

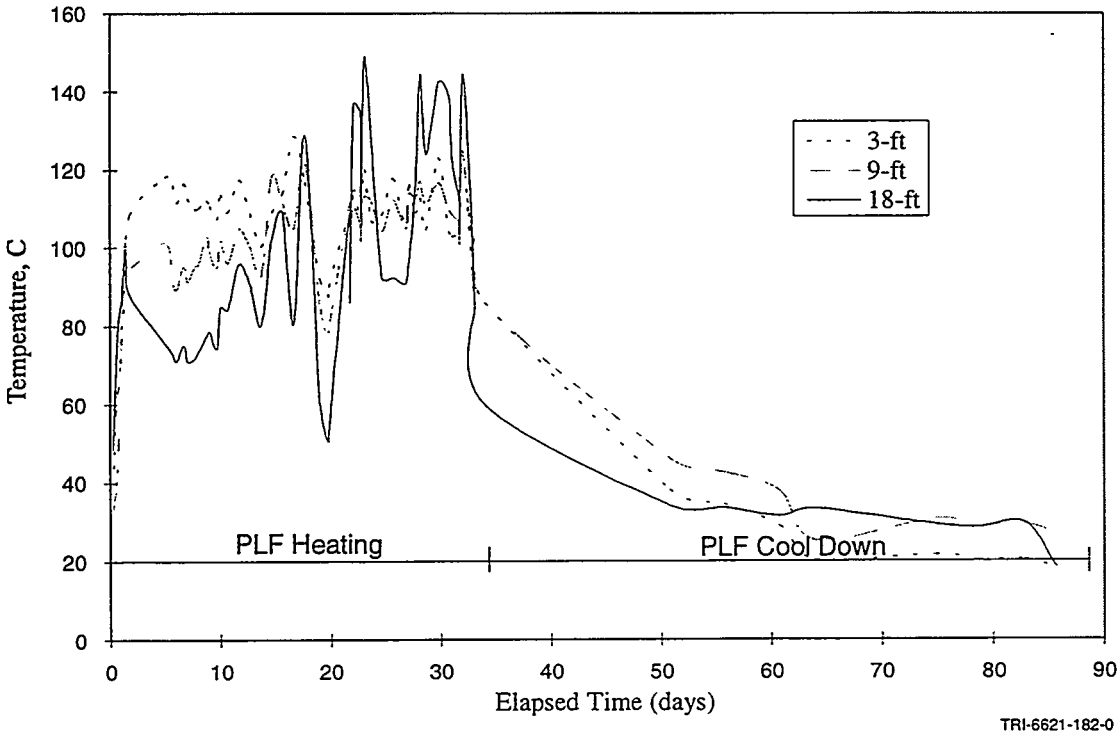

Figure 4-8. PLF heating, center row electrode temperatures.

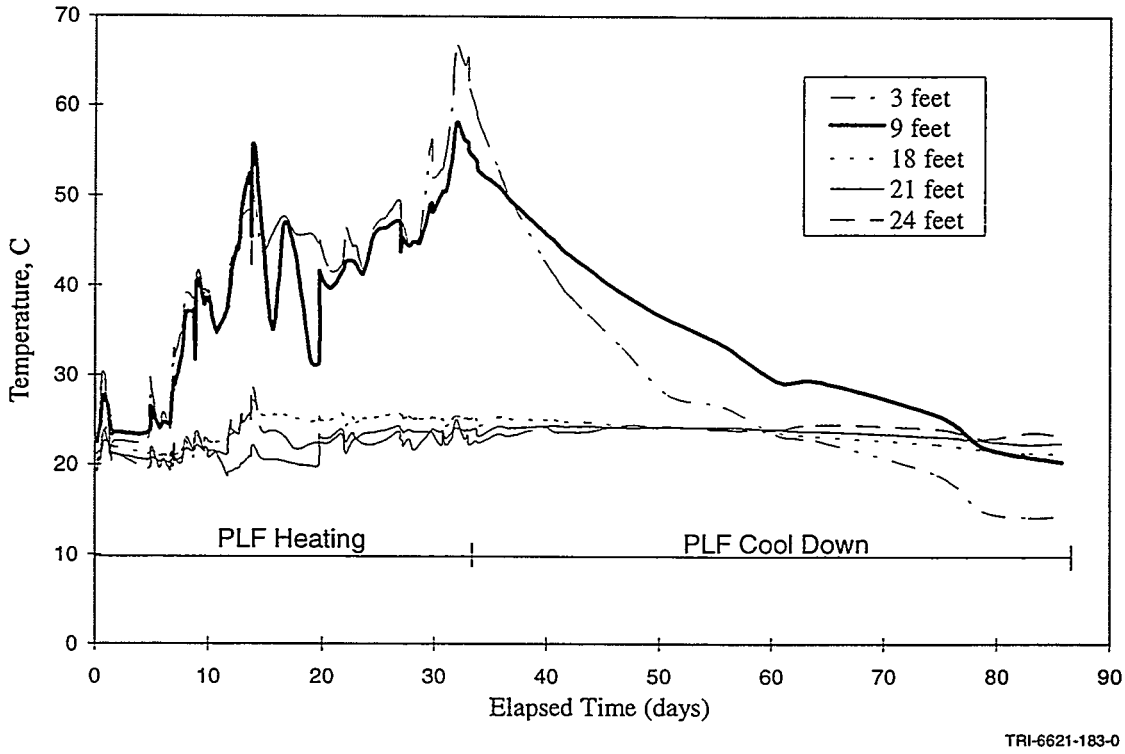

Figure 4-9. PLF heating, outer rows electrode temperatures.

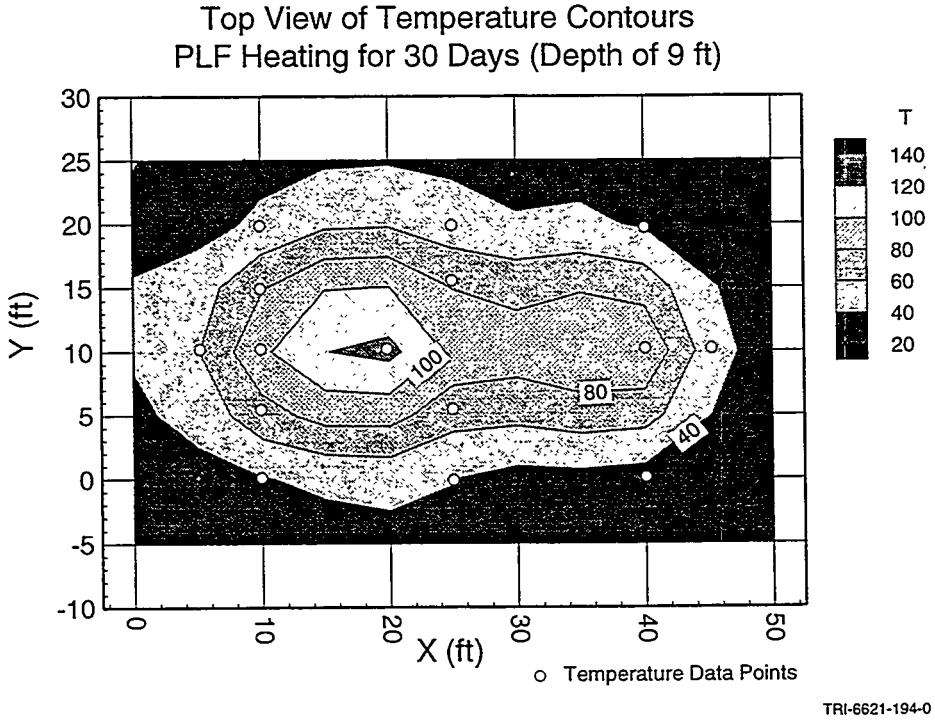

Figure 4-10. PLF heating, combined final temperature contours, plan view.

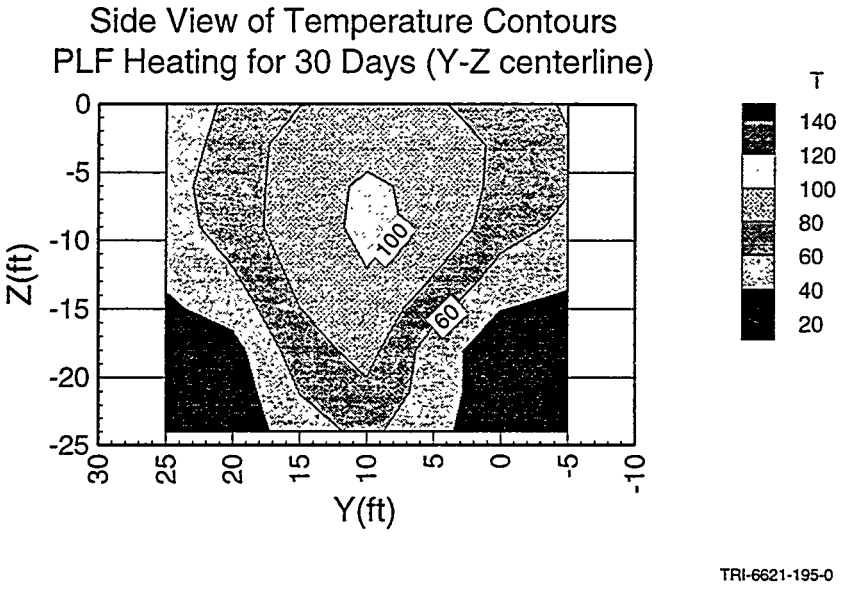

Figure 4-11. PLF heating, combined final temperature contours, long-side view.

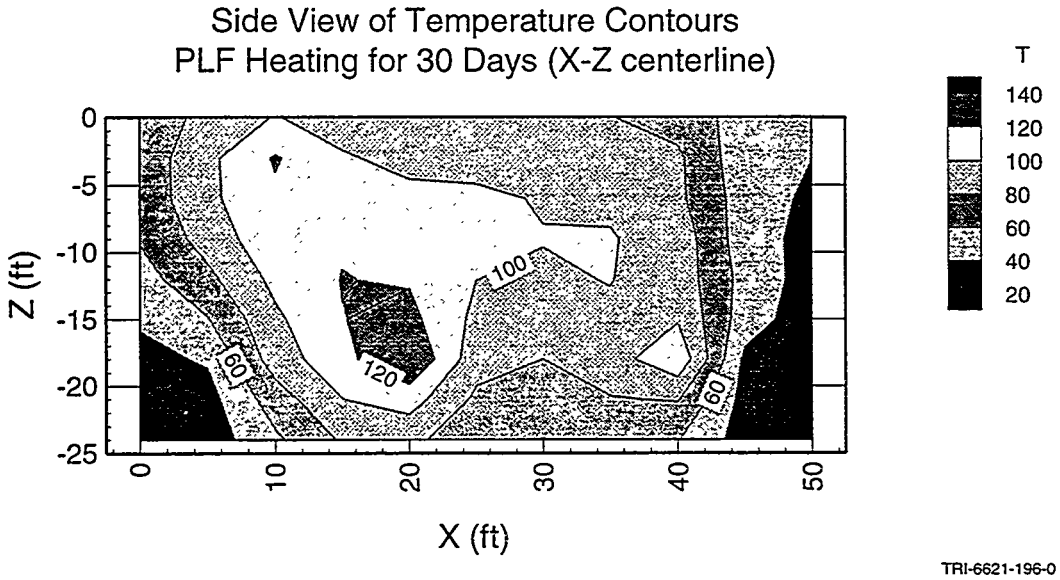

Figure 4-12. PLF heating, combined final temperature contours, short-side view.

Table 4-2. Heat Balance for PLF Heating Test

Contribution	Heat (Btu)	% of Input
Heat in:	1.54×10^8	
Heat Out:		
(1) Line Loss	3.9×10^6	2.5
(2) Heating Soil	5.6×10^7	36.4
(3) Evaporating Water	5.93×10^7	38.5
(4) Heating Water	6.5×10^6	4.2
(5) Heating Extracted Air	1.09×10^7	7.1
(6) Conduction loss to surrounding soil	1.8×10^6	1.2
(7) Loss through insulated top	4.5×10^6	2.9
Total Out	1.43×10^8	92.8

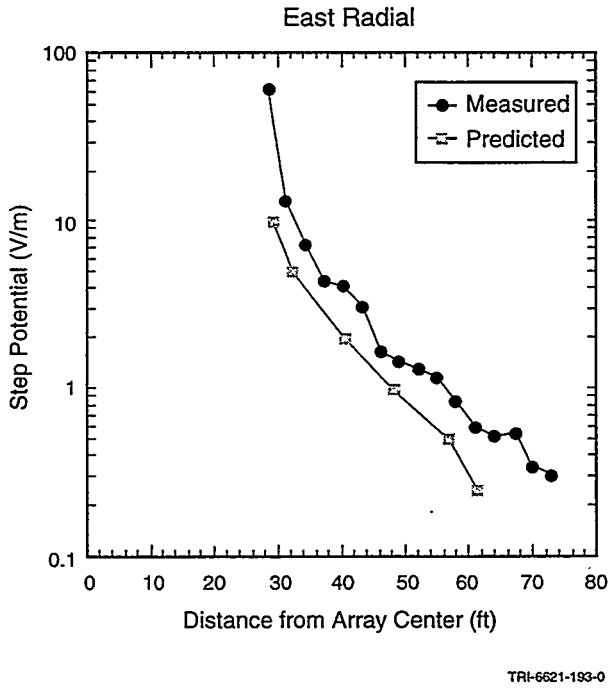

Figure 4-13. Comparison of calculated versus measured step potential (East radial).

5.0 RADIOFREQUENCY HEATING RESULTS

5.1 Applied Energy

Figure 5–1 shows the power input during the 29-day Radiofrequency (RF) heating period. Figure 5–2 shows the applied energy, which is an integration of Figure 5–1 over time. The figure shows that the total applied energy was 30,000 kWH, or 1.02×10^8 Btu.

5.2 Soil Temperatures

During the 87-day PLF cooldown period, rain and snowmelt water drained into the thermal insulation covering the treatment zone within the RF shield. A decision was made to remove the water soaked insulation and not replace it before the start of the RF heating phase.

Figure 5–3 shows the thermowell temperature profiles over time at the different depths in the heated area. These temperatures are the averaged temperature over the whole area. Similar to what occurred during the PLF heating, the temperatures at the 3-ft and 9-ft depths were significantly higher than at the lower depths. Figures 5-4 through 5-6 show temperatures at the individual wells at depths of 3 ft, 9 ft, and 18 ft respectively. The temperatures are not homogenous with respect to location. The TW7 and 8 wells, located in the middle of the array, had higher temperatures than the TW2, 3, and 4 wells located on the west side of the array. The TW11 well had the lowest temperatures which was the same case during PLF heating. The highest temperatures were attained at the 9-ft depth with a significant temperature gradient from the 9-ft to the 3-ft depth. By comparison, there was not much difference in temperatures between the 9-ft and 3-ft depths during the PLF heating. Figure 5–7 shows the center row temperatures at the 3-ft and 9-ft depths, were about 150°C and at the 18-ft depth, about 90°C. Figure 5-8 shows the combined outer row temperatures with the 3-ft depth reaching 75°C, the 9-ft depth reaching 50°C, and the lower depths near background temperature at 20°C. Figures 5-9 through 5-11 show the temperature contours from all data sources for the plan view, long-side view, and short-side view, respectively. Using a kriging routine with all data from day 29, the average temperature for the target treatment volume of 15 ft wide by 45 ft long by 18.5 ft deep was estimated to be 112°C. Using the total applied energy of 30,000 kWH, a volumetric energy requirement for the RF heating test amounted to 0.73 kWH/yd^3–°C.

5.3 Heat Balance

Contributions to the energy consumption consist of,

(1) line losses,
(2) heating the soil,
(3) vaporizing water,

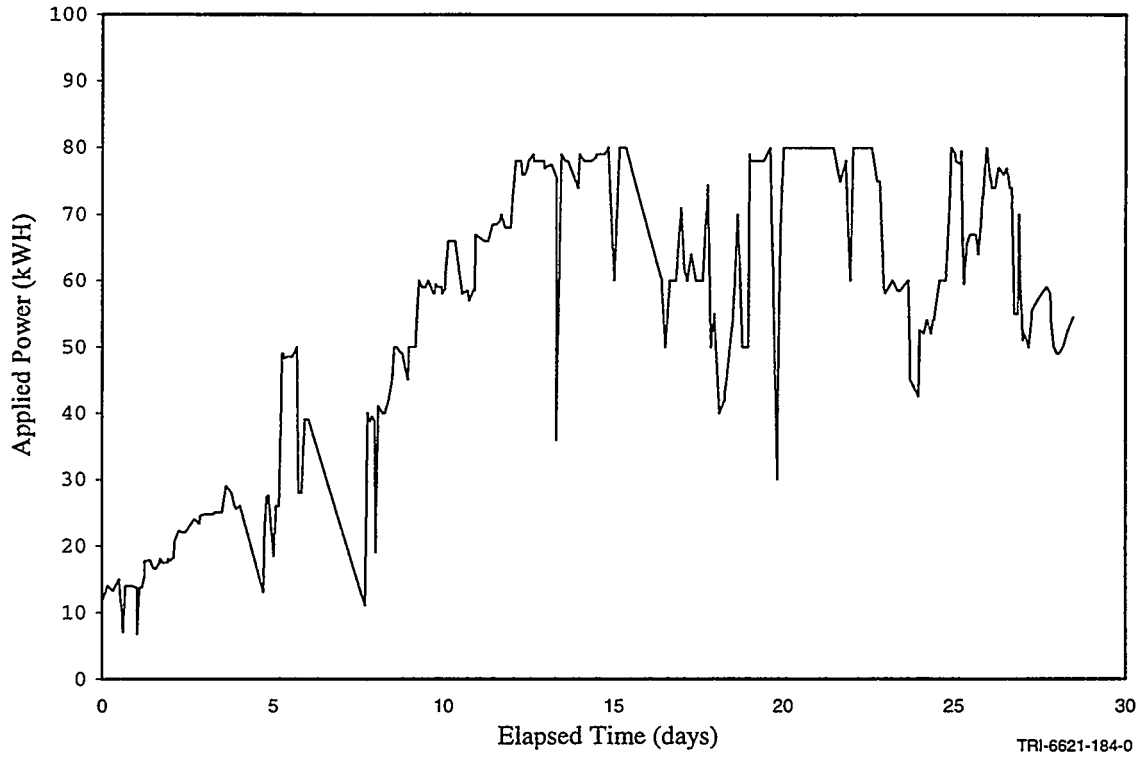

Figure 5-1. RF heating, applied power.

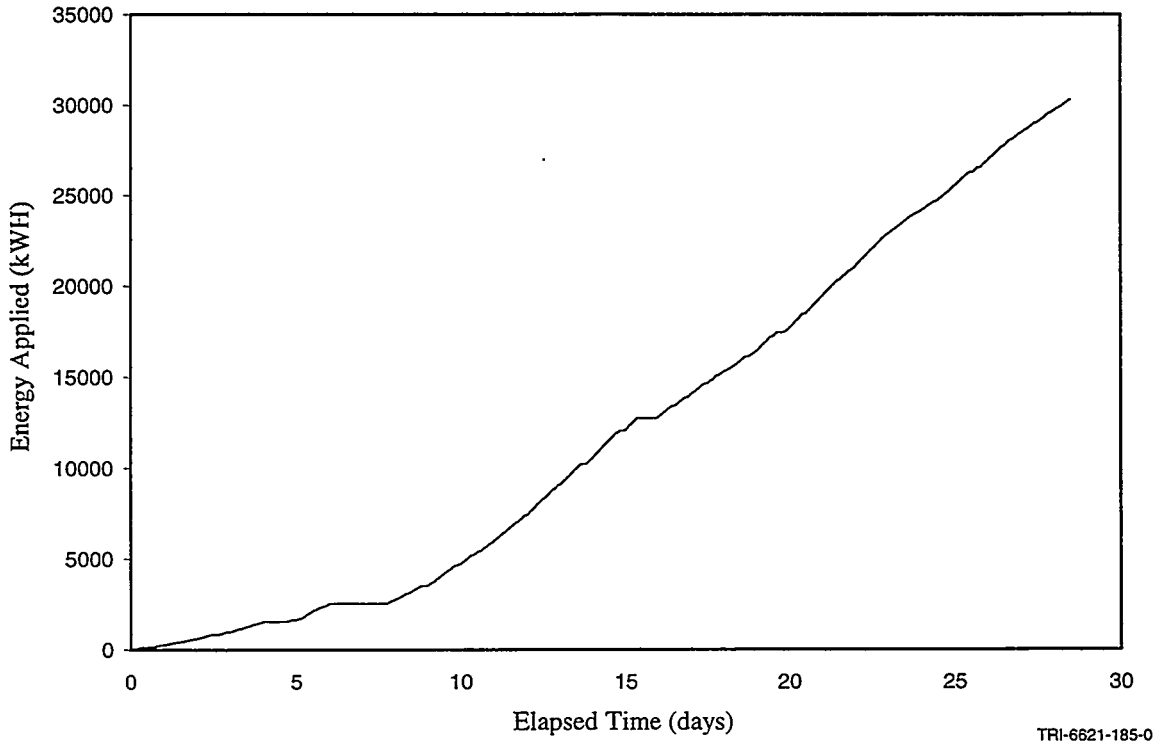

Figure 5-2. RF heating, cumulative applied energy.

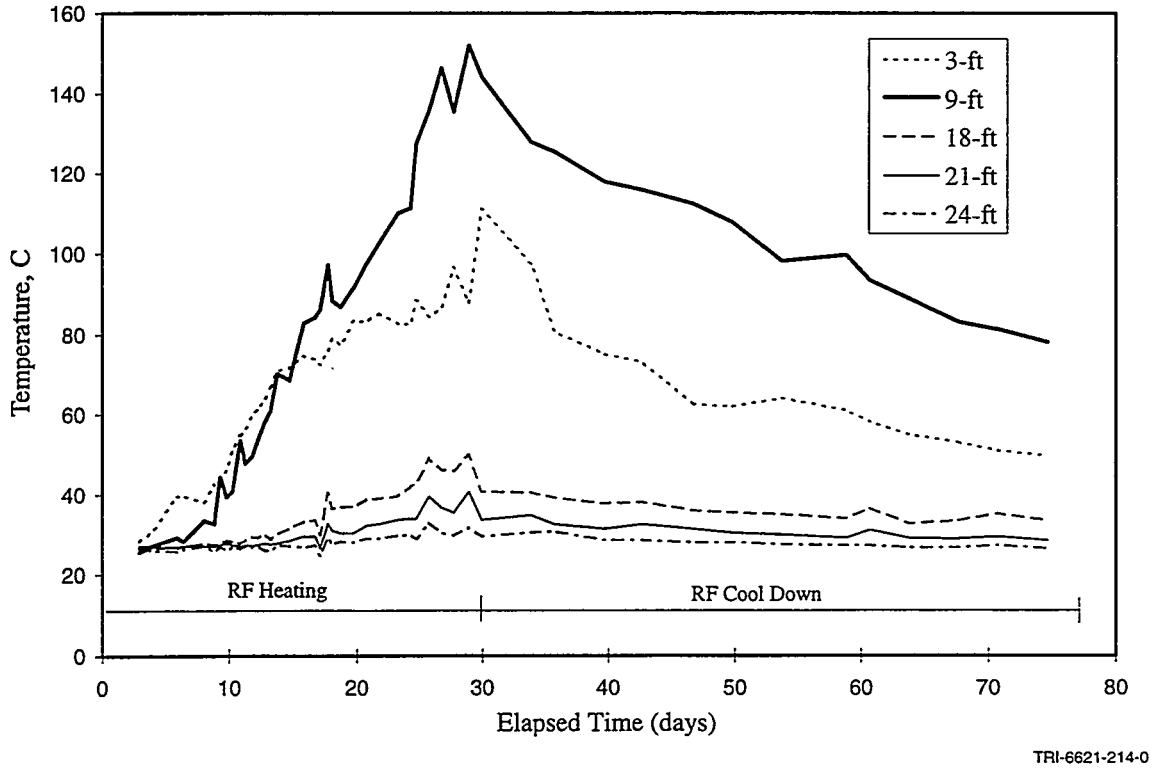

Figure 5-3. RF heating, thermowell temperatures.

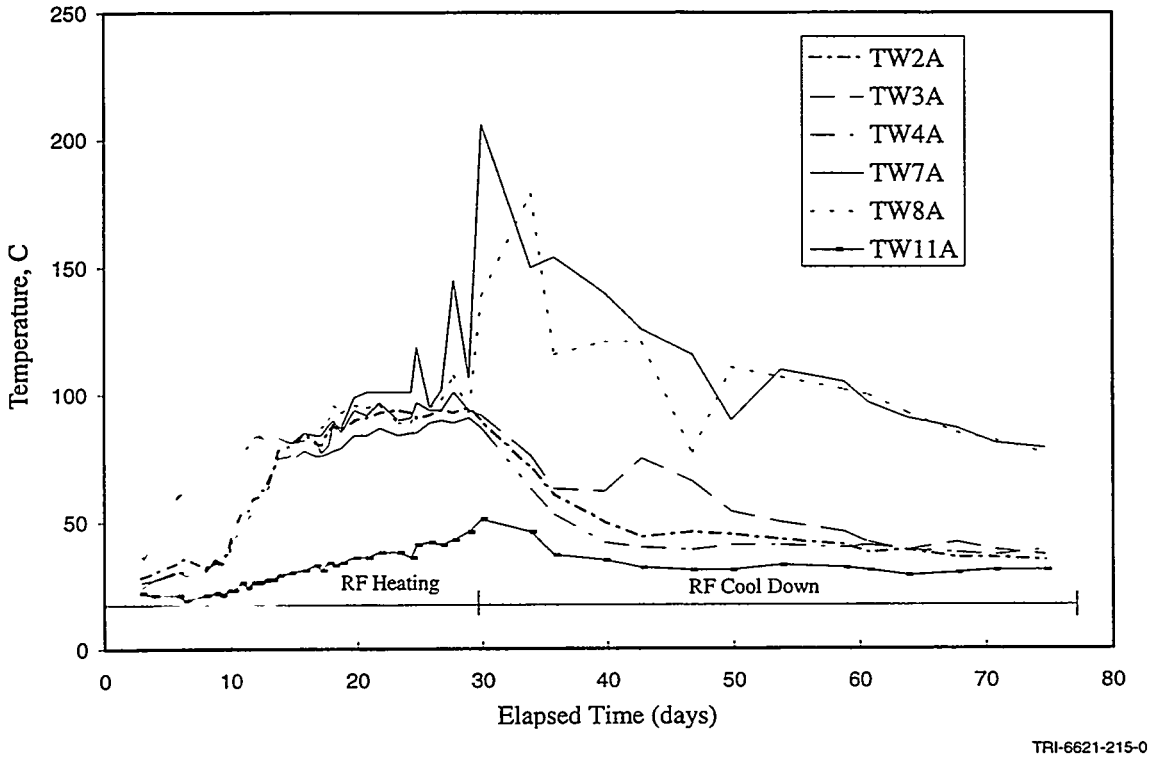

Figure 5-4. Thermowell temperatures at 3 ft. depth during RF heating.

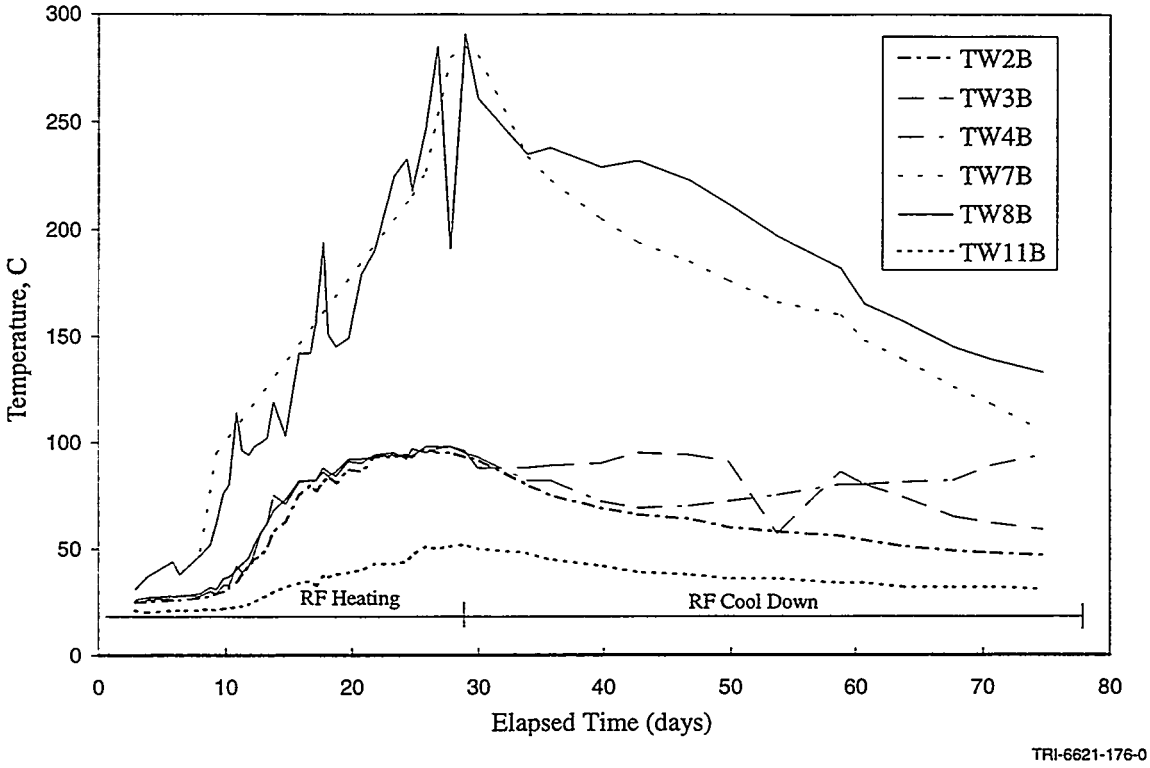

Figure 5-5. Thermowell temperatures at 9-ft. depth during RF heating.

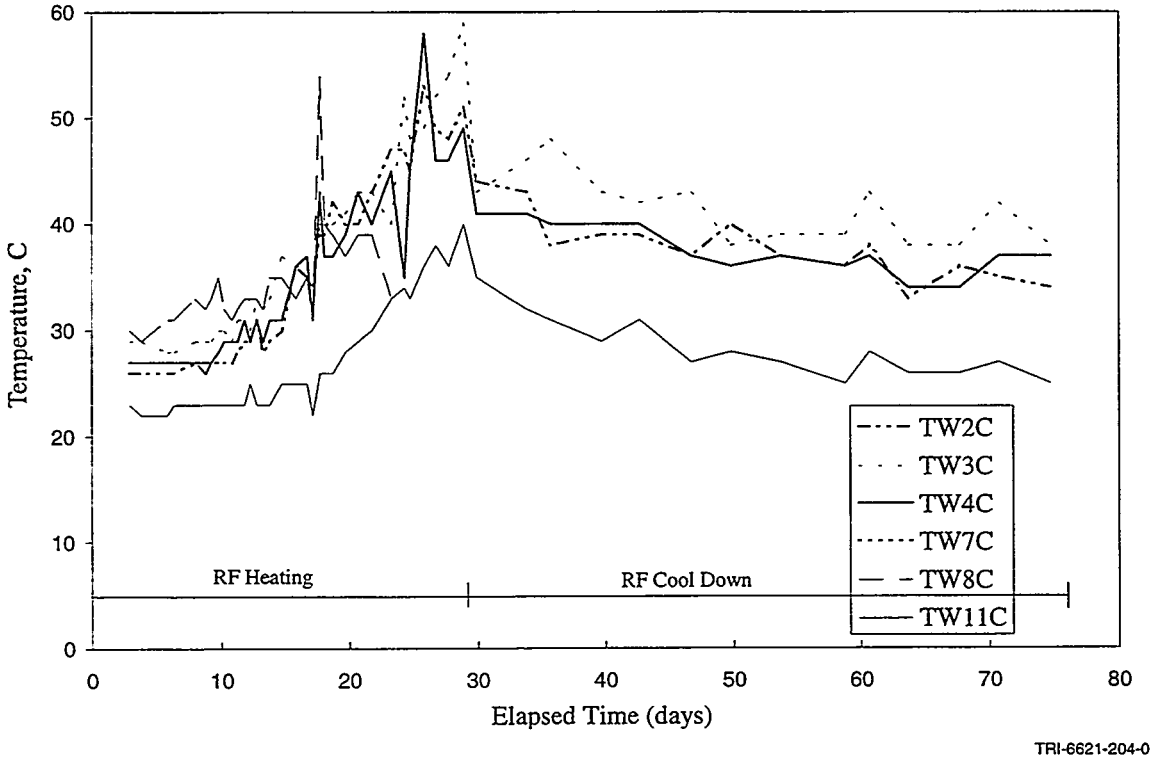

Figure 5-6. Thermowell temperatures at 18-ft. depth during RF heating.

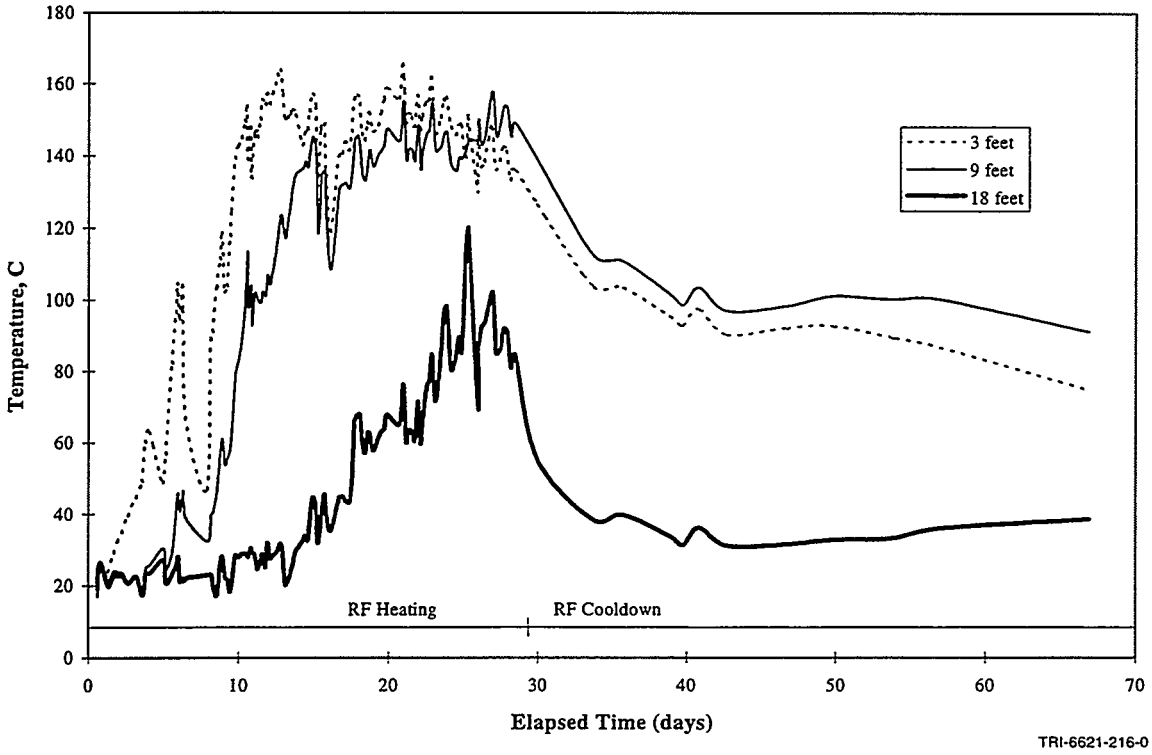

Figure 5-7. RF heating, center row electrode temperatures.

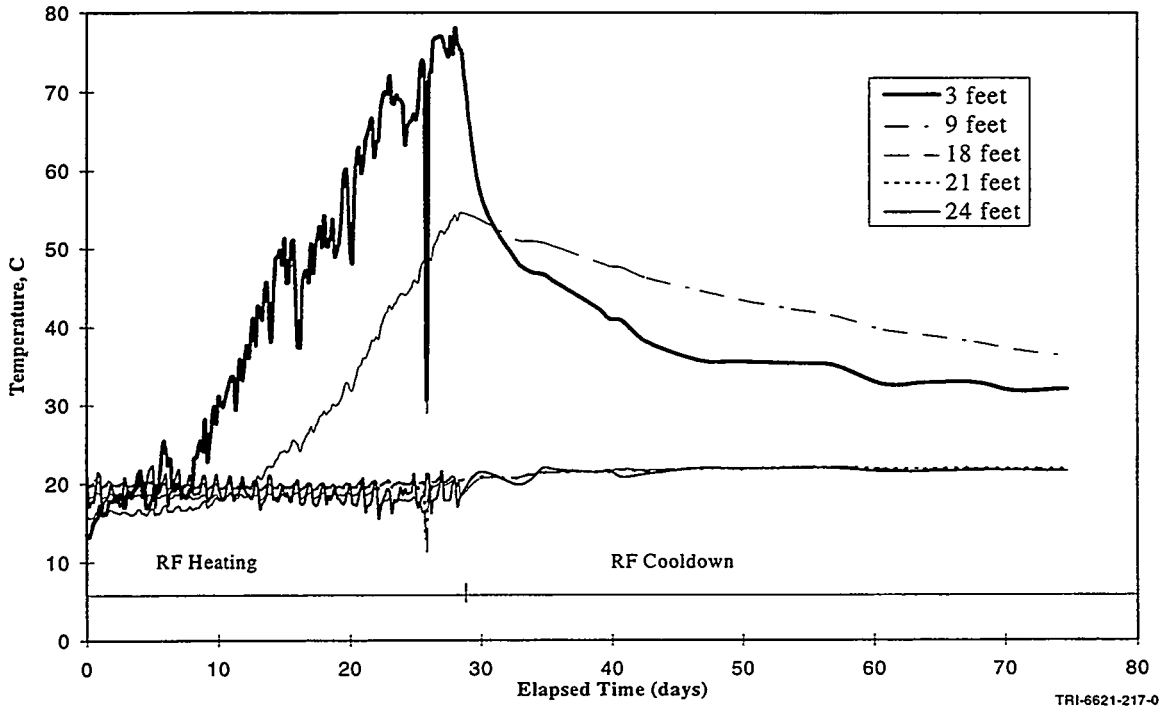

Figure 5-8. RF heating, outer row electrode temperatures.

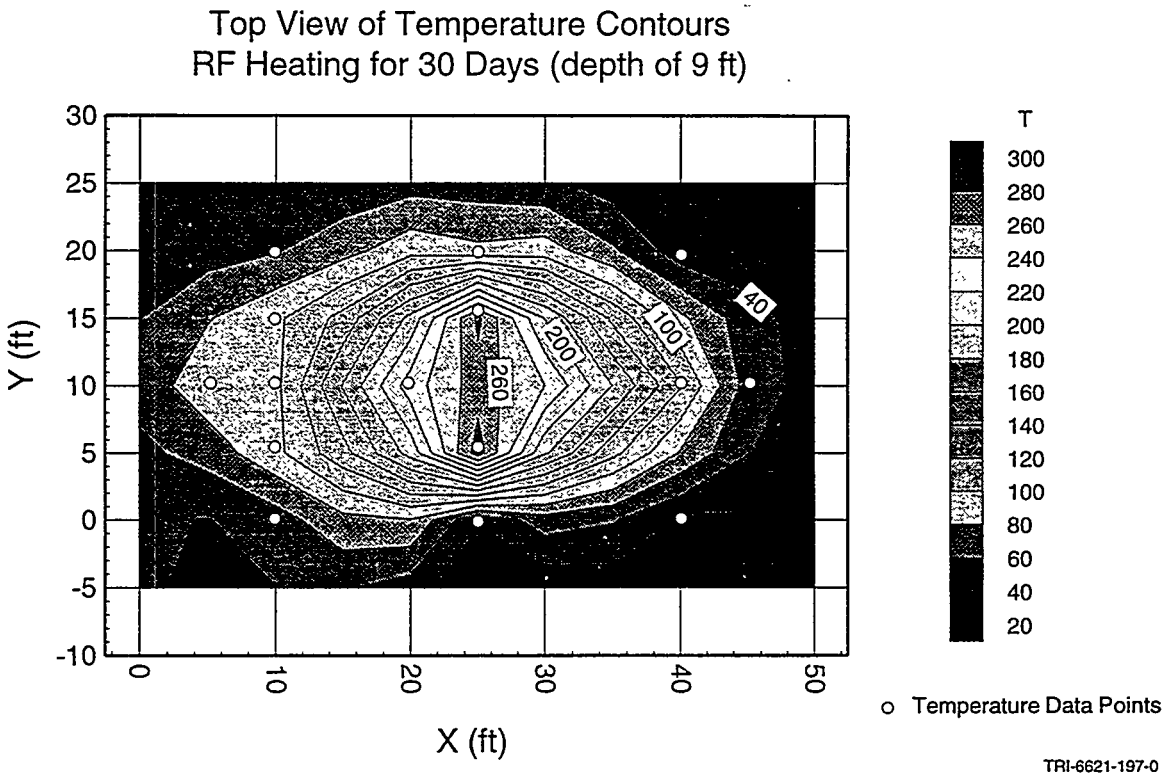

Figure 5-9. RF heating, combined final temperature contours, plan view.

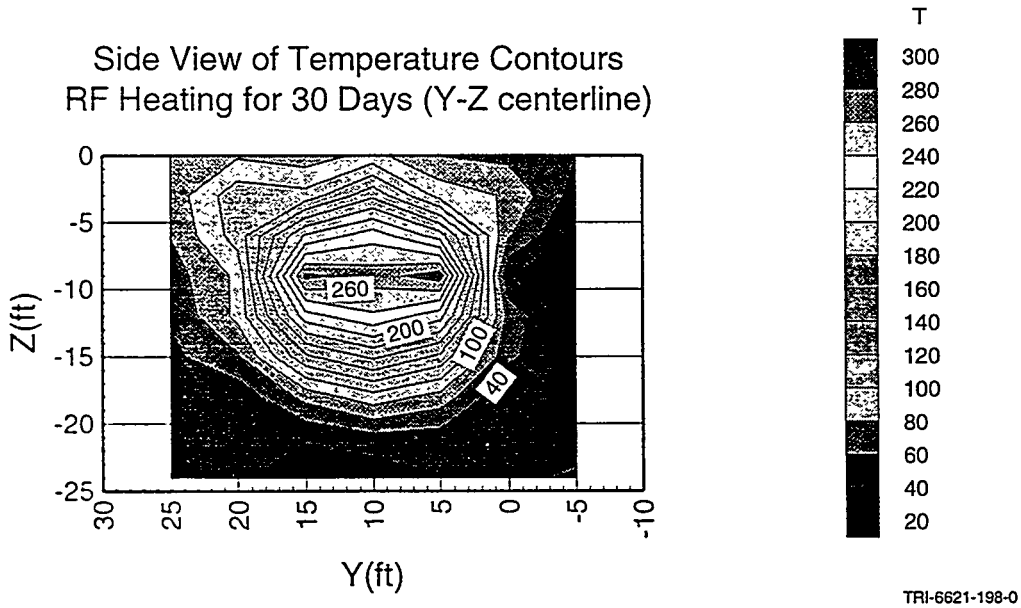

Figure 5-10. RF heating, combined final temperature contours, long-side view.

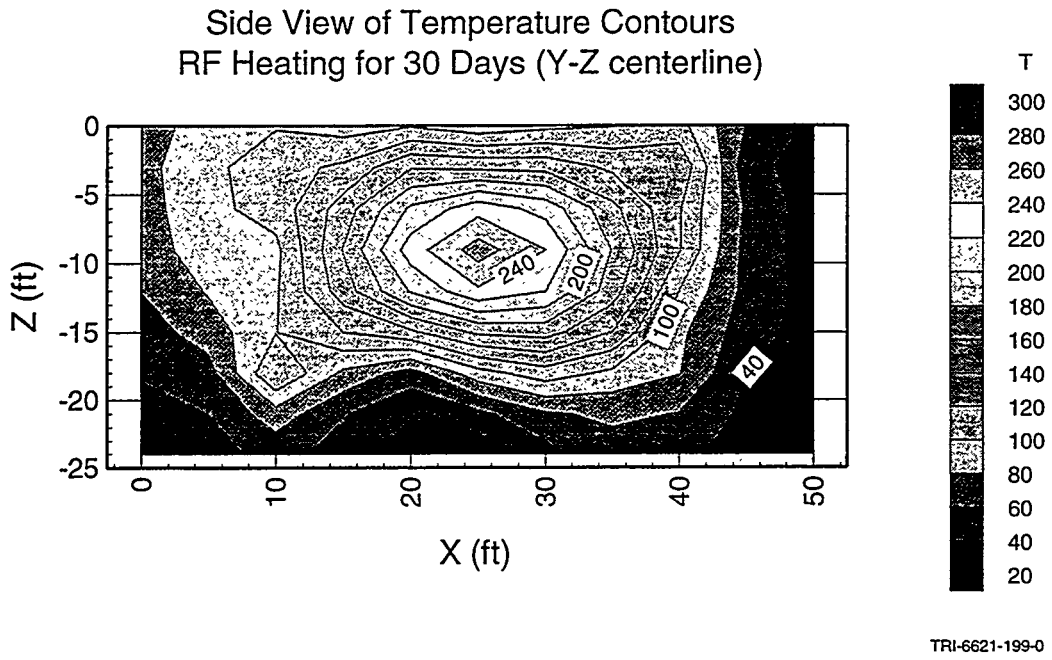

Figure 5-11. RF heating, combined final temperature contours, short-side view.

(4) heating pore water to vaporization temperature,
(5) heating extracted soil gas and ambient air drawn by the vacuum extraction wells,
(5) conduction heat loss to surrounding soil, and
(6) conduction heat loss through the uninsulated vapor barrier at the top of the heated zone.

Detailed calculations of these contributions are shown in Appendix B. Table 5–1 summarizes the results. Other contributions to the heat balance that are not accounted for are heat loss due to condensation of water vapor on the inside of the vapor barrier and radiation heat losses.

5.4 RFI Measurements

Near and far field electromagnetic field intensities were extensively measured at the TEVES demonstration site, and at locations 1/8 to 1 mile from the test site. The purpose of these measurements was to ensure that any radiated RF power levels were below the permissible Federal Communications Commission (FCC) standards, that no interference was generated with airport or SNL communications, and that no personnel safety problem areas existed.

The first set of measurements were taken with RF power levels at about 10 kW. Both site safety and radio frequency interference (RFI) levels were measured and found to be acceptable. The second set of measurements were taken during the TEVES test with full RF power, up to 100 kW. These measurements consisted of recording power densities resulting from both the electric and magnetic fields with a hand-held field strength or exposure probe. The area-wide

average power density, attributable to the electric and magnetic fields, was found to be <0.02 and <0.2 mW/cm^2, respectively. These are less than 1% of the maximum permissible exposure limits of 3.92 mW/cm2 for electric field and 217.5 mW/cm^2 for magnetic field as specified by IEEE C95.1 - 1991 (Standard for Safety Levels with Respect to Human Exposure to Radio Frequency Fields, 3 kHz to 300 GHz). The maximum RF power density found within 1 inch of any conductor, at or near the exclusion zone boundary, with full power applied, was 2.0 mW/cm^2. This is still less than 1/2 the electric field's exposure limit for uncontrolled access.

Seven sites were identified for repeated electric and magnetic field intensity measurements at and around the TEVES demonstration site. RFI measurements consisted of measuring and recording the electric and magnetic field intensity at the fundamental frequency and the first four harmonics at each location, as well as scanning all frequencies in-between. Ambient field intensities were also recorded for each frequency measured.

Table 5-2 identifies the maximum electric field intensity measured at the applied frequency of 6.78 MHz as a function of distance from the electrode array as compared with the IEEE (Institute of Electrical and Electronics Engineers) standard.

Table 5-3 shows the maximum magnetic field intensity measured at the applied frequency of 6.78 MHz as a function of distance from the electrode array, indicating that the maximum measured magnetic field intensity of 12.5 μG is less than 0.1% of the IEEE limit of 30 mG.

Out-of-band electric field intensity measurements were also taken. Out-of-band refers to measurements at frequencies other than the operating frequency, directly generated as part of its operation. These were also less than 1% of the acceptable FCC limit as described in 47 CFR 18. In addition, no electromagnetic interference was experienced by any SNL or airport communication staff throughout the duration of the RF heating demonstration.

Table 5-1. RF Heating Heat Balance

Contribution	Heat (Btu)	% of Input
Heat in:	1.02×10^8	
Heat Out:		
(1) Line Loss	2.6×10^6	2.6
(2) Heating Soil	5.6×10^7	54.9
(3) Vaporizing Water	2.4×10^7	23.5
(4) Heating Pore Water	2.4×10^6	2.4
(5) Heating Extracted Air	7.6×10^6	7.5
(6) Conduction Loss to Surrounding Soil	1.8×10^6	1.8
(7) Conduction Loss through Un-Insulated Top	5.6×10^6	5.3
Total Out		98.0

Table 5-2. Maximum Electric Field RFI Measurements. Near/Far Field Applied Frequency = 6.78 MHz; applied Power = 60 kW

Distance from Array (meters)	Electric Field Intensity (V/m)	Personnel Safety Continuous Exposure Electric Field Standards IEEE/ANSI (V/m)
25	0.560	121.5
300	0.032	121.5
800	0.007	121.5
1600	0.003	121.5

Table 5-3. Maximum Magnetic Field RFI Measurements. Near/Far Field Applied Frequency = 6.78 MHz; Applied Power = 60 kW

Distance from Array (meters)	Magnetic Field Intensity (μG)	Personnel Safety Continuous Exposure Magnetic Field Standards IEEE/ANSI (mG)
25	12.5	30
300	1.1	30
800	0.2	30
1600	0.06	30

5.5 Impedance Tracking and Matching

The RF power source used for the heating demonstration was an AN/FRT-86 HF band radio frequency transmitter with a maximum output power of 200 kW. Several pre-demonstration operational tests were conducted into a 50 ohm dummy load. The RF power source was checked out up to 150 kW at each of the three frequencies: 3.39, 6.78 and 13.6 MHz. The operational performance of the RF heating system used in the TEVES demonstration was evaluated by monitoring the RF power delivered and absorbed by the subsurface array by tracking the electrode array's complex input impedance. A matching network was utilized to deliver RF energy from the power source to the widely varying impedance of the electrode array load. Both the forward and reflected power at the output of the RF power source were

continuously monitored throughout the demonstration. By periodically adjusting the variable components of the matching network's final stage, the reflected power was minimized or maintained at zero.

The matching network was capable of handling high standing wave ratios (SWR) and efficiently delivering up to 100 kW to the load. The electrical impedance, measurable immediately exterior to the RF shield, presented a very high SWR, directly related to the length and geometry of the feed conductor and RF shield structure connected to the subsurface electrode array. Two fixed element stages were used in series, each of which employed a fixed value high voltage vacuum series capacitor followed by a fixed length of coaxial transmission line (i.e. a line stretcher). These two fixed stages preceded the final variable element stage. Four separate configurations of this composite matching network were utilized during the demonstration. Figure 5-12 and Table 5-4 illustrate a schematic representation of the complete matching network and list the various component values used in each of the configurations.

By recording the complex voltage measurements obtained from the IITRI designed and fabricated in-line impedance meter, changes in trends in the input impedance to the electrode array were tracked as a function of time. By monitoring these trends in the impedance, a qualitative assessment of the RF heating system's performance was conducted.

The initial operating frequency for the RF heating portion of the TEVES demonstration was 6.78 MHz, a designated industrial, scientific and medical (ISM) frequency band. The measured temperature profiles for the heated soil array, while operating at this frequency showed heating was occurring to depth. This combined with the real-time monitoring of the array impedance indicated that this frequency would achieve the desired extent of volumetric heating as the test progressed. Therefore, switching to a lower operating frequency (i.e. 3.39 MHz), was not selected.

Figure 5-13 shows a calculated Smith chart representation of the electrode array's input impedance as would be measured at the soil surface, if possible, as a function of time for the entire demonstration. The data presented is a running average of the numerous log entries of the complex impedance. This data corresponds to tracking the average impedance on a 12 to 24 hour basis throughout the demonstration.

The soil loaded array had already been pre-dried, for the most part, at the end of the PLF heating demonstration. Figure 5-13 shows an expected trend in input impedance from points 1 through 27, during the first two weeks of heating. Between impedance points 27 and 38, during the next 3 to 4 days, the trend in impedance is erratic and may be a result of subsurface electrode array changes or vapor production/collection system abnormalities. The trend in impedance seems to track more as expected from points 38 to 43, during the next 2 days. However, after point 43 until the end of the demonstration, the erratic pattern of the input impedance indicates that major impedance variations were occurring within the subsurface electrode array throughout the balance of the last 9 days of heating.

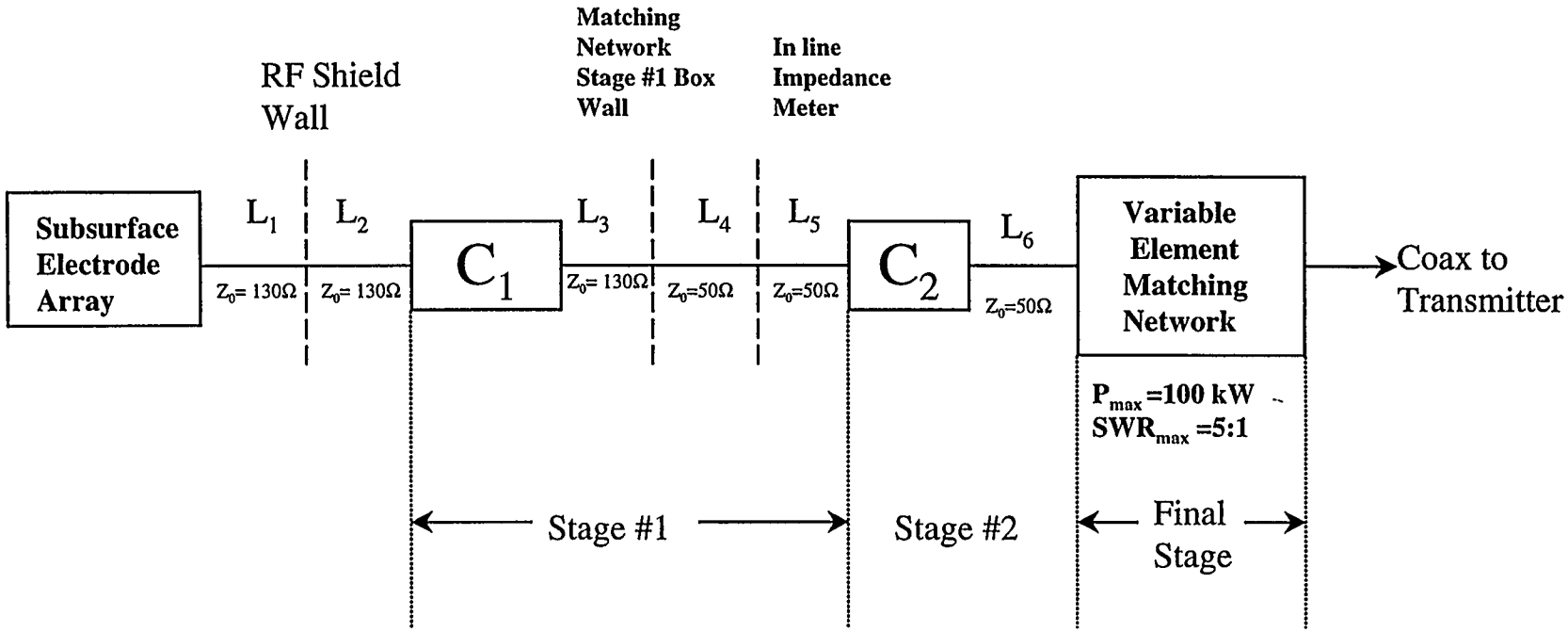

Figure 5-12. Matching network configuration schematic.

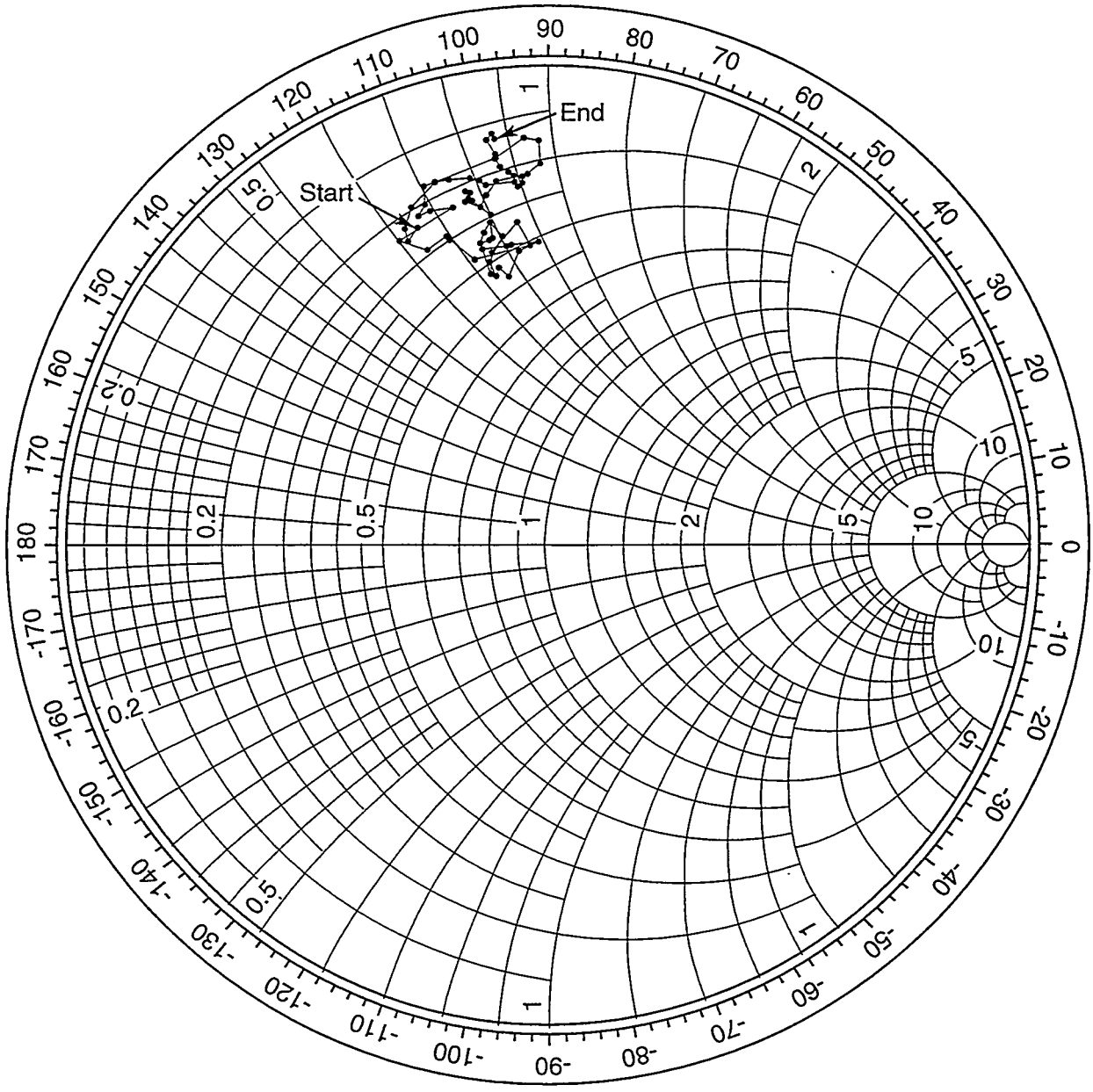

Figure 5-13. Smith chart for TEVES demonstration.

Table 5-4. Matching Network Fixed Component Values for four Configurations

Configuration #		Stage #1				Stage #2	
	L_2 (in)	C_1(pF)	L_3 (in)	L_4(in)	L_5(in)	C_2 (pF)	L_6(in)
1	17	N/A	21	703	137	50	12
2	17	25	21	701	113	100	36
3	20	16.67	18	701	113	100	36
4	20	12.5	18	701	113	100	36

This page intentionally left blank.

6.0 AIR AND WATER VAPOR EXTRACTION

6.1 Soil Gas Flow Rates

Figure 6-1 shows the soil vapor flow rates during the entire demonstration period. For most of the operation, the flow rates were between 150 and 180 standard cubic feet per minute (scfm). The numerous low or zero flow rate periods were due to the operation of the air stripper when the condensate tank became full (see Section 3.3.2.2, Air Stripper). These periods lasted approximately 12.5 minutes and occurred approximately once per hour during active soil heating periods. Figure 6-2 shows the manifold vacuum measured just upstream of the off-gas treatment system. This figure also shows a drop in manifold vacuum during the air stripper runs, which were more prevalent during the PLF heating period.

Actual flow from subsurface soils was diluted at two locations to manage high contaminant extraction rates. A 1-in gate valve on the distill end of the extraction manifold was left fully open during the entire demonstration period. Appendix B shows a calculation that the amount of air flowing through the 1-in gate valve was about 73 scfm or about 40 to 48% of the total flow measured by the Pitot tube. A larger 3-in gate valve was installed after the PLF heating period, just prior to the vacuum blower, as an additional vapor flux controller. This was necessary due to the large increases in contaminant extraction rates that occurred during the PLF heating and were expected to reoccur during the RF heating. The indicated flow rates for the RF heating were lower due to opening this 3-in gate valve one-quarter to one-half.

On day 28 of the PLF heating period, the vacuum extraction system was switched from the two primary extraction wells in the center row to the four backup extraction wells in the ground rows. The water vapor extraction rate and the condensate generation rate dropped to near zero. After five days, the extraction system was changed back to the primary center row extraction wells.

6.2 Condensate Oil

During the PLF heating test, one quart of oil was collected via the condenser/day tank. During the RF heating, 55 gallons of oil were collected via the condenser/day tank. Figure 6-3 shows the results of the American Society of Testing and Materials (ASTM) D-2887 simulated distillation test on these two oils. The tests show that the first fractions boiled at 280°F to 360°F (138°C to 182°C) with significant fractions boiling at temperatures much higher than those attained by either the PLF or the RF tests.

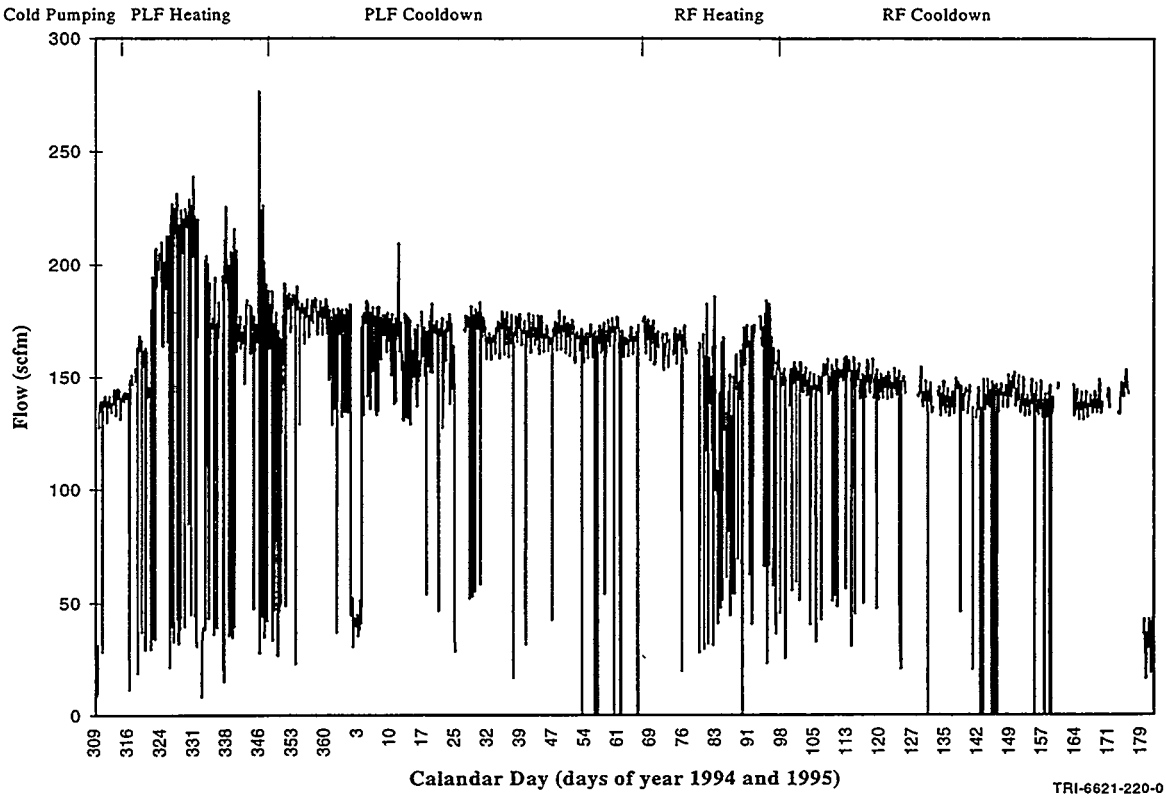

Figure 6-1. Manifold vapor flow rate during entire demonstration period.

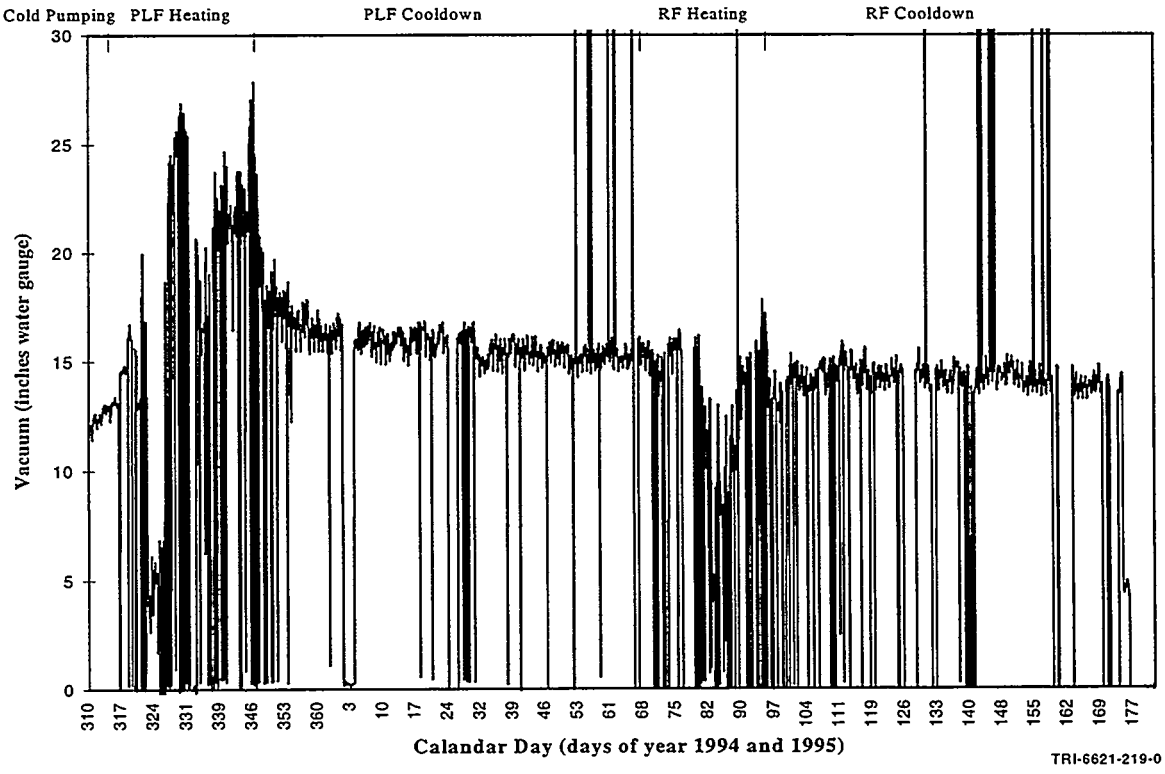

Figure 6-2. Manifold vacuum during entire demonstration period.

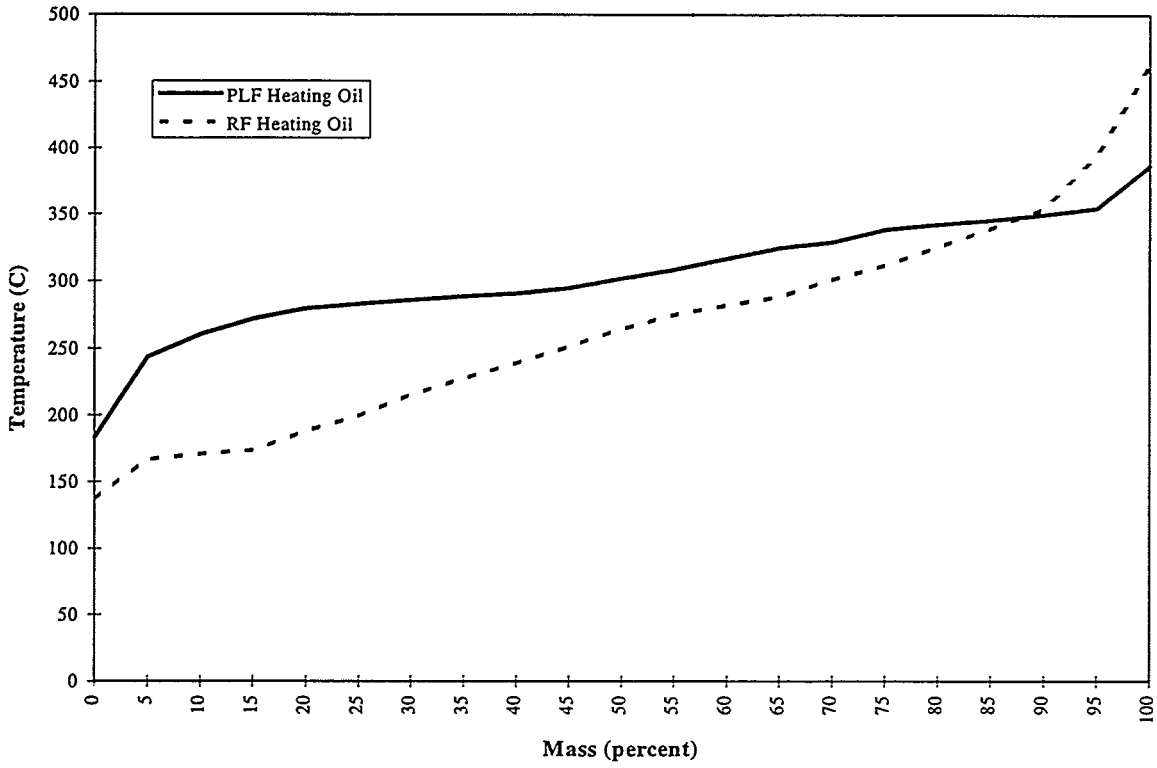

Figure 6-3. Simulated distillation for oil condensate (ASTM D-2887).

6.3 Water as Condensate

Figure 6-4 shows the condensate production rate and the accumulated condensate over the period of the PLF and RF heating tests. The condensate collection rates were higher during the PLF heating period than during the RF heating period since water was injected during PLF heating. The very large spike of condensate generated during the PLF heating occurred when extraction from the backup extraction wells was changed back to the primary center row. During the cooling period between PLF and RF heating periods, the condensate generation rates were significantly lower because of the lower vapor pressure of water at the reduced temperatures. The cumulative condensate was used in the energy balance calculations for both the PLF and RF heating periods.

The condensate water was passed through an activated carbon bed in order to remove toxic organic compounds. The effluent from the carbon bed was stored in a large tank. Analysis of the water in the tank at the end of the RF test period showed that the total toxic organics content was below the city of Albuquerque Discharge Standard of 5 ppm. Acetone was found at 7.4 ppm in this condensate; however, acetone is not on the total toxic organics list and the condensate was allowed to be discharged to the sanitary sewer.

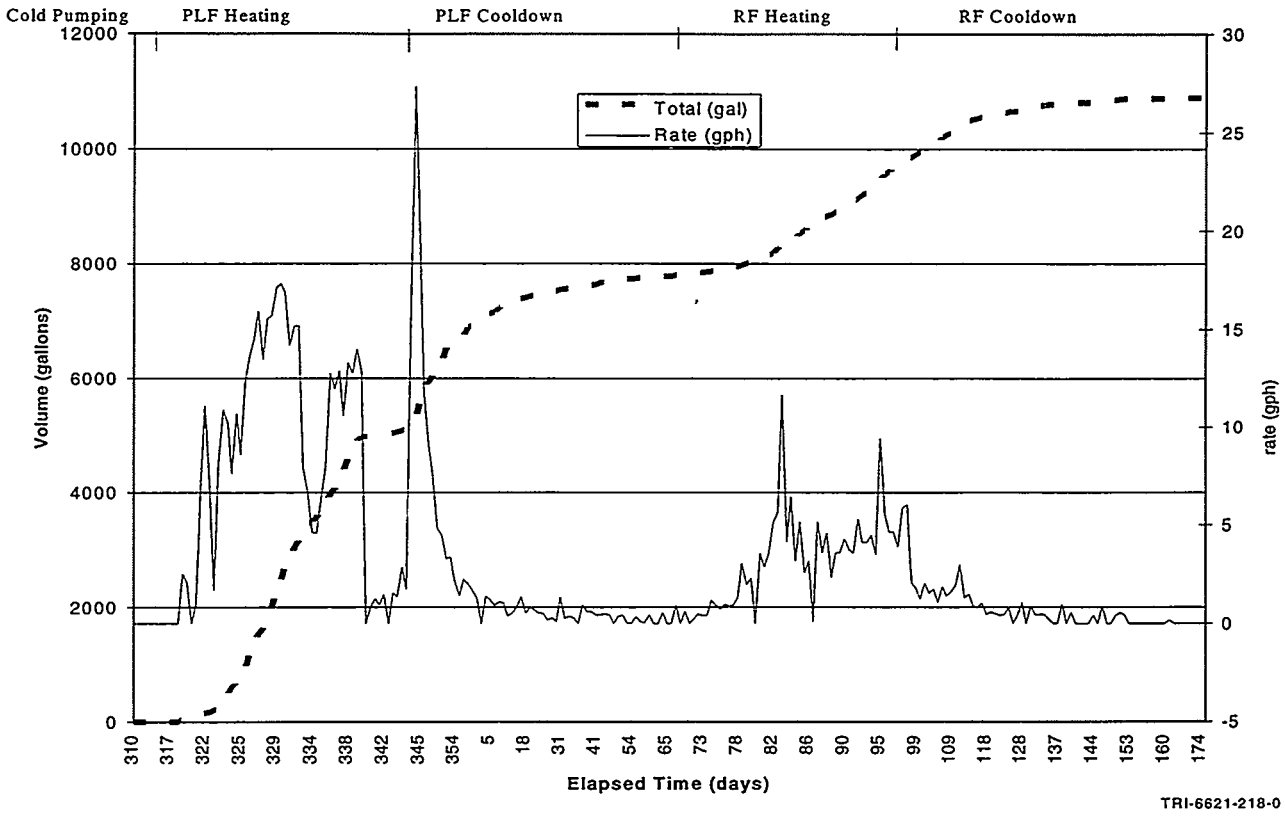

Figure 6-4. Condensate production.

6.4 Uncondensed Water Vapor

A relative humidity sensor was located downstream of the condenser to measure percent water by volume entering the thermal catalytic oxidizer. During the PLF heating period the sensor worked well; however, as more oil vapor began to be extracted from the treatment zone, the sensor became coated with oil and gave unreliable results. Attempts to reposition the sensor further downstream were unsuccessful and use of the sensor was abandoned.

7.0 VAPOR ANALYSIS AND VOC EXTRACTION RATES

The vapor extraction chemical monitoring system operated continuously from the test initiation to the final shutdown. Graphical presentation of the monitored contaminants are shown for the entire demonstration period. Table 7-1 shows the initial cold pumping, heating periods, and cooldown periods with the actual dates, sequential day of the calendar year, and the duration for each period.

Table 7-1. Demonstration Period Activities

Activity	Start Date	Calendar Day	Duration
Cold Pumping	11/05/94	309	4
PLF Heating	11/09/94	313	33
PLF Cooldown	12/12/94	346	87
RF Heating	3/9/95	68	29
RF Cooldown	4/7/95	97	84
System Shutdown	6/30/95	181	-

Nine compounds were analyzed twice per day to assess system performance (see section 3.4.5.1 Vapor Composition Analysis). Figure 7-1 shows all nine compounds plotted together during all the periods shown in Table 7-1. During the heating periods, sharp increases in the concentrations of all the measured contaminants occurred. Figures 7-1 through 7-10 show the individual contaminant concentrations during the demonstration period.

Figure 7-11 shows the sum of the 9 VOC concentrations plotted with the average thermowell temperature at 3 ft. depth. Similarly, Figure 7-12 shows the total GC count plotted with the average thermowell temperature at 3 ft. depth.

The steady increases in total VOC concentration were a result of the increased temperature on the vapor pressure of the soil contaminants; however, the large spikes were most likely a result of liquid filled containers in the treatment zone that quickly released vapors when the vapor pressure exceeded the pressure capacity of the container. The large residuals during the PLF and RF cooldown periods for Freon and Trichloroethylene shown in Figures 7-4 and 7-8 are most likely caused by the widespread vapor plume that exists at this site. These compounds were pulled from outside the treatment zone by the vapor extraction system. Figure 7-13 shows the normalized total GC counts as a function of the operating date. The GC counts were normalized to the value at operating day 4 when the unheated extraction stopped and the extraction with PLF heating began. This was the baseline. Figure 7-13 also shows the average thermowell temperature at a 3 ft. depth. Normalized GC counts reached a high of 3.5 during PLF heating, with the exception of what is suspected to be a drum burst on day 38. During RF heating, the high normalized GC counts was about 3 without counting the drum bursts. The normalized GC count was less than 1 during the cooldown period after the PLF heating and also after the RF heating. This

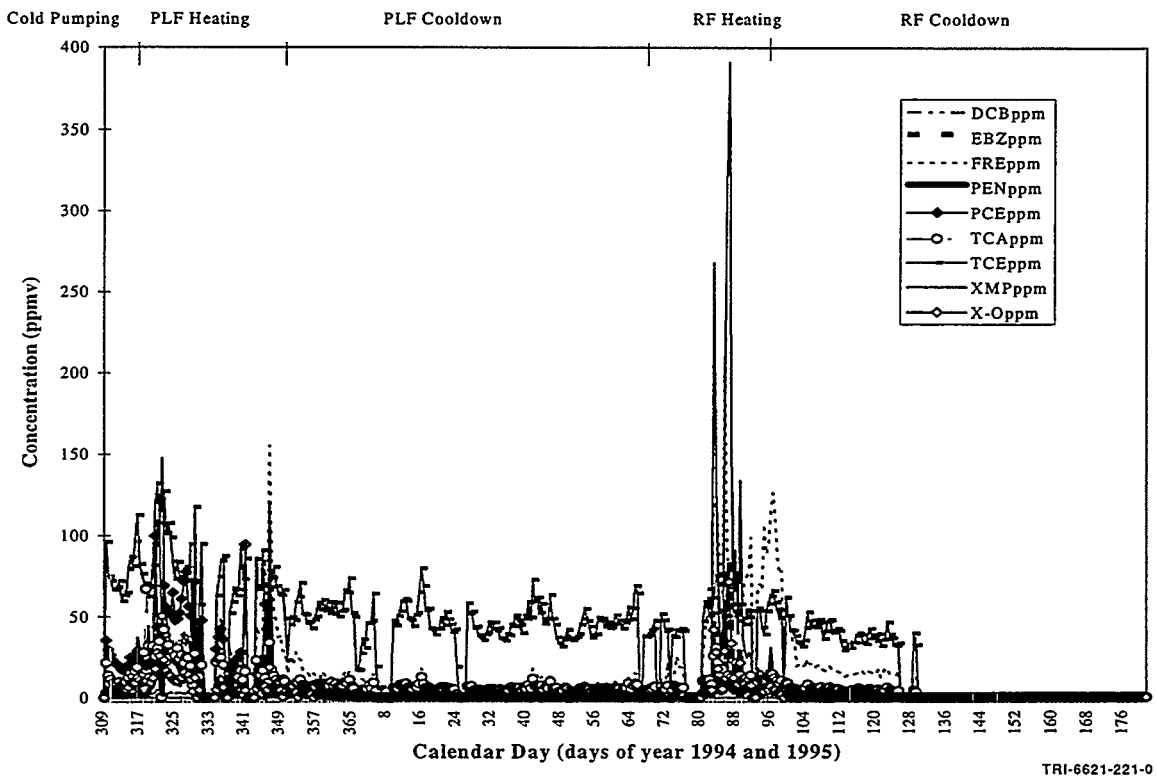

Figure 7-1. Chemical vapor concentrations from the extraction manifold.

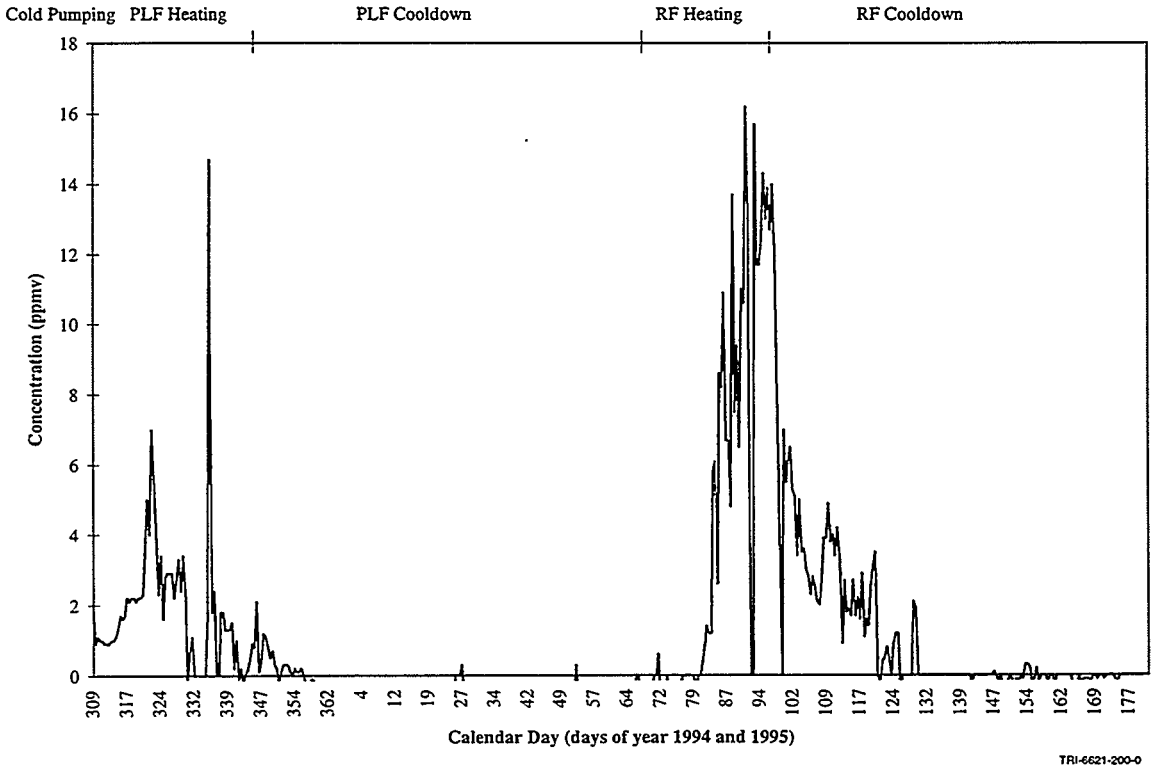

Figure 7-2. Dichlorobenzene concentration from the extraction manifold.

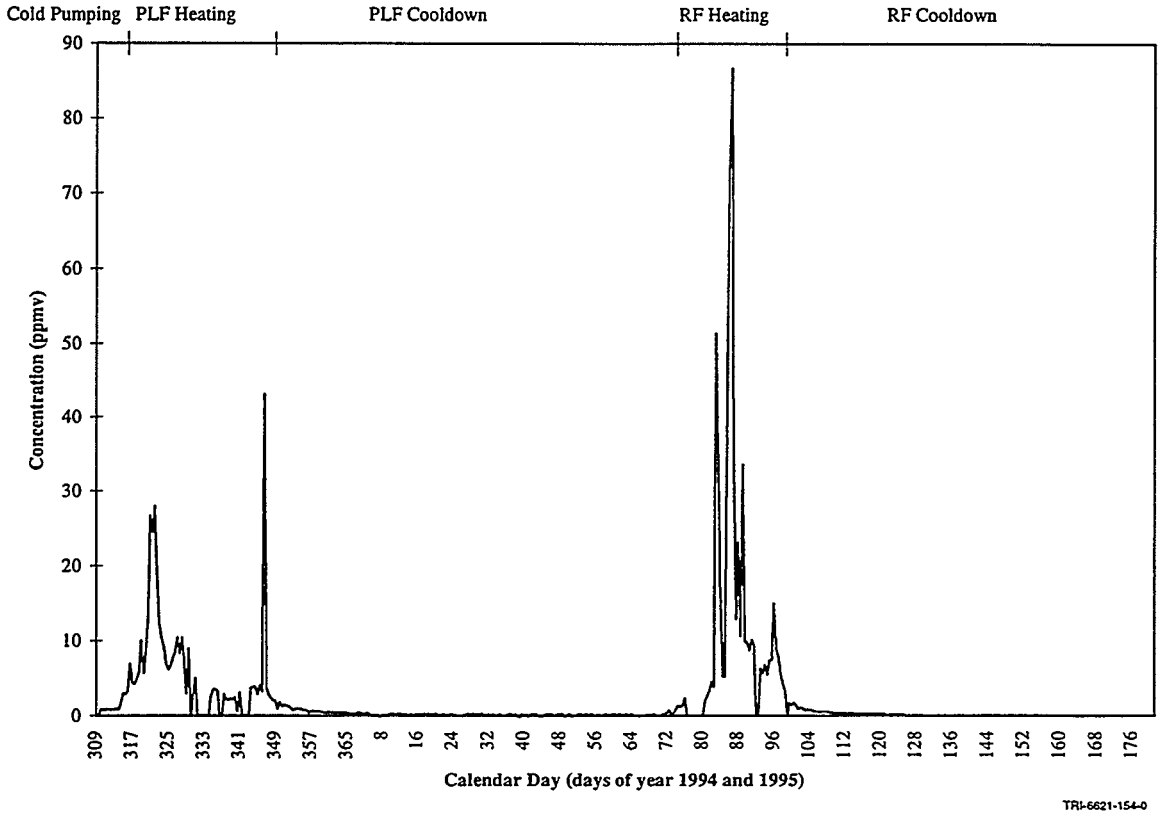

Figure 7-3. Ethylbenzene concentration from the extraction manifold.

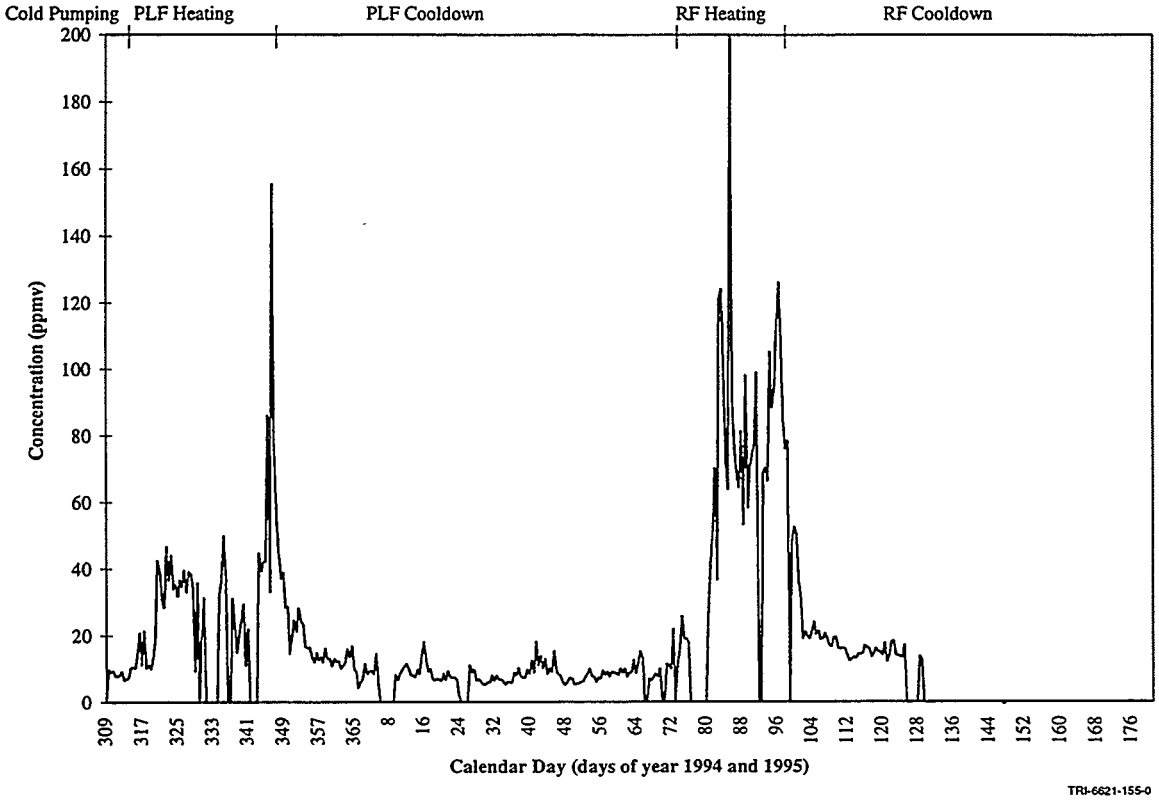

Figure 7-4. Freon 113 concentration from the extraction manifold.

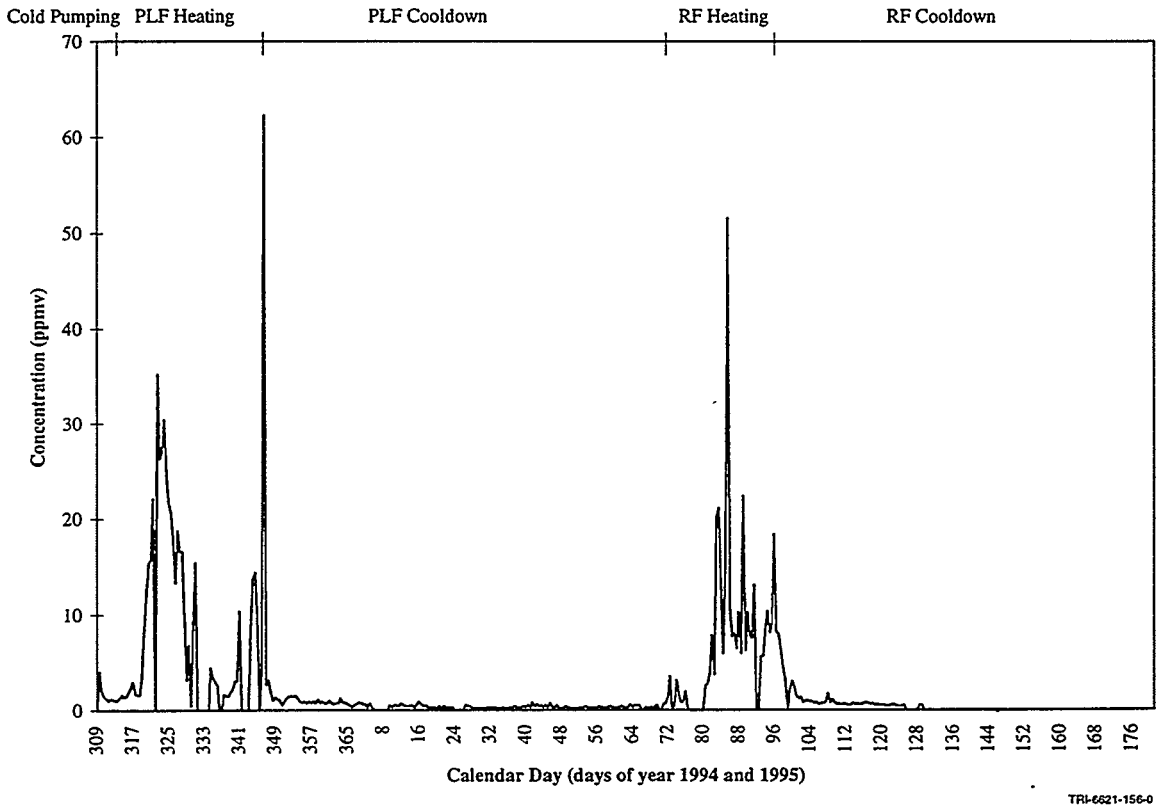

Figure 7-5. Pentane concentration from the extraction manifold.

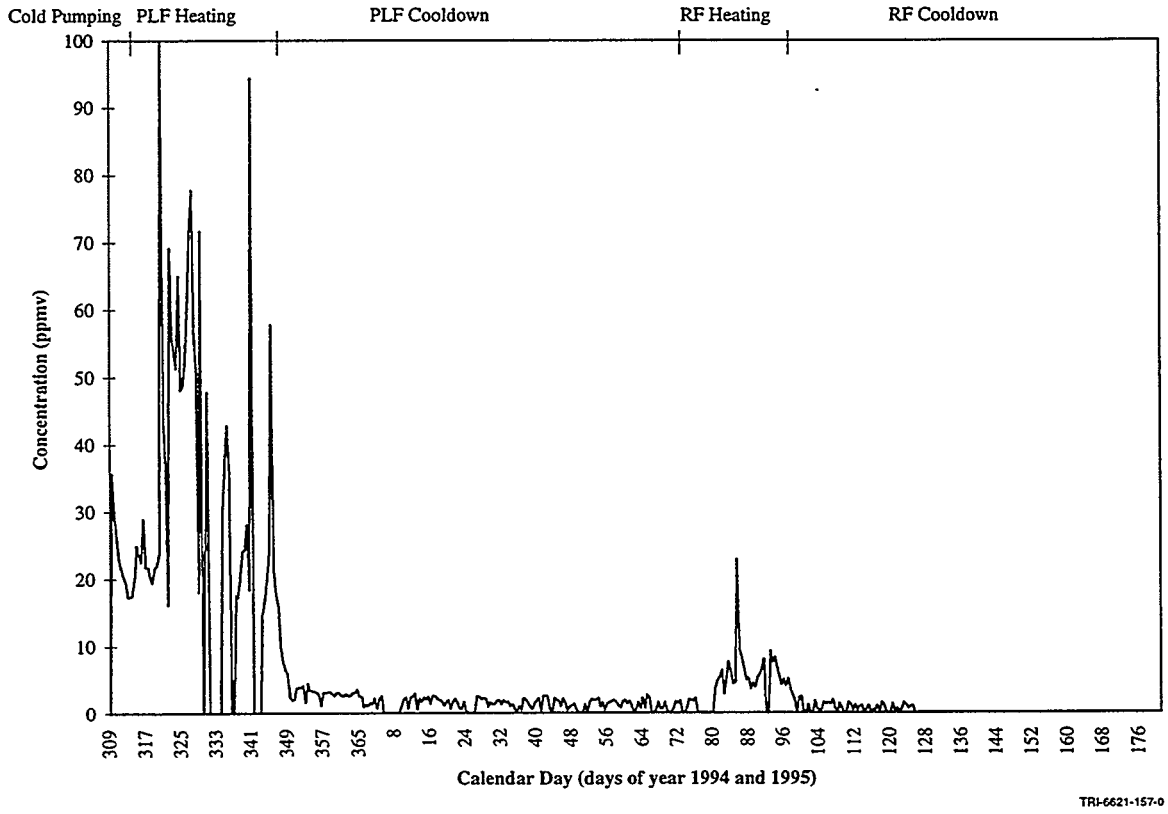

Figure 7-6. Tetrachlorethylene concentration from the extraction manifold.

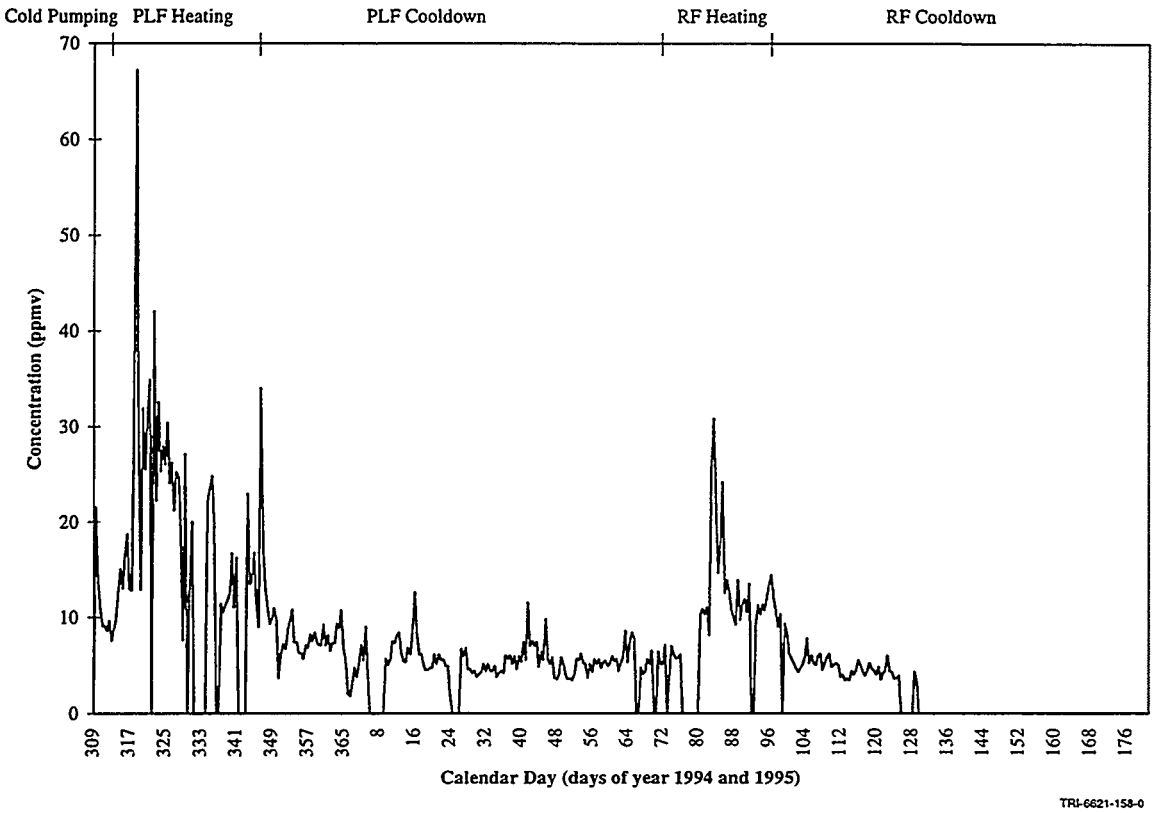

Figure 7-7. Trichlorethane concentration from the extraction manifold.

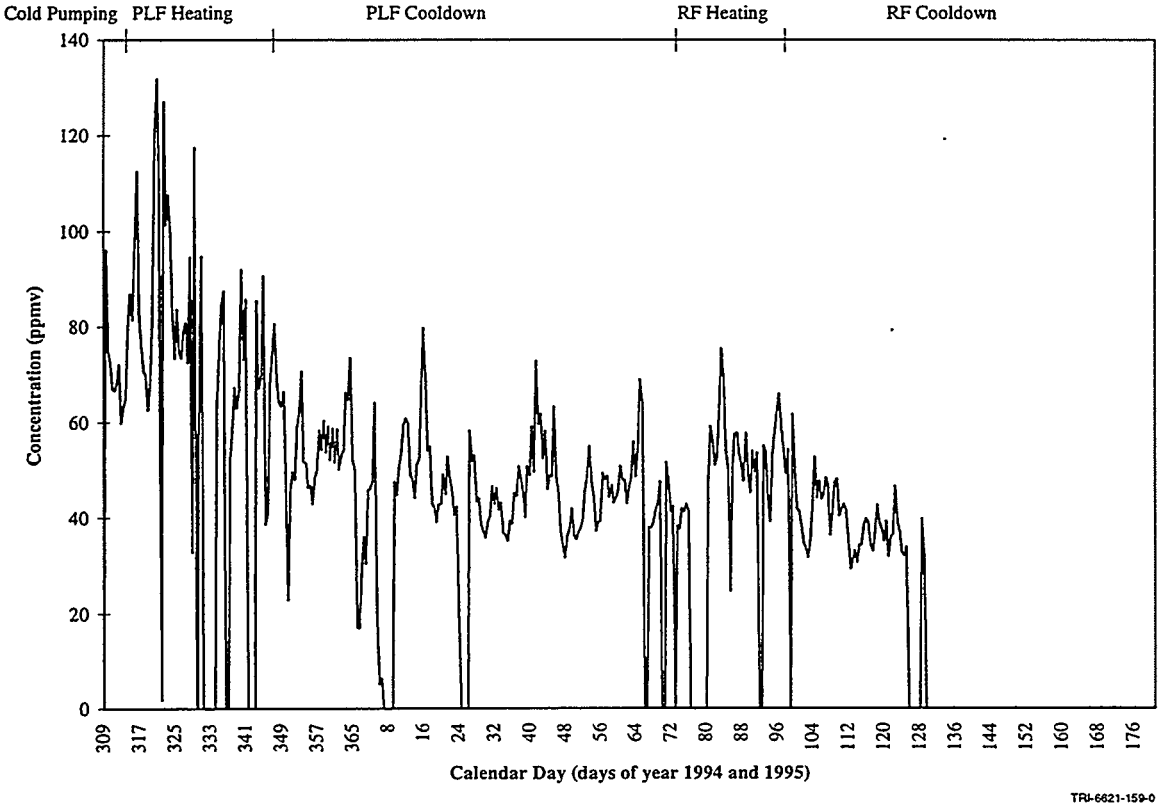

Figure 7-8. Trichloroethylene concentration from the extraction manifold.

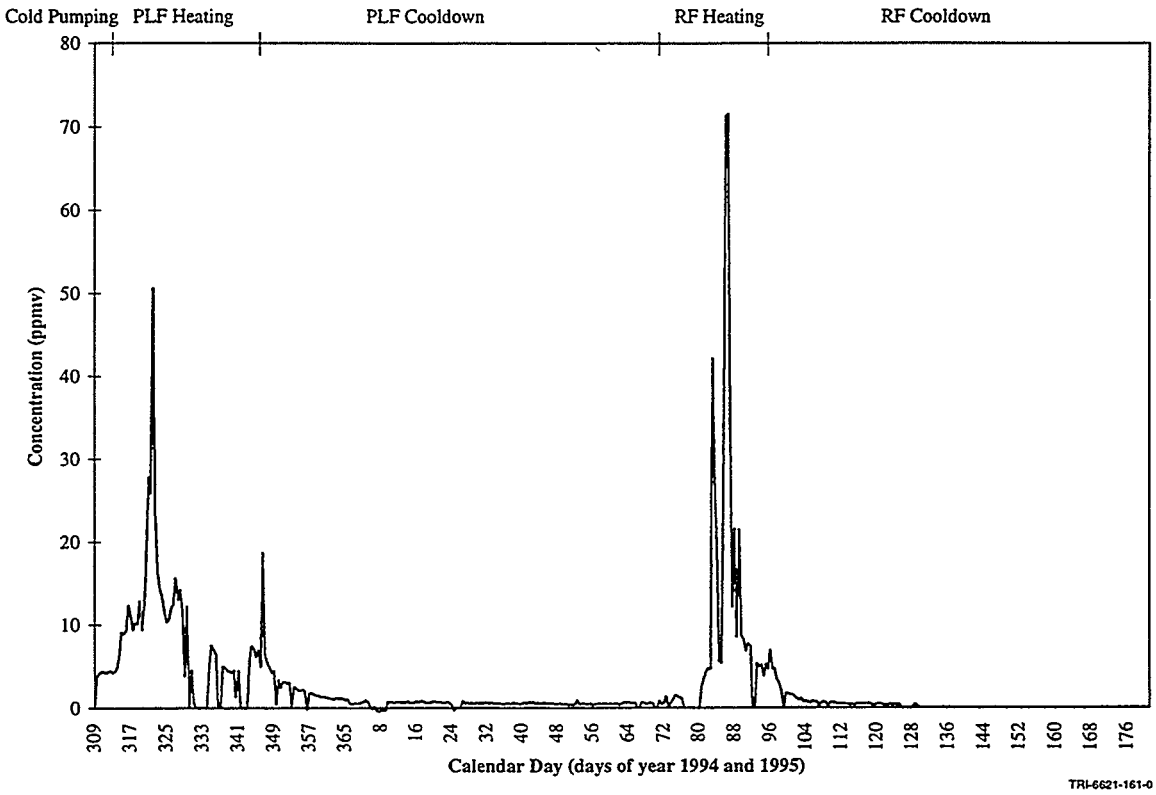

Figure 7-9. Xylene-m/p concentration from the extraction manifold.

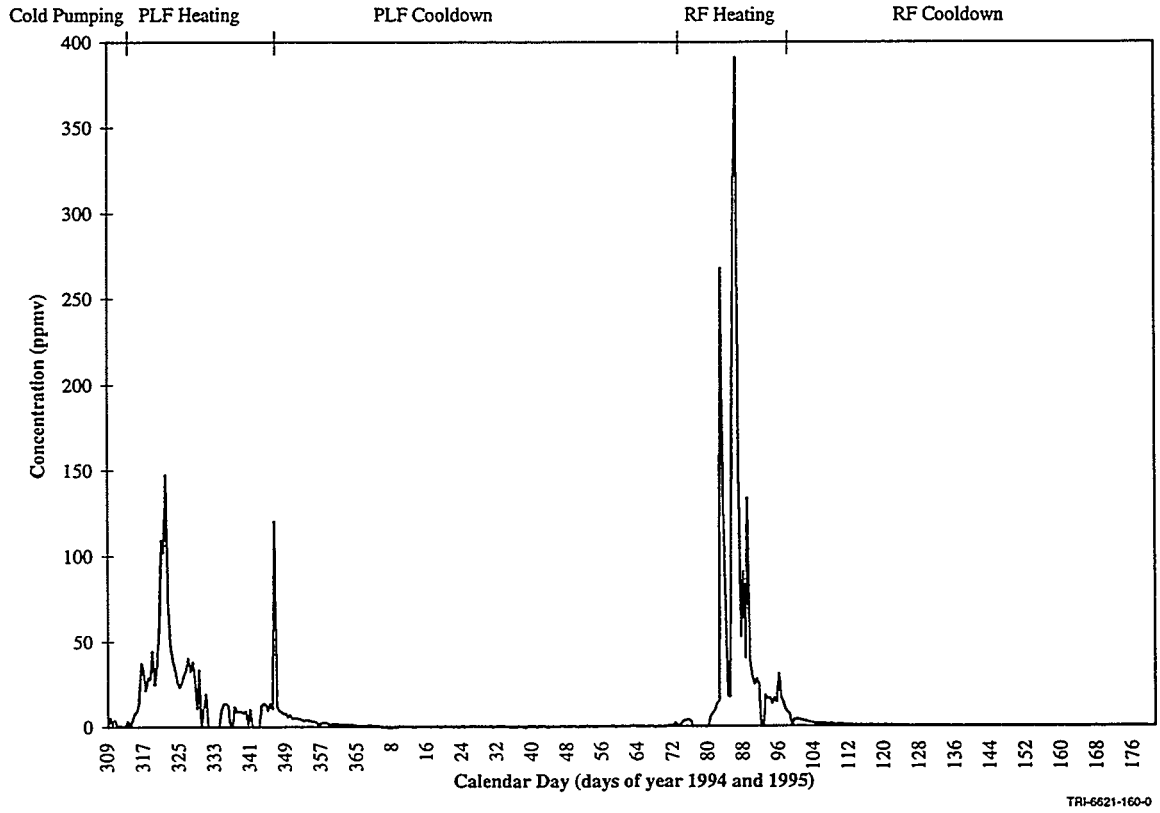

Figure 7-10. Xylene-o concentration from the extraction manifold.

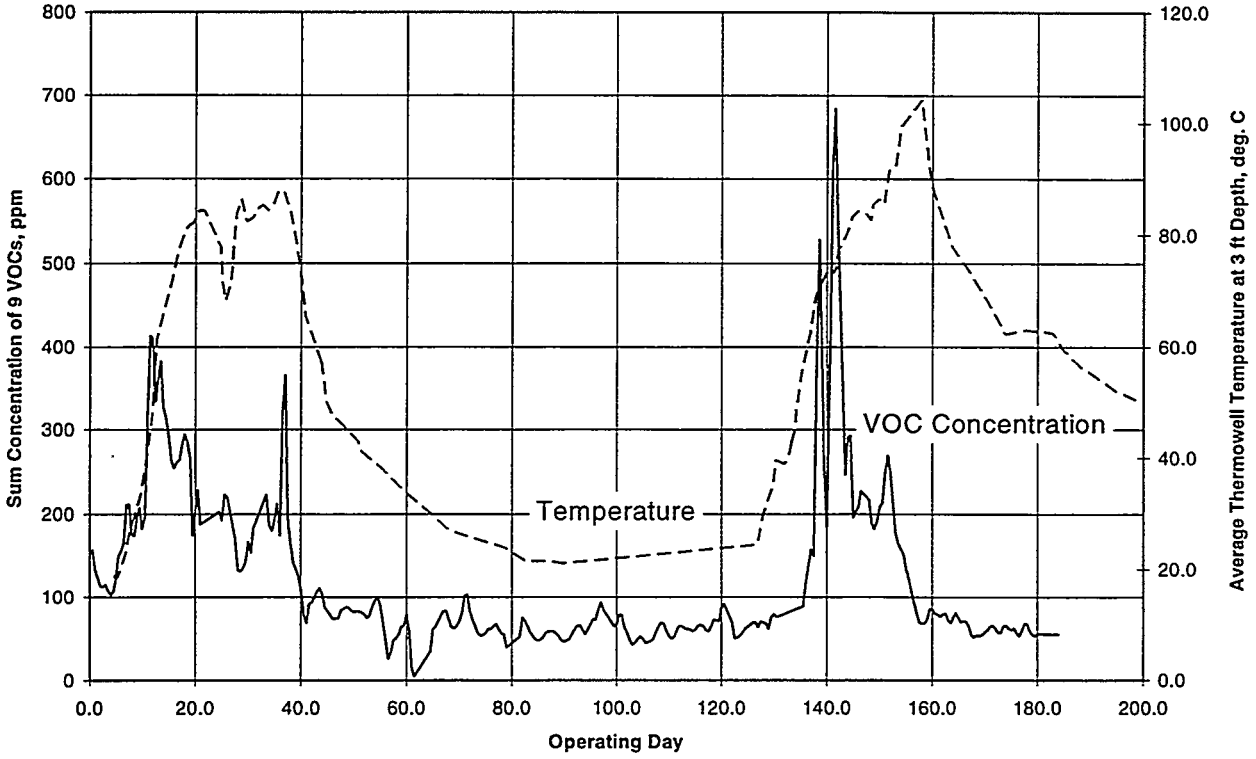

Figure 7-11. Thermowell temperature and VOC concentration at manifold (9 VOCs).

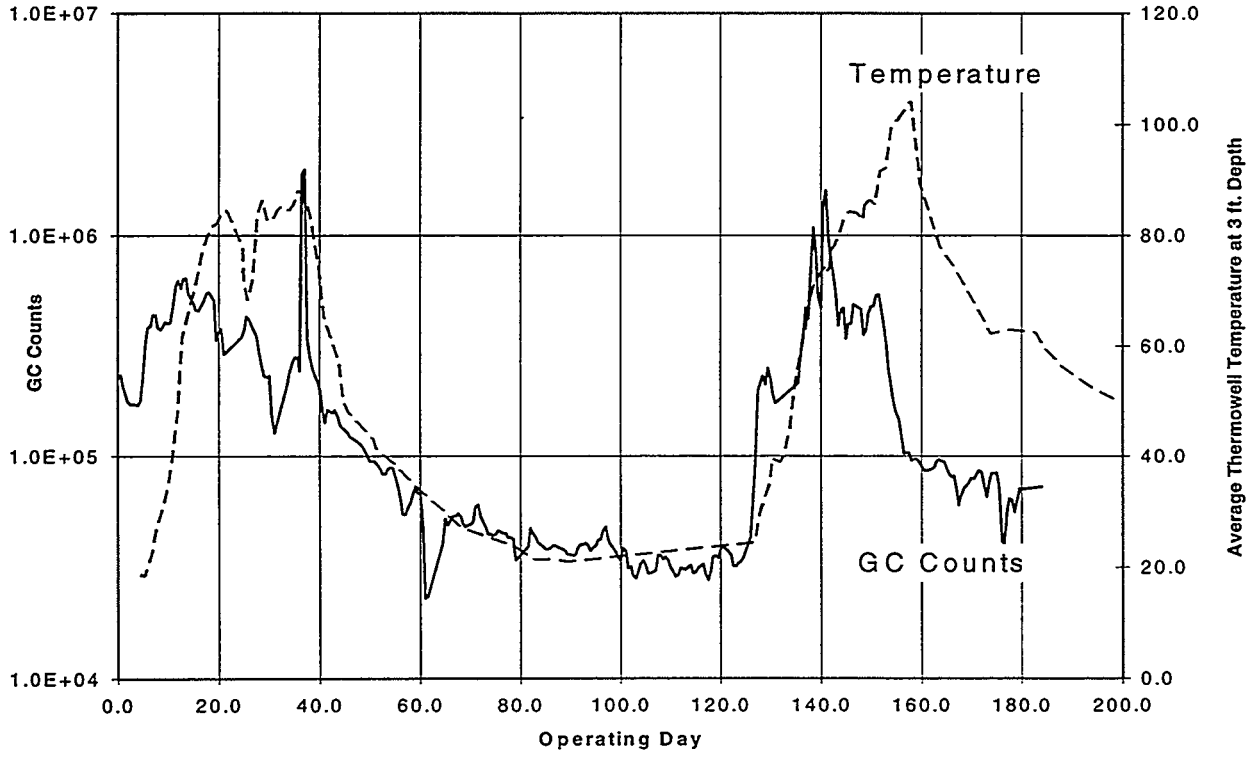

Figure 7-12. Thermowell temperature and total VOC concentration (total GC counts).

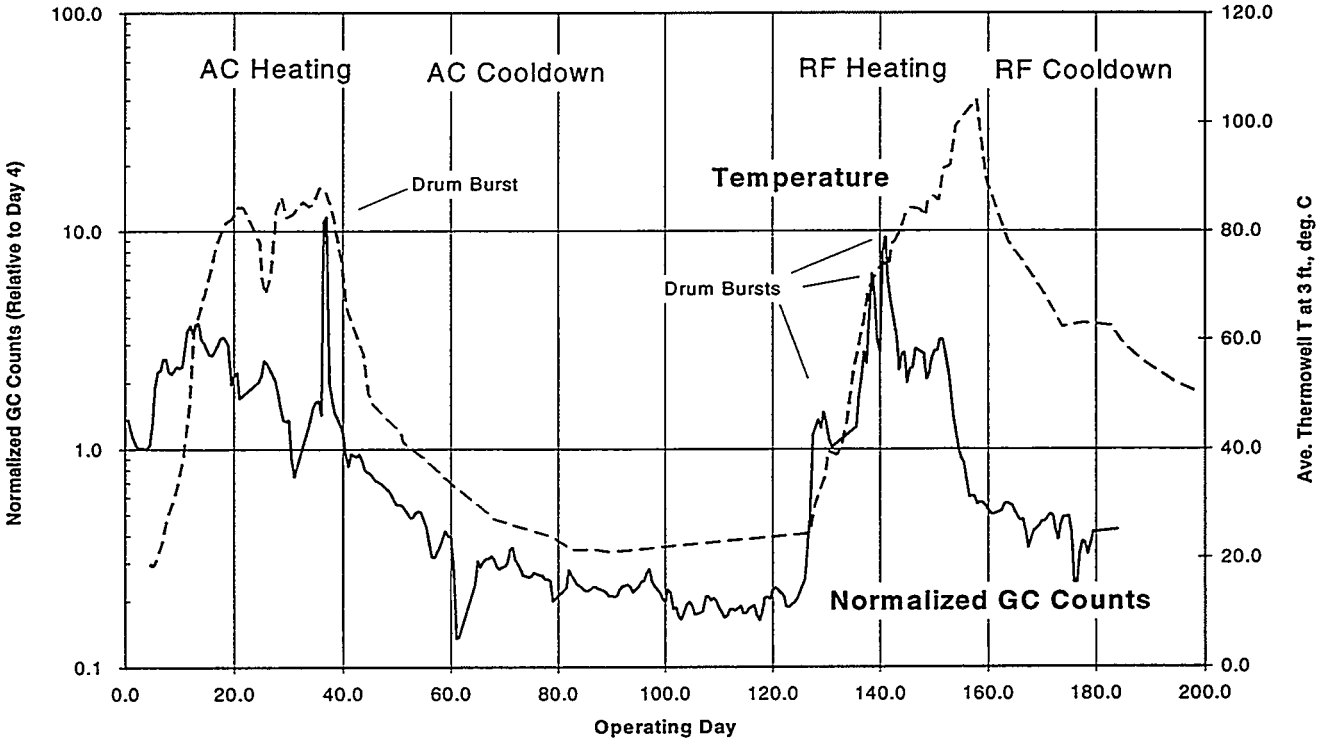

Figure 7-13. Normalized GC counts and thermowell temperature.

can be interpreted as depletion of organic compounds from the soil. The depletion is especially clear after the RF heating, because while the temperatures were still high, the normalized GC counts were much less than 1. The automated data collection system summed the mass removal rate for each monitored compound over the duration of the demonstration. Table 7-2 shows the total mass of monitored contaminants removed.

Table 7-2. Total Mass of Removed Contaminants

Contaminant	Mass Removed (lbs)	Contaminant	Mass Removed (lbs)
DCB	4.88	TCA	18.86
EBZ	4.18	TCE	106.46
FRE	62.06	XMP	16.74
PEN	2.92	X-O	5.22
PCE	21.92		
		Total	243.24

8.0 SUBSURFACE PRESSURE MEASUREMENTS

Results of the subsurface pressure scanning system were used to evaluate vapor containment in the heated zone. Pressure measurements above atmospheric pressure indicated a potential driving force away from the vapor collection wells in the center of the heated zone. Figures 8-1 through 8-12 show the variations in subsurface pressure at each one of the sampled locations (e.g., North side, 15-ft depth). These charts show a trend of 1 to 3 mbar subatmospheric pressure for most of the duration of the testing. The numerous spikes of pressure increases are a consequence of the off-gas treatment system switching to process condensate water through the air stripper. When this happens, the valve to the air extraction manifold is closed 90% for the 15 minute duration of the air stripper cycle. An evaluation of the occurence of superatmospheric pressures showed that these were infrequent and subatmospheric pressures were reestablished quickly after the stripper cycle. Figure 8-1 through 8-12 all show an anomaly for 5 days around day 323. This is due to flooding of the pressure scanning system due to the addition of water during PLF heating. The pressure readings returned to normal when this problem was corrected.

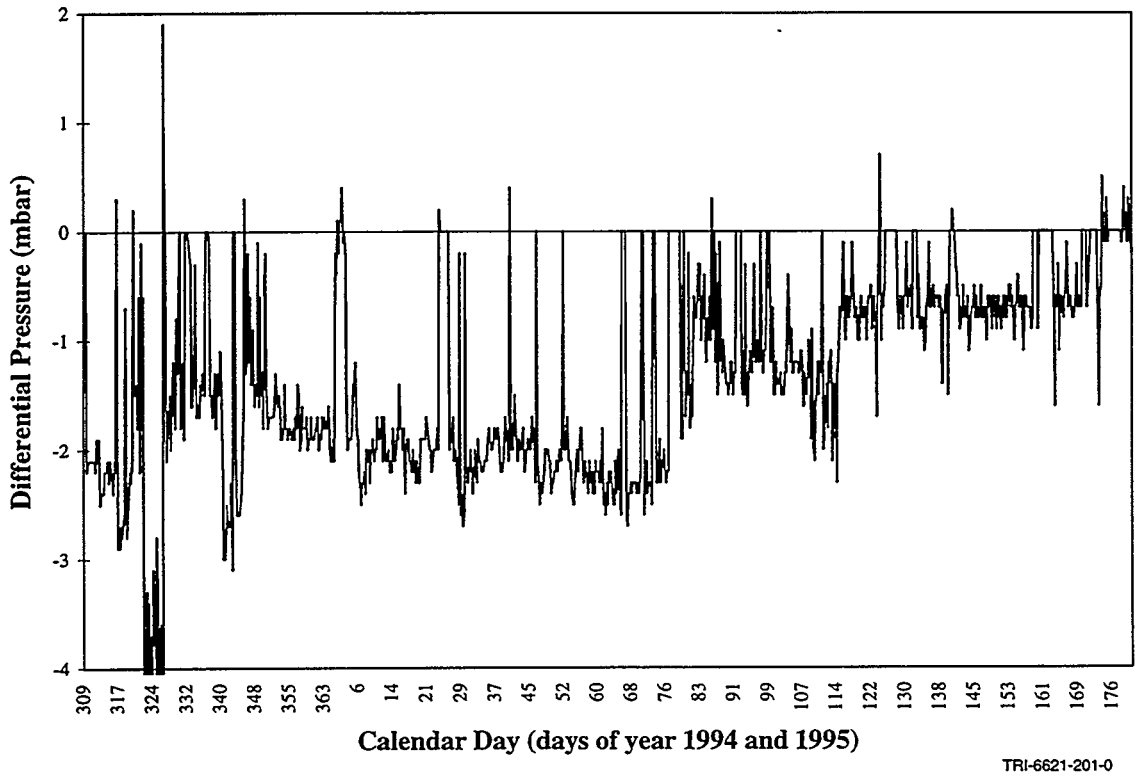

Figure 8-1. Subsurface pressure at North side, 8-ft depth.

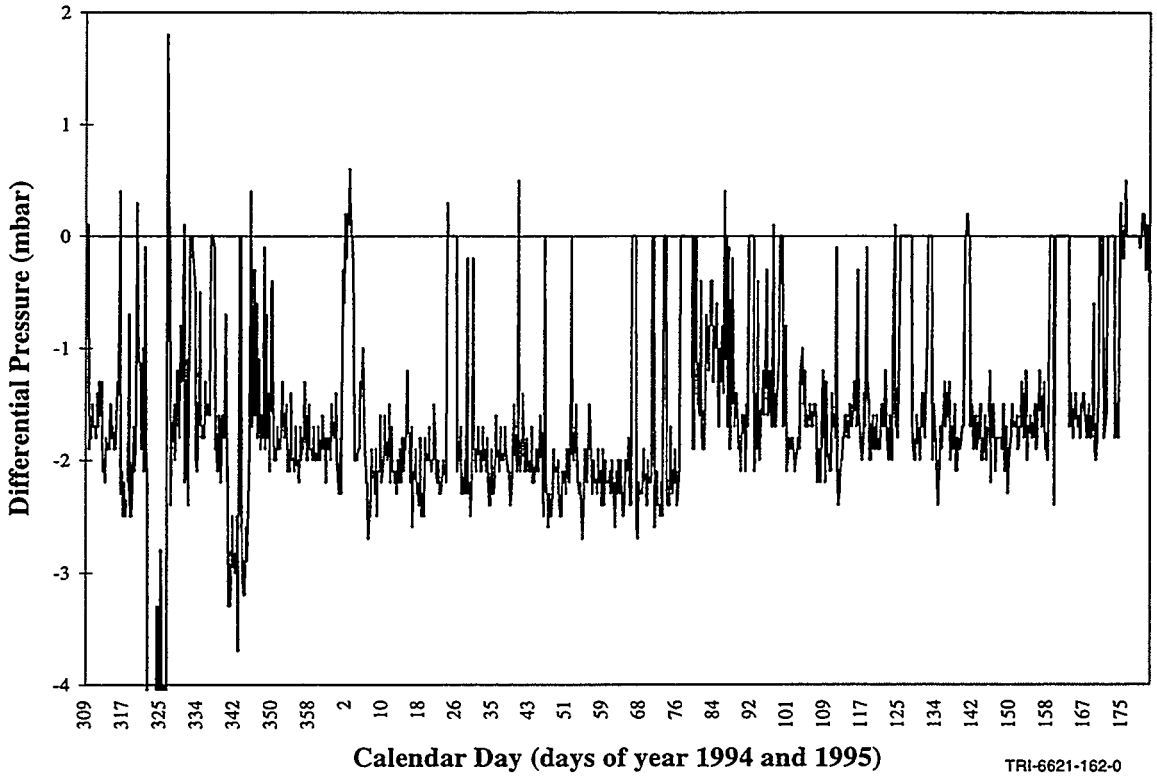

Figure 8-2. Subsurface pressure at North side, 15-ft depth.

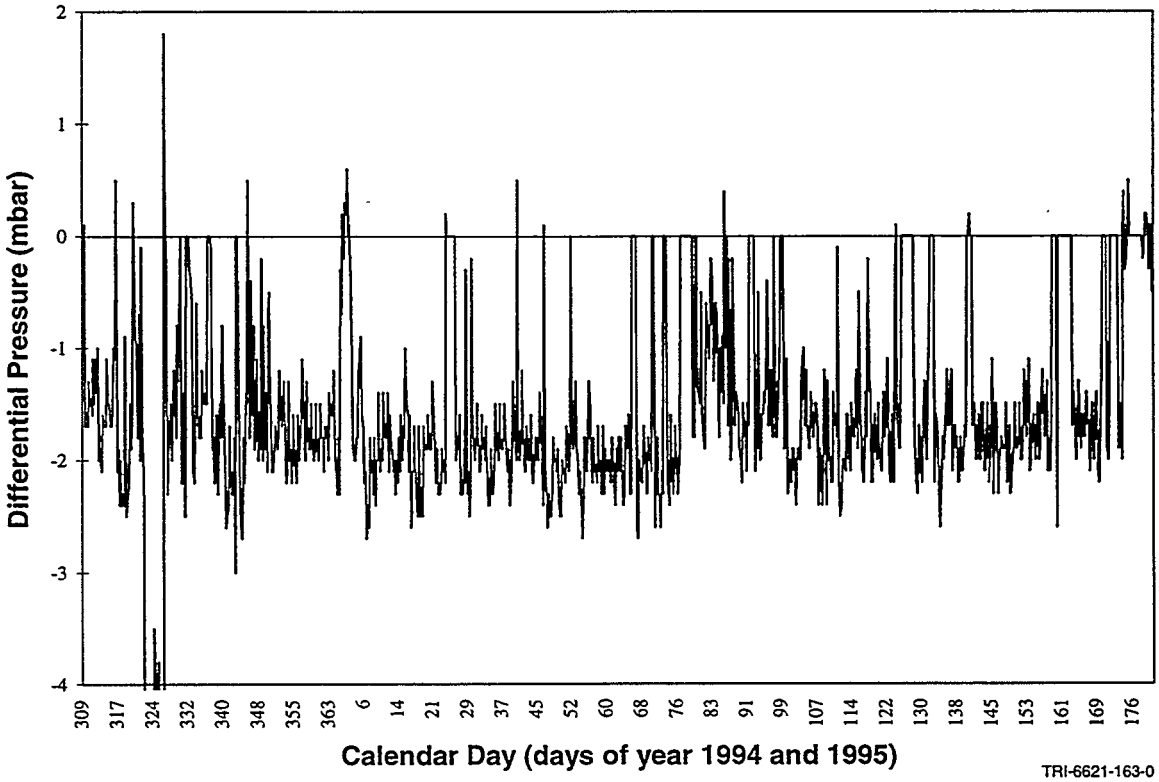

Figure 8-3. Subsurface pressure at North side, 25-ft depth.

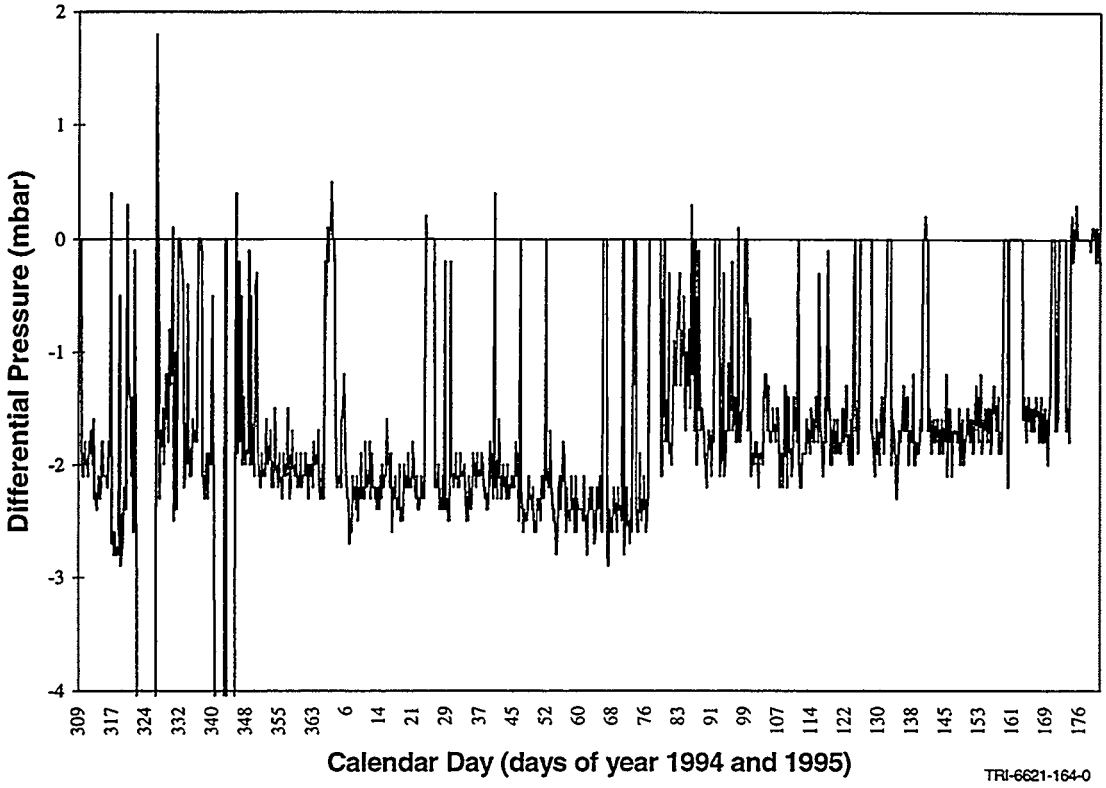

Figure 8-4. Subsurface pressure at South side, 8-ft depth.

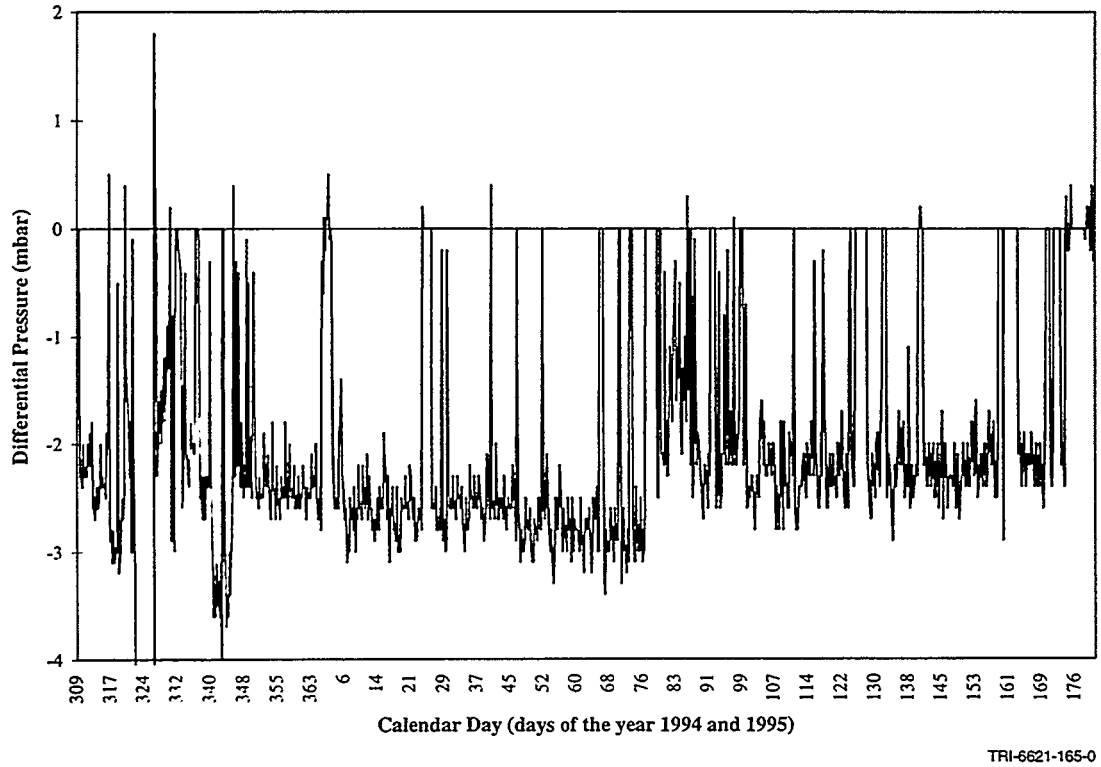

Figure 8-5. Subsurface pressure at South side, 15-ft depth.

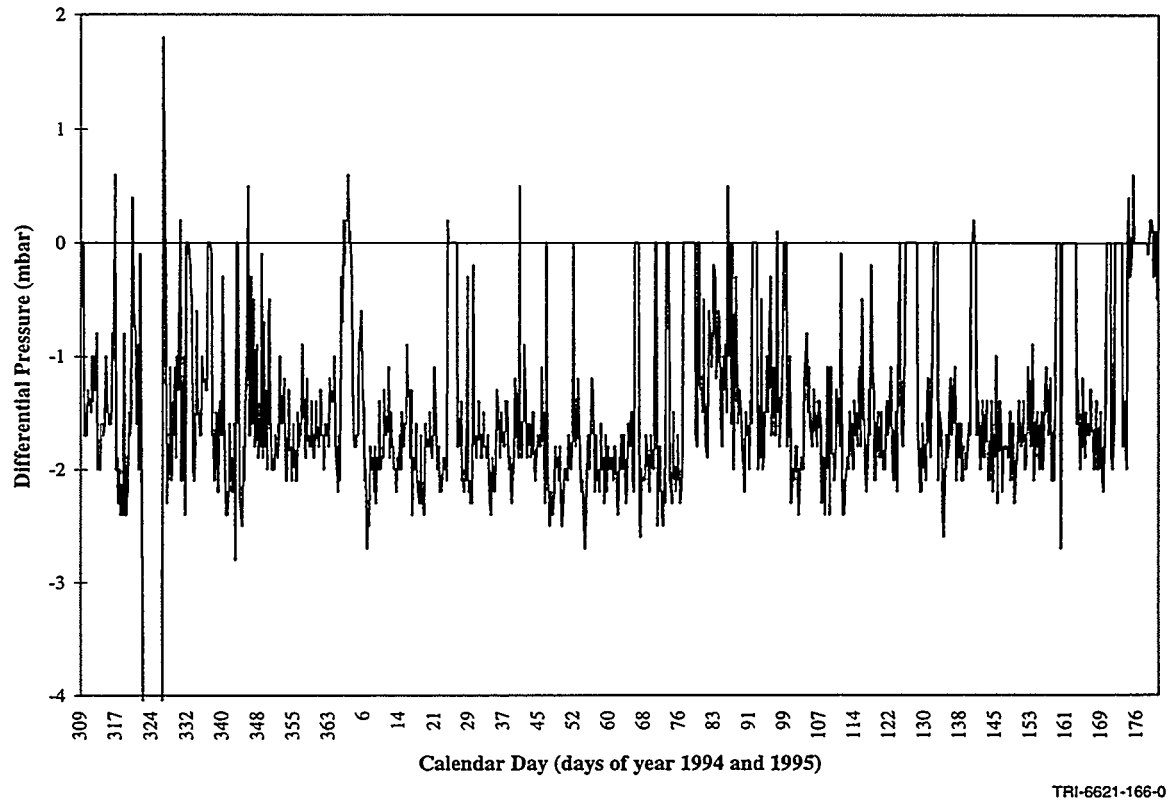

Figure 8-6. Subsurface pressure at South side, 25-ft depth.

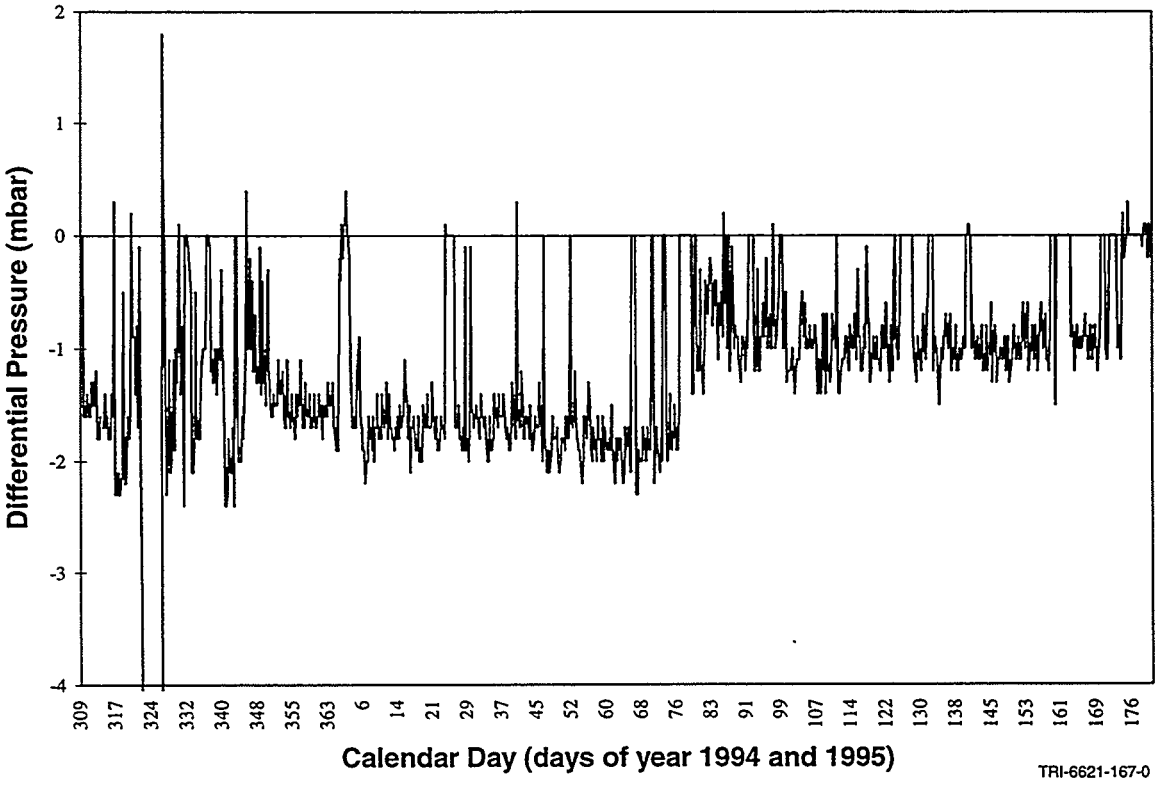

Figure 8-7. Subsurface pressure at West side, 8-ft depth.

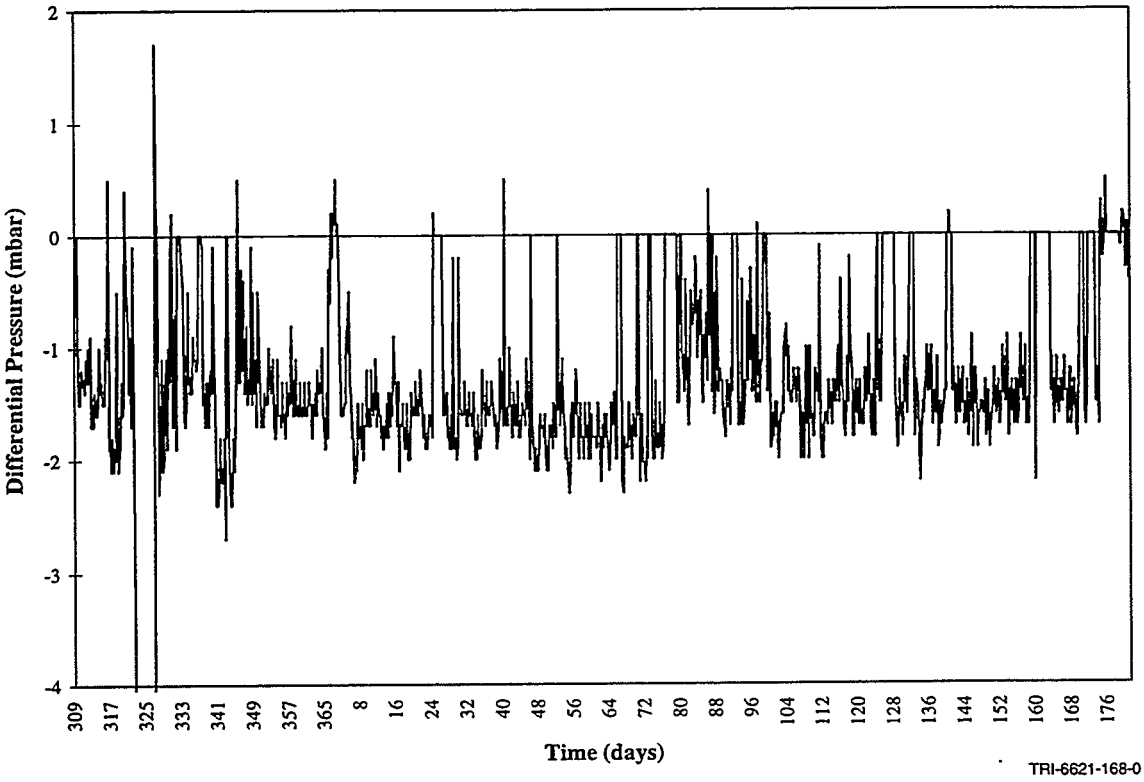

Figure 8-8. Subsurface pressure at West side, 15-ft depth.

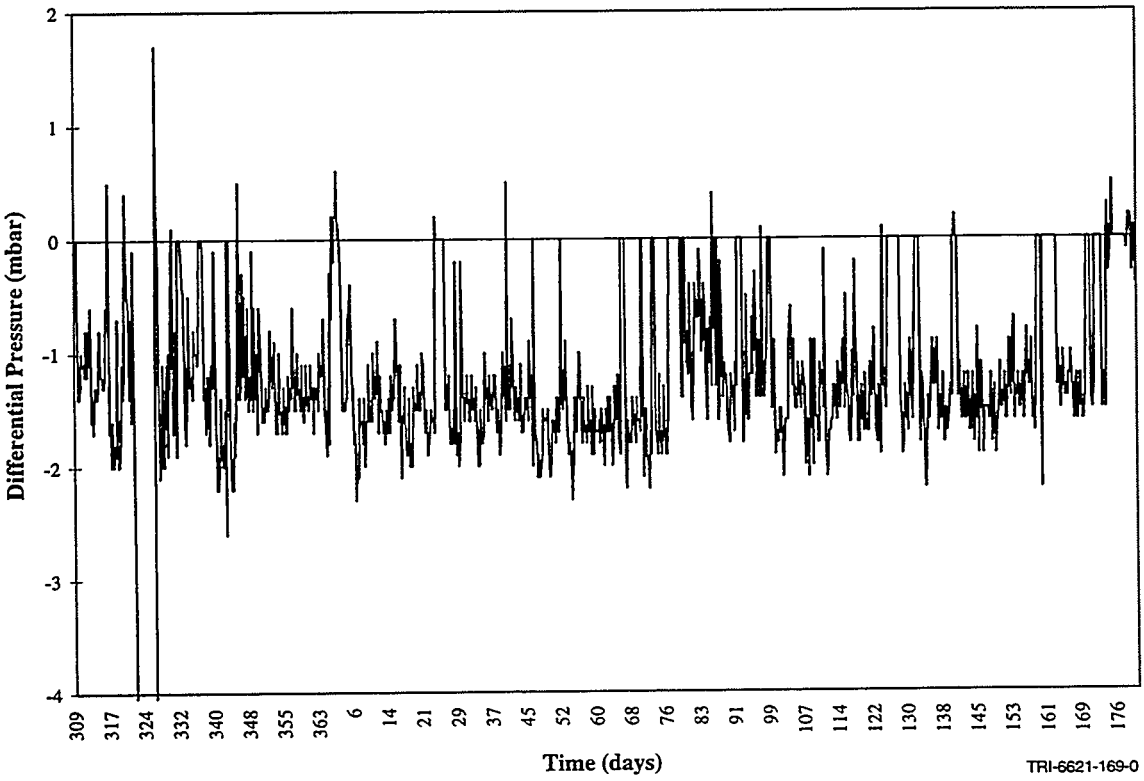

Figure 8-9. Subsurface pressure at West side, 25-ft depth.

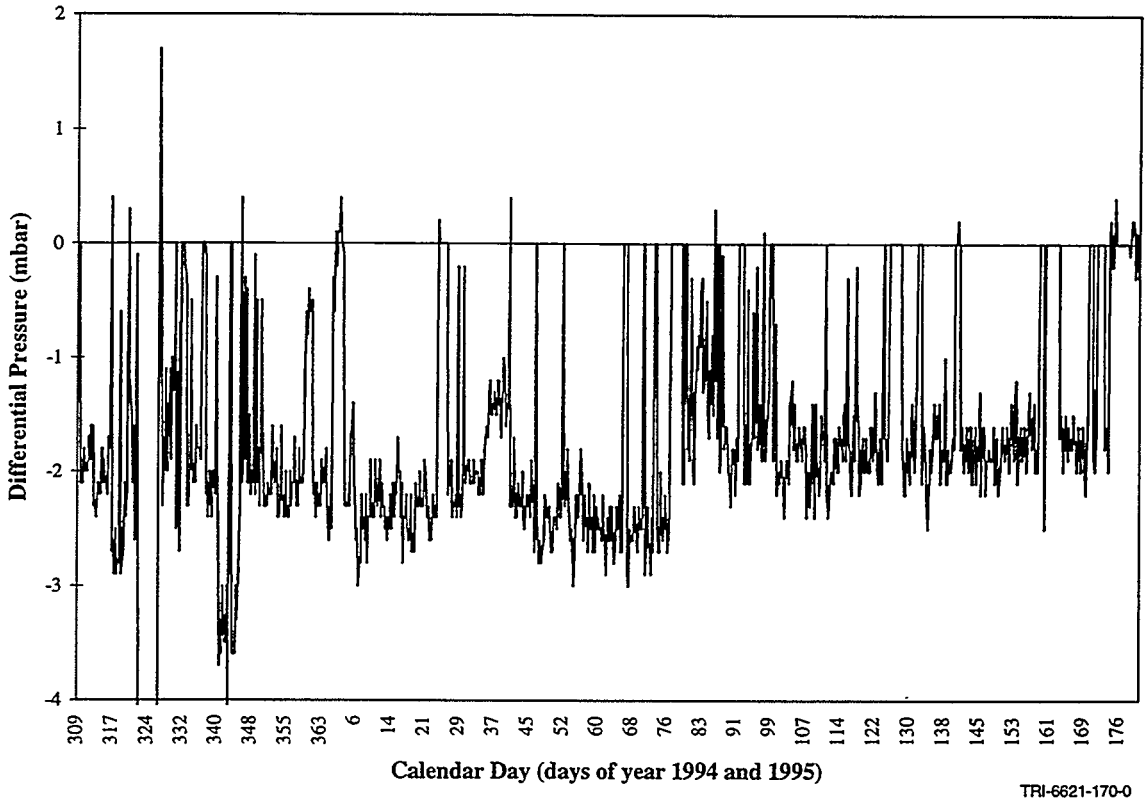

Figure 8-10. Subsurface pressure at East side, 8-ft depth.

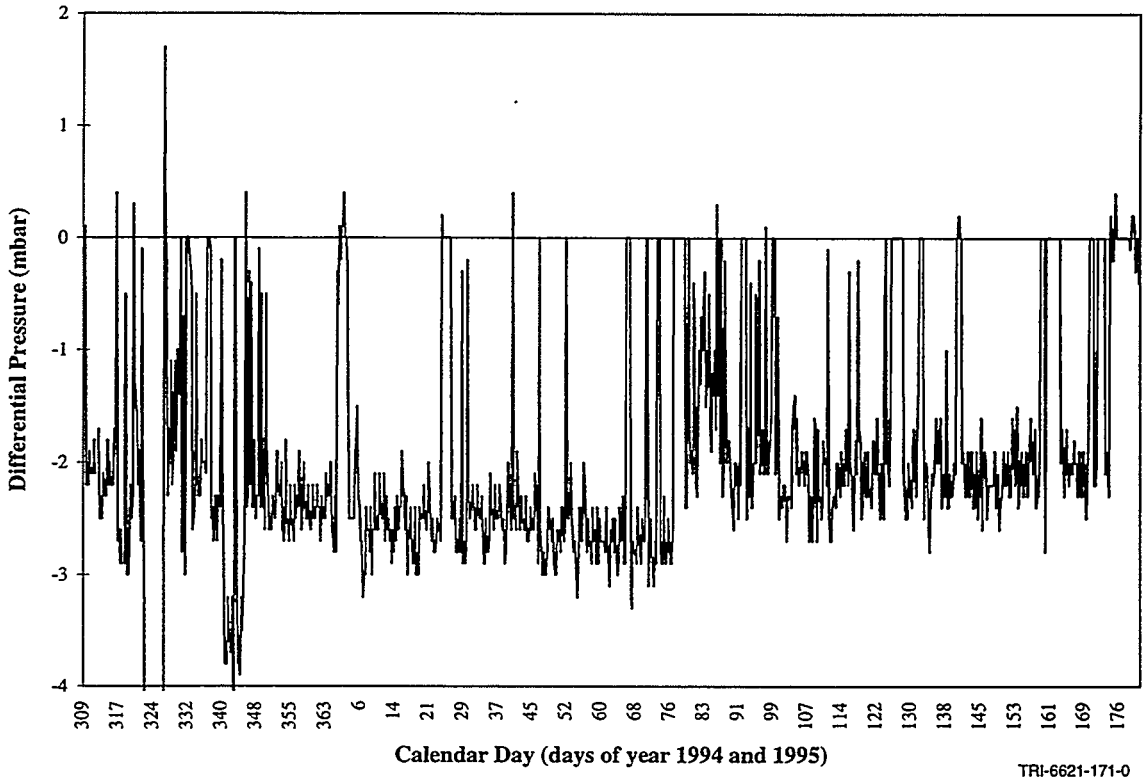

Figure 8-11. Subsurface pressure at East side, 15-ft depth.

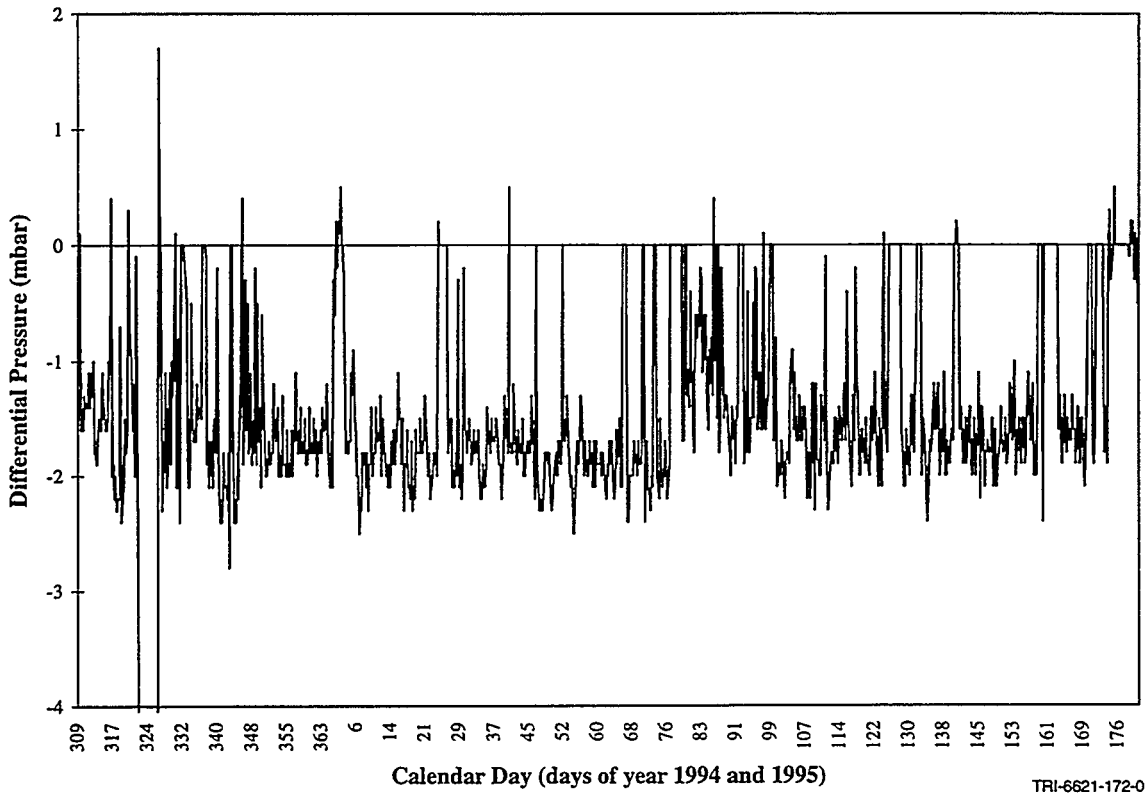

Figure 8-12. Subsurface pressure at East side, 25-ft depth.

This page intentionally left blank.

9.0 AIR PERMEABILITY

9.1 Pre-Test

Permeability data were gathered during the Phase I Site Investigation (See Section 3.2.2 Air Permeability Tests). Table 9-1 shows the results obtained from the SEAMIST™ tool at different depths just prior to the completion of the two extraction wells, TEVES1 and TEVES2. The estimated radius of influence of the 4-in extraction well installed during Phase I was about 40 ft based on previous field experience on other vacuum extraction projects (Johnson 1990).

Table 9-1. Air Permeability Test Results

	Permeability, Darcy	
Depth (ft)	TEVES1	TEVES2
20	5	63
30	11	6
40	11	5
50	17	7
60	16	47
75	7	17

9.2 Permeability During Test

The average permeability of the soil during the TEVES operation can be calculated from the vapor extraction rate and the manifold vacuum using the simple cylindrical model:

$$k = \frac{Q \bullet P_w \bullet \mu \bullet \ln(r_w / r_i)}{L \bullet \pi \bullet (P_w^2 - P_{atm}^2)}$$

where k is the permeability,
L is the length of the withdrawal zone,
μ is the viscosity of the gas,
r_i is the radius of influence,
r_w is the radius of the collector well,
P_w is the pressure in the collector well,
P_{atm} is the atmospheric pressure, and
Q is the flow,
all in consistent units

Using a flow of 138 scfm, P_{atm} of 830 mbar, P_w of 810 mbar, μ of 1.8E-7 mbar-sec, r_w of 4 inches, r_i of 15 ft, and L of 60 ft (total for both wells), the calculated k was 23 darcies. This result is about same the order of magnitude as the SEAMIST™ determinations prior to the test.

9.3 Post-Test Permeabilities

The SEAMIST™ system was used to determine permeabilities before and after the TEVES operation. Table 9-2 shows the pre-test/post-test comparison of permeabilities determined using SEAMIST™. In general, the post-test permeabilities were somewhat smaller than the pre-test permeabilities, which is consistent with observations of subsidence discussed in Section 11.1.

Table 9-2. Pre- and Post-Test Air Permeability Results

	Pre-Test Permeability, Darcy	Post-Test Permeability, Darcy
	Borehole B1	Boreholes PT5
Depth, ft		
5	28	9
10	20	4
15	23	5
25	7	2
35	22	12
45	5	2
55	13	7
	Borehole B4	Borehole PT6
Depth, ft		
5	56	N/A
10	27	30
15	30	13
25	6	2
35	28	17
45	6	5
55	25	185

However, there were significant technical problems achieving a good borehole seal with the SEAMIST™ liner in the post-test survey. This prevents a direct comparison to the pre-test data and making specific conclusions regarding changes in soil air permeability as a result of the TEVES operation.

10.0 PRE-TEST AND POST-TEST SOIL AND SOIL GAS SAMPLING/ANALYSIS

10.1 Pre-Test and Post-Test Soil Analysis

Table E-1 in Appendix E shows a comparison of the pre-test and post-test soil analyses for the TEVES site. The soil was analyzed for various organic compounds in the standard EPA protocols (Table 3-1). Figure 10-1 shows the locations of the pre-test and post-test boreholes. Table 10-1 shows the comparison of TCO analysis for the pre-test boreholes and the corresponding post-test boreholes at different depths. The total chromatographable organic (TCO) varied widely at the different borehole locations and depths. The results indicate that there was not much difference between pre-test and post-test soil TCO concentrations in the A-row boreholes, and very significant decreases in concentrations in the B-row boreholes, from 83 to 99.9% for corresponding boreholes. This is consistent with the significantly higher temperatures in the center of the heated zone. The post-test increases can be explained as incomplete removal of all contamination since the target end temperature of 200°C was not achieved because of the unplanned cooldown period after completion of the PLF heating period. The average percent removal, determined by averaging the TCO before and after treatment, was 84.1%.

Table 10-1. Pre-Test and Post-Test Soil Analysis Comparison.

Total Chromatographable Organics				
Pre-Test		Post-Test		
Location, Depth, ft	Conc., mg/kg	Conc., mg/kg	Location, Depth ft	% Removal
Ground Row				
A3,10	13	4.4	PT3,10	66.2
A3,15	2.1	3.8	PT3,15	-81.0
A6,10	3.5	170	PT4,10	-4757.1
A6,25	2.8	ND	PT4,25	ND
Center Row				
B1,5	11,000	5.3	PT5,5	99.95
B1,12	2,900	1800	PT5,10	37.9
B1,15	190	510	PT5,15	-168.4
B1,25	4.2	79	PT5,25	-1781.0
B1,45	14	2.2	PT5,45	84.3
B1,55	19	2.3	PT5,55	87.9
B4,5	11,000	23	PT6,5	99.79
B4,10	9300	2600	PT6,10	72.0
B4,25	45	270	PT6,25	-500.0
B4,55	4.2	ND	PT6,55	ND
Average	2874	456		84.1

ND - Non-Detect

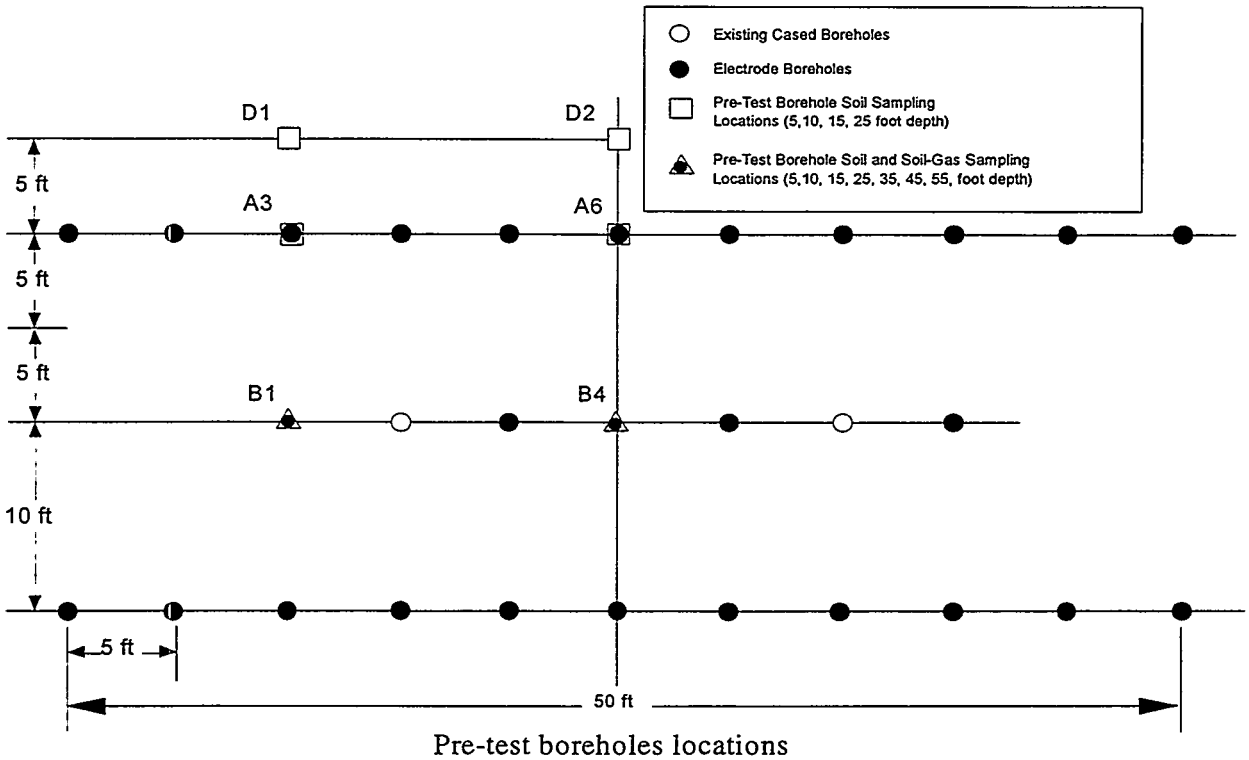

Pre-test boreholes locations

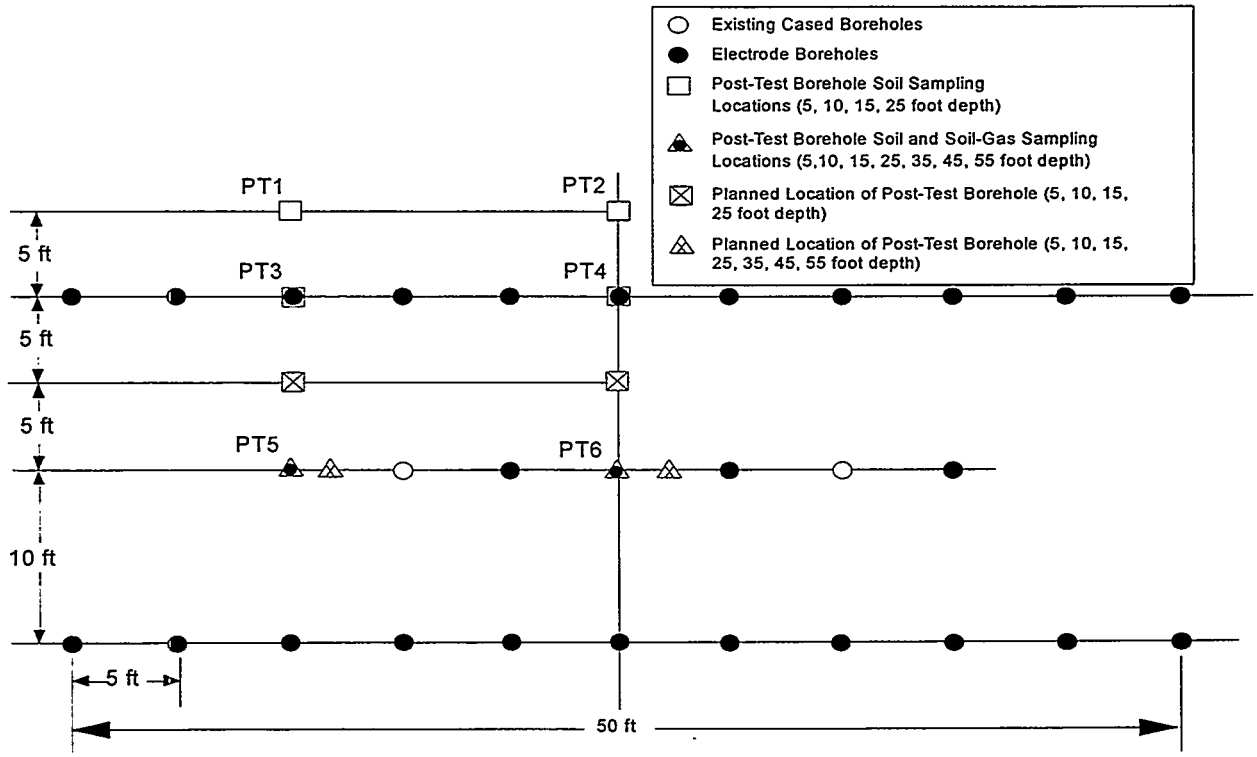

Post-test boreholes locations

Figure 10-1. Pre- and post-test borehole locations.

10.2 Pre-Test and Post-Test Soil Gas Analysis

Table E-2 in Appendix E gives a comparison of the pre-test to post-test gas analysis at boreholes in the center row. The samples were analyzed by EPA compendium method, TO-14. Tables 10.2 and 10.3 give the comparisons for Benzene and TCE, respectively, at the pre-test and post-test boreholes. The contaminant concentrations in the post-test boreholes are lower than in the pre-test boreholes in general. In cases where concentrations are higher, it is postulated that the vacuum extraction system pulled in contaminants from outside of the heated zone during the cooldown period. Nevertheless, it is the contaminant concentration in the soil rather than in the soil vapor that is more indicative of the effectiveness of the decontamination using thermal enhancement methods.

Table 10-2. Comparison of Pre-Test and Post-Test Benzene Concentrations in Soil-Gas

Pre-Test Location	Depth (ft)	Concentration (ppm)	Post-Test Location	Concentration (ppm)
B1	5	1.5	PT5	0.26
	10	0.57		0.22
	15	0.44		0.26
	45	0.59		0.30
	55	0.53		0.38
B4	5	14	PT6	0.066
	10	33		
	15	4.0		0.1
	55	0.15		0.43

Table 10-3. Pre-Test and Post-Test Concentrations of TCE in Soil Vapor

Pre-Test Location	Depth (ft)	Concentration (ppm)	Post-Test Location	Concentration (ppm)
B1	5	110	PT5	29
	10	42		30
	15	25		15
	25	22		47
	35	15		51
	45	16		40
	55	35		0.45
B4	10	47	PT6	0.37
	15	11		6.7
	15	12		8.9
	25	14		2.2
	35	12		40
	45	15		20
	55	2.8		47

11.0 POST-TEST EXCAVATION AND EVALUATION

On July 19, 1995, disassembly of the energy feed, temperature measurement, and vacuum extraction system was completed. The RF shield was lifted off the outer row electrode supports and set aside.

11.1 Soil Subsidence

Visual inspection showed that the soil beneath the vapor barrier had subsided. Removal of the vapor barrier showed that the central portion of the treatment zone had subsided with an oval shape nearly reaching the outer row electrodes and extending to the ends of the center row electrodes. Figure 11-1 shows the dimensions of the subsidence with the approximate depths across several transects. Figure 11-2 shows a picture from the short-side view.

11.2 Electrode Removal

The outer row electrodes were easily removed with the use of a small crane. The copper pipe bus bar was cut to facilitate removal of the center row electrodes. Electrode B4 could not be pulled after several rigging methods and was left for exploration during the excavation effort. Electrode B5 was found to have melted about 2 ft from the top and about 2 inches below the upper thermocouple fitting. All other center row electrodes were removed and appeared in good condition.

11.3 Buried Metal Object Excavation Exploration

Pre-test evaluations with a magnetometer towed array showed that there was a group of buried metal objects in the south-east quadrant of the treatment zone (NMSU 1996). Figure 11-3 shows the results of an enhanced magnetometer evaluation and the likely locations of buried metal objects. A permit condition stipulated in the RCRA RD&D Permit for the project (NMED 1994) called for an exploratory excavation effort to determine whether there were any containers that continued to have liquid waste after completion of the demonstration. The exploration work was performed with a small backhoe with a reach of about 10 ft. Excavation began in the southeast corner and proceeded west to approximately the midpoint of the treatment zone. A variety of solid waste materials were found in the treatment zone along this path including items looking like large rolls of film and glass containers. One metal drum (about 55 gal size) located in the extreme southeast corner was found to still contain liquid materials. This material was a light-brown liquid with a viscosity similar to water. From the mid-point, the exploration moved north across the pit. At the north pit boundary, several metal objects

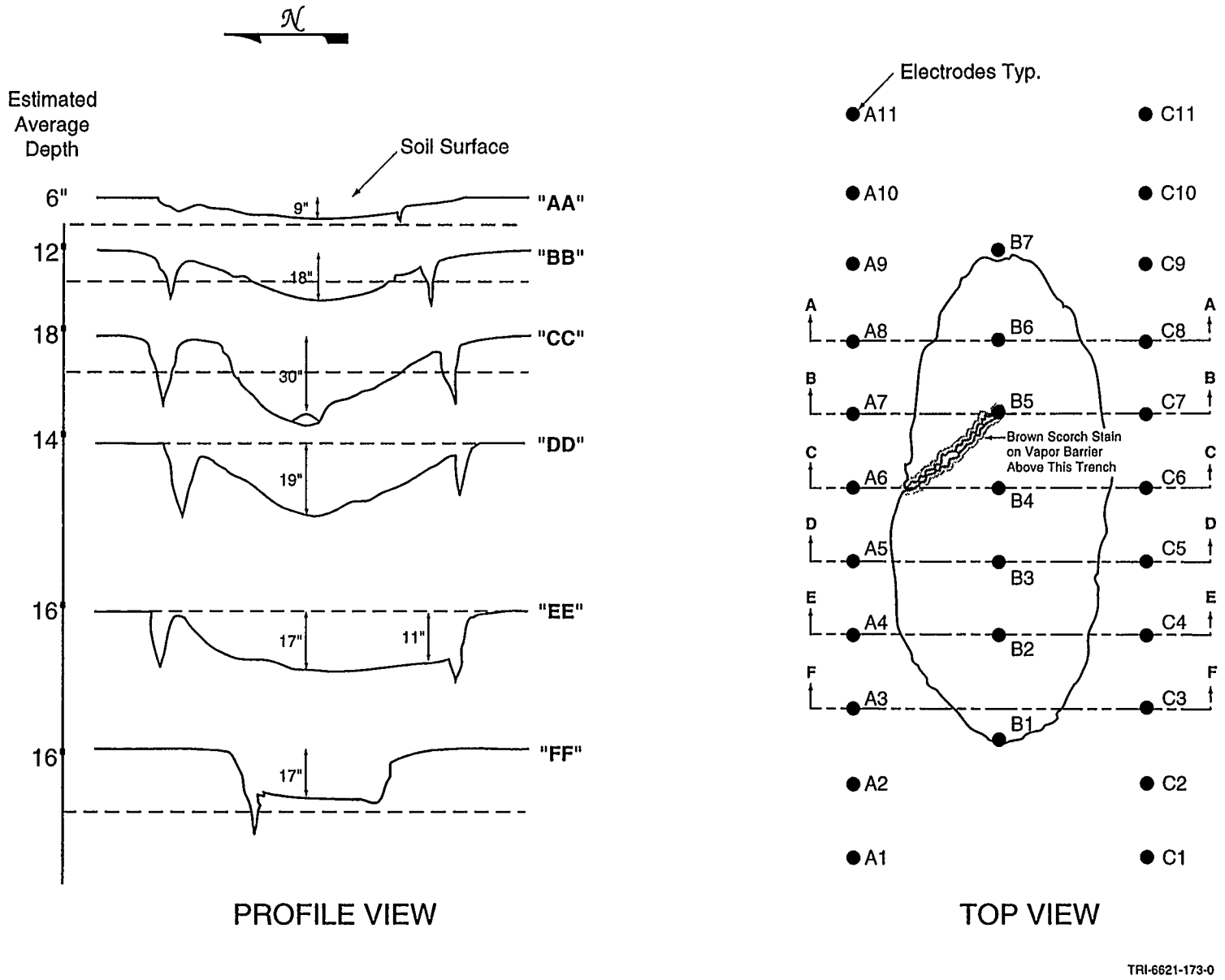

Figure 11-1. Dimensions of subsidence with approximate depths across several transects.

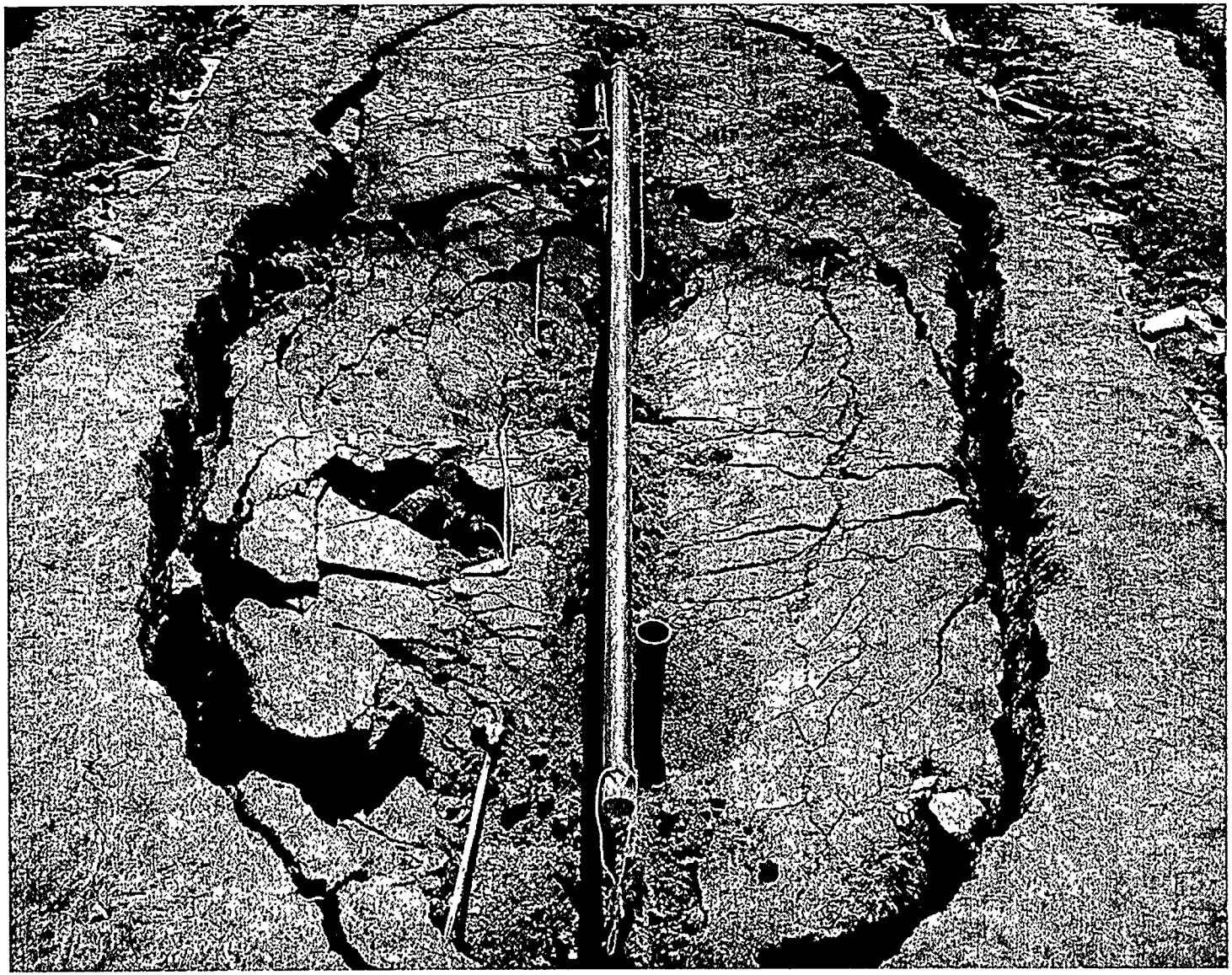

ET-716-0

Figure 11-2. Photograph of Subsidence Zone.

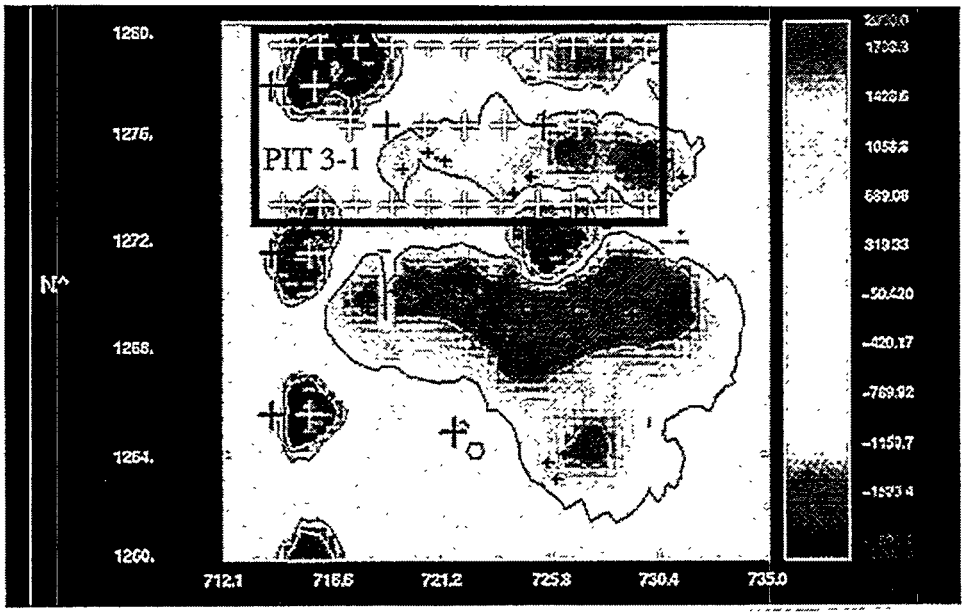

Figure 11-3. Enhanced magnetometer evaluation of the treatment zone and likely locations of buried metal objects.

(about 55 gallon size) were encountered but none were found that contained any liquids. The container with liquid wastes in the southeast corner was found in a location that was very poorly heated (see Figures 4-10 to 4-12 and 5-9 to 5-11). The density of buried metal objects in the southeast corner of the treatment zone was much lower than expected, based on the magnetometer survey results.

During the exploration work, the soil in the very center of the treatment zone was found to be powder dry as a result of the soil heating and vacuum extraction removal of soil contaminants and moisture. Soil with such low moisture content has little strength and may likely have settled into voids in the uncompacted disposal cell leading to the subsidence noted on the surface.

12.0 COST EVALUATION

Projected costs on a unit volume of treated soil basis is presented for the TEVES in this section. The SITE guidelines were used (Evans 1990) in order to have a comparable cost basis with other innovative technologies. Information gathered from the demonstration were used for the twelve cost categories. Implementation proceed in a modular fashion by repeating the treatment on adjacent volumes of soil in series until the entire area has been treated. While the electricity and site operations costs are linear with the size of the project (either by volume, number of modules or time), the electrode installation and operations setup costs were estimated with fractional cost factors for subsequent modules. For electrode installation, a fraction of 0.66 is used for drilling and a fraction of 0.1 is used for piping material costs for modules subsequent to the first module. For the setup cost of other components, a fraction of 0.5 was used for subsequent modules. A comparison to the baseline technology of excavation and thermal treatment will be made. Other costs for excavation and treatment are also included in this section for comparison.

12.1 TEVES Cost Estimated Using SITE Method

For innovative technologies, the Superfund Innovative Technologies Evaluation (SITE) program uses a twelve category format for evaluating projected treatment costs (Evans 1990). This format is also used for TEVES in comparison with other innovative technologies and put into a unit volume basis. In the SITE program, total treatment cost is evaluated without accounting for site characterization and pilot studies, which are acknowledged to be substantial cost factors. To compare TEVES with the other innovative technologies, site characterization and pilot study costs will not be included.

The TEVES cost estimates are based upon 6,000 yd^3 of volume treated 2,000 yd^3 at a time. Each "batch" will require 2 months so that 6 months of operation will be required. Each PLF and RF unit will have a 200 kW capacity.

12.1.1 Site Preparation

The site preparation includes well drilling and preparation, building enclosure, utility connections, and system installation. These are summarized in Table 12–1. The assumptions are:

- $1,300/extraction well.
- 2 wells per 1,000 yd^3 of treated soil.
- 8 man-weeks required for installation at $50/manhour.

Table 12-1. TEVES Site Preparation Cost

Item	Cost	Cost/yd^3
Extraction Wells	15,600	2.60
Building Enclosure	10,000	1.67
Utility Connections	10,000	1.67
System Installation (Exclusively Electrodes)	16,000	2.67
Total Site Preparation	51,600	8.61

12.1.2 Permitting

Permit preparation took about 1 man-month for the TEVES project. The primary uncertainty in determining cost is due to the amount of interaction with regulators required to allow the permit. An amount of $30,000 is included for permitting. Distributed over 6,000 yd^3, this amounts to $5/yd^3.

12.1.3 Installed Capital Cost

A summary of the installed capital cost for TEVES is given below (Table 12-2). The assumptions for the capital cost calculations are the following:

- 5 year amortization (for PLF, RF and offgas treatment units) at 7% interest rate. Annuity Factor = 0.244. There is one project per year.
- No amortization for piping.
- Electrode installation is not amortized since the cost is incurred at each site.

Total capital cost is $27.50/yd^3. With the addition of $277,890 ($46.32/yd^3) for installation of electrodes, the total installed capital cost is $73.82/yd^3.

Table 12-2. TEVES Capital Cost

Item	Cost	Cost/yd^3
PLF Transformer	60,000	2.44
RF Transmitter	200,000	8.14
Offgas Treatment	175,000	7.12
Piping	10,000	1.67
Electrodes and Installation	277,890	46.32
Total Installed Capital Cost		65.69

12.1.4 Startup

The assumptions for startup costs are the following:

- 100 man-hours at $50/man-hour = $5,000.
- Insurance and taxes taken as 10% of annualized capital equipment cost - $15,730. Note: since the electrode installation costs already include insurance, they are not included again here.

Total startup cost is $20,738 or $3.46/yd^3.

12.1.5 Consumables and Supplies

The consumables consist of the catalyst for the Catox unit and the activated carbon. The catalyst costs $7,000. Distributed over 6,000 yd^3, this amounts to $1.17/yd^3. Activated carbon costs about $2/lb. Assuming a 55 gal drum (700 lb) is used for each 1,000 yd^3, the cost is $1.40/yd^3. Propane cost for the offgas treatment system is about $0.38/yd^3 of treated soil. Total consumables is $2.95/yd^3.

12.1.6 Labor

The assumptions for the labor calculation are the following:

- Two people are required on site.
- They are required to be there 12 hours per day.
- The cost of an operator is $50/hr.
- 30 days per month, 6 months of operation.

This amounts to $216,000 or $36/yd^3.

12.1.7 Utilities

The assumptions for the utilities calculation are the following:

- The PLF heating will run first, followed by the RF unit. Both units require 200 kW.
- Other power requirements include a 7 Hp blower and a 1 Hp condensate pump.
- 0.5 kW is required for night lighting.
- Electricity cost is $0.10/kWH.

The total electricity requirement is 206.5 kW. A 6-month period in which 6,000 yd^3 of soil is treated amounts to $ 14.87/ yd^3.

12.1.8 Effluent Treatment and Disposal Cost

The offgas treatment system destroys the VOCs in the vapor stream. However, during the PLF heating operation, water is added to the soil to improve conductance. The vaporized water is condensed, treated with an air stripper, then polished with activated carbon. Activated carbon cost is included under "Consumables and Supplies". Hazardous waste disposal charges at SNL are $9/kg, which also pays for pollution prevention programs. Assuming a $4.5/kg cost for an industrial disposal contractor, each 1,000 yd^3 treated requires one 55 gal Granular Activated Carbon (GAC) drum, the GAC disposal amounts to $1.00/$yd^3$.

12.1.9 Residuals and Waste Shipping and Handling

Items such as contaminated drill cuttings are included in the boring and electrode emplacement costs. GAC used for liquid effluent is included in effluent treatment.

12.1.10 Analytical

A $20,000 cost is assumed for analytical as a typical cost from SITE reports. This amounts to $3.33/$yd^3$.

12.1.11 Maintenance and Modifications

This item is taken as total of 10% of equipment cost (Table 12-2 total minus Electrodes and Installation) or $44,500, which amounts to $7.42/$yd^3$.

12.1.12 Demobilization

Assuming eight man-weeks at $50/hr, the cost amounts to $16,000 or $2.67/$yd^3$.

12.1.13 Total Treatment Cost

Total treatment cost, shown in Table 12–3, is about $151.00/$yd^3$.

Table 12-3. TEVES Treatment Cost Using SITE Format

Item	Cost	%
Site Preparation	8.61	5.7
Permitting	5.00	3.3
Capital Equipment (Installed)	65.69	43.5
Startup	3.46	2.3
Consumables	2.95	2.0
Labor	36.00	23.8
Utilities	14.87	9.8
Effluent Treatment	1.00	0.7
Residuals (Included in Effluent Treatment)	0	0
Analytical	3.33	2.2
Maintenance	7.42	4.9
Demobilization	2.67	1.8
Total	**151.00**	**100**

12.2 Comparison of TEVES Costs with that of Other Options

There are several critical factors that affect the cost of implementing TEVES. These consist of the following:

- The number or spacing of locations where soil analysis is required for adequate characterization. Pre-treatment site characterization and post-treatment characterization requirements depend upon the judgement of state environmental officials.
- The number of operator hours required during active heating periods.
- The offgas treatment system selected.
- The volume of soil treated. TEVES is somewhat modular in implementation because extremely large PLF and RF energy systems are not practical and electrode spacings cannot be very large.
- The time required for treatment. The PLF and RF heating operations greatly expedite the extraction operation so that less time is required, thus reducing the total lifecycle restoration period. The expedited operation also allows for the equipment to be used for other projects so that the equipment cost can be distributed over more treated volume than for the baseline SVE.
- Operator attention. Because TEVES requires high-power equipment, more operator attention is required than for baseline SVE, thus resulting in a higher operating costs.

Without considering site characterization and pilot studies, the cost of TEVES, Subsurface Volatilization and Ventilation System (SVVS), Steam Enhanced Recovery Process (SERP), and for excavation/treatment using thermal desorption are as shown in Table 12–4. Costs were developed by the technology developers using the twelve-category SITE format.

Table 12-4. Comparison of Costs for Treatment Options

Treatment Option	Treatment Cost, $/yd^3
SVVS[1]	10
SERP[2]	29 to 46
TEVES[3]	151
Excavation[4]	480

[1] Data provided by Billings and Associates, and Brown and Root Environmental based on operation at Electro-voice facility, Buchanan, MI (EPA, 1995d)
[2] Data provided by Hughs Environmental Systems based on operation at Rainbow Disposal Site, Huntington Beach, CA (EPA, 1995b)
[3] Data from present study
[4] Data provided by International Technology Corporation (IT, 1995)

TEVES can be compared with these processes on this basis, although several variables were not the same during the tests of the competing technologies. Some examples of the variables are: the volume of the contaminated site, concentrations of the contaminants, water content of the soil, and residence time of the soil in the desorption unit. EPA (1992), (1993), (1995a) and (1995c) give costs for four thermal desorption technologies used with excavation. Figure 12–1 shows a plot of cost estimates for TEVES, relative to that of various thermal desorption technologies and enhanced vapor extraction technologies as a function of treated volume. In addition to the cost information generated for TEVES in this study, the LANL Environmental Technology Costs-Savings Analysis Project (ETCAP) has developed cost comparisons for TEVES and conventional technologies under different situations (LANL 1996). These costs are shown in Table 12-5 and incorporated in Figure 12-1.

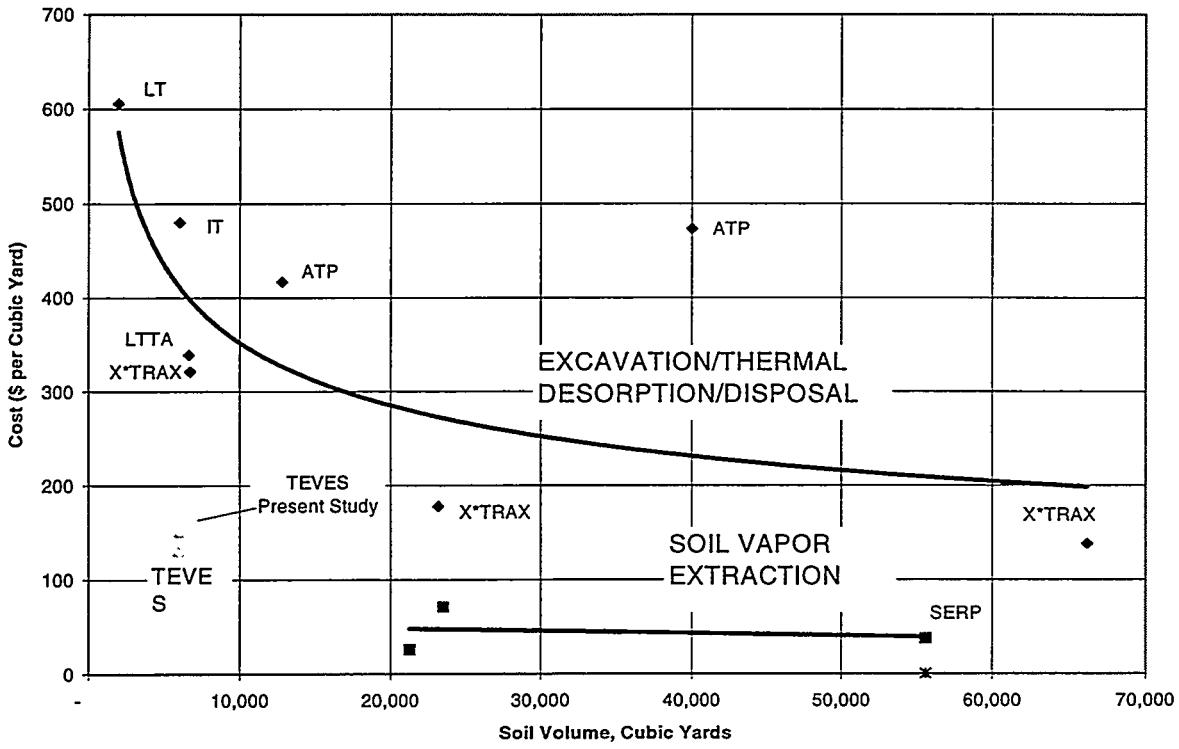

Figure 12-1. Treatment option costs.

Table 12-5. Cost Comparisons Developed by ETCAP (LANL, 1996)

	TEVES	Excavate and Treat	SVE
Cost, $/yd^3 Treated	130	590	ND*

*ND - Not Determined

Other costs have also been determined for excavation and offsite treatment/disposal at a RCRA site. These are summarized in Table 12–6.

Table 12-6. Costs for Excavation and Treatment/Disposal at a RCRA Site*

	55 gal. drum	$/yd^3
No Stabilization	155	368
Stabilization	204	545

*Data from Sandia National Laboratories-Environmental Restoration (SNL-ER) studies

This page intentionally left blank.

13.0 CONCLUSIONS

13.1 Performance and Process Improvements

The TEVES project was designed to be a fully integrated, near-full scale application of soil heating, vapor extraction and off-gas treatment in an application with unsaturated zone free phase contamination and containerized wastes. The large amount of oil co-disposed with organic solvents created a long term source that would continue to supply contamination to the surrounding soils. The objectives of the TEVES project were met by demonstrating how powerline frequency and radiofrequency heating technologies could be integrated with a single electrode array, and demonstrating an off-gas treatment system that could manage both vapor and condensate treatment within an integrated system.

A pre-test design estimate of PLF energy needs showed 0.68 kW-hr/yd^3-°C to bring the treatment zone up to 90°C. Heat balance calculations from test data showed an actual value of 1.63 kW-hr/yd^3-°C. However, the pre-test design estimate did not include the energy requirement for the water injected to maintain the electrical conductivity. If this is accounted for, the pre-test design energy needs is about 1.67 kWH/yd^3-°C, which is close to the results from the test.

For the RF pre-test design, the energy needs were estimated to be 0.63 kW-hr/yd^3-°C. The test results showed a figure of 0.73 kW-hr/yd^3-°C, which is, again, close to the pre-test design estimate. It appears that the RF is more efficient at heating the soils because the PLF system requires the addition of such a large volume of water to moderate electrode resistivity increases. However, with the utility costs only about 10% of the total system costs, the selection of heating technology should be more based on the contaminant type and soil rather than efficiency of heating (see 13.3 Application Niche).

In the heated zone, TEVES resulted in the removal of up to 99% of the total chromatographable organics in spite of the unplanned cooldown period between the PLF and RF heating periods. If there were no delay between the heating modes, then a higher temperature would have been attained over a larger volume and the removal would have been even more complete.

13.2 Process Improvements

During the PLF heating, water was injected at the surface in order to improve electrical conductivity and thus soil heating. At the lower depths, 18 and 24 ft., average temperatures reached about 40°C as compared with 80°C at the shallower depths (3 to 9 ft.). This difference may be a result of water addition only at the surface which did not penetrate to the deeper regions. It is recommended that several deeper water injection points be included in future electrode designs.

This was the first operation of an integrated, stand-alone vapor and condensate treatment system. The integrated system worked well; however, during operations several improvements in system components were identified. During the heating periods, a large amount of water vapor was generated as expected. However, to conserve propane costs, the catalyst heater was fed by the extracted vapors from treatment zone. When large pulses of contaminants occurred during the later stages of the PLF heating, the catalyst bed temperature would experience high temperature excursions. Materials like xylene were identified in the process monitoring system during these temperature excursions which also have high heats of combustion. Future designs should include a fresh air dilution system to moderate the catalyst bed temperatures when large pulses of high heat value contaminants can be expected.

The water vapor was moderated very well by the air-to-air heat exchanger; however, more condensate was generated than expected. In addition, this condensate included a large amount of chemicals and oil during the RF heating phase. The operation of the condensate treatment system would have been improved if an oil separator was included in the process flow.

At present, the TEVES requires almost full-time operator monitoring during RF operations to manually tune the impedance matching system to attain full energy delivery efficiency. A better control system that would automatically account for changes in soil load impedance with an automated impedance matching network has been under development and will be available soon.

13.3 Application Niche

The TEVES has an application niche in which it is competitive with other available technologies. For example, in low-permeability soils SVE is not effective; however, TEVES is effective and competitive with excavation and off-site disposal. For sites contaminated with SVOCs, SVE is also not very effective; but the TEVES is effective and is competitive with excavation. Table 13–1 shows a summary of competing alternatives as functions of contaminant type, soil type, and contamination depth.

Table 13–1. Comparison of Technologies for Various Soil Remediation Applications

Technology	Applications							
	VOC				SVOC			
	High Perm. Soil		Low Perm. Soil		High Perm. Soil		Low Perm. Soil	
	Shallow	Deep	Shallow	Deep	Shallow	Deep	Shallow	Deep
SVE	1	1	2	2	2	2	3	3
Steam Injection	1	1	2	2	2	2	3	3
Excavation	2	3	1	3	1	3	1	3
TEVES (RF)	2	3	1	3	1	3	1	3
TEVES (PLF)	2	2	1	1	2	2	2	2

1 Competitive Technology
2 Marginally Competitive Technology
3 Non-Competitive Technology

PLF and RF heating have the advantage of faster cleanup and lower residual contamination. SVE, when applied to low permeability soils, requires a long remediation period.

Cleanup cost depends upon the acceptable residual. With SVE alone, perhaps due to diffusion limitations and sorption phenomena, there will still be a residual left. Johnson (1990) suggests that after SVE, enhanced biodegradation may be needed to achieve lower cleanup levels. TEVES would be able to attain lower residual concentrations than SVE due to the higher temperatures used.

This page intentionally left blank.

14.0 REFERENCES

Anderholm, S.K. *Groundwater geochemistry of the Albuquerque-Belen Basin, Central New Mexico*: U.S. Geological Survey Water-Resources Investigation Report 86-4094, 110 p., 1988.

ANSI/IEEE Standard 80 - 1986. *IEEE Guide for Safety in AC Substation Grounding.* Wiley InterScience.

Bjorklund, L.J. and B.W. Maxwell. *Availability of Groundwater in the Albuquerque Area, Bernalillo and Sandoval Counties.* New Mexico State Engineer Report 21, 117 p. 1961.

Boublik, T., Fried, V. and Hala, E., The Vapor Pressures of Pure Substances: Selected Values of the Temperature Dependence of the Vapour Pressures of Some Pure Substances in the Normal and Low Pressure Region. Vol. 17; Amsterdam, Netherlands: *Elsevier Science Publication*; 1984.

Buck, F.A.M. and Seider, E.L.. "State-of-the-art VOC Abatement from Soil-Venting Operations." *Remediation*, Winter 1991/92.

Dalton, K.E., "Electromagnetic Modeling of Solid Waste Landfills." *Proceedings: International Topical Meeting on Nuclear and Hazardous Waste Management-Spectrum 92. Boise, Idaho, August 23-27, 1992.*

DOE (1995a) *Dynamic Underground Stripping: Innovative Technology Summary Report.* U.S. Department of Energy, Office of Environmental Management, Office of Technology Development, April 1995.

DOE (1995b) *Six Phase Soil Heating: Innovative Technology Summary Report.* U.S. Department of Energy, Office of Environmental Management, Office of Technology Development, April 1995.

EPA (1992) Risk Reduction Engineering Laboratory, Office of Research and Development, U.S. Environmental Protection Agency, *Low Temperature Thermal Treatment (LT) Technology, Roy F. Weston, Inc., Applications Analysis Repor.* EPA/540/AR–92/019, December 1992.

EPA (1993) Risk Reduction Engineering Laboratory, Office of Research and Development, U.S. Environmental Protection Agency, *SoilTech APT Systems, Inc., Anaerobic Thermal Processor, Applications Analysis Report, Wide Beach Development Site and Waukegan Harbor Superfund Site.* Draft, EPA/540/A__. May 1993.

EPA (1995a) Risk Reduction Engineering Laboratory, Office of Research and Development, U.S. Environmental Protection Agency, *X*TRAX™ Model 200 Thermal Desorption System, RUST Remedial Services, Inc. —Draft Applications Analysis Report.* EPA/540/AR–95/xxx, April 1995.

EPA(1995b). National Risk Management Research Laboratory Office of Research and Development, U.S. Environmental Protection Agency, *In Situ Steam Enhanced Recovery Process, Hughes Environmental Systems, Inc., Innovative Technology Evaluation Report.* EPA/540/R–94/510, July 1995.

EPA (1995c) National Risk Management Research Laboratory Office of Research and Development, U.S. Environmental Protection Agency, *Low Temperature Thermal Aeration (LTTA) Process Canonie Environmental Services, Inc., Applications Analysis Report.* EPA/540/AR–93/504, July 1995.

EPA (1995d). National Risk Management Research Laboratory Office of Research and Development, U.S. Environmental Protection Agency, *Subsurface Volatilization and Ventilation System (SVVS), Innovative Technology Report.* EPA/540/R–94/529, August, 1995.

Evans, G., Estimating Innovative Technology Costs for the SITE Program, in *Journal of the Air and Waste Management Association* 40:7 (pp.1047–1051), 1990.

Grant, P.R., *Geothermal Potential on Kirtland Air Force Base Lands, Bernalillo County, New Mexico.* SAND81-7141, Sandia National Laboratories, Albuquerque, New Mexico, 1981.

Hensel, E. and Dalton, K.E. Non-Intrusive Characterization of Waste Sites, *Proceedings of the International Topical Meeting on Nuclear and Hazardous Waste Management-Spectrum 92,* in Boise, Idaho, August 23-27, 1992.

Hensel, E. and Dalton, K.E. *Heterogeneous Sensors and Data Interpretation, Fifth Topical Meeting on Robotics and Remote Systems*, April, 1993.

IITRI, *Thermal Enhanced Vapor Treatment System Demonstration Phase III—Design Report,* Prepared by R. Snow and T. Bajzek, IITRI, for James Phelan, Sandia National Laboratories. IITRI Project No., C06763, March 17, 1993.

IT (1992a). *Site Specific Sampling and Analysis Plan for TEVES Phase I Site Investigation,* International Technologies Corporation, Albuquerque, New Mexico, March, 1992.

IT (1992b). *Results of the TEVES Phase I Site Investigation,* International Technologies Corporation, Albuquerque, New Mexico, July, 1992.

IT (1995). Bremser, J., Booth, S., Silva, M., *Cost Effectiveness of Thermally Enhanced In-Situ Soil Remediation Technologies*, LAUR–95–xxxx, November 1995.

Jarosch, T.R., R.J. Beleski, and D. Faust, 1994. *Final Report: In-Situ Radio Frequency Heating Demonstration.* Westinghouse Savannah River Company, WSRC-TR-93-673.

Johnson, P.C., Stanley, C.C., Kemblowski, M.W., Byers, D.L. and Colthart, J.D., A Practical Approach to the Design, Operation and Monitoring of In Situ Soil-Venting Systems, *Groundwater Monitoring Review* , Spring 1990, p. 159–178.

Jones, D., T. Bajzek, L. Ploense, and H. Dev. 1990. *Treatment of Soil at Chemical Waste Landfill, Task I Final Report, Soil Treatability and Measurement of Electrical Properties,* IIT Research Institute, Chicago, IL. March 1993.

Kelley, V.C., *Geology of the Albuquerque Basin, New Mexico*, New Mexico Bureau of Mines and Mineral Resources Memoir 33, Socorro, New Mexico, 1977.

Kues, G., *Groundwater Levels and Directions of Ground Water Flow in the Central Part of Bernalillo County, New Mexico, Summer 1983*, U.S. Geological Survey, Water Resources Investigations Report 85-4325, Washington D.C., 1986.

LANL (1996). LANL Environmental Technology Costs-Savings Analysis Project (ETCAP). *Cost Studies of Thermally Enhanced In-Situ Soil Remediation Technologies,* Los Alamos National Laboratories, May 1996.

Lowry, W.E. and S.M. Narbutovskih, High Resolution Gas Permeability Measurements with the SEAMIST System, *proceedings of the Fifth National Outdoor Active Conference on Aquifer Restoration, Ground Water Monitoring and Geophysical Methods*, May 1991.

Machette, M.N., *Quaternary and Pliocene Faults in the la Jencia and Southern Part of the Albuquerque-Belen Basins, New Mexico: Evidence of Fault History From Fault-Scarp Morphology and Quaternary Geology*, U.S. Geological Survey, New Mexico Geological Society Guidebook, 33rd Field Conference, 1982.

McCabe, W.L. and J.C. Smith. *Unit Operations of Chemical Engineering*. 3rd Ed. McGraw Hill, 1976.

McCorkle, R.W., Analysis of Selected DOE Waste Sites. Masters Thesis in Mechanical Engineering. New Mexico State University, Las Cruces, NM. December 1993.

Narbutovskih, S.. *The Accuracy and Adequacy of SEAMIST Applied to Gas Permeability Measurements. Science and Engineering Associates Topical Report SEATR-91-C*, Science and Engineering Associates, Santa Fe, NM. April 125, 1991.

NAVSHIPS, *Technical Manual for the AN/FRT-86(V) Radio Transmitting Set,* NAVSHIPS 0967-293-2010. Department of the Navy, Naval Electronic Systems Command, May 1970, Change No. 1, September 1970.

NIOSH, *Pocket Guide the Chemical Hazards*, National Institute for Occupational Safety and Health, June, 1990.

Oster, C.C., Connell, P. and Wenck, N.C., *Vacuum Extraction of Volatile Organics from Soils.*

Peter, F.J. and G.R. Laguna, *Autonomous Gas Chromatograph System for Thermal Enhanced Vapor Extraction System (TEVES),* Proof of Concept Demonstration. Sandia National Laboratories. SAND96-2302. September 1996.

Peterson, T.A. and Curtis, J.T., *Soil Vapor Extraction Technology: Reference Handbook,* for Risk Reduction Engineering Laboratory, Office of Research and Development, U.S. Environmental Protection Agency, EPA/540/2–91/003, February 1991.

Phelan, J.M. *Field Measurements of Soil Air Permeability at the Chemical Waste Landfill,* Sandia National Laboratories, Environmental Restoration Technologies Department, Albuquerque, NM. September 1993.

Phelan, J.M., Reavis, B., Cheng W.C., *Passive Soil Venting at the Chemical Waste Landfill Site at Sandia National Laboratories, Albuquerque, New Mexico,* SAND95–0776, May 1995.

RCRA. Resource Conservation and Recovery Act Research, Development and Demonstration Permit for Thermal Enhanced Vapor Extraction System (TEVES) Demonstration. May 1994. Permittee: U.S. Department of Energy/Sandia National Laboratories I.D. No. NM5890110518, Permit No. NM5890110518–3, 1994.

Reeder, H.O., L.J. Bjorklund and G.A. Dinwiddie, *Quantitative Analysis of Water Resources in the Albuquerque Area, New Mexico, Computed Effects on the Rio Grande of Pumpage of Ground Water*, New Mexico State Engineer Technical Report 33, Santa Fe, New Mexico, 1967.

Sandia National Laboratories (SNL). *Chemical Waste Landfill Final Closure Plan and Post-Closure Permit Application,* Environmental Impact and Restoration Division 7723, Sandia National Laboratoris, Albuquerque, NM, December 1991.

Titus, F. B., *Geology and Groundwater Conditions in Eastern Valencia County, New Mexico,* Ground-Water Report No. 7, State Bureau of Mines and Mineral Resources, New Mexico Institute of Mining and Technology, Socorro, NM, 1963.

Webb, S.W., *TOUGH2 Simulations of the TEVES Project Including the Behavior of a Single-Component NAPL,* Sandia National Laboratories, SAND94-1639. May 1996.

Appendix A
Site Geology and Hydrology

This page intentionally left blank.

Appendix A

Site Geology and Hydrology

Geology

SNL is near the east-central edge of the Albuquerque Basin, one of a north-south-trending line of basins that make up the Rio Grande rift zone. On the east and west, the basin is bound by uplifted fault blocks. The Sandia, Manzanita, and Manzano Mountains are uplifted on the eastern boundary. The western side of the basin is bound by the Lucero uplift, with the Ladron Mountains on the south side and little physiographic relief on the northwest side of the basin (see Figure A-1).

The Albuquerque Basin is filled with a thick (up to 12,000 ft [3,658 m] deep) sequence of sediments. This sequence of sediments, called the Santa Fe Group, thins toward the edges of the basin and is truncated at the uplifted boundaries. Basin-fill alluvial fans of the Santa Fe Group consist of channels, debris flows, floodplain deposits, and eolian deposits. Santa Fe Group sediments are overlain in places by Pliocene Ortiz gravel deposits and Rio Grande fluvial deposits and are interbedded with Tertiary and Quaternary basalts and pyroclastics (Bjorklund and Maxwell 1961).

The geology of the eastern section of KAFB shows evidence of major faulting. The Hubbell Springs and Sandia faults are a set of north-south trending faults, which form a series of down-to-the-west blocks (Machette 1982; Grant 1981; Kelley 1977). The Compliance Agreement Report (SNL 1991), which was submitted to New Mexico Environmental Division (NMED) in May 1991, describes these features in more detail. Lithologic data from CWL wells confirm the presence of a complex interlayered section (SNL 1991). Detailed geologic cross sections are provided in the Compliance Agreement Report (SNL 1991). According to geophysical log correlations, three large sediment sections can be correlated among the monitor wells at the CWL (SNL 1991). The overall trend of the section down to about 500 ft (152 m) below ground level (BGL) is predominantly coarser starting at ground level and becoming finer moving downward. These three sediment sections are not separate geologic units but represent large-scale changes in the stratigraphic section.

Hydrology

SNL is within the Albuquerque Basin hydrologic area. The basin is approximately 161 km (100 mi) long and from 32 to 64 km (20 to 40 mi) wide. The Rio Grande, flowing north to south, is the main drainage in the basin; the Jemez River, Rio Puerco, and Rio Salado are major tributaries in the basin. The Albuquerque-Belen Basin is hydraulically connected to the Santo Domingo Basin to the north and the Socorro Basin to the south (Anderholm 1988).

The major aquifer in the Albuquerque Basin is principally composed of Santa Fe Group sediments. Groundwater in the basin generally exists under water-table conditions; however, confined or semiconfined conditions may exist locally. Semiconfined conditions can result from the presence of intermittent and discontinuous beds of silt and clay-rich sedimentary layers, which are relatively impermeable. The depth to groundwater in the basin ranges from 5 ft (1.5 m) BGL near the Rio Grande to more than 1400 ft (427 m) BGL near the edges of the basin (Anderholm 1988).

The Sandia and Manzano Mountains act as recharge zones for deep, regional saturated flow. Recharge to the Santa Fe Formation is probably from both groundwater percolating through interstices and fractures in pre-Tertiary rocks, and surface runoff and recharge in lowland areas, most of which occurs through infiltration in alluvial fans (Titus 1963). The faults affect the groundwater flow system in the region. In general, on the east side of the fault system the water table is approximately 100 ft (30 m) BGL; to the west, groundwater is approximately 400 to 500 ft (122 to 152 m) BGL.

Before the extensive development in the City of Albuquerque and on KAFB, the apparent direction of groundwater flow in the KAFB area was to the west or southwest (Bjorklund and Maxwell 1961). Municipal pumping, however, had the effect of lowering the water table elevation in the Albuquerque area (Reeder et al., 1967; Kues 1987). The KAFB production wells have a large effect on the hydraulic gradient in this area, creating a cone of depression in the groundwater surface elevation in the northern portion of the region. At the CWL, the water table is approximately 485 ft (148 m) BGL. According to analysis of water-level data, the regional hydraulic gradient at the CWL is to the west, but the gradient is affected locally by heterogeneous media located to the northwest. The regional hydrologic system is described in more detail by SNL (1991).

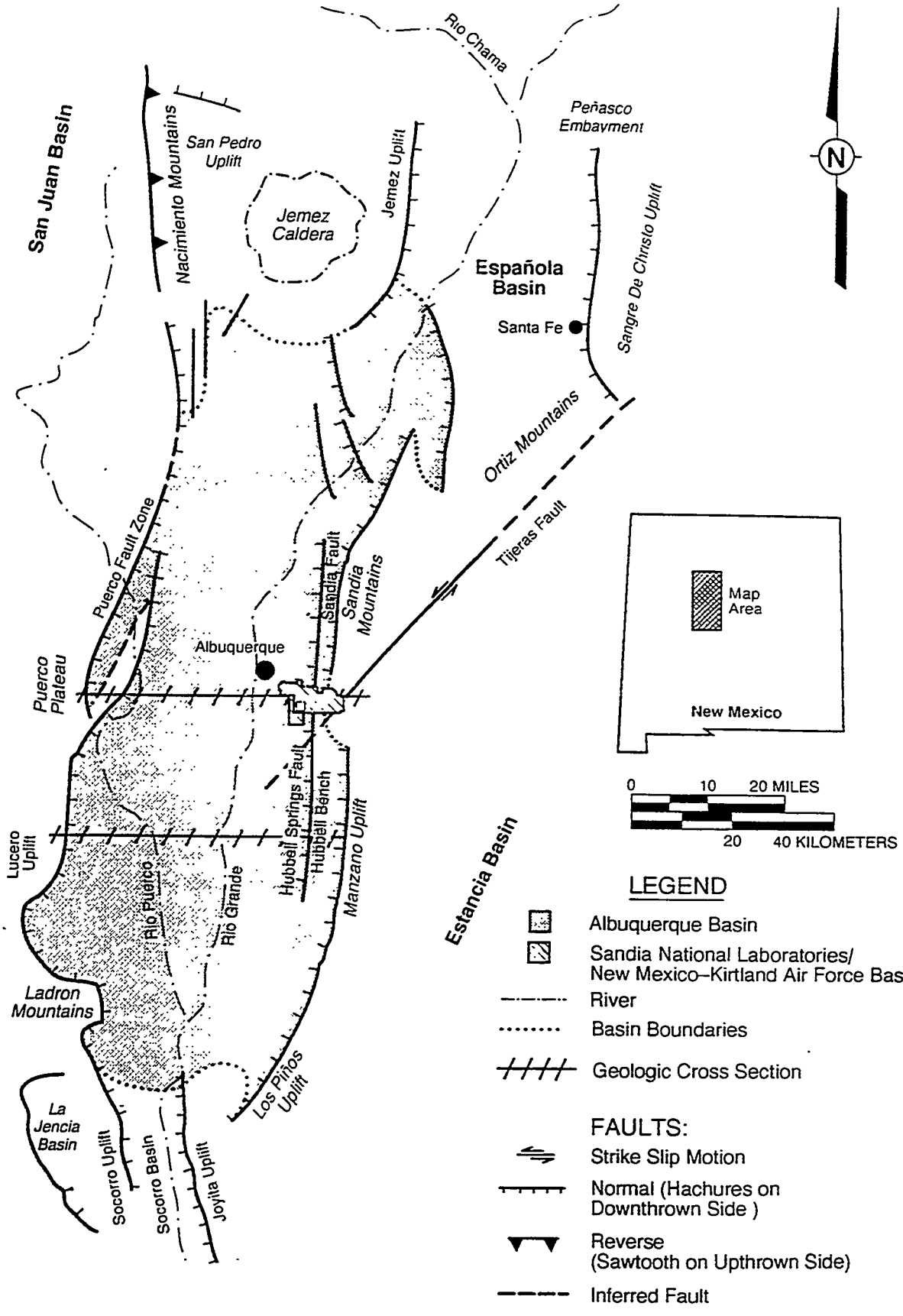

Figure A-1. Regional tectonic setting of the Albuquerque Basin, North Central New Mexico, Sandia National Laboratories/New Mexico and Kirtland Air Force Base.

This page intentionally left blank.

Appendix B
Heat Balance Calculations

This page intentionally left blank.

Appendix B

Heat Balance Calculations

PLF Heating

Assumptions for PLF Heating:

1. Electrical line losses are 2.5% as per previous ITRI experience
2. Conduction losses are determined from a linear temperature gradient between thermowell and outer row temperatures with the average gradient being half the temperature gradient at the end of the heating period since the initial gradient is zero.
3. The krigging method is adequate for determining average soil volume temperatures given the temperatures measured in the thermowells and center and outer rows.
4. The total water evaporated due to heating is equal to the condensate collected plus the amount of water vapor in the air flow downstream of the condenser. This water vapor is estimated assuming a saturated condition at the average condenser temperature.
5. Water content in the soil is 20% of the pore volume during PLF heating
6. Pore water is heated to ¾ of the final soil temperature, on average, before being evaporated.
7. Soil gas temperature was at 50° F on average.
8. Dilution air was at 50° F on average.
9. The presence of water vapor does not significantly affect the heat capacity of the air.
10. Conduction heat losses through the bottom of the heated volume was insignificant compared to that lost through the sides and top.
11. The volume averaged temperature used here included the entire volume measured by the temperature monitoring date to better account for heat balance (chapters 4 and 5 used smaller volumes that are more representative of the volume heated to target temperatures).

PLF Heat Balance Calculation:

- Figure 4-1 shows the PLF power applied to the soil during the 33-day test period.
- Figure 4-3 shows the accumulated energy input of 45,000 kW-hr.

  45,000 kW-hr x 3412 Btu/kW-hr = 1.54×10^8 Btu

- Figures 4-10 through 4-12 show x-y, x-z, and y-z temperature profiles at the end of PLF heating. A krigging method produced an average soil temperature of 58.4°C for the 30 ft wide by 50 ft long by 24 ft deep volume (36,000 ft^3).

1) Line Loss
From past IITRI experience, line losses are about 2.5% for PLF lines. This amounts to

$0.025 \times 1.54 \times 10^8 = \underline{3.9 \times 10^6 \text{ Btu}}$

2) Soil Heating
- The heat capacity of sand is 0.191 Btu/lb-°F (Perry's Chemical Engineers' Handbook, 6th ed. p. 3-146).
- The baseline temperature for the PLF heating was 23°C.
- The affected soil volume was 30 ft x 50 ft by 24 ft deep, or 36,000 ft^3.
- The average soil temperature after 33 days of heating was 58.4°C as determined from a kriging technique.
- Therefore, the heat required to heat the soil to the maximum temperature was:

$36{,}000\ ft^3 \times 112\ lb/ft^3 \times 0.19\ Btu/lb\text{-}°F \times (58.4\text{-}23°C) \times 1.8°F/°C = \underline{4.9 \times 10^7 \text{ Btu}}$

- In addition, the heating was shut down from day 18 to day 21, allowing the thermowell temperatures at the 3 ft. depth to drop from 85°C to 65°C and at the 9 ft depth to drop from 70°C to 65°C. A very rough estimate of this loss would assume a 15°C drop for the top 3 ft and a 12.5°C drop for the 6 ft between the 3 ft and 9 ft depths. This would then account for:

$1500\ ft^2 \times 3\ ft \times 112\ lb/ft^3 \times 0.191\ Btu/lb\text{-}°F \times (15°C \times 1.8°F/°C) +$
$1500 \times 6 \times 112 \times 0.19 \times 12.5 \times 1.8 = 6.9 \times 10^6 \text{ Btu}$

- The total heat duty for soil heating is thus $\underline{5.6 \times 10^7 \text{ Btu.}}$

3) Water Vapor Generation
- Figure 6-4 shows the cummulative condensate collected for the PLF heating period was about 5600 gallons.

- The heat required for boiling this water was

$5600\ gal \times 8.3\ lb/gal \times 1008\ Btu/lb = \underline{4.69 \times 10^7 \text{ Btu}}$

- In addition, there was uncondensed water vapor which went to the Catox unit. This can be accounted for by assuming that the vapor exiting the condenser was saturated with water vapor at the condenser temperature. At 80°F, the saturation of water in air is 0.02 lb water vapor per lb of dry air (Perry's Chemical Engineers' Handbook, 6th edition, p.20-6).

$175\ scfm \times 28.3\ liter/ft^3 \times mole/24.4\ liter \times 29\ g/mole \times lb/454g = 13\ lb/min\ air$

$0.02 \times 13\ lb/min = 0.259\ lb/min\ water\ vapor$

0.259 lb/min x 60 min/hr x 24 hr/day x 33 days = 12,300 lb

12,300 lb x 1008 Btu/lb = $\underline{1.24 \times 10^7 \text{ Btu}}$

- The total energy required for vaporizing water was then $\underline{5.93 \times 10^7 \text{ Btu}}$.

4) Heating Pore Water - Sensible Heat
   - Pore water is estimated at 20% of the pore volume (30%). This amounts to

     $36{,}000 \text{ ft}^3 \times 0.3 \times 0.2 = 2160 \text{ ft}^3$

   - The heat capacity of liquid water is 1 Btu/lb-°F.
   - Average soil temperature, and thus pore water temperature, at the end of 33 days was 58.4°C. However, not all of the water had to be heated to this temperature before vaporizing. Assume the water was heated 3/4 of the way to this temperature before boiling. The average water temperature before boiling would then have been

     $23 + 0.75 (58.4 - 23) = 49.6°C$

   - The sensible heat required would then have been

     $mC_p \Delta T = 2160 \text{ ft}^3 (62.4 \text{ lb/ft}^3)(1 \text{ Btu/lb-°F})(49.6\text{-}23°C)(1.8°F/°C) = \underline{6.5 \times 10^6 \text{ Btu}}$

5) Heating Extracted Air
   - Pitot tube reading was about 175 scfm.
   - Assume air comes out of soil at about 50°F. Dilution air is also about 50°F.
   - Heat capacity of air @ 100°F is 0.25 Btu/lb-°F (Perry, p.3-140).
   - Note: no accounting is made for the effect of water vapor on heat capacity.
   - Average manifold air temperature was about 120°F (from log book).
   - At STP (20°C, 1 atm) the molar volume of air is 24.4 liters.
   - Air flow rate was

     175 scfm x 28.3 liter/ft^3 x mole/24.2 liter x 29 g/mole x lb/454 g = 13.1 lb/min.

   - Total air was

     13.1 lb/min x 60 min/hr x 24 hr/day x 33 days = 623,000 lb.

   - Heat added to air was

     $mC_p\Delta T = 623{,}000 \text{ lb} \times 0.25 \text{ Btu/lb-°F} \times (120 - 50°F) = \underline{1.09 \times 10^7 \text{ Btu}}$.

6) Conduction Loss to Surrounding Soil

- Assume the temperature gradient at the boundary is estimated by the average thermowell temperature minus the average outer row temperature divided by the distance between the thermowell and the outer row (5 ft). The gradients at the different depths at the end of the test are then:

Depth ft	Thermowell °C	Outer Row °C	ΔT °C	ΔT/ΔX °C/ft
3	87	65	22	4.4
9	85	58	27	5.4
18	45	25	20	4
21	37	23	14	2.8
24	32	22	10	2

- Since these gradients represent the gradients at the end of the heating period and the gradients at the beginning of the heating period was zero, the average gradient is roughly half of these values.
- The perimeter is 2 x 30 + 2 x 50 =160 ft.
- Because the vertical temperature gradient at the 21 and 24 ft depths are small, conduction loss through the bottom of the heated region is neglected.
- The thermal conductivity of the soil is 0.19 Btu/hr-ft-°F (Perry, p. 3-260).
- The thermal conductivity of water is 0.39 Btu/hr-ft-°F.
- Since the porosity of the soil is 0.3 and the saturation is 20%, the effective thermal conductivity of the wet soil is taken as
- 0.19 x (1-0.3) + 0.39 x 0.3 x 0.2 = 0.156 Btu/hr-ft-°F.
- It is acknowledged that tortuosity is not accounted for in the conduction path.
- The contributions to the heat flow can be taken as the sum of the flows at the different depths, which are taken as the average gradient in the section, times the thermal conductivity (K), the depth (ΔZ), and perimeter (P).

$Q = -K\Sigma(DT/DX)\Delta A = -K\Sigma\,(\Delta T/\Delta X)\,P\,\Delta Z$

Depth ft	Ave. Grad. °C/ft	1/2 Grad °F/ft	(ΔT/ΔX) P ΔZ °F-ft	K (ΔT/ΔX) P ΔZ Btu/hr
0 to 3	4.4	4.0	1920	300
3 to 9	4.9	4.4	4224	659
9 to 18	4.7	4.2	6048	943
18 to 21	3.4	3.1	1488	232
21 to 24	2.4	2.2	1056	164
Total				2300

- The conduction heat loss to the surrounding soil is thus

2300 Btu/hr x 24 hr/day x 33 days = $\underline{1.8 \times 10^6}$ Btu

1) Conduction loss through top of heated soil

Basis and Calcuation:

- A 0.010 inch layer of silicone-impregnated fiberglass (as a vapor barrier) and 2 inches of fiberglass insulation and is provided on top of the heated soil.
- In addition, the top 3 feet of soil is considered to be an insulating layer.
- The thermal conductivity of fiberglass insulation is 0.27 Btu/(hr-ft^2-°F/in).
- The thermal conductivity of silicone is 2.9 Btu/(hr-ft^2-°F/in).
- The thermal conductivity of wet soil, as estimated in item (6) is 0.16 Btu/hr-ft-°F.
- From Figure 4-4, the average temperature of the soil at 3 ft. depth during the PLF heating period was about 70°C or 158°F.
- Assuming the ambient temperature under the RF cover was 60°F, the total temperature gradient from the soil at 3 ft depth to the ambient air was 158 °F-60°F = 98°F.
- Even though a portion of the heat transfer mechanism involves evaporation of water, vapor phase transport of water and then condensation, the heat transfer is modeled as conduction only.
- The effective heat transfer coefficient is evaluated from:

$$1/h_{eff} = 1/(k_{ins}/w_{ins}) + 1/(k_{vb}/w_{vb}) + 1/(k_{soil}/w_{soil})$$

where "ins" is fiberglass insulation and "vb" is the vapor barrier

$$1/h_{eff} = 1/(0.27/2) + 1/(2.9/0.010) + 1/(0.16/3)$$

$$h_{eff} = 0.038 \text{ Btu/hr-ft}^2\text{-°F}$$

- The PLF heating period was 33 days.
- The area above the heated zone was 30 ft x 50 ft or 1500 ft^2.
- The heat loss is through the top of the soil is then

$$Q\ t = h_{eff}\ (\Delta T)\ A\ t = 0.038\ (98)\ (1500)\ (33 \times 24) = 4.5 \times 10^6 \text{ Btu}$$

- Heat Balance Summary for PLF Heating

Contribution	Heat, Btu	% of Input
Heat in:	1.54×10^8	
Heat Out:		
Line Loss	3.9×10^6	2.5
Heating Soil	5.6×10^7	36.4
Evaporating Water	5.93×10^7	38.5
Heating Water	6.5×10^6	4.2
Heating Extracted Air	1.09×10^7	7.1
Conduction loss to surrounding soil	1.8×10^6	1.2
Loss through insulated top	4.5×10^6	2.9
Total Out	$\mathbf{1.43 \times 10^8}$	**92.8**

- The closure on the Heat Balance is 92.8%
  Other possible contributions to the heat consumption are radiant heat losses, heat loss due to the condensation of water vapor onto the vapor barrier, and inaccuracies due to the assumptions made, i.e., averaging methods.

RF Heat Balance

RF Heat Balance Assumptions:

1) Line losses are 2.5% as per previous IITRI experience.
2) Total water evaporated is equal to the condensate collected plus the amount of water vapor in the air flow downstream of the condenser. This water vapor is estimated as that in saturated air at the condenser temperature.
3) Soil moisture content was 1/3 of that during the PLF heating.
4) Soil gas and dilution air are at 50° F.
5) Conduction losses are the same as for during PLF heating.
6) Since the soil surface insulation was removed, the cover losses are greater than for the PLF heating.

RF Heat Balance Calculation:

- Heat Input:
  Figure 5-2 shows the cummulative RF energy applied to the site. At the end of 29 days, the cummulative energy applied is about 30,000 kW-hr. Using the conversion factor of 3412 Btu/kW-hr, this amounts to 1.02×10^8 Btu.

1) Line Losses :
   - According to IITRI experience, line losses for RF transmission is about 2.5%. This amounts to $0.025 \times 1.02 \times 10^8 = 2.6 \times 10^6$ Btu.

2) Heating Soil
   Figure 5-3 shows the average temperatures at different depths in the heated region over time. The maximum temperature occurs just when the RF heating is stopped at 29 days.

   The maxium temperatures attained at the different depths are as follows:

Depth	Temperature, °C
3	110
9	150
18	50
21	40
24	30

   - Using a kriging method, the average soil temperature is 65.2°C for the 30 ft x 50 ft by 24 ft deep affected volume, 36,000 ft^3.
   - Figure 5-3 also shows that the baseline temperature, before initiation of the RF heating, was about 25°C.
   - The bulk density of sand is about 1.8 g/cm^3 or 112 lb/ft^3

- The heat capacity of sand is 0.191 Btu/lb-°F (Perry's Chemical Engineers' Handbook, 6th edition, p. 3-146).
- The enthalpy change due to the increase in sand temperature is then:

$\Delta H = mC_p\Delta T = 36{,}000\ ft^3 \times 112\ lb/ft^3 \times 0.191\ Btu/lb\text{-}°F \times (65.2\text{-}250C) \times 1.8°F/°C$
$= \underline{5.6 \times 10^7\ Btu}$

3) Vaporizing Water
   - As shown in Figure 6-3, the volume of water collected in the condenser during the RF heating period, day 68 through 97 on the calendar year, was 1800 gallons.
   - The heat required to vaporize 1800 gallons of water is:

1800 gal x 8.3 lb/gal x 1008 Btu/gal = $\underline{1.5 \times 10^7\ Btu/lb}$

   - Since the vapor stream exiting the condenser still contained some moisture, an estimate of this amount of water should be made. It is assumed that the vapor is saturated with water vapor at the condenser temperature of 80°F.
   - At 80°F, the saturation of water in air is 0.02 lb water vapor per lb of dry air (Perry's Chemical Engineers' Handbook, 6th edition, p.20-6).
   - For 29 days of extraction, the amount of air extracted is:

144 scfmx28.3 liter/ft^3 xmole/24.4 liter x 29g/mole x lb/454 g = 10.7 lb/min

10.7 lb/min x 60 min/hr x 24 hr/d x 29 d = 4.46×10^5 lb

   - The amount of water vapor is then $4.46 \times 10^5 \times 0.02 = 8920$ lb
   - The heat required to vaporize this water is then:

8920 lb x 1008 Btu/lb = $\underline{9.0 \times 10^6\ Btu}$

   - The total heat for vaporizing water vapor is then $\underline{2.4 \times 10^7\ Btu}$.

4) Heating pore water

   - The pore water in the soil must be heated to the temperature of the soil, although some of the water would have vaporized before the soil temperature reached maximum. Assume that on the average, the soil moisture reached ¾ of the way to the maximum soil temperature.
   - The temperature that the water must reach is then

25 + 0.75 (65.2 - 25°C) = 55.2°C

Assume the soil moisture during the RF heating was 1/3 of that during PLF heating or 2160 ft^3 /3 =720 ft^3
720 ft^3 x 62.4 lb/ft^3 = 45,000 lb

- The sensible heat is thus

  45,000 lb x 1 Btu/lb-°F x (55.2 -25°C) x 1.8 °F/°C =$\underline{2.4 \times 10^6 \text{ Btu}}$

5) Heating Extracted Air
   - Pitot tube reading was about 144 scfm.
   - Assume air comes out of soil at about 50°F. Dilution air is also about 50°F.
   - Heat capacity of air @ 100°F is 0.25 Btu/lb-°F. (Perry, p.3-140).
   - Note: No accounting is made for the effect of water vapor on heat capacity.
   - Average manifold air temperature was about 120°F (from log book).
   - At STP (20°C, 1 atm) the molar volume of air is 24.4 liters.
   - Air flow rate was

     140 scfm x 28.3 liter/ft^3 xmole/24.2 liter x 29 g/mole x lb/454 g = 10.5 lb/min.

   - Total air was

     10.5 lb/min x 60 min/hr x 24 hr/day x 29 days = 437,000 lb.

   - Heat added to air was

     $mC_p\Delta T$ = 437,000 lb x 0.25 Btu/lb-°F x (120 - 50°F) = $\underline{7.6 \times 10^6 \text{ Btu}}$.

6) Conduction Loss to Surrounding Soil
   - Because this term is relatively small and should be similar to that during the PLF heating period, it is assumed to be the same as for AC heating, $\underline{1.8 \times 10^6 \text{ Btu}}$.

7) Heat loss through the top of soil during RF heating period
   Basis and Calculation
   - Because the fiberglass insulation was soaked after the PLF heating, it was removed prior to the RF heating period.
   - From Figure 5-3, the average temperature of the soil at 3 ft depth during RF heating was about 70°C or 158 °F.
   - Assuming the air temperature in the RF shield above the soil was 60°F, the temperature gradient from the 3 ft. depth to the air in the RF shield was 158-60= 98°F.
   - The effective heat transfer coefficient is then

     $1/h_{eff} = 1/(k_{vb}/w_{vb}) + 1/(k_{soil}/w_{soil})$

     $= 1/(2.9/0.010) + 1/(0.16/3)$

     h_{eff} = 0.053 Btu/hr-ft^2-°F

- The heat loss is through the top of the soil is then

  $Q\ t = h_{eff}\ (\Delta T)\ A\ t\ = 0.053\ (98\ )\ (1500)\ (29 \times 24) = 5.4 \times 10^{6}$ Btu

- Summary of Heat Balance for RF heating

Contribution	Heat, Btu	% of Input
Heat in:	1.02×10^{8}	
Heat Out:		
(1) Line Loss	2.6×10^{6}	2.6
(2) Heating Soil	5.6×10^{7}	54.9
(3) Vaporizing Water	2.4×10^{7}	23.5
(4) Heating Pore Water	2.4×10^{6}	2.4
(5) Heating Extracted Air	7.6×10^{6}	7.5
(6) Conduction loss to surrounding soil	1.8×10^{6}	1.8
(7) Conduction Loss through insulated top	5.4×10^{6}	5.3
Total Out	**1.08×10^{8}**	**98.0**

Appendix C
Dilution Air Flow Calculations

This page intentionally left blank.

Appendix C

Dilution Air Flow Calculations

Dilution air at the manual valve on the Catox Unit

- The offgas treatment system unit has an orifice plate and digital readout of airflow entering the system. This device was indicating about 230 scfm throughout the RF test period as recorded in the log book.

- Figure 6-1 shows the pitot tube reading upstream of the Offgas treatment unit. For the duration of the test, the flow was in the range of 150 to 175 scfm.

- By difference, the dilution air at the manual dilution valve on the Catox unit was about 55 to 80 scfm.

Dilution air at the 1 inch gate valve at the RF enclosure

- Although there was not a flow measurement at this location, the pressure in the manifold (MV3 in Figure 3-2) was recorded throughout the test. From the pressure drop, the flow can be estimated. The readings show a consistent 20 mbar vacuum which is equivalent to 0.291 psi or 41.9 lb_f/ft^2.

- The main contributions to the pressure drop are the flow of air through the gate valve and the gas expansion from the 1 inch line into the 3 inch manifold piping.

- The relationship for energy loss due to flow through a piping element is:

$$h_f = \frac{K_f V^2}{2g_c}$$

where K_f is the friction factor, V is the velocity and g_c is a conversion factor equal to 32.2 lb_m - ft/lb_f-s^2.

(McCabe and Smith, Unit Operations of Chemical Engineering, 3rd ed., p. 109, McGraw-Hill, 1976)

- The energy loss is related to the pressure drop by:

$$h_f = -\frac{\Delta P}{\rho}$$

where ρ is the gas density

- Combining the two equations and rearranging gives:

$$V^2 = -\frac{2g_c \Delta P}{\rho K_f}$$

- The value of K_f for a fully open gate valve is 0.2 (McCabe and Smith, p.109).
- The value of K_f for a contraction is $(1-S_a/S_b)^2$ where S_a is the cross-sectional area of the inlet pipe and S_b is the cross-sectional area of the outlet pipe. (McCabe and Smith, p. 107).
- For a 1 inch schedule 40 pipe, the inside diameter is 1.05 inch; for a 3 inch diameter schedule 40 pipe, it is 3.07 inches. (McCabe and Smith, Appendix 6).
- Since the ratio of cross-sectional areas is the ratio of diameters squared, $S_a/S_b = (1.05/3.07)^2 = 0.117$
- K_f for expansion is then (1-0.117) = 0.883
- The total K_f is then 0.2 + 0.883 = 1.083
- The density of air is:

$$\rho = \frac{n(MW)}{Vol} = \frac{P(MW)}{RT} = \frac{(630/760\ atm)(29\ g/mole)(28.3\ L/ft^3)}{(0.0821\ L-atm/mole-K)(288K)(454\ g/lb)} = 0.0643\ lb/ft^3$$

- $V^2 = 2(32.2)(41.9)/[(0.0634)(1.083)] = 39{,}300\ ft^2/s^2$
- V=198 ft/s
- The flow rate is then:

$$V*(\pi D^2/4) = [(198\ ft/s)*3.14*(1.05/12\ ft)^2]/4 * 60s/min = 71.5\ ft^3/min$$

- Corrected to standard conditions (1 atm, 0 ^{0}C), the dilution gas at the 1 inch valve is

$$71.5\ ft^3/min \times (630/760\ atm) \times (273K/288K) = \underline{56.1\ scfm}$$

- The assumption that the flow was turbulent should be checked:

$$Re = \rho VD/\mu = (0.0634\ lb/ft^3)\ (198\ ft/s)(1.05/12\ ft)/(1.14 \times 10^{-5}\ lb/ft\text{-}s) = 9.6 \times 10^4$$

Turbulent flow

Note: the viscosity of air at 15°C is 0.017 cp or 1.14 x 10-5 lb/ft-s (Smith, 1996).

Appendix D
Step Potential Predictions and Measurements

This page intentionally left blank.

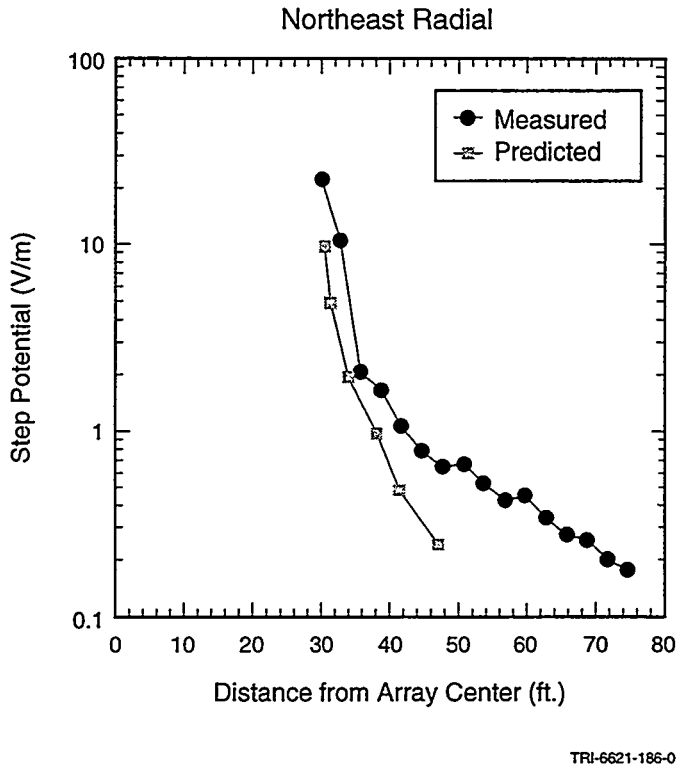

Figure D-1. Comparison of calculated versus measured step potential (Northeast radial).

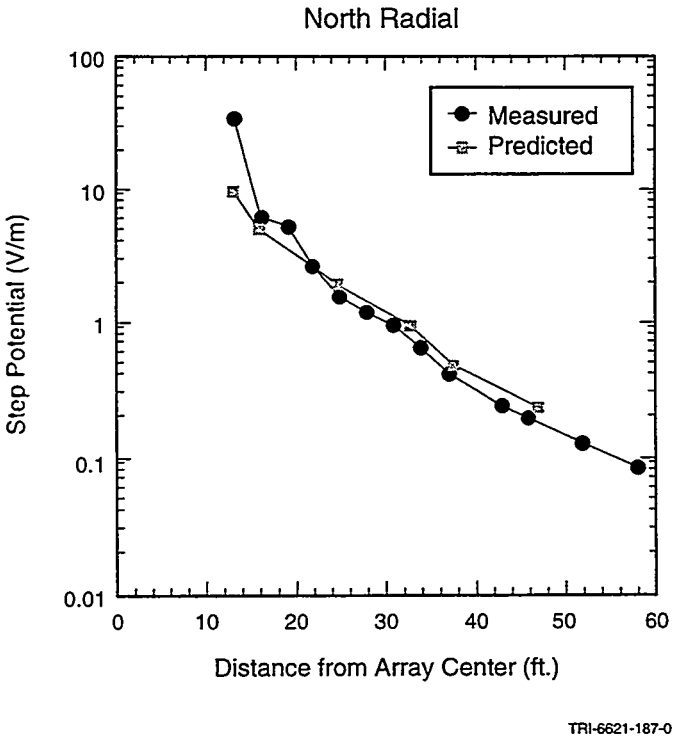

Figure D-2. Comparison of calculated versus measured step potential (North radial).

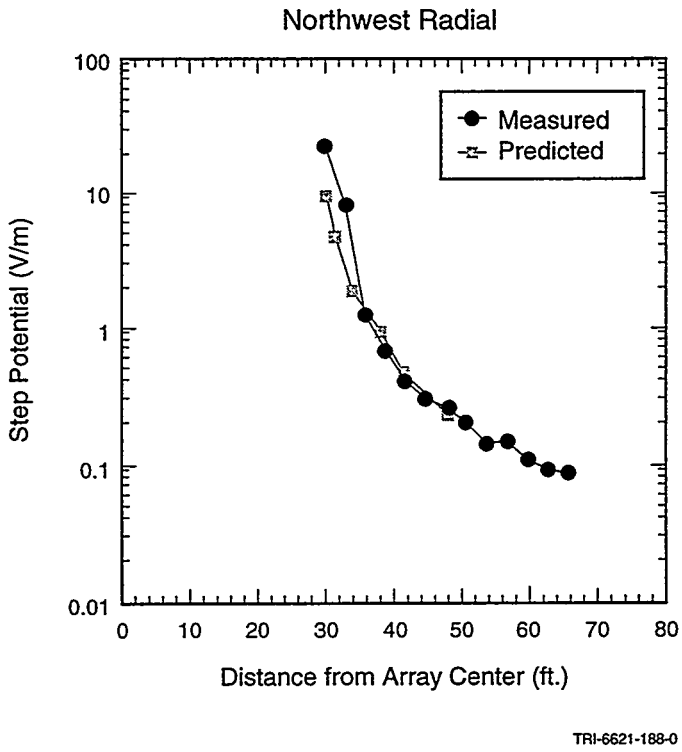

Figure D-3. Comparison of calculated versus measured step potential (Northwest radial).

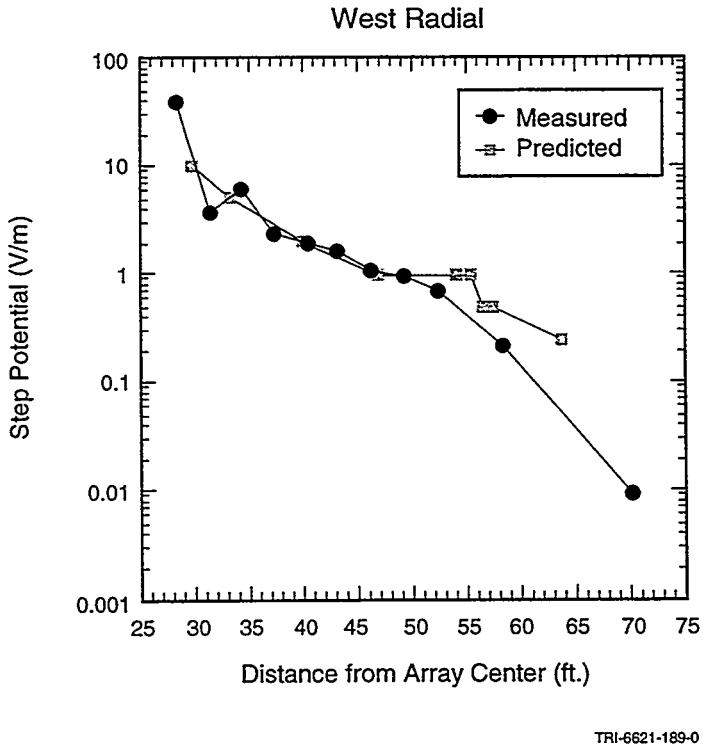

Figure D-4. Comparison of calculated versus measured step potential (West radial).

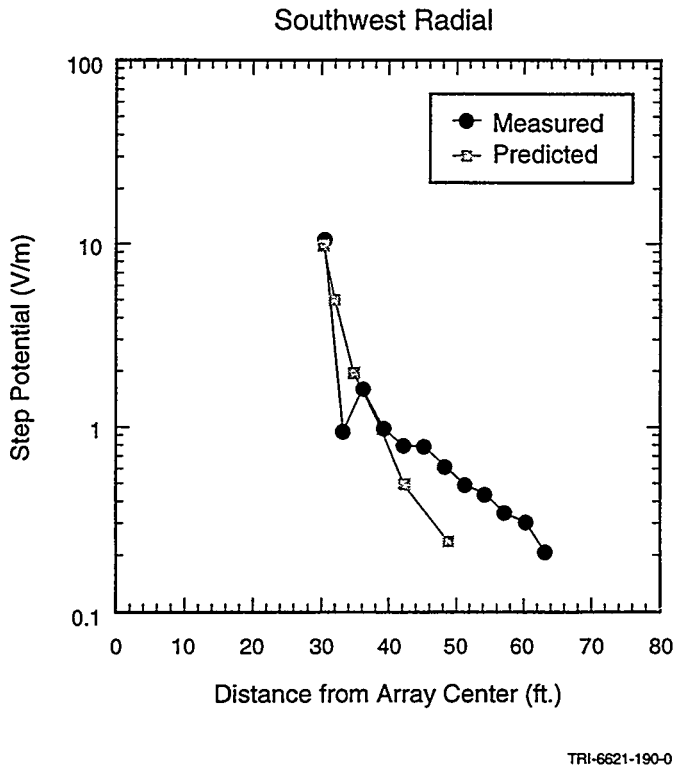

Figure D-5. Comparison of calculated versus measured step potential (Southwest radial).

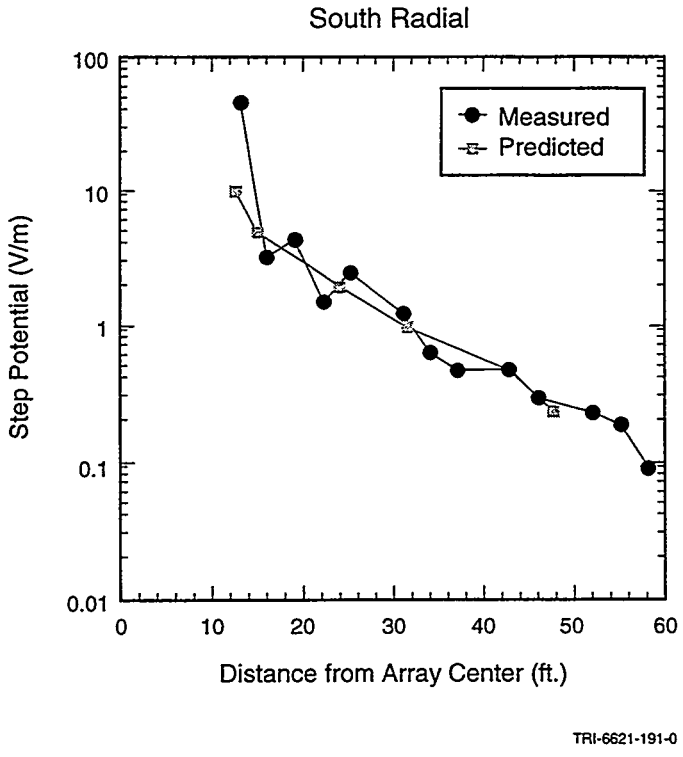

Figure D-6. Comparison of calculated versus measured step potential (South radial).

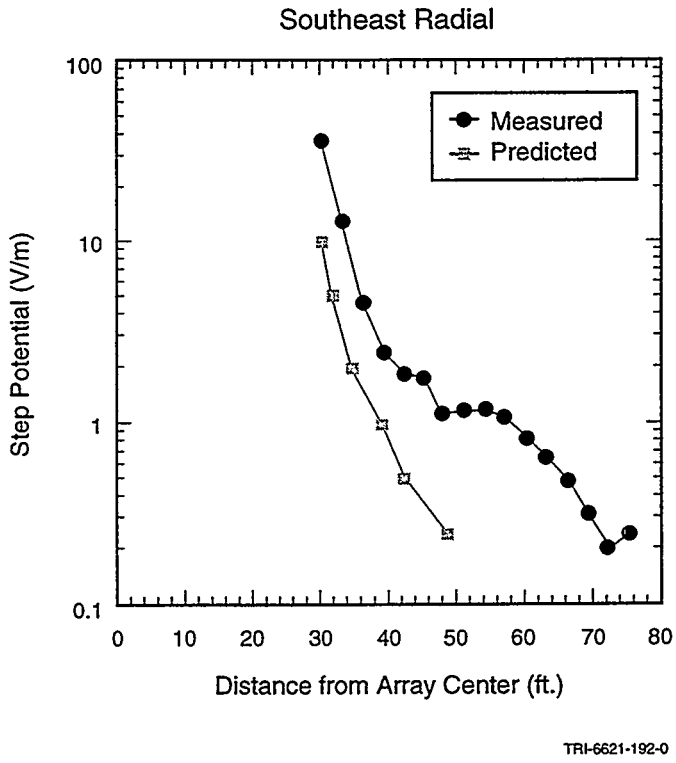

Figure D-7. Comparison of calculated versus measured step potential (Southeast radial).

Appendix E
Pre-Test and Post-Test Soil and Soil Gas Analysis Data

This page intentionally left blank.

Table E-1. Pre-Test and Post-Test Soil Analysis

Pre-test Soil Analysis		Detected Results Only		Detected Results Only		Post-Test Soil Analysis	
Sample No.	Location, Depth	Contaminant	Concentration	Concentration	Contaminant	Location, Depth	Sample No.
Outside Treatment Zone Data							
				2.4 mg/kg	Total Chromatographable Organics (TCO)	PT1,5	25406-05
				ND < 8.0 mg/kg	Total Chromatographable Organics (TCO)	PT1,10	25407-05
017161-2	D1,10	bis(2-Ethylhexyl) phthalate	0.034 mg/kg				
				ND < 4.0 mg/kg	Total Chromatographable Organics (TCO)	PT1,15	25408-05
				ND < 4.0 mg/kg	Total Chromatographable Organics (TCO)	PT1,25	25409-05
017163-2	D1,25	bis(2-Ethylhexyl) phthalate	0.063 mg/kg				
				ND < 4.0 mg/kg	Total Chromatographable Organics (TCO)	PT2,5	25410-05
				ND < 4.0 mg/kg	Total Chromatographable Organics (TCO)	PT2,10	25411-05
017165-1	D2,10	Acetone	0.020 mg/kg				
017165-1	D2,10	Methylene chloride	0.0019 mg/kg				
017165-2	D2,10	bis(2-Ethylhexyl) phthalate	0.043 mg/kg				
				ND < 4.0 mg/kg	Total Chromatographable Organics (TCO)	PT2,15	25412-05
				0.005 mg/kg	Methylene chloride	PT2,25	25413-04
				ND < 4.0 mg/kg	Total Chromatographable Organics (TCO)	PT2,25	25413-05
017167-1	D2,25	Toluene	0.003 mg/kg				
Ground Row Electrode Data							
				3.4 mg/kg	Total Chromatographable Organics (TCO)	PT3,5	25414-05
017151-1	A3,5	Methylene chloride	0.0023 mg/kg				
017152-1	A3,10	Methylene chloride	0.0027 mg/kg	0.005 mg/kg	Methylene chloride	PT3,10	25415-04
017152-2	A3,10	Total Chromatographable Organics (TCO)	13 mg/kg	4.4 mg/kg	Total Chromatographable Organics (TCO)	PT3,10	25415-05
017152-1	A3,10	Acetone	0.0076 mg/kg				
017152-2	A3,10	Phenanthrene	0.044 mg/kg				
017152-2	A3,10	bis(2-Ethylhexyl) phthalate	0.11 mg/kg				
017153-1	A3,15	Methylene chloride	0.0028 mg/kg	0.006 mg/kg	Methylene chloride	PT3,15	25416-04
017153-2	A3,15	Total Chromatographable Organics (TCO)	2.1 mg/kg	3.8 mg/kg	Total Chromatographable Organics (TCO)	PT3,15	25416-05

Table E-1. Pre-Test and Post-Test Soil Analysis

Pre-test Soil Analysis		Detected Results Only			Detected Results Only		Post-Test Soil Analysis	
Sample No.	Location, Depth	Contaminant	Concentration		Concentration	Contaminant	Location, Depth	Sample No.
017153-2	A3,15	bis(2-Ethylhexyl) phthalate	0.45 mg/kg					
017153-2	A3,15	Di-n-octyl phthalate	0.04 mg/kg					
					3.6 mg/kg	Total Chromatographable Organics (TCO)	PT3,25	25417-05
017154-1	A3,25	Acetone	0.0058 mg/kg					
017154-1	A3,25	Ethylbenzene	0.0019 mg/kg					
017154-1	A3,25	Methylene chloride	0.0031 mg/kg					
017154-1	A3,25	Tetrachloroethene	0.0015 mg/kg					
017154-1	A3,25	Toluene	0.0011 mg/kg					
017154-1	A3,25	Trichloroethene	0.0015 mg/kg					
017154-1	A3,25	Xylenes	0.0056 mg/kg					
					7.2 mg/kg	Total Chromatographable Organics (TCO)	PT4,5	25418-05
017155-1	A6,5	Acetone	0.005 mg/kg					
017155-1	A6,5	Methylene chloride	0.0039 mg/kg					
017155-1	A6,5	Tetrachloroethene	0.0014 mg/kg					
					0.45 mg/kg	Dibenzofuran	PT4,10	25419-01
					0.35 mg/kg	2, 4-Dimethylphenol	PT4,10	25419-01
					1.0 mg/kg	2-Methylphenol (o-cresol)	PT4,10	25419-01
					0.95 mg/kg	4-Methylphenol (p-cresol)	PT4,10	25419-01
017156-2	A6,10	Total Chromatographable Organics (TCO)	3.5 mg/kg		170 mg/kg	Total Chromatographable Organics (TCO)	PT4,10	25419-05
017156-1	A6,10	Methylene chloride	0.011 mg/kg					
017156-2	A6,10	bis(2-Ethylhexyl) phthalate	0.034 mg/kg					
017157-1	A6,15	Tetrachloroethene	5.5 mg/kg					
017157-1	A6,15	Trichloroethene	0.77 mg/kg					
Duplicate of 017157-1								
017158-1	A6,15	Methylene chloride	0.11 mg/kg					
017158-1	A6,15	Tetrachloroethene	4.1 mg/kg					
017158-1	A6,15	Toluene	0.14 mg/kg					
017157-2	A6,15	Total Chromatographable Organics (TCO)	5.5 mg/kg					
017157-2	A6,15	Phenanthrene	0.034 mg/kg					
017157-2	A6,15	bis(2-Ethylhexyl) phthalate	0.11 mg/kg					
Duplicate of 017157-2								
017158-2	A6,15	Acenaphthene	0.47 mg/kg					
017158-2	A6,15	Dibenzofuran	0.61 mg/kg					
017158-2	A6,15	Fluorene	2.1 mg/kg					

Table E-1. Pre-Test and Post-Test Soil Analysis

Pre-test Soil Analysis		Detected Results Only			Detected Results Only		Post-Test Soil Analysis	
Sample No.	Location, Depth	Contaminant	Concentration		Concentration	Contaminant	Location, Depth	Sample No.
017158-2	A6,15	Phenanthrene	7.8 mg/kg					
017158-2	A6,15	Fluoranthene	1.4 mg/kg					
017158-2	A6,15	Pyrene	5.4 mg/kg					
017158-2	A6,15	Benzo(a)anthracene	0.24 mg/kg					
017158-2	A6,15	bis(2-Ethylhexyl) phthalate	5.1 mg/kg					
017158-2	A6,15	Chrysene	0.48 mg/kg					
017158-2	A6,15	Benzo(b)fluoranthene	0.28 mg/kg					
017158-2	A6,15	Benzo(g,h,i)perylene	0.17 mg/kg					
017158-2	A6,15	Total Chromatographable Organics (TCO)	1700 mg/kg					
017159-2	A6,25	Total Chromatographable Organics (TCO)	2.8 mg/kg		ND < 4.0 mg/kg	Total Chromatographable Organics (TCO)	PT4,25	25421-05
017159-1	A6,25	Methylene chloride	0.0041 mg/kg					
Center Row Electrode Data								
					0.44 mg/kg	Di-n-butyl phthalate	PT5,5	25422-01
017168-2	B1,5	Total Chromatographable Organics (TCO)	11000 mg/kg		5.3 mg/kg	Total Chromatographable Organics (TCO)	PT5,5	25422-05
017168-1	B1,5	Acetone	2.3 mg/kg					
017168-1	B1,5	Ethylbenzene	3.0 mg/kg					
017168-1	B1,5	Methylene chloride	0.54 mg/kg					
017168-1	B1,5	Tetrachloroethene	45 mg/kg					
017168-1	B1,5	Toluene	1.4 mg/kg					
017168-1	B1,5	1,1,1-Trichloroethane	1.2 mg/kg					
017168-1	B1,5	1,1,2-Trichloroethane	1.4 mg/kg					
017168-1	B1,5	Trichloroethene	14 mg/kg					
017168-1	B1,5	Xylenes	31 mg/kg					
017168-2	B1,5	1,2-Dichlorobenzene	2.4 mg/kg					
017168-2	B1,5	2-Methylnaphthalene	2.7 mg/kg					
017168-2	B1,5	Acenaphthene	6.0 mg/kg					
017168-2	B1,5	Dibenzofuran	6.0 mg/kg					
017168-2	B1,5	Diethyl phthalate	2.0 mg/kg					
017168-2	B1,5	Fluorene	39 mg/kg					
017168-2	B1,5	Phenanthrene	96 mg/kg					
017168-2	B1,5	Carbazole	25 mg/kg					
017168-2	B1,5	Fluoranthene	16 mg/kg					
017168-2	B1,5	Pyrene	56 mg/kg					
017168-2	B1,5	Benzo(a)anthracene	3.1 mg/kg					
017168-2	B1,5	Chrysene	6.5 mg/kg					
017168-2	B1,5	Benzo(b)fluoranthene	3.4 mg/kg					
017168-2	B1,5	Benzo(a)pyrene	1.6 mg/kg					
017168-2	B1,5	Benzo(g,h,i)perylene	2.2 mg/kg					
017169-2	B1,12	Benzo(a)anthracene	1.6 mg/kg		0.41 mg/kg	Benzo(a)anthracene	PT5,10	25423-01
017169-2	B1,12	Benzo(b)fluoranthene	1.4 mg/kg		0.48 mg/kg	Benzo(b)fluoranthene	PT5,10	25423-01
017169-2	B1,12	Chrysene	1.8 mg/kg		0.83 mg/kg	Chrysene	PT5,10	25423-01
017169-2	B1,12	Dibenzofuran	2.3 mg/kg		0.4 mg/kg	Dibenzofuran	PT5,10	25423-01

Table E-1. Pre-Test and Post-Test Soil Analysis

Pre-test Soil Analysis		Detected Results Only			Detected Results Only		Post-Test Soil Analysis	
Sample No.	Location, Depth	Contaminant	Concentration		Concentration	Contaminant	Location, Depth	Sample No.
					0.49 mg/kg	Di-n-butyl phthalate	PT5,10	25423-01
017169-2	B1,12	Fluoranthene	5.4 mg/kg		1.3 mg/kg	Fluoranthene	PT5,10	25423-01
017169-2	B1,12	Phenanthrene	21 mg/kg		29 mg/kg	Phenanthrene	PT5,10	25423-01
017169-2	B1,12	Pyrene	14 mg/kg		3.8 mg/kg	Pyrene	PT5,10	25423-01
					0.013 mg/kg	Benzene	PT5,10	25423-04
017169-1	B1,12	Methylene chloride	0.32 mg/kg		0.009 mg/kg	Methylene chloride	PT5,10	25423-04
017169-1	B1,12	Toluene	1.0 mg/kg		0.006 mg/kg	Toluene	PT5,10	25423-04
					1800 mg/kg	Total Chromatographable Organics (TCO)	PT5,10	25423-05
017169-1	B1,12	Acetone	1.4 mg/kg					
017169-1	B1,12	Ethylbenzene	1.6 mg/kg					
017169-1	B1,12	Tetrachloroethene	7.5 mg/kg					
017169-1	B1,12	1,1,1-Trichloroethane	0.83 mg/kg					
017169-1	B1,12	1,1,2-Trichloroethane	0.33 mg/kg					
017169-1	B1,12	Trichloroethene	1.9 mg/kg					
017169-1	B1,12	Xylenes	11 mg/kg					
017169-2	B1,12	Phenol	0.71 mg/kg					
017169-2	B1,12	1,2-Dichlorobenzene	0.3 mg/kg					
017169-2	B1,12	2-Methylphenol	0.43 mg/kg					
017169-2	B1,12	4-Methylphenol	1.2 mg/kg					
017169-2	B1,12	2,4-Dimethylphenol	0.43 mg/kg					
017169-2	B1,12	Naphthalene	1.0 mg/kg					
017169-2	B1,12	2-Methylnaphthalene	1.9 mg/kg					
017169-2	B1,12	Acenaphthene	1.7 mg/kg					
017169-2	B1,12	Anthracene	1.4 mg/kg					
017169-2	B1,12	Carbazole	7.2 mg/kg					
017169-2	B1,12	Benzo(a)pyrene	1.0 mg/kg					
017169-2	B1,12	Indeno(1,2,3-cd)pyrene	0.65 mg/kg					
017169-2	B1,12	Benzo(g,h,i)perylene	1.0 mg/kg					
017169-2	B1,12	Total Chromatographable Organics (TCO)	2900 mg/kg					
017170-2	B1,15	Benzo(a)anthracene	0.2 mg/kg		0.52 mg/kg	Benzo(a)anthracene	PT5,15	25424-01
017170-2	B1,15	Fluoranthene	0.8 mg/kg		1.4 mg/kg	Fluoranthene	PT5,15	25424-01
017170-2	B1,15	Phenanthrene	2.8 mg/kg		11 mg/kg	Phenanthrene	PT5,15	25424-01
017170-2	B1,15	Pyrene	2.5 mg/kg		6.5 mg/kg	Pyrene	PT5,15	25424-01
					0.006 mg/kg	Benzene	PT5,15	25424-04
					0.037 mg/kg	Trichloroethene	PT5,15	25424-04
					0.005 mg/kg	Xylenes	PT5,15	25424-04
017170-2	B1,15	Total Chromatographable Organics (TCO)	190 mg/kg		510 mg/kg	Total Chromatographable Organics (TCO)	PT5,15	25424-05
017170-2	B1,15	Fluorene	0.8 mg/kg					
017170-2	B1,15	Anthracene	0.2 mg/kg					
017170-2	B1,15	Carbazole	0.57 mg/kg					
017170-2	B1,15	Di-n-butyl phthalate	0.095 mg/kg					
017170-2	B1,15	bis(2-Ethylhexyl) phthalate	1.4 mg/kg					
017170-2	B1,15	Chrysene	0.56 mg/kg					

Table E-1. Pre-Test and Post-Test Soil Analysis

Pre-test Soil Analysis		Detected Results Only			Detected Results Only		Post-Test Soil Analysis	
Sample No.	Location, Depth	Contaminant	Concentration		Concentration	Contaminant	Location, Depth	Sample No.
017170-2	B1,15	Benzo(b)fluoranthene	0.17 mg/kg					
017170-2	B1,15	Benzo(a)pyrene	0.14 mg/kg					
017170-2	B1,15	Indeno(1,2,3-cd)pyrene	0.095 mg/kg					
017170-2	B1,15	Benzo(g,h,i)perylene	0.16 mg/kg					
017170-2	B1,15	Naphthalene	0.079 mg/kg					
017170-2	B1,15	2-Methylnaphthalene	0.16 mg/kg					
017170-2	B1,15	Acenaphthene	0.22 mg/kg					
017170-2	B1,15	Dibenzofuran	0.2 mg/kg					
017171-2	B1,25	Total Chromatographable Organics (TCO)	4.2 mg/kg		79 mg/kg	Total Chromatographable Organics (TCO)	PT5,25	25425-05
					3.3 mg/kg	Total Chromatographable Organics (TCO)	PT5,35	25426-05
017173-2	B1,45	Total Chromatographable Organics (TCO)	14 mg/kg		2.2 mg/kg	Total Chromatographable Organics (TCO)	PT5,45	25427-05
017173-2	B1,45	Fluorene	0.076 mg/kg					
017173-2	B1,45	Phenanthrene	0.3 mg/kg					
017173-2	B1,45	Anthracene	0.035 mg/kg					
017173-2	B1,45	Carbazole	0.088 mg/kg					
017173-2	B1,45	Fluoranthene	0.073 mg/kg					
017173-2	B1,45	Pyrene	0.2 mg/kg					
017173-2	B1,45	bis(2-Ethylhexyl) phthalate	0.086 mg/kg					
017174-2	B1,55	Total Chromatographable Organics (TCO)	19 mg/kg		2.3 mg/kg	Total Chromatographable Organics (TCO)	PT5,55	25428-05
017174-1	B1,55	Methylene chloride	0.003 mg/kg					
017174-2	B1,55	Fluorene	0.079 mg/kg					
017174-2	B1,55	Phenanthrene	0.33 mg/kg					
017174-2	B1,55	Anthracene	0.035 mg/kg					
017174-2	B1,55	Carbazole	0.098 mg/kg					
017174-2	B1,55	Fluoranthene	0.086 mg/kg					
017174-2	B1,55	Pyrene	0.23 mg/kg					
017174-2	B1,55	bis(2-Ethylhexyl) phthalate	0.12 mg/kg					
016936-2	B4,5	Total Chromatographable Organics (TCO)	11000 mg/kg		23 mg/kg	Total Chromatographable Organics (TCO)	PT6,5	25439-03
016936-1	B4,5	Acetone	1.3 mg/kg					
016936-1	B4,5	Benzene	0.11 mg/kg					
016936-1	B4,5	Ethylbenzene	10 mg/kg					
016936-1	B4,5	Methylene chloride	0.31 mg/kg					
016936-1	B4,5	Tetrachloroethene	0.96 mg/kg					
016936-1	B4,5	Toluene	0.38 mg/kg					
016936-1	B4,5	Trichloroethene	0.52 mg/kg					
016936-1	B4,5	Xylenes	24 mg/kg					
016936-2	B4,5	1,2-Dichlorobenzene	3.8 mg/kg					

Table E-1. Pre-Test and Post-Test Soil Analysis

Pre-test Soil Analysis		Detected Results Only			Detected Results Only		Post-Test Soil Analysis	
Sample No.	Location, Depth	Contaminant	Concentration		Concentration	Contaminant	Location, Depth	Sample No.
016936-2	B4,5	4-Methylphenol	3.0 mg/kg					
016936-2	B4,5	Naphthalene	21 mg/kg					
016936-2	B4,5	2-Methylnaphthalene	13 mg/kg					
016936-2	B4,5	Acenaphthene	2.6 mg/kg					
016936-2	B4,5	Dibenzofuran	4.2 mg/kg					
016936-2	B4,5	Fluorene	7.0 mg/kg					
016936-2	B4,5	Phenanthrene	21 mg/kg					
016936-2	B4,5	Carbazole	3.0 mg/kg					
016936-2	B4,5	Fluoranthene	3.0 mg/kg					
016936-2	B4,5	Pyrene	9.4 mg/kg					
016936-2	B4,5	Butyl benzyl phthalate	1.8 mg/kg					
016936-2	B4,5	bis(2-Ethylhexyl) phthalate	35 mg/kg					
016936-2	B4,5	Chrysene	0.86 mg/kg					
					25 mg/kg	chromium (Cr)	PT6,10	25440-01
					3.3 mg/kg	Bis(2-ethylhexyl) phthalate	PT6,10	25440-01
					7.2 mg/kg	Chrysene	PT6,10	25440-01
					7.4 mg/kg	n-Nitrosodiphenylamine	PT6,10	25440-01
					17 mg/kg	Phenanthrene	PT6,10	25440-01
					1.7 mg/kg	Pyrene	PT6,10	25440-01
016937-1	B4,10	Benzene	30 mg/kg		0.024 mg/kg	Benzene	PT6,10	25440-02
016937-1	B4,10	Toluene	160 mg/kg		0.013 mg/kg	Toluene	PT6,10	25440-02
016937-2	B4,10	Total Chromatographable Organics (TCO)	9300 mg/kg		2600 mg/kg	Total Chromatographable Organics (TCO)	PT6,10	25440-03
016937-1	B4,10	Acetone	38 mg/kg					
016937-1	B4,10	1,1-Dichloroethane	11 mg/kg					
016937-1	B4,10	Ethylbenzene	140 mg/kg					
016937-1	B4,10	4-Methyl-2-pentanone(MIBK)	11 mg/kg					
016937-1	B4,10	Tetrachloroethene	130 mg/kg					
016937-1	B4,10	1,1,1-Trichloroethane	83 mg/kg					
016937-1	B4,10	1,1,2-Trichloroethane	14 mg/kg					
016937-1	B4,10	Trichloroethene	210 mg/kg					
016937-1	B4,10	Xylenes	420 mg/kg					
016937-2	B4,10	Fluorene	9.8 mg/kg					
016937-2	B4,10	Phenanthrene	22 mg/kg					
016937-2	B4,10	Carbazole	2.1 mg/kg					
016937-2	B4,10	Fluoranthene	4.3 mg/kg					
016937-2	B4,10	Pyrene	9.9 mg/kg					
016937-2	B4,10	Butyl benzyl phthalate	0.71 mg/kg					
016937-2	B4,10	Benzo(a)anthracene	0.77 mg/kg					
016937-2	B4,10	bis(2-Ethylhexyl) phthalate	12 mg/kg					
016937-2	B4,10	Chrysene	1.1 mg/kg					
016937-2	B4,10	Benzo(b)fluoranthene	0.5 mg/kg					

Table E-2. Pre-Test and Post-Test Soil Gas Analysis

Pre-test Soil Gas Analysis		Detected Results Only			Detected Results Only		Post-Test Soil Gas Analysis	
Sample No.	Location, Depth	Contaminant	Concentration		Concentration	Contaminant	Location, Depth	Sample No.
Center Row Electrode Data								
017168-3	B1,5	Benzene	1.5 ppm		0.26 ppm	Benzene	PT5,5	25431-01
017168-3	B1,5	Chloroform	1.0 ppm		0.42 ppm	Chloroform	PT5,5	25431-01
017168-3	B1,5	Dichlorodifluoromethane	3.0 ppm		0.36 ppm	Dichlorodifluoromethane	PT5,5	25431-01
					0.45 ppm	1,2-Dichloropropane	PT5,5	25431-01
					0.90 ppm	Methylene chloride	PT5,5	25431-01
017168-3	B1,5	Tetrachloroethene	64 ppm		0.79 ppm	Tetrachloroethene	PT5,5	25431-01
017168-3	B1,5	1,1,1-Trichloroethane	40 ppm		3.3 ppm	1,1,1-Trichloroethane	PT5,5	25431-01
017168-3	B1,5	Trichloroethene	110 ppm		29 ppm	Trichloroethene	PT5,5	25431-01
017168-3	B1,5	1,1,2-Trichloro-1,2,2-tri-fluoroethane	5.2 ppm		7.1 ppm	1,1,2-Trichloro-1,2,2-tri-fluoroethane	PT5,5	25431-01
017168-3	B1,5	Trichlorofluoromethane	4.1 ppm					
017168-3	B1,5	1,1-Dichloroethene	1.3 ppm					
017168-3	B1,5	1,1-Dichloroethane	1.6 ppm					
017168-3	B1,5	Toluene	10 ppm					
017168-3	B1,5	Ethylbenzene	5.1 ppm					
017168-3	B1,5	Xylenes	20 ppm					
017169-3	B1,10	Benzene	0.57 ppm		0.22 ppm	Benzene	PT5,10	25432-01
017169-3	B1,10	Chloroform	0.49 ppm		0.43 ppm	Chloroform	PT5,10	25432-01
017169-3	B1,10	Dichlorodifluoromethane	2.1 ppm		0.37 ppm	Dichlorodifluoromethane	PT5,10	25432-01
017169-3	B1,10	1,2-Dichloropropane	0.47 ppm		0.41 ppm	1,2-Dichloropropane	PT5,10	25432-01
					0.86 ppm	Methylene chloride	PT5,10	25432-01
017169-3	B1,10	Tetrachloroethene	39 ppm		0.83 ppm	Tetrachloroethene	PT5,10	25432-01
017169-3	B1,10	1,1,1-Trichloroethane	20 ppm		3.4 ppm	1,1,1-Trichloroethane	PT5,10	25432-01
017169-3	B1,10	Trichloroethene	42 ppm		30 ppm	Trichloroethene	PT5,10	25432-01
017169-3	B1,10	1,1,2-Trichloro-1,2,2-tri-fluoroethane	2.5 ppm		7.3 ppm	1,1,2-Trichloro-1,2,2-tri-fluoroethane	PT5,10	25432-01
017169-3	B1,10	Trichlorofluoromethane	2.3 ppm					
017169-3	B1,10	1,1-Dichloroethene	0.56 ppm					
017169-3	B1,10	1,1-Dichloroethane	0.69 ppm					
017169-3	B1,10	Toluene	8.7 ppm					
017169-3	B1,10	Ethylbenzene	3.3 ppm					
017169-3	B1,10	Xylenes	14 ppm					
017170-3	B1,15	Chloroform	0.28 ppm		0.22 ppm	Chloroform	PT5,15	25433-01
017170-3	B1,15	1,2-Dichloropropane	0.35 ppm		0.21 ppm	1,2-Dichloropropane	PT5,15	25433-01
017170-3	B1,15	Methylene chloride	0.22 ppm		0.44 ppm	Methylene chloride	PT5,15	25433-01
017170-3	B1,15	Tetrachloroethene	24 ppm		0.43 ppm	Tetrachloroethene	PT5,15	25433-01
017170-3	B1,15	1,1,1-Trichloroethane	9.8 ppm		1.8 ppm	1,1,1-Trichloroethane	PT5,15	25433-01
017170-3	B1,15	Trichloroethene	25 ppm		15 ppm	Trichloroethene	PT5,15	25433-01
017170-3	B1,15	1,1,2-Trichloro-1,2,2-tri-fluoroethane	1.3 ppm		3.9 ppm	1,1,2-Trichloro-1,2,2-tri-fluoroethane	PT5,15	25433-01
017170-3	B1,15	Dichlorodifluoromethane	0.57 ppm					
017170-3	B1,15	Trichlorofluoromethane	0.84 ppm					
017170-3	B1,15	1,1-Dichloroethene	0.33 ppm					
017170-3	B1,15	Acetone	1.2 ppm					
017170-3	B1,15	1,1-Dichloroethane	0.36 ppm					
017170-3	B1,15	Benzene	0.44 ppm					

Table E-2. Pre-Test and Post-Test Soil Gas Analysis

Pre-test Soil Gas Analysis		Detected Results Only			Detected Results Only		Post-Test Soil Gas Analysis	
Sample No.	Location, Depth	Contaminant	Concentration		Concentration	Contaminant	Location, Depth	Sample No.
017170-3	B1,15	4-Methyl-2-pentanone	0.26 ppm					
017170-3	B1,15	Toluene	5.4 ppm					
017170-3	B1,15	Ethylbenzene	2.7 ppm					
017170-3	B1,15	Xylenes	12 ppm					
017170-3	B1,15	4-Ethyl toluene	0.21 ppm					
017170-3	B1,15	1,2,4-Trimethylbenzene	0.12 ppm					
017170-3	B1,15	1,2-Dichlorobenzene	0.13 ppm					
Duplicate of 017170-3								
					0.26 ppm	Benzene	PT5,15	25438-01
					0.53 ppm	Chloroform	PT5,15	25438-01
016396-3	B1,15	Dichlorodifluoromethane	0.45 ppm		0.43 ppm	Dichlorodifluoromethane	PT5,15	25438-01
					0.27 ppm	1,2-Dichloroethane	PT5,15	25438-01
					0.59 ppm	1,2-Dichloropropane	PT5,15	25438-01
					1.1 ppm	Methylene chloride	PT5,15	25438-01
016396-3	B1,15	Tetrachloroethene	20 ppm		1.0 ppm	Tetrachloroethene	PT5,15	25438-01
016396-3	B1,15	1,1,1-Trichloroethane	7.9 ppm		4.2 ppm	1,1,1-Trichloroethane	PT5,15	25438-01
016396-3	B1,15	Trichloroethene	22 ppm		39 ppm	Trichloroethene	PT5,15	25438-01
016396-3	B1,15	Trichlorofluoromethane	0.67 ppm		2.5 ppm	Trichlorofluoromethane	PT5,15	25438-01
016396-3	B1,15	1,1,2-Trichloro-1,2,2-tri-fluoroethane	1.1 ppm		8.6 ppm	1,1,2-Trichloro-1,2,2-tri-fluoroethane	PT5,15	25438-01
016396-3	B1,15	Toluene	4.2 ppm					
016396-3	B1,15	Ethylbenzene	2.0 ppm					
016396-3	B1,15	Xylenes	8.8 ppm					
					0.31 ppm	Benzene	PT5,25	25434-01
017171-3	B1,25	Chloroform	0.44 ppm		0.62 ppm	Chloroform	PT5,25	25434-01
017171-3	B1,25	Dichlorodifluoromethane	2.4 ppm		0.48 ppm	Dichlorodifluoromethane	PT5,25	25434-01
017171-3	B1,25	1,2-Dichloropropane	0.45 ppm		0.69 ppm	1,2-Dichloropropane	PT5,25	25434-01
					1.3 ppm	Methylene chloride	PT5,25	25434-01
017171-3	B1,25	Tetrachloroethene	9.5 ppm		1.3 ppm	Tetrachloroethene	PT5,25	25434-01
017171-3	B1,25	1,1,1-Trichloroethane	7.0 ppm		4.7 ppm	1,1,1-Trichloroethane	PT5,25	25434-01
017171-3	B1,25	Trichloroethene	22 ppm		47 ppm	Trichloroethene	PT5,25	25434-01
017171-3	B1,25	1,1,2-Trichloro-1,2,2-tri-fluoroethane	3.0 ppm		9.7 ppm	1,1,2-Trichloro-1,2,2-tri-fluoroethane	PT5,25	25434-01
017171-3	B1,25	Trichlorofluoromethane	1.7 ppm					
017171-3	B1,25	1,1-Dichloroethene	0.58 ppm					
017171-3	B1,25	Toluene	1.4 ppm					
017171-3	B1,25	Ethylbenzene	0.5 ppm					
017171-3	B1,25	Xylenes	2.9 ppm					
017172-3	B1,35	Chloroform	0.26 ppm		0.69 ppm	Chloroform	PT5,35	25435-01
					0.24 ppm	1,2-Dibromoethane	PT5,35	25435-01
017172-3	B1,35	Dichlorodifluoromethane	1.3 ppm		0.54 ppm	Dichlorodifluoromethane	PT5,35	25435-01
					0.37 ppm	1,2-Dichloroethane	PT5,35	25435-01
					0.75 ppm	1,2-Dichloropropane	PT5,35	25435-01
017172-3	B1,35	Methylene chloride	0.21 ppm		1.6 ppm	Methylene chloride	PT5,35	25435-01
017172-3	B1,35	Tetrachloroethene	7.7 ppm		1.4 ppm	Tetrachloroethene	PT5,35	25435-01
017172-3	B1,35	1,1,1-Trichloroethane	4.3 ppm		4.9 ppm	1,1,1-Trichloroethane	PT5,35	25435-01

Table E-2. Pre-Test and Post-Test Soil Gas Analysis

Pre-test Soil Gas Analysis		Detected Results Only		Detected Results Only		Post-Test Soil Gas Analysis	
Sample No.	Location, Depth	Contaminant	Concentration	Concentration	Contaminant	Location, Depth	Sample No.
017172-3	B1,35	Trichloroethene	15 ppm	51 ppm	Trichloroethene	PT5,35	25435-01
017172-3	B1,35	1,1,2-Trichloro-1,2,2-tri-fluoroethane	1.8 ppm	11 ppm	1,1,2-Trichloro-1,2,2-tri-fluoroethane	PT5,35	25435-01
017172-3	B1,35	Trichlorofluoromethane	0.84 ppm				
017172-3	B1,35	1,1-Dichloroethene	0.37 ppm				
017172-3	B1,35	Benzene	0.32 ppm				
017172-3	B1,35	Toluene	0.73 ppm				
017172-3	B1,35	Ethylbenzene	0.36 ppm				
017172-3	B1,35	Xylenes	1.8 ppm				
017173-3	B1,45	Benzene	0.59 ppm	0.30 ppm	Benzene	PT5,45	25436-01
017173-3	B1,45	Chloroform	0.28 ppm	0.55 ppm	Chloroform	PT5,45	25436-01
017173-3	B1,45	Dichlorodifluoromethane	2.6 ppm	0.48 ppm	Dichlorodifluoromethane	PT5,45	25436-01
				0.28 ppm	1,2-Dichloroethane	PT5,45	25436-01
017173-3	B1,45	1,2-Dichloropropane	0.21 ppm	0.60 ppm	1,2-Dichloropropane	PT5,45	25436-01
017173-3	B1,45	Methylene chloride	0.47 ppm	1.3 ppm	Methylene chloride	PT5,45	25436-01
017173-3	B1,45	Tetrachloroethene	5.7 ppm	1.0 ppm	Tetrachloroethene	PT5,45	25436-01
017173-3	B1,45	1,1,1-Trichloroethane	5.5 ppm	4.3 ppm	1,1,1-Trichloroethane	PT5,45	25436-01
017173-3	B1,45	Trichloroethene	16 ppm	40 ppm	Trichloroethene	PT5,45	25436-01
017173-3	B1,45	1,1,2-Trichloro-1,2,2-tri-fluoroethane	2.4 ppm	9.5 ppm	1,1,2-Trichloro-1,2,2-tri-fluoroethane	PT5,45	25436-01
017173-3	B1,45	Trichlorofluoromethane	1.4 ppm				
017173-3	B1,45	1,1-Dichloroethene	0.65 ppm				
017173-3	B1,45	Toluene	0.8 ppm				
017173-3	B1,45	Ethylbenzene	0.22 ppm				
017173-3	B1,45	Xylenes	1.2 ppm				
017174-3	B1,55	Benzene	0.53 ppm	0.38 ppm	Benzene	PT5,55	25437-01
				0.64 ppm	Chloroform	PT5,55	25437-01
				0.24 ppm	1,2-Dibromoethane	PT5,55	25437-01
017174-3	B1,55	Dichlorodifluoromethane	1.2 ppm	0.46 ppm	Dichlorodifluoromethane	PT5,55	25437-01
017174-3	B1,55	1,2-Dichloropropane	0.21 ppm	0.75 ppm	1,2-Dichloropropane	PT5,55	25437-01
017174-3	B1,55	Methylene chloride	0.32 ppm	1.5 ppm	Methylene chloride	PT5,55	25437-01
017174-3	B1,55	Tetrachloroethene	5.4 ppm	1.3 ppm	Tetrachloroethene	PT5,55	25437-01
017174-3	B1,55	1,1,1-Trichloroethane	3.6 ppm	4.8 ppm	1,1,1-Trichloroethane	PT5,55	25437-01
017174-3	B1,55	Trichloroethene	11 ppm	48 ppm	Trichloroethene	PT5,55	25437-01
017174-3	B1,55	1,1,2-Trichloro-1,2,2-tri-fluoroethane	0.98 ppm	9.3 ppm	1,1,2-Trichloro-1,2,2-tri-fluoroethane	PT5,55	25437-01
017174-3	B1,55	Trichlorofluoromethane	0.61 ppm				
017174-3	B1,55	1,1-Dichloroethene	0.4 ppm				
017174-3	B1,55	Toluene	0.96 ppm				
017174-3	B1,55	Xylenes	1.8 ppm				
016936-3	B4,5	Benzene	14 ppm	0.066 ppm	Benzene	PT6,5	25452-01
016936-3	B4,5	Methylene chloride	1.4 ppm	0.025 ppm	Methylene chloride	PT6,5	25452-01
				0.025 ppm	1,1,2,2-tetrachlorethane	PT6,5	25452-01
016936-3	B4,5	Tetrachloroethene	9.5 ppm	0.025 ppm	Tetrachloroethene	PT6,5	25452-01
016936-3	B4,5	Toluene	17 ppm	0.026 ppm	Toluene	PT6,5	25452-01
016936-3	B4,5	1,1,1-Trichloroethane	18 ppm	0.036 ppm	1,1,1-Trichloroethane	PT6,5	25452-01

Table E-2. Pre-Test and Post-Test Soil Gas Analysis

Pre-test Soil Gas Analysis		Detected Results Only			Detected Results Only		Post-Test Soil Gas Analysis	
Sample No.	Location, Depth	Contaminant	Concentration		Concentration	Contaminant	Location, Depth	Sample No.
016936-3	B4,5	Trichloroethene	35 ppm		0.45 ppm	Trichloroethene	PT6,5	25452-01
016936-3	B4,5	1,1,2-Trichloro-1,2,2-tri-fluoroethane	1.7 ppm		0.049 ppm	1,1,2-Trichloro-1,2,2-tri-fluoroethane	PT6,5	25452-01
016936-3	B4,5	Dichlorodifluoromethane	0.67 ppm					
016936-3	B4,5	Trichlorofluoromethane	1.5 ppm					
016936-3	B4,5	1,1-Dichloroethene	0.3 ppm					
016936-3	B4,5	Acetone	1.1 ppm					
016936-3	B4,5	1,1-Dichloroethane	1.8 ppm					
016936-3	B4,5	Chloroform	0.32 ppm					
016936-3	B4,5	1,2-Dichloroethane	0.52 ppm					
016936-3	B4,5	Ethylbenzene	25 ppm					
016936-3	B4,5	Xylenes	40 ppm					
016936-3	B4,5	1,3,5-Trimethylbenzene	0.38 ppm					
016937-3	B4,10	Methylene chloride	1.0 ppm		0.025 ppm	Methylene chloride	PT6,10	25453-01
016937-3	B4,10	1,1,1-Trichloroethane	17 ppm		0.022 ppm	1,1,1-Trichloroethane	PT6,10	25453-01
016937-3	B4,10	Trichloroethene	47 ppm		0.37 ppm	Trichloroethene	PT6,10	25453-01
016937-3	B4,10	Dichlorodifluoromethane	1.5 ppm					
016937-3	B4,10	Trichlorofluoromethane	2.4 ppm					
016937-3	B4,10	1,1,2-Trichloro-1,2,2-tri-fluoroethane	3.1 ppm					
016937-3	B4,10	1,1-Dichloroethane	1.4 ppm					
016937-3	B4,10	Benzene	33 ppm					
016937-3	B4,10	Toluene	9.4 ppm					
016937-3	B4,10	Tetrachloroethene	13 ppm					
016937-3	B4,10	Ethylbenzene	5.3 ppm					
016937-3	B4,10	Xylenes	13 ppm					
					0.23 ppm	Methylene chloride	PT6,15	25454-01
016938-3	B4,15	1,1,1-Trichloroethane	3.2 ppm		0.78 ppm	1,1,1-Trichloroethane	PT6,15	25454-01
016938-3	B4,15	Trichloroethene	11 ppm		6.7 ppm	Trichloroethene	PT6,15	25454-01
016938-3	B4,15	Trichlorofluoromethane	0.48 ppm		0.49 ppm	Trichlorofluoromethane	PT6,15	25454-01
016938-3	B4,15	1,1,2-Trichloro-1,2,2-tri-fluoroethane	0.73 ppm		1.6 ppm	1,1,2-Trichloro-1,2,2-tri-fluoroethane	PT6,15	25454-01
016938-3	B4,15	Dichlorodifluoromethane	0.33 ppm					
016938-3	B4,15	Benzene	3.7 ppm					
016938-3	B4,15	Toluene	2.9 ppm					
016938-3	B4,15	Tetrachloroethene	3.5 ppm					
016938-3	B4,15	Ethylbenzene	3.4 ppm					
016938-3	B4,15	Xylenes	7.8 ppm					
016938-3	B4,15	1,3,5-Trimethylbenzene	0.55 ppm					
Duplicate of 016938-3								
016939-3	B4,15	Benzene	4.0 ppm		0.10 ppm	Benzene	PT6,15	25459-01
					0.22 ppm	Chloroform	PT6,15	25459-01
016939-3	B4,15	Dichlorodifluoromethane	0.33 ppm		0.12 ppm	Dichlorodifluoromethane	PT6,15	25459-01
					0.12 ppm	1,2-Dichloropropane	PT6,15	25459-01
					0.30 ppm	Methylene chloride	PT6,15	25459-01
016939-3	B4,15	Tetrachloroethene	4.1 ppm		0.25 ppm	Tetrachloroethene	PT6,15	25459-01

Table E-2. Pre-Test and Post-Test Soil Gas Analysis

Pre-test Soil Gas Analysis		Detected Results Only			Detected Results Only		Post-Test Soil Gas Analysis	
Sample No.	Location, Depth	Contaminant	Concentration		Concentration	Contaminant	Location, Depth	Sample No.
016939-3	B4,15	1,1,1-Trichloroethane	3.5 ppm		1.1 ppm	1,1,1-Trichloroethane	PT6,15	25459-01
016939-3	B4,15	Trichloroethene	12 ppm		8.9 ppm	Trichloroethene	PT6,15	25459-01
016939-3	B4,15	1,1,2-Trichloro-1,2,2-tri-fluoroethane	0.72 ppm		2.0 ppm	1,1,2-Trichloro-1,2,2-tri-fluoroethane	PT6,15	25459-01
016939-3	B4,15	Trichlorofluoromethane	0.48 ppm					
016939-3	B4,15	Toluene	3.0 ppm					
016939-3	B4,15	Ethylbenzene	3.6 ppm					
016939-3	B4,15	Xylenes	8.0 ppm					
016939-3	B4,15	1,3,5-Trimethylbenzene	0.59 ppm					
016940-3	B4,25	Chloroform	0.29 ppm		0.044 ppm	Chloroform	PT6,25	25455-01
016940-3	B4,25	Methylene chloride	0.3 ppm		0.078 ppm	Methylene chloride	PT6,25	25455-01
016940-3	B4,25	Tetrachloroethene	3.2 ppm		0.063 ppm	Tetrachloroethene	PT6,25	25455-01
016940-3	B4,25	1,1,1-Trichloroethane	4.6 ppm		0.10 ppm	1,1,1-Trichloroethane	PT6,25	25455-01
016940-3	B4,25	Trichloroethene	14 ppm		2.2 ppm	Trichloroethene	PT6,25	25455-01
016940-3	B4,25	Trichlorofluoromethane	0.99 ppm		0.046 ppm	Trichlorofluoromethane	PT6,25	25455-01
016940-3	B4,25	1,1,2-Trichloro-1,2,2-tri-fluoroethane	1.6 ppm		0.13 ppm	1,1,2-Trichloro-1,2,2-tri-fluoroethane	PT6,25	25455-01
016940-3	B4,25	Dichlorodifluoromethane	1.0 ppm					
016940-3	B4,25	1,1-Dichloroethene	0.44 ppm					
016940-3	B4,25	Benzene	3.0 ppm					
016940-3	B4,25	1,2-Dichloropropane	0.21 ppm					
016940-3	B4,25	Toluene	2.4 ppm					
016940-3	B4,25	Ethylbenzene	2.0 ppm					
016940-3	B4,25	Xylenes	4.3 ppm					
016941-3	B4,35	Chloroform	0.26 ppm		0.79 ppm	Chloroform	PT6,35	25456-01
016941-3	B4,35	Dichlorodifluoromethane	0.72 ppm		0.33 ppm	Dichlorodifluoromethane	PT6,35	25456-01
					0.44 ppm	1,2-Dichloroethane	PT6,35	25456-01
016941-3	B4,35	1,2-Dichloropropane	0.2 ppm		0.58 ppm	1,2-Dichloropropane	PT6,35	25456-01
016941-3	B4,35	Methylene chloride	0.35 ppm		1.2 ppm	Methylene chloride	PT6,35	25456-01
016941-3	B4,35	Tetrachloroethene	2.7 ppm		1.2 ppm	Tetrachloroethene	PT6,35	25456-01
016941-3	B4,35	1,1,1-Trichloroethane	3.0 ppm		4.0 ppm	1,1,1-Trichloroethane	PT6,35	25456-01
016941-3	B4,35	Trichloroethene	12 ppm		40 ppm	Trichloroethene	PT6,35	25456-01
016941-3	B4,35	Trichlorofluoromethane	0.57 ppm		1.9 ppm	Trichlorofluoromethane	PT6,35	25456-01
016941-3	B4,35	1,1,2-Trichloro-1,2,2-tri-fluoroethane	0.92 ppm		6.7 ppm	1,1,2-Trichloro-1,2,2-tri-fluoroethane	PT6,35	25456-01
016941-3	B4,35	1,1-Dichloroethene	0.29 ppm					
016941-3	B4,35	Benzene	2.2 ppm					
016941-3	B4,35	Toluene	1.7 ppm					
016941-3	B4,35	Ethylbenzene	2.1 ppm					
016941-3	B4,35	Xylenes	4.2 ppm					
016942-3	B4,45	Chloroform	0.37 ppm		0.40 ppm	Chloroform	PT6,45	25457-01
016942-3	B4,45	Dichlorodifluoromethane	1.4 ppm		0.25 ppm	Dichlorodifluoromethane	PT6,45	25457-01
016942-3	B4,45	1,2-Dichloroethane	0.21 ppm		0.21 ppm	1,2-Dichloroethane	PT6,45	25457-01
016942-3	B4,45	1,2-Dichloropropane	0.34 ppm		0.40 ppm	1,2-Dichloropropane	PT6,45	25457-01
016942-3	B4,45	Methylene chloride	0.63 ppm		1.0 ppm	Methylene chloride	PT6,45	25457-01
016942-3	B4,45	Tetrachloroethene	2.9 ppm		0.48 ppm	Tetrachloroethene	PT6,45	25457-01

Table E-2. Pre-Test and Post-Test Soil Gas Analysis

Pre-test Soil Gas Analysis		Detected Results Only			Detected Results Only		Post-Test Soil Gas Analysis	
Sample No.	Location, Depth	Contaminant	Concentration		Concentration	Contaminant	Location, Depth	Sample No.
016942-3	B4,45	1,1,1-Trichloroethane	4.4 ppm		2.7 ppm	1,1,1-Trichloroethane	PT6,45	25457-01
016942-3	B4,45	Trichloroethene	15 ppm		20 ppm	Trichloroethene	PT6,45	25457-01
016942-3	B4,45	Trichlorofluoromethane	0.96 ppm		1.6 ppm	Trichlorofluoromethane	PT6,45	25457-01
016942-3	B4,45	1,1,2-Trichloro-1,2,2-tri-fluoroethane	1.6 ppm		5.4 ppm	1,1,2-Trichloro-1,2,2-tri-fluoroethane	PT6,45	25457-01
016942-3	B4,45	1,1-Dichloroethene	0.6 ppm					
016942-3	B4,45	1,1-Dichloroethane	0.24 ppm					
016942-3	B4,45	Benzene	2.3 ppm					
016942-3	B4,45	Toluene	1.6 ppm					
016942-3	B4,45	Ethylbenzene	1.3 ppm					
016942-3	B4,45	Xylenes	2.6 ppm					
016943-3	B4,55	Benzene	1.1 ppm		0.43 ppm	Benzene	PT6,55	25458-01
					0.81 ppm	Chloroform	PT6,55	25458-01
016943-3	B4,55	Dichlorodifluoromethane	0.15 ppm		0.50 ppm	Dichlorodifluoromethane	PT6,55	25458-01
					0.40 ppm	1,2-Dichloroethane	PT6,55	25458-01
016943-3	B4,55	1,2-Dichloropropane	0.079 ppm		0.95 ppm	1,2-Dichloropropane	PT6,55	25458-01
016943-3	B4,55	Methylene chloride	0.16 ppm		2.1 ppm	Methylene chloride	PT6,55	25458-01
016943-3	B4,55	Tetrachloroethene	0.75 ppm		1.1 ppm	Tetrachloroethene	PT6,55	25458-01
016943-3	B4,55	1,1,1-Trichloroethane	0.81 ppm		5.3 ppm	1,1,1-Trichloroethane	PT6,55	25458-01
016943-3	B4,55	Trichloroethene	2.8 ppm		47 ppm	Trichloroethene	PT6,55	25458-01
016943-3	B4,55	Trichlorofluoromethane	0.11 ppm		3.0 ppm	Trichlorofluoromethane	PT6,55	25458-01
016943-3	B4,55	1,1,2-Trichloro-1,2,2-tri-fluoroethane	0.16 ppm		10 ppm	1,1,2-Trichloro-1,2,2-tri-fluoroethane	PT6,55	25458-01
016943-3	B4,55	1,1-Dichloroethene	0.081 ppm					
016943-3	B4,55	Toluene	0.91 ppm					
016943-3	B4,55	Ethylbenzene	0.86 ppm					
016943-3	B4,55	Xylenes	1.8 ppm					

Appendix F
Construction Diagrams of Vapor Extraction Wells TEVES1 and TEVES2

This page intentionally left blank.

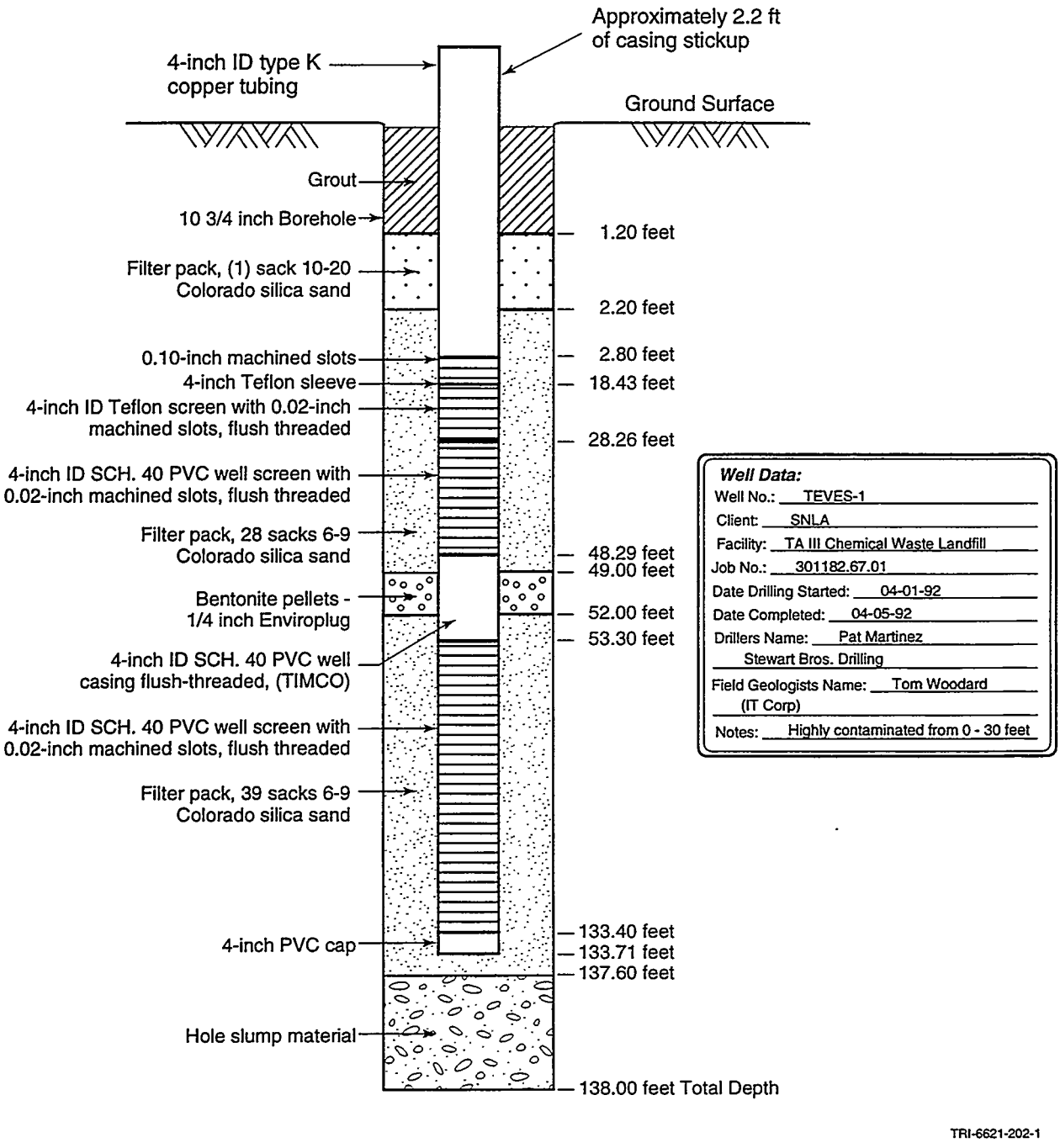

Figure F-1. Well construction schematic (Vapor Extraction Well No. TEVES-1).

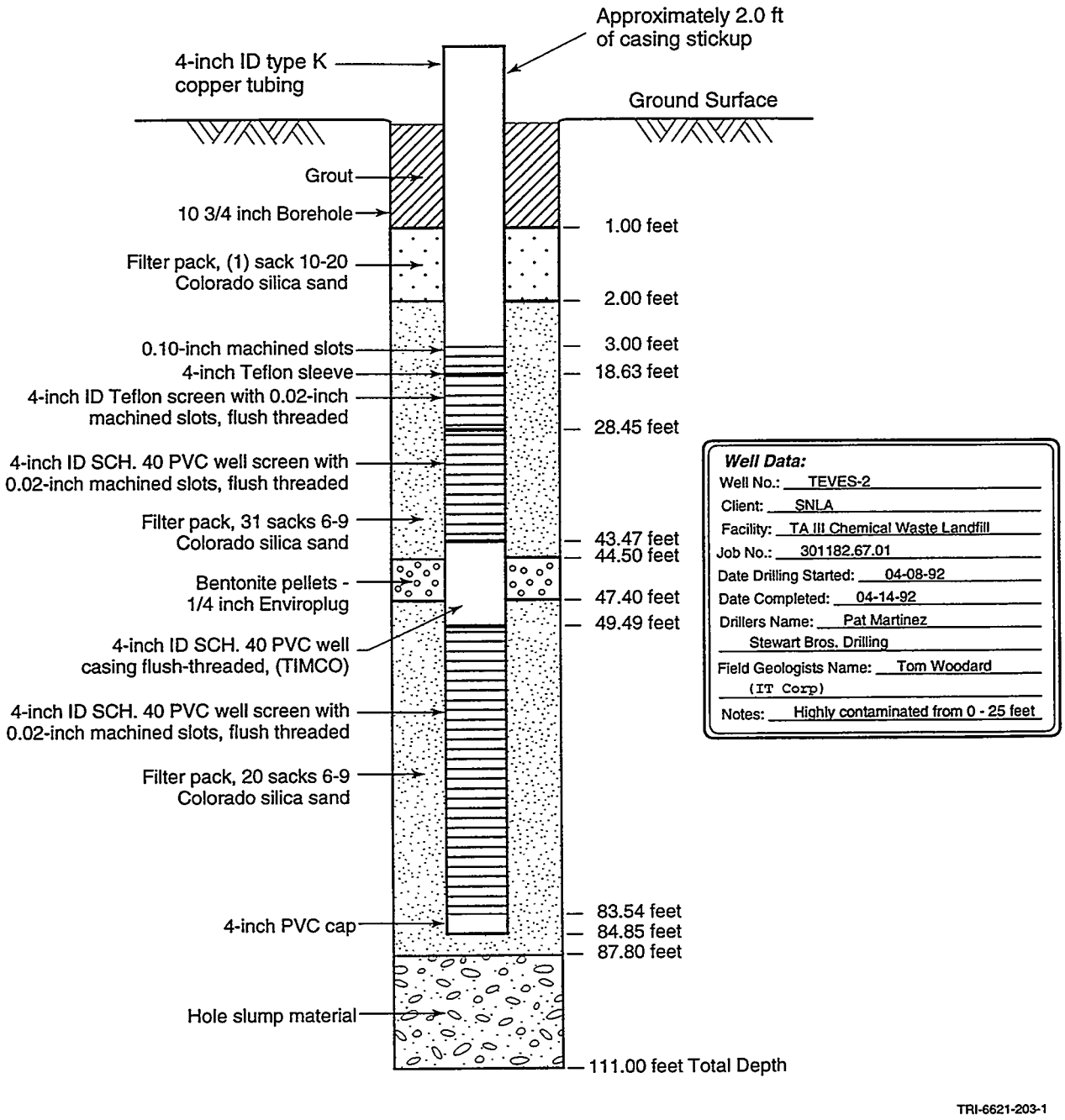

Figure F-2. Well construction schematic (Vapor Extraction Well No. TEVES-2).

DISTRIBUTION:

1 Kim Abott
U.S. Department of Energy
Oakland Operations Office
1301 Clay Street
Oakland, CA
94612-5208

1 Roger Aines
Lawrence Livermore National Lab
7000 East Avenue
Livermore, CA
94550

1 Cheryl Allen
Techreps Inc.
5000 Marble N.E.
Albuquerque, NM
87110

1 Cindy Ardito
Intera Inc.
1650 University Blvd. N.E.
Albuquerque, NM
87102

1 Paul Beam
U.S. Department of Energy
EM-40, Cloverleaf Building
19901 Germantown Rd.
Germantown, MD
20874-1290

1 Theresa Bergsman
Pacific Northwest Laboratories
Battelle Boulevard
P.O. Box 999
Richland, WA
99352

1 Mike Buettner
Lawrence Livermore National Lab, L-1
7000 East Avenue
Livermore, CA
94550-9900

1 Skip Chamberlain
U.S. Department of Energy
EM-53, Cloverleaf Building
19901 Germantown Rd.
Germantown, MD
20874-1290

1 David Daniel
University of Texas at Austin
Dept. of Civil Engineering
Cockrell Hall
Room 9.102
Austin, TX
78712

1 D. Dresp
Thomas Branigan Library
106 W. Hadley St.
Las Cruces, NM
88003

1 Tom Early
Oak Ridge National Laboratory
P.O. Box 2008
Oak Ridge, TN
37831-6317

1 Bruce Erdal
Los Alamos National Laboratory
EM-TD, MS J591
Los Alamos, NM
87545

1 Elizabeth Fiedler
Oak Ridge National Laboratory
P.O. Box 2008
Oak Ridge, TN
37831-6317

1 Philip Gauglitz
Pacific Northwest Laboratories
Battelle Boulevard
P.O. Box 999
Richland, WA 99352

1 John Geiger
U.S. Department of Energy
Savannah River Operations Office
P.O. Box A
Aiken, SC
29802

1 Ralph Gruebel
AGRA Earth & Environmental, Inc.
4700 Lincoln Rd. NE
Albuquerque, NM
87109

1 Thomas Hicks
U.S. Department of Energy
Savannah River Operations Office
P.O. Box A, Bldg. 703-46A
Aiken, SC
29802

1 Tim Jarosch
Westinghouse Savannah River Co.
Road SR-1
Bldg. 773-42A
Aiken, SC
29808

1 Jeff Lenhert
U.S. Department of Energy
Albuquerque Operations Office
Pennsylvania & H Street
Kirkland Air Force Base
Albuquerque, NM
87116

1 Julianne Levings
U.S. Department of Energy
Albuquerque Operations Office
Pennsylvania & H Street
Kirkland Air Force Base
Albuquerque, NM
87116

1 Brian Looney
Westinghouse Savannah River Co.
Road SR-1
Bldg. 773-42A
Aiken, SC
29808

1 Bill Lowry
Science and Engineering Assoc., Inc.
1570 Pacheco St.
Suite D1
Santa Fe, NM
87505

1 Dennis Olona
U.S. Department of Energy
Albuquerque Operations Office
Pennsylvania & H Street
Kirkland Air Force Base
Albuquerque, NM
87116

1 Joseph Paladino
U.S. Department of Energy
H17 Cloverleaf Gtn-HQ/OST
19901 Germantown Rd.
Germantown, MD
20874-1290

1 Arturo Palomares
Environmental Protection Agency,
Region 8
999 18th Street
Suite 500
Denver, CO
80202

1 James Paulson
U.S. Department of Energy
Chicago Operations Office
9800 S. Cass Ave.
Argonne, IL
60439

1 Elizabeth Phillips
U.S. Department of Energy
P.O. Box 2001
Oak Ridge, TN
37830

1 Caroline Purdy
U.S. Department of Energy
EM-53, Cloverleaf Building
19901 Germantown Rd.
Germantown, MD
20874-1290

1 Amy Regan
Los Alamos National Laboratory
P.O. Box 1663, MS H827
Los Alamos, NM
87545

1 Richard Renn
MDM/Lamb, Inc.
6121 Indian School Rd., N.E.
Suite 105
Albuquerque, NM
87110

1 Eric Rogoff
MDM/Lamb, Inc.
6121 Indian School Rd., N.E.
Suite 105
Albuquerque, NM
87110

1 Nina Rosenberg
Los Alamos National Laboratory
EES-DO, MS D446
Los Alamos, NM
87545

1 John Stormont
University of New Mexico
Dept. of Civil Engineering
Albuquerque, NM
87131-1351

1 James E. Stangel
IIT Research Istitute
10 West 35th Street
Chicago, IL
60616-3799

1 Jim Studer
Intera Inc.
1650 University Blvd. N.E.
Albuquerque, NM
87102

1 Guggilam C. Sresty
IIT Research Institute
10 West 35th Street
Chicago, IL
60616-3799

1 Bruce Thomson
University of New Mexico
Dept. of Civil Engineering
Albuquerque, NM
87131-1351

1 Jef Walker
U.S. Department of Energy
EM-53, Cloverleaf Building
19901 Germantown Rd.
Germantown, MD
20874-1290

1 Philip Washer
U.S. Department of Energy
Savannah River Operations Office
P.O. Box 616, Bldg. 773-A
Aiken, SC
29803

1 James Wright
U.S. Department of Energy
Savannah River Operations Office
P.O. Box A, Bldg. 703-46A
Aiken, SC
29803

1 Paul Zielinski
U.S. Department of Energy
EM-443, Cloverleaf Building
19901 Germantown Rd.
Germantown, MD
20874-1290

1 Harsh Dev
IIT Research Istitute
10 West 35th Street
Chicago, IL
60616-3799

1 Gorm Heron
National Risk Management
Research Laboratory
U.S. Environmental Protection
Agency
919 Kerr Research Dr.
Ada, OK
74820

1 MS 0329 Frank Peter, 2643
1 0503 George Laguna, 2338
1 0719 George Allen, 6621
1 0719 Tom Burford, 6621
1 0719 Bob Helgesen, 6621
50 0719 James Phelan, 6621
1 0719 Bruce Reavis, 6621
1 0719 Steve Webb, 6621
1 0720 Wu-Ching Cheng, 6626
1 0720 Ken Sorenson, 6626
1 0724 Joan Woodard, 6000
1 0726 James Rice, 6600
1 1147 Warren Cox, 6681
1 1148 Dick Fate, 6685
1 0968 James Swanson, 5716
1 9018 Central Technical Files,
8940-2
5 0899 Technical Library, 4916
2 0619 Review & Approval Desk
For DOE/OSTI, 12690
1 0161 Patent & Licensing, 11500